SECURITY CLASSIFICATION OF THIS PAGE

(2)

REPORT DOCUME

AD-A256 014

DTIC ELECTE OCT 7 1992 S C D

1a. REPORT SECURITY CLASSIFICATION: Unclassified	1b
2a. SECURITY CLASSIFICATION AUTHORITY	3. DISTRIBUTION/AVAILABILITY OF REPORT: Approved for public release distribution unlimited
2b. DECLASSIFICATION/DOWNGRADING SCHEDULE	
4. PERFORMING ORGANIZATION REPORT NUMBER(S)	5. MONITORING ORGANIZATION REPORT NUMBER(S): AFOSR-TR- 92 0855
6a. NAME OF PERFORMING ORGANIZATION: UCLA School of Medicine; 6b. OFFICE SYMBOL (If applicable)	7a. NAME OF MONITORING ORGANIZATION: Air Force Office of Scientific Research /NL
6c. ADDRESS (City, State, and ZIP Code): Mental Retardation Research Center, 760 Westwood Plaza (NPI 58-258), Los Angeles, CA 90024	7b. ADDRESS (City, State, and ZIP Code): Bldg. 410, Bolling AFB, DC 20332-6448
8a. NAME OF FUNDING/SPONSORING ORGANIZATION: AFSOR; 8b. OFFICE SYMBOL (If applicable): NL	9. PROCUREMENT INSTRUMENT IDENTIFICATION NUMBER: AFSOR-90-0056
8c. ADDRESS (City, State, and ZIP Code): Bldg. 410, Bolling AFB, DC 20331	10. SOURCE OF FUNDING NUMBERS: PROGRAM ELEMENT NO. 61102F; PROJECT NO. 2312; TASK NO. A3; WORK UNIT ACCESSION NO.

11. TITLE (Include Security Classification): Intracellular Physiology of the Rat Suprachiasmatic Nucleus: Electrical Properties, Neurotransmission, and Effects of Neuromodulators

12. PERSONAL AUTHOR(S): F. Edward Dudek

13a. TYPE OF REPORT	13b. TIME COVERED	14. DATE OF REPORT (Year, Month, Day)	15. PAGE COUNT
Final	FROM 11/01/89 TO 6/30/92	1992 Aug 24	

16. SUPPLEMENTARY NOTATION

17. COSATI CODES			18. SUBJECT TERMS (Continue on reverse if necessary and identify by block number)
FIELD	GROUP	SUB-GROUP	Hypothalamus, GABA, suprachiasmatic nucleus, excitatory amino acids, glutamate, electrophysiology

19. ABSTRACT (Continue on reverse if necessary and identify by block number)

The aim of this research has been to gain an understanding of the neurophysiology of the suprachiasmatic nucleus (SCN), with emphasis on intrinsic electrical properties, synaptic and non-synaptic transmission, and neuromodulation. We have studied the role of excitatory and inhibitory amino acids (i.e., glutamate and GABA) in fast synaptic transmission. Our work has provided strong evidence that these transmitters mediate most, if not all, of the synaptic potentials in SCN neurons. Experiments with extracellular recordings indicate that a circadian rhythm of electrical activity persists after pharmacological blockade of these transmitter systems. Intracellular recordings showed that the intrinsic membrane properties are not homogeneous across the SCN, that some neurons have low-threshold Ca^{2+} spikes and inward rectification, and that the firing pattern depends on firing rate. We have recently found that synchronous bursts of action potentials can occur in the SCN after chemical synapses have been blocked with low-calcium solutions and amino-acid-transmitter antagonists. Finally, we have continued to study the supraoptic and paraventricular nuclei and the preoptic area of the hypothalamus, thus allowing a direct comparison between the SCN and other areas of the hypothalamus. Our experiments should provide a rigorous understanding of how neurotransmitters, local neuronal circuits and intrinsic membrane properties regulate the electrical activity of neurons in the SCN and other hypothalamic areas.

20. DISTRIBUTION/AVAILABILITY OF ABSTRACT	21. ABSTRACT SECURITY CLASSIFICATION
☒ UNCLASSIFIED/UNLIMITED ☐ SAME AS RPT ☐ DTIC USERS	Unclassified
22a. NAME OF RESPONSIBLE INDIVIDUAL: Dr. Genevieve Haddad	22b. TELEPHONE (Include Area Code): (202) 767-5021 — 22c. OFFICE SYMBOL: NL

DD FORM 1473, 84 MAR — 83 APR edition may be used until exhausted. All other editions are obsolete.

SECURITY CLASSIFICATION OF THIS PAGE

28 AUG 1992

Final Technical Report
11-1-89 to 6-30-92
(2 yr funding & 7 mo no-cost extension)

P.I.-F.E. Dudek
AFSOR 90-0056

TABLE OF CONTENTS

Final Technical Report
11-1-89 to 6-30-92
(2 yr funding & 7 mo no-cost extension)

P.I.-F.E. Dudek
AFSOR 90-0056

I. RESEARCH OBJECTIVES

The general aim of this research project has been to test several important hypotheses about the electrophysiology of the suprachiasmatic nucleus (SCN). We have used the hypothalamic slice preparation and a combination of electrophysiological techniques (i.e., extracellular single- and multi-unit recording, intracellular recording, and whole-cell patch clamp). Our first project was to determine whether glutamate is the transmitter mediating the retinal input to the SCN, and in particular whether non-NMDA and NMDA receptors generate EPSPs in SCN neurons. We have also tested the hypothesis that activation of $GABA_A$ receptors and increased chloride conductance mediate fast inhibitory input to SCN neurons. We have studied the intrinsic electrophysiological properties of SCN neurons, and have tested the hypothesis that they are homogeneous across the SCN. We have attempted to identify distinct groups of cells with different electrophysiological properties, and in particular test for the presence of low-threshold calcium spikes and inward rectification. Another set of experiments has examined the role of amino acid transmitters in generation of the circadian rhythm of electrical activity observed in the SCN. These latter experiments have also provided exciting new data for the presence of non-synaptic mechanisms of synchronization in the SCN. Thus, several interrelated projects, directly in line with our original proposal, have been completed or are underway concerning the electrophysiology of SCN neurons.

Under the partial support of the AFOSR, we have also undertaken electrophysiological studies of other hypothalamic nuclei. The paraventricular nucleus (PVN) contains a diverse population of neuroendocrine cells responsible for the secretion of such important hormones as vasopressin and corticotropin-releasing factor. We completed an extensive series of experiments on the PVN; these studies were aimed at defining the different classes of neurons based on their electrophysiological properties, and then evaluating the role that glutamate plays as an excitatory transmitter to the different cell types of this nucleus. The preoptic area is another hypothalamic area responsible for a variety of homeostatic mechanisms, and we have performed experiments aimed at defining the electrophysiological properties and neurotransmitters of neurons in the preoptic area. Recently, we completed a patch-clamp analysis of spontaneous synaptic currents of supraoptic nucleus (SON) neurons with the goal of understanding synaptic mechanisms of neuroendocrine cells in more detail.

II. STATUS OF RESEARCH

A. Suprachiasmatic nucleus (SCN)

1. Intracellular electrophysiology

a. Excitatory amino acids

Intracellular recordings were obtained from over 100 SCN neurons in horizontal or

parasagittal slices from rats and guinea pigs. Retinal input activated by optic nerve stimulation evoked excitatory postsynaptic potentials (EPSPs) and virtually no inhibitory postsynaptic potentials (IPSPs) in SCN neurons. Our experiments documented that the antagonist for AMPA/kainate-type amino acid receptors, 6,7-dinitroquinoxaline-2,3-dione (DNQX, 1-10 μM), blocked EPSPs in a concentration-dependent and reversible manner. The selective N-methyl-D-aspartate (NMDA) receptor antagonist, DL-2-amino-5-phosphonopentanoic acid (AP5, 50-100 μM) did not significantly and consistently affect the EPSPs at resting or hyperpolarized membrane potentials; however, when SCN neurons were depolarized, AP5 blocked or depressed a slow component of the EPSPs. Similar data were obtained for EPSPs in response to stimulation at other sites. These results demonstrate that both non-NMDA and NMDA receptors mediate excitatory synaptic transmission from both retinal input and from other CNS sites, and that NMDA receptors are important when SCN cells are depolarized. A paper on this work was published in the *Journal of Physiology* (Kim and Dudek, 1991), and reprints are enclosed.

b. Gamma-amino-butyric acid (GABA)

Another series of experiments were aimed at studying inhibitory synaptic mechanisms in the SCN. Electrical stimulation dorsocaudal to the SCN evoked ISPSs in 33 of 36 neurons, and spontaneous IPSPs were present in every neuron. Spontaneous and evoked fast IPSPs were hyperpolarizing at resting potential and had a reversal potential $\sim$-75 mV. With KCl electrodes, the IPSPs were positive going. The IPSPs were blocked by bicuculline, a $GABA_A$ receptor antagonist. Bicuculline-resistant hyperpolarizing potentials, similar in time-course to the fast IPSPs, also occurred spontaneously and could be evoked by electrical stimulation of the optic nerve or dorsocaudal site. A fast prepotential always preceded these hyperpolarizing potentials, and injection of hyperpolarizing currents blocked these events, thus indicating they were not synaptic in origin. No slow IPSPs were detected in SCN neurons. These data provide evidence that SCN neurons receive extensive GABAergic input and that $GABA_A$ receptors and an increase in chloride conductance mediate these inhibitory synaptic mechanisms. A paper on these data is in press in the *Journal of Physiology* (Kim and Dudek, 1992), and copies of the proofs are enclosed.

c. Membrane properties

Recent studies have been aimed at evaluating whether the electrophysiological properties of SCN neurons are homogeneous or heterogeneous, and whether distinct classes of neurons can be identified. We focused on the subpopulation of neurons that demonstrably received retinal input, as determined by recording short-latency EPSPs to optic nerve stimulation (Kim and Dudek, 1991). Considerable effort has been spent on a quantitative analysis of the electrophysiology of SCN neurons, primarily with sharp electrodes (but also more recently with patch electrodes). The experiments with sharp electrodes have indicated that individual action potentials are relatively short in duration, and are followed by a pronounced hyperpolarizing afterpotential. Spike inactivation, spike broadening and frequency accommodation occurred consistently during depolarizing current pulses, and an after-hyperpolarization routinely followed a burst of action potentials. The membrane

time constant of these neurons ranged from 7 to 21 msec (mean 11.4 $\pm$ 0.7 msec). The input resistance of these neurons was 105 to 626 megohms (mean 301 $\pm$ 23 megohms) with sharp electrodes. Although there was some variability in these properties, no distinct groups were found when analyses were made across the neuronal population. Some neurons did show slight time- and voltage-dependent inward rectification, and these neurons had a higher spontaneous firing rate and were more excitable. Some neurons also had low-threshold calcium spikes, although other neurons clearly lacked them. Most neurons fired spontaneously; those neurons with a firing rate >6 Hz had a regular firing pattern, whereas neurons that fired <4 Hz had an irregular pattern. Altering the firing rate with injected current changed the firing pattern. These results suggest that: (1) SCN neurons receiving optic nerve input are not electrophysiologically homogeneous, and yet they do not appear to form distinct classes of electrophysiological cell types, (2) time-dependent inward rectification and the capacity to generate low-threshold calcium spikes are limited to only a sub-population of neurons, (3) inward rectification is associated with an increased spontaneous firing rate, and (4) firing pattern is related to firing rate, probably more than to cell type. These electrophysiological properties have also been observed with whole-cell patch-clamp techniques, but voltage-clamp studies on these properties are needed. Another manuscript is in press in the *Journal of Physiology* concerning the sharp-electrode experiments on membrane properties.

2. Role of amino acid transmitters in the circadian rhythm of electrical activity in the SCN

Preliminary experiments have been performed on the long-term objective of understanding the possible role of glutamate and GABA in the expression of the circadian rhythm of electrical activity in the SCN. Yona Bouskila, a graduate student in our laboratory, developed a procedure for using multi-unit extracellular recordings to study the circadian rhythm of electrical activity. This technique has the advantage over single-unit recordings of being less labor-intensive because one does not have to continuously search for single-unit action potentials during an experiment to sample the population. Furthermore, it is more objective because it removes any possibility of experimental bias in obtaining recordings from cells. We undertook a series of experiments examining the effects of excitatory and inhibitory amino-acid-receptor antagonists on the circadian rhythm of electrical activity. Our preliminary data indicate that there is a circadian rhythm of multi-unit activity even when these transmitter receptors are blocked pharmacologically. We have so far only recorded for slightly more than one day, and we wish to extend the duration of our recordings so that we can evaluate 2 or even 3 days of electrical activity. We also plan to use animals whose circadian rhythm has been shifted by 12 hours, so that if we perform the experiment at the same time of the day, we can control for any other variables that could generate this apparent circadian rhythm of electrical activity in our hypothalamic slices. Future experiments will thus provide a more definitive test of the hypothesis that the circadian rhythm of electrical activity can persist after blockade of amino acid receptors and fast synaptic potentials.

3. Non-chemical-synaptic mechanisms of synchronization of the SCN

Several independent observations in the literature concerning the SCN and circadian rhythms have suggested that the electrical activity of SCN neurons can be synchronized by mechanisms that do not involve chemical synaptic transmission. We found that bursts of electrical activity occurred when hypothalamic slices were bathed in a low-calcium solution for several hours. Multi-unit recordings showed that populations of SCN neurons had their bursts of activity roughly synchronized, and dual recordings from adjacent areas confirmed that in one SCN the bursts occurred synchronously across the population. The bursts in one SCN were not, however, synchronized with bursts in the contralateral SCN. A mixture of NMDA, non-NMDA, and $GABA_A$ receptor antagonists had no effect upon the synchronicity of the bursts. Whole-cell patch-clamp recordings confirmed that the low-calcium solution blocked the evoked EPSPs and IPSPs, and the mixture of antagonists blocked the remaining spontaneous PSPs. These results indicate that synchronous neuronal activity can occur in the SCN without active chemical synapses, thus strongly suggesting that a different mechanism of communication exists in the SCN. The possible mechanisms include electrotonic coupling via gap junctions among SCN neurons, ephaptic interactions, and shifts in the concentration of extracellular ions such as potassium; future experiments will attempt to evaluate these mechanisms in the SCN. This approach derives from our earlier AFOSR-supported research on non-synaptic mechanisms of synchronization in the hippocampus (Dudek, Obenaus, and Tasker, 1990). An abstract (Bouskila and Dudek, 1992) has been submitted and a manuscript on these findings is enclosed.

B. Other hypothalamic regions

1. Paraventricular nucleus (PVN)

We have undertaken an extensive series of experiments involving intracellular recording and staining with subsequent immunohistochemical identification of neurons in the PVN. Three general types of neurons, based on electrophysiological properties, have been identified in and around the PVN. Combined electrophysiological, anatomical and immunohistochemical studies indicate that one can delineate (1) magnocellular neuroendocrine cells, (2) parvocellular neurons, and (3) other types of neurons outside the PVN. In essence, these studies showed that distinct electrophysiological properties are associated with anatomically specific cell types in the PVN (Tasker and Dudek, 1991; Hoffman, Tasker and Dudek, 1991). Selective non-NMDA receptor antagonists effectively blocked EPSPs in all of these different types of PVN cells (van den Pol, Wuarin and Dudek, 1990, Wuarin and Dudek, 1991). More recent studies have shown that these different types of PVN neurons have NMDA receptors that mediate excitatory synaptic transmission when the cells are depolarized (Wuarin and Dudek, 1991). Reprints of these papers are enclosed.

2. Supraoptic nucleus (SON)

Using whole-cell patch clamp techniques with the hypothalamic slice preparation, we have re-examined synaptic mechanisms in the SON. Our earlier work supported by this grant provided electrophysiological evidence that glutamate acting on non-NMDA receptors mediates fast EPSPs in this nucleus. Other studies suggest that GABA mediates IPSPs in the SON. We analyzed spontaneous synaptic currents with the whole-cell patch-clamp technique because of the improved signal-to-noise ratio available with this technique. Bicuculline blocked all fast inhibitory postsynaptic currents (IPSCs), and CNQX blocked all of the excitatory postsynaptic currents (EPSCs). Thus, we have confirmed with the more sensitive technique of whole-cell patch recording that all of the fast EPSCs and IPSCs appear to be mediated by glutamate and GABA acting of AMPA/kainate and $GABA_A$ receptors respectively. An abstract has been submitted (Wuarin and Dudek, 1992) and a copy of a submitted manuscript is also included.

3. Preoptic area

We have undertaken electrophysiological and anatomical studies in the preoptic area of the hypothalamus. We tested the hypothesis that this anatomically heterogeneous population of neurons is electrophysiologically heterogeneous. A series of intracellular electrophysiological experiments demonstrated that virtually all the cells have low-threshold calcium spikes and linear current-voltage relations. Additional evidence with the whole-cell patch-clamp technique has been obtained that glutamate and GABA mediate synaptic events here, as in other hypothalamic regions. A manuscript on this work is enclosed (Hoffman et al, in preparation), and an abstract on the patch-clamp recordings has been submitted (Hoffman, Wuarin and Dudek, 1992).

C. Conclusions

Retinal input generates fast EPSPs and no IPSPs, and stimulation of other sites around the SCN causes both fast EPSPs and fast IPSPs. Glutamate and GABA mediate most if not all fast EPSPs and IPSPs in the SCN. Glutamate acts on non-NMDA receptors at resting potential, but NMDA receptors contribute to the EPSPs when the neurons are depolarized. Only fast IPSPs (no slow IPSPs) have been observed in SCN neurons; $GABA_A$ receptors and an increase in Cl^- conductance generate these IPSPs. These pharmacological and ionic properties of synaptic events appear to be identical to other hypothalamic neurons, including those in the SON, PVN, arcuate nucleus and preoptic area.

In terms of intrinsic membrane properties, the SCN appears more similar to the PVN than to the SON or preoptic area. That is, the latter two hypothalamic areas are relatively homogeneous in terms of cell types, whereas the PVN is not homogeneous and does have relatively distinct cell types. Although we have not yet identified distinct cell types in the SCN, when future electrophysiological data with patch electrodes are combined with anatomical and

immunocytochemical results (including intracellular staining), distinct groups of neurons may become apparent.

Combined extracellular and intracellular recordings on groups of SCN neurons indicate that synchronization can occur without active chemical synaptic mechanisms. Additional research from our lab and others suggests that non-chemical-synaptic mechanisms synchronize SCN neurons during the circadian rhythm. Future research needs to be aimed at identifying the synaptic and non-synaptic mechanisms of local neuronal communication that operate in the SCN, and determine if and how they contribute to the circadian rhythm of electrical activity in the SCN.

III. PUBLICATIONS

Refereed Publications (* indicates research on the suprachiasmatic nucleus)

Dudek, F.E., Obenaus, A. and Tasker, J.G. (1990) Osmolality-induced changes in extracellular volume alter epileptiform bursts independent of chemical synapses in the rat: importance of non-synaptic mechanisms in hippocampal epileptogenesis. Neurosci. Lett. 120:267-270.

van den Pol, A.N., Wuarin, J.P. and Dudek, F.E. (1990) Glutamate, the dominant excitatory transmitter in neuroendocrine regulation. Science 250:1276-1278.

Tasker, J.G. and Dudek, F.E. (1991) Electrophysiological properties of neurones in the region of the paraventricular nucleus in slices of rat hypothalamus. J. Physiol., London 434:271-293.

Wuarin, J.P. and Dudek, F.E. (1991) Excitatory amino acid antagonists inhibit synaptic responses in the guinea pig hypothalamic paraventricular nucleus. J. Neurophysiol. 65:946-951.

Hoffman, N.W., Tasker, J.G. and Dudek, F.E. (1991) Immunohistochemical differentiation of electrophysiologically defined neuronal populations in the region of the rat paraventricular nucleus. J. Comp. Neurol. 307:405-416.

Tasker, J.G., Hoffman, N.W. and Dudek, F.E. (1991) A comparison of three intracellular markers for combined electrophysiological, anatomical and immunohistochemical analyses. J. Neurosci. Meth. 38:129-143.

*Kim, Y.I. and Dudek, F.E. (1991) Intracellular electrophysiological study of suprachiasmatic nucleus neurones in rodents: excitatory synaptic mechanisms. J. Physiol., London 444:269-287.

*Kim, Y.I. and Dudek, F.E. (1992) Intracellular electrophysiological study of suprachiasmatic nucleus neurones in rodents: inhibitory synaptic mechanisms. J. Physiol., London (in press).

*Kim, Y.I. and Dudek, F.E. Membrane properties of rat suprachiasmatic nucleus neurons receiving optic nerve input. J. Physiol., London (in press).

Manuscripts submitted or in preparation

Hoffman, N.W., Kim, Y.I., Gorski, R.A. and Dudek, F.E. Intracellular membrane and synaptic properties in medial preoptic slices containing the sexually dimorphic nucleus of the rat.

*Bouskila, Y. and Dudek, F.E. New type of synchronization without active calcium-dependent synaptic transmission in the hypothalamus.

Tasker, J.G. and Dudek, F.E. Local synaptic inhibitory inputs to neurones of the paraventricular nucleus in slices of rat hypothalamus.

Wuarin, J.P. and Dudek, F.E. Patch clamp analysis of spontaneous synaptic currents in supraoptic neurons of the rat hypothalamus.

Abstracts (1992 only)

*Bouskila, Y. and Dudek, F.E. (1992) Synchronous neuronal activity in the suprachiasmatic nucleus (SCN) independent of chemical synaptic transmission. Soc. Neurosci. Abstr. (submitted).

Wuarin, J.P. and Dudek, F.E. (1992) Patch-clamp analysis of spontaneous synaptic currents in rat supraoptic neurons. Soc. Neurosci. Abstr. (submitted).

Hoffman, N.W., Wuarin, J.P. and Dudek, F.E. (1992) Whole-cell patch clamp recordings of spontaneous synaptic currents and their block by amino acid neurotransmitter antagonists in medial preoptic slices from immature male rats. Soc. Neurosci. Abstr. (submitted).

IV. PROFESSIONAL PERSONNEL (* indicates primary personnel paid from this grant)

* Mr. Yona Bouskila
  Dr. Neil H. Hoffman
* Dr. Yang I. Kim
  Dr. Jeffrey G. Tasker
  Dr. Jean-Pierre Wuarin

V. INTERACTIONS

At the 1990 Winter Conference on Brain Research, Drs. E. Dudek, M. Gillette, M. Rea and A. van den Pol participated in a workshop on the SCN. All of us also attended the 1991 meeting and have several informal discussions on our research.

VI. NEW DISCOVERIES, INVENTIONS OR PATENT DISCLOSURES--none, other than the research findings described below.

VII. OTHER STATEMENTS

In the next month or two, I plan to submit a renewal grant application to follow-up the progress we have made over the last few years toward gaining an understanding of the function of the SCN at a cell and membrane level. At the present time my plan is to focus the grant on local neuronal interactions. We will use glutamate microstimulation and whole-cell patch-clamp recordings to test the hypothesis that *local* GABAergic neurons generate the fast IPSCs to SCN neurons. We will also modify our slice preparation (possibly use sterile techniques, etc.) to obtain recordings that hopefully last for 2-3 days so that we can test more rigorously the hypothesis that the circadian rhythm of electrical activity in the SCN does not depend on amino-acid-mediated neurotransmission. If these experiments support our preliminary data (above), this will strongly suggest that non-synaptic mechanisms are important in synchronizing neurons during the circadian rhythm of SCN electrical activity. Finally, several possible experiments are being considered to study non-chemical-synaptic mechanisms of synchronization, with particular emphasis on electrotonic coupling and gap junctions.

Neuroscience Letters, 120 (1990) 267–270
Elsevier Scientific Publishers Ireland Ltd.

NSL 07373

Osmolality-induced changes in extracellular volume alter epileptiform bursts independent of chemical synapses in the rat: importance of non-synaptic mechanisms in hippocampal epileptogenesis

F. Edward Dudek, Andre Obenaus and Jeffrey G. Tasker

Mental Retardation Research Center, UCLA School of Medicine, Los Angeles, CA (U.S.A.)

(Received 6 July 1990; Revised version received 24 August 1990; Accepted 24 August 1990)

Key words: Hippocampus; Epilepsy; Synchrony; Osmolality; Calcium

The contribution of non-synaptic mechanisms to the seizure susceptibility of rat CA1 hippocampal pyramidal cells was examined in vitro by testing the effects of osmolality on synchronous neuronal activity, using solutions which blocked chemical synaptic transmission both pre- and postsynaptically. Decreases in osmolality, which shrink the extracellular volume, caused or enhanced epileptiform bursting. Increases in osmolality with membrane-impermeant solutes, which expand the extracellular volume, blocked or greatly reduced epileptiform discharges. Reductions in the extracellular volume, therefore, can enhance synchronization among CA1 hippocampal neurons through non-synaptic mechanisms. Since similar osmotic treatments are known to modify epileptiform discharges in several models of epilepsy, non-synaptic mechanisms are probably more important in hippocampal epileptogenesis than previously realized and may contribute to the high susceptibility of this brain region to epileptic seizures in animals and humans. These data also provide a possible explanation for the observation in humans that decreased plasma osmolality, which can be associated with a wide range of clinical syndromes, leads to seizures.

Chemical synapses are clearly the dominant form of neuronal communication under normal conditions, but non-synaptic mechanisms (i.e. electrical field effects or ephaptic interactions, changes in extracellular $[K^+]$, and electrotonic coupling through gap junctions) may be critically important in abnormal states, such as epilepsy [12, 28]. Several laboratories independently showed that low-$[Ca^{2+}]$ solutions, which block chemical synaptic transmission, give rise to spontaneous bursts of synchronized activity in hippocampal slices [17, 20, 25]; this suggests that mechanisms other than chemical synapses can synchronize the electrical activity of hippocampal neurons. However, whether chemical synapses were *completely* blocked and thus whether non-synaptic mechanisms are sufficient for neuronal synchronization in the hippocampus has been questioned [9]. Changes in the osmolality of the extracellular fluid alter cellular volume [15] and would be expected to modify the effectiveness of non-synaptic mechanisms of neuronal synchronization. Experiments on cortical brain slices [2, 27] and on animal models of epilepsy [5, 6] have shown that changes in the osmolality of the extracellular fluid alter epileptiform activity, but the mechanisms underlying the effects of osmolality have been unclear because chemical synapses were operative. We now test the hypothesis that the extracellular volume determines the strength of non-synaptic mechanisms of neuronal interaction and is therefore an important factor in hippocampal epileptogenesis. This study shows that even when chemical synapses have been demonstrably blocked both pre- and postsynaptically, synchronized electrical activity of CA1 hippocampal pyramidal cells is still sensitive in a predictable manner to changes in the osmolality of the extracellular fluid. These data emphasize the important role that non-synaptic mechanisms play in synchronizing the electrical activity of CA1 hippocampal neurons, which may contribute to their high sensitivity to seizure- and hypoxia-induced damage under clinical conditions.

Conventional techniques were used for the preparation and in vitro maintenance of rat hippocampal slices (400 μm). The normal extracellular solution contained (in mM): NaCl 124, KCl 3.0, $CaCl_2$ 2.4, $NaHCO_3$ 26, $MgSO_4$ 2.0, NaH_2PO_4 1.24 and glucose 10. The low-$[Ca^{2+}]$ solution contained (in mM): $CaCl_2$ 0, EGTA 1.0, 6,7-dinitroquinoxaline-2,3-dione (DNQX) 0.03 and D,L-2-amino-5-phosphonopentanoate (AP5) 0.03. The solutions were saturated with 95% O_2 and 5% CO_2 (pH = 7.4) and maintained at 34°C. Intracellular and

Correspondence: F.E. Dudek, Mental Retardation Research Center, UCLA School of Medicine, 760 Westwood Plaza (NPI 58-258), Los Angeles, CA 90024, U.S.A.

extracellular recordings were obtained from the cell body layer of CA1. The osmolality of these solutions was measured with a vapor-pressure osmometer.

The interpretation that chemical synaptic transmission is blocked in low-[Ca^{2+}] solutions has been questioned on two grounds [9]. First, although low-[Ca^{2+}]-solutions block synaptic responses to single stimuli [17, 20, 25], they may not block completely the facilitated response to repetitive stimulation [19]. Second, previous studies [17, 20, 25] could not rule out a possible contribution of depolarization-induced, calcium-independent transmitter release; although such a hypothetical mechanism might not cause synaptic potentials, it could lead to increased transmitter levels in the extracellular space. In the present study, we used both a low-[Ca^{2+}] solution (i.e. Ca^{2+} omitted) with 1 mM EGTA as a presynaptic block, and high concentrations (30 μM) of the excitatory amino acid antagonists DNQX and AP5 to block the postsynaptic effects of glutamate. Numerous studies have clearly shown that these concentrations (or lower ones) of quinoxalinediones and AP5 are sufficient to abolish excitatory chemical synaptic transmission and/or synaptically mediated epileptiform bursts in the hippocampus [7, 14, 16, 22, 23]. A γ-aminobutyric acid (GABA) antagonist was not added to the extracellular solution (even though spontaneous release of GABA might occur in low-[Ca^{2+}] solutions), because GABA would tend to depress activity, and inhibitory postsynaptic potentials (IPSPs) would not synchronize neurons under these conditions. Intracellular and extracellular synaptic responses to both single and repetitive (12 and 24 Hz) stimuli were completely eliminated (Fig. 1A,B).

Within 30–120 min after application of low-[Ca^{2+}] solution, spontaneous bursts of synchronized compound action potentials ('population spikes') usually occurred at regular intervals (Fig. 1C). Low-[Ca^{2+}] solutions increase neuronal excitability by lowering threshold for action potential generation [13]. The increased excitability and repetitive firing of action potentials probably initiate the synchronous bursts that occur in these solutions [26].

Dilution of the extracellular medium with 5–20% H_2O, which causes cell swelling and a reduction of the extra-

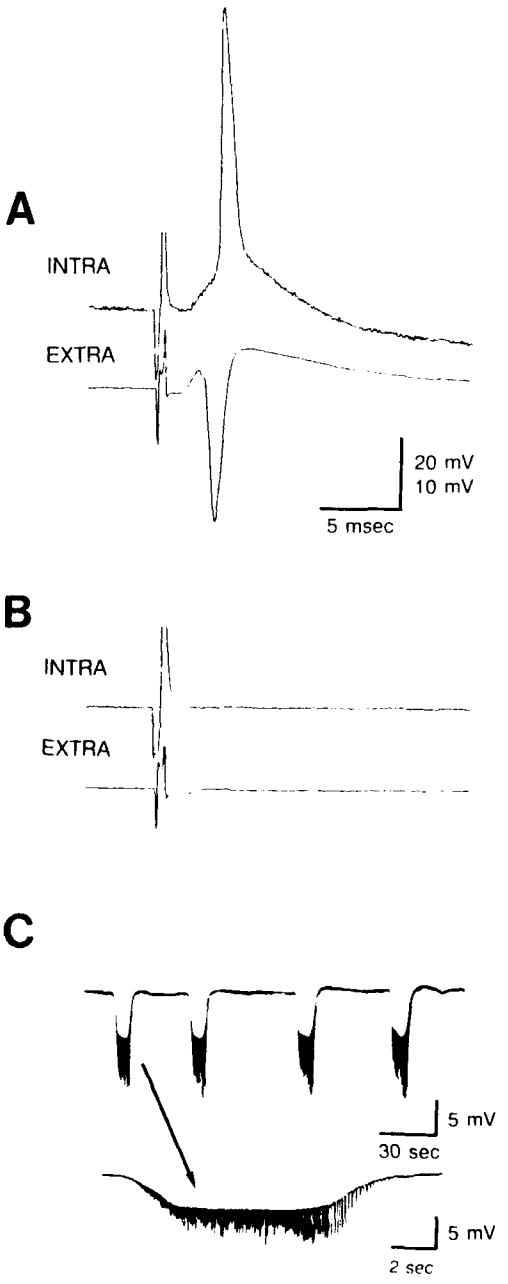

Fig. 1. Pre- and postsynaptic blockade of chemical synapses and subsequent development of epileptiform activity in the CA1 area of rat hippocampal slices. A: synaptic responses to electrical stimulation of stratum radiatum in normal medium. Intracellular recordings (INTRA: single response) showed a typical excitatory postsynaptic potential (EPSP) with a superimposed action potential. Extracellular field potentials (EXTRA: average of 5 responses) displayed a positive-going population EPSP and a faster, negative-going population spike. B: pre- and postsynaptic block of chemical synaptic transmission. Ca^{2+}-dependent release of synaptic transmitter from presynaptic terminals was blocked with low-[Ca^{2+}] solutions (i.e. Ca^{2+} omitted) containing 1 mM EGTA. Postsynaptic excitatory amino acid receptors were blocked with the non-NMDA antagonist, 6,7-dinitroquinoxaline-2,3-dione (DNQX, 30 μM), and the NMDA antagonist, D,L-2-amino-5-phosphonopentanoate (AP5, 30 μM). In normal solutions, DNQX and AP5 (30 μM) abolished synaptic responses in CA1 pyramidal cells. Synaptic responses were consistently and completely eliminated to single and repetitive stimuli (12 and 24 Hz, 0.5 ms for 10 s). The intracellular and extracellular responses are averages of the last 20 responses to 24 Hz stimulation. Calibrations are the same as in (A). C: spontaneous bursts of population spikes after blockade of chemical synaptic transmission. Within 40 min, most slices had spontaneous bursts of population spikes in the CA1 area. During each burst, a negative shift in extracellular potential was followed by repetitive population spikes, which are shown at slow (above) and fast (below) time scales.

cellular volume [15], induced or greatly enhanced epileptiform bursts in 5–10 min ($n=9$, Fig. 2A). Conversely, addition of a membrane-impermeant solute (i.e. 5–40 mM sucrose or mannitol), which causes cell shrinkage and a resultant increase of the extracellular volume, reversibly blocked or depressed the spontaneous epileptiform bursts in 15–30 min ($n=9$, Fig. 2B). Changes in extracellular resistance, indicative of alterations in extracellular volume, have been measured previously in the CA1 area during similar changes in osmolality [27]. Glycerol (5–40 mM), a membrane-permeant solute, had little or no effect on the bursts during a 30-min application ($n=6$, Fig. 2C). These experiments demonstrate that increases or decreases in the osmolality of the extracellular medium and their associated effects on extracellular volume can depress or enhance, respectively, epileptiform bursts. These effects occur even when chemical synaptic transmission has been unequivocally blocked. Therefore, mechanisms that depend on the size of the extracellular space and are independent of chemical synapses are responsible for the generation and/or synchronization of these epileptiform bursts.

If non-synaptic mechanisms play a major role in the synchronization of hippocampal neurons, and thus significantly augment the susceptibility of the hippocampus to epileptic seizures, then experimental alteration of the extracellular volume should affect epileptiform bursting. Previous studies have shown that changes in osmolality can alter epileptiform activity both in vitro and in vivo [2, 5, 6, 27]. Although there is evidence that the observed osmotic effects were not due to chemical synapses [2, 27], it is impossible to rule out a contribution from chemical transmission in these studies. Indeed, some of the available data have suggested that these osmotic effects potentially involve or depend upon chemical synapses [2, 6]. Increased extracellular space under hyperosmotic conditions could allow faster diffusion of transmitter away from synaptic receptors; on the other hand, the concentration of transmitter could be increased if the extracellular space was reduced in solutions of lowered osmolality. In the present study, however, non-synaptic mechanisms must account for the effects of osmolality on epileptiform activity, since chemical synapses were completely blocked.

Intense activity of cortical neurons is known to cause cell swelling and concomitant shrinkage of the extracellular volume [10, 11], similar to what would be expected in hypoosmotic solutions. Our data strongly suggest that activity-dependent reductions in extracellular volume and subsequent enhancement of non-synaptic mechanisms of neuronal excitation are part of an important positive-feedback loop that contributes to the induction and maintenance of epileptogenesis. Non-synaptic mechanisms of neuronal interaction may contribute to the high seizure susceptibility of CA1 pyramidal cells, and to the sensitivity of this area to seizure- and

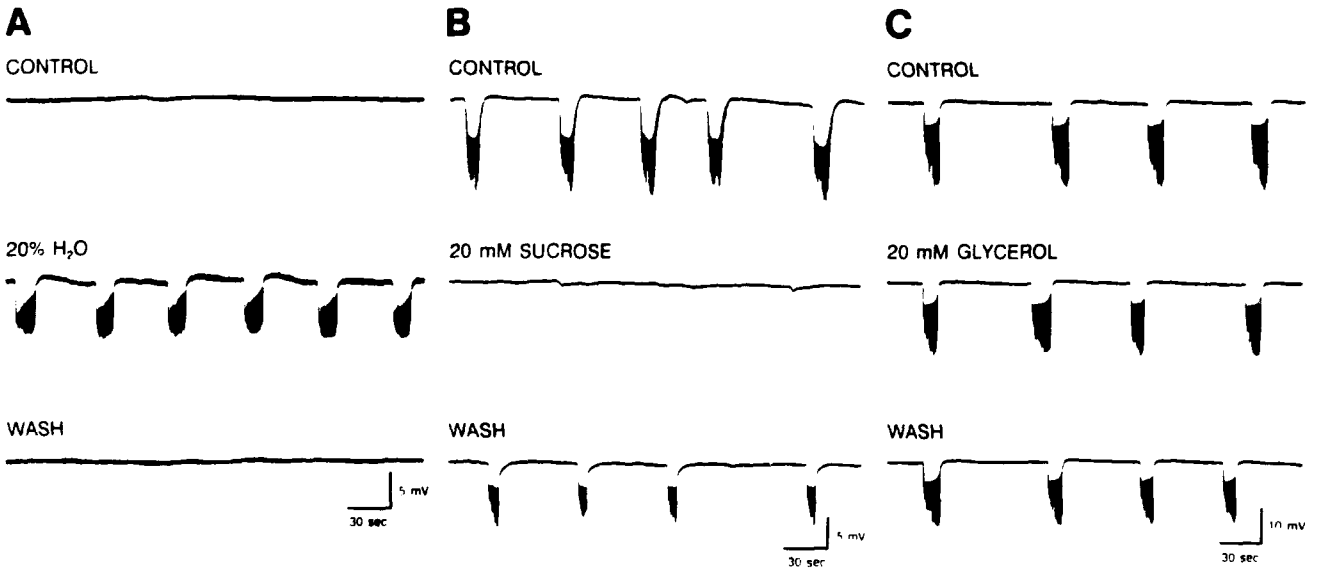

Fig. 2. Effects of osmolality on epileptiform bursts after blockade of chemical synapses. It is well-known that water moves into cells and causes swelling in hypoosmotic solutions, and that water moves out of cells and leads to shrinkage in hyperosmotic solutions if the added solutes are membrane impermeant [15]. A: induction of epileptiform bursts by hypoosmotic medium (20% H_2O; −35 mOsm). In those slices where spontaneous bursts did not occur, dilution of the fluid reversibly induced synchronous bursts of population spikes. B: block of spontaneous epileptiform bursts with hyperosmotic medium. Addition of 20 mM sucrose (+30 mOsm), an impermeant solute, to the perfusion medium blocked epileptiform bursts. C: lack of effect of a membrane-permeant solute. Addition of glycerol had no effect on spontaneous epileptiform bursts.

hypoxia-induced damage [3, 4, 8, 18, 21, 24]. Finally, numerous clinical syndromes, such as hyponatremia and psychogenic polydipsia, are associated with reduced plasma osmolality and seizures; increases in plasma osmolality reliably block these seizures [1]. Our data provide a possible explanation for how non-synaptic mechanisms could contribute significantly to the seizures that occur clinically when plasma osmolality is lowered.

This research was supported by a grant from the United States Air Force Office of Scientific Research to F.E.D. and by a National Institute of Health postdoctoral fellowship to J.G.T. We are grateful to Drs. C. Houser, C. Wasterlain, and G. Zampighi for their constructive criticisms. We thank C. Kinney for secretarial assistance.

1 Andrew, R.D., Seizure and acute osmotic change: clinical and neurophysiological aspects, J. Neurol. Sci., in press.
2 Andrew, R.D., Fagan, M., Ballyk, B.A. and Rosen, A.S., Seizure susceptibility and the osmotic state, Brain Res., 498 (1989) 175–180.
3 Auer, R.N. and Siesjö, B.K., Biological differences between ischemia, hypoglycemia, and epilepsy, Ann. Neurol., 24 (1988) 699–707.
4 Balestrino, M., Aitken, P.G. and Somjen, G.G., Spreading depression-like hypoxic depolarization in CA1 and fascia dentata of hippocampal slices: relationship to selective vulnerability, Brain Res., 497 (1989) 102–107.
5 Baran, H., Lassmann, H., Sperk, G., Seitelberger, F. and Hornykiewicz, O., Effect of mannitol treatment on brain neurotransmitter markers in kainic acid-induced epilepsy, Neuroscience, 47 (1986) 679–684.
6 Baxter, C.F., Wasterlain, C.G., Hallden, K.L. and Pruess, S.F., Effect of altered blood plasma osmolalities on regional brain amino acid concentrations and focal seizure susceptibility in the rat, J. Neurochem., 47 (1986) 617–624.
7 Blake, J.F., Brown, M.W. and Collingridge, G.L., CNQX blocks acidic amino acid induced depolarizations and synaptic components mediated by non-NMDA receptors in rat hippocampal slices, Neurosci. Lett., 89 (1988) 182–186.
8 Dam, A.G., Epilepsy and neuronal loss in the hippocampus, Epilepsia, 21 (1980) 617–629.
9 Dichter, M.A. and Ayala, G.F., Cellular mechanisms of epilepsy: a status report, Science, 237 (1987) 157–164.
10 Dietzel, I., Heinemann, U., Hofmeier, G. and Lux, H.D., Stimulus-induced changes in extracellular Na^+ and Cl^- concentration in relation to changes in the size of the extracellular space, Exp. Brain Res., 46 (1982) 73–84.
11 Dietzel, I., Heinemann, U. and Lux, H.D., Relations between slow extracellular potential changes, glial potassium buffering, and electrolyte and cellular volume changes during neuronal hyperactivity in cat brain, Glia, 2 (1989) 25–44.
12 Dudek, F.E., Snow, R.E. and Taylor, C.P., Role of electrical interactions in synchronization of epileptiform bursts, Adv. Neurol., 44 (1986) 593–617.
13 Frankenhaeuser, B. and Hodgkin, A.L., The action of calcium on the electrical properties of squid axons, J. Physiol., 137 (1957) 218–244.
14 Herreras, O., Menendez, N., Herranz, A.S., Solis, J.M. and Martin del Rio, R., Synaptic transmission at the Schaffer-CA1 synapse is blocked by 6,7-dinitro-quinoxaline-2,3-dione. An in vivo brain dialysis study in the rat, Neurosci. Lett., 99 (1989) 119–124.
15 Hoffman, E.K. and Simmonsen, L.O., Membrane mechanisms in volume and pH regulation in vertebrate cells, Physiol. Rev., 69 (1989) 315–382.
16 Honore, T., Davies, S.N., Drejer, J., Fletcher, E.J., Jacobsen, P., Lodge, D. and Nielsen, F.E., Quinoxalinediones: potent competitive non-NMDA glutamate receptor antagonists, Science, 241 (1988) 701–703.
17 Jefferys, J.G.R. and Haas, H.L., Synchronized bursting of CA1 hippocampal pyramidal cells in the absence of synaptic transmission, Nature, 300 (1982) 448–450.
18 Kawasaki, K., Traynelis, S.F. and Dingledine, R., Different responses of CA1 and CA3 regions to hypoxia in rat hippocampal slice, J. Neurophysiol., 63 (1990) 385–394.
19 Konnerth, A. and Heinemann, U., Presynaptic involvement in frequency facilitation in the hippocampal slice, Neurosci. Lett., 42 (1983) 255–260.
20 Konnerth, A., Heinemann, U. and Yaari, Y., Slow transmission of neural activity in hippocampal area CA1 in absence of active chemical synapses, Nature, 307 (1983) 69–71.
21 McBain, C.J., Traynelis, S.F. and Dingledine, R., Regional variation of extracellular space in the hippocampus, Science, 249 (1990) 674–677.
22 Neuman, R.S., Ben-Ari, Y. and Cherubini, E., Antagonism of spontaneous and evoked bursts by 6-cyano-7-nitroquinoxaline-2,3-dione (CNQX) in the CA3 region of the in vitro hippocampus, Brain Res., 474 (1988) 201–203.
23 Neuman, R.S., Ben-Ari, Y., Gho, M. and Cherubini, E., Blockade of excitatory synaptic transmission by 6-cyano-7-nitroquinoxaline-2,3-dione (CNQX) in the hippocampus in vitro, Neurosci. Lett. 92 (1988) 64–68.
24 Sagar, H.J. and Oxbury, J.M. Hippocampal neuron loss in temporal lobe epilepsy: correlation with early childhood convulsions, Ann. Neurol., 22 (1987) 334–340.
25 Taylor, C.P. and Dudek, F.E., Synchronous neural afterdischarges in rat hippocampal slices without active chemical synapses, Science, 218 (1982) 810–812.
26 Traub, R.D., Dudek, F.E., Taylor, C.P. and Knowles, W.D., Simulation of hippocampal afterdischarges synchronized by electrical interactions, Neuroscience, 14 (1985) 1033–1038.
27 Traynelis, S.F. and Dingledine, R., Role of extracellular space in hyperosmotic suppression of potassium-induced electrographic seizures, J. Neurophysiol., 61 (1989) 927–938.
28 Yaari, Y. and Jensen, M.S., Nonsynaptic mechanisms and interictal-ictal transitions in the mammalian hippocampus. In M. Dichter (Ed.), Mechanisms of Epileptogenesis, Plenum, New York, 1988, pp. 183–197.

Glutamate, the Dominant Excitatory Transmitter in Neuroendocrine Regulation

ANTHONY N. VAN DEN POL,* JEAN-PIERRE WUARIN, F. EDWARD DUDEK

Glutamate has been found to play an unexpectedly important role in neuroendocrine regulation in the hypothalamus, as revealed in converging experiments with ultrastructural immunocytochemistry, optical physiology with a calcium-sensitive dye, and intracellular electrical recording. There were large amounts of glutamate in boutons making synaptic contact with neuroendocrine neurons in the arcuate, paraventricular, and supraoptic nuclei. Almost all medial hypothalamic neurons responded to glutamate and to the glutamate agonists quisqualate and kainate with a consistent increase in intracellular calcium. In all magnocellular and parvocellular neurons of the paraventricular and arcuate nuclei tested, the non-NMDA (non–*N*-methyl-D-aspartate) glutamate antagonist CNQX (cyano-2,3-dihydroxy-7-nitroquinoxaline) reduced electrically stimulated and spontaneous excitatory postsynaptic potentials, suggesting that the endogenous neurotransmitter is an excitatory amino acid acting primarily on non-NMDA receptors. These results indicate that glutamate plays a major, widespread role in the control of neuroendocrine neurons.

THE NEUROENDOCRINE HYPOTHALAMUS has been a fertile ground for the discovery of neuroactive substances. In the search for new transmitters one important classical neurotransmitter, glutamate, has practically been ignored with respect to its contribution to neuroendocrine regulation (*1, 2*). However, our data suggest that glutamate accounts for the majority of excitatory synapses in the neuroendocrine hypothalamus. We tested whether glutamate occurs in high concentrations in a subset of presynaptic axons; whether hypothalamic neurons respond to glutamate, to what extent, and through which receptor; and whether the postsynaptic response to the naturally released neurotransmitter can be blocked by glutamate antagonists.

Characterized rabbit antisera raised against glutamate (*3*) were used to label hypothalamic ultrathin sections with postembedding silver-intensified gold particles (*4, 5*). Immunoreactive axons were found in synaptic contact with dendrites and cell bodies in all regions of the neuroendocrine mediobasal hypothalamus examined, including the magnocellular and parvocellular paraventricular (Fig. 1), supraoptic, and arcuate nuclei. These regions represent the final common neuronal pathway regulating endocrine secretions. Serial ultrathin sections revealed that all cells (n = 14) studied in the paraventricular and arcuate nuclei received synaptic contact from axons exhibiting glutamate immunoreactivity (*6*). The postsynaptic neurons (n = 9) in the paraventricular nucleus were large (28 to 35 μm in diameter) magnocellular neurons containing large (200 nm) dense-core vesicles immunoreactive for oxytocin and vasopressin-neurophysin. Glutamate-immunoreactive boutons contained small, clear, round vesicles apposed to an asymmetrical synaptic specialization; dense-core vesicles, suggestive of peptide colocalization, were also found in the presynaptic boutons. The ratio of immunogold particles over axons to their postsynaptic dendrites was 5:1, a ratio similar to that found with immunogold staining in glutamatergic axons in other brain regions (*7–9*).

Fig. 1. Electron micrograph of glutamate-immunoreactive presynaptic bouton in the paraventricular nucleus making an asymmetrical synapse (black arrow) with a dendrite (DEN). The axon is filled with small round vesicles and with a few dense-core vesicles (open arrow). Two other axons (AX) also contact the same central dendrite in the paraventricular nucleus. The black dots are silver-intensified gold particles, which identify the three axons as containing high levels of glutamate. Width of micrograph, 0.95 μm.

Neurons responding to glutamate show an increase in intracellular Ca^{2+} (*10*), which mediates a wide variety of biochemical events in the cell. To study the Ca^{2+} response of neurons from the medial hypothalamus, we grew cells in monolayer primary tissue culture on glass cover slips (*11*); after the development of synaptic contacts, the response of neurons to glutamate was studied with the Ca^{2+} indicator dye fluo-3 by digital video microscopy (*12*). We examined the response of neurons to glutamate and related substances in a microscope perfusion chamber where glutamate and its agonists could be serially added to the perfusion medium. Nearly all neurons (93.1% of 522 cells) showed an increase in Ca^{2+} in response to glutamate (1 to 100 μM) (Fig. 2). Similarly, the glutamate agonists kainate and quisqualate induced a Ca^{2+} rise in almost all the cells (kainate: 90.1% of 121 cells; quisqualate: 92.8% of 168 cells). Cells that responded to one agonist generally responded to all three. A minor response to the glutamate agonist *N*-methyl-D-aspartate (NMDA) was seen in some cells.

To investigate the nature of the endogenous neurotransmitter, we used intracellular recording from coronal hypothalamic slices (500 μm) and tested whether the non-NMDA glutamate antagonist cyano-2,3-dihydroxy-7-nitroquinoxaline (CNQX) blocked the excitatory postsynaptic potentials (EPSPs) in the arcuate and paraventricular nuclei. If glutamate is an important endogenous transmitter in neuroendocrine circuits, EPSPs should be blocked by agents that block activation of the glutamate receptor. Bath application of 3 μM CNQX reduced, and 30 μM CNQX blocked almost completely, spontaneous EPSPs. Electrical stimulation lateral to the paraventricular nucleus or dorsal to the arcuate nucleus elicited EPSPs in the respective areas. Although many axons and pathways were electrically stimulated in these experiments, CNQX blocked EPSPs in a dose-dependent manner (Fig. 3) (*13*). This effect was observed in every cell of the 26 tested (20 in the paraventricular nucleus; 6 in the arcuate nucleus); at higher doses (30 μM) the EPSPs were virtually eliminated. Of the 20 cells in the paraventricular nucleus, 13 were determined to be neurosecretory on the basis of their electrophysiological properties (*14*). Kynurenic acid, a broad-spectrum glutamate antagonist, also reduced the amplitude of the EPSPs in the paraventricular nucleus, as had been previously reported in

A. N. van den Pol, Section of Neurosurgery, Yale University School of Medicine, New Haven, CT 06510. J.-P. Wuarin and F. E. Dudek, Mental Retardation Research Center, UCLA School of Medicine, Los Angeles, CA 90024.

*To whom correspondence should be addressed.

the supraoptic nucleus (*15*). Together, these data support the suggestion that most of the fast excitatory input to the arcuate and paraventricular nuclei is mediated by glutamate.

The widespread response to glutamate in almost all hypothalamic neurons examined with both optical and intracellular physiological techniques is in seeming contrast to the apparent low level of binding found in autoradiographic analysis of hypothalamic receptors (*16*). Similarly, a number of reports have shown that hypothalamic neurons appear relatively resistant to excitatory amino acid toxicity (*17*). We suggest that these results are caused not by the absence of glutamate receptors in the hypothalamus but rather by the lower number of receptors or to differences in second messenger systems. Although the hypothalamus has a lower density of glutamate-binding sites than cortical areas such as the hippocampus, neurotransmission mediated by glutamate may be equally important in the hypothalamus because neurons there tend to be less extensively branched (*18*), with smaller surface areas and higher input resistances; therefore, equal single-channel currents through a glutamate-activated channel would have a proportionately larger effect in a hypothalamic neuron than in a cortical one.

Although glutamate has been recognized as a major neurotransmitter in other brain systems such as the neocortex and hippocampus (*8, 9, 19*), investigations of the neural control of the endocrine system have focused on other possible neuroactive substances. On the basis of data from ultrastructural immunocytochemistry, intracellular electrophysiology, and optical digital physiology, we suggest that the major excitatory neurotransmitter regulating neuroendocrine neurons is glutamate. Our data argue that, not only does glutamate play an important role in neuroendocrine regulation, but also that it is probably the major excitatory neurotransmitter inducing release of neuroendocrine hormones from axons terminating in both the median eminence and the posterior pituitary. Combining our results on glutamate with work on the inhibitory transmitter γ-aminobutyrate acid (GABA) (*4, 20, 21*), we suggest that amino acid neurotransmitters account for the majority of all presynaptic axons involved in neuroendocrine regulation, greatly outnumbering amines, peptides, or other neuroactive substances. Since peptide colocalization may be found in most if not all cells with amino acid transmitters (*22*), this conclusion would suggest that glutamate and GABA would be responsible for the majority of fast excitatory and inhibitory synaptic potentials, while peptides and other neuroactive substances in the neuroendocrine hypothalamus may be coreleased. These other neurotransmitters could work synergistically and function at longer intervals, perhaps with longer lasting effects. Our data support a general hypothesis that glutamate is the major fast excitatory neurotransmitter that controls not only the neuroendocrine system but also other hypothalamic regions as well.

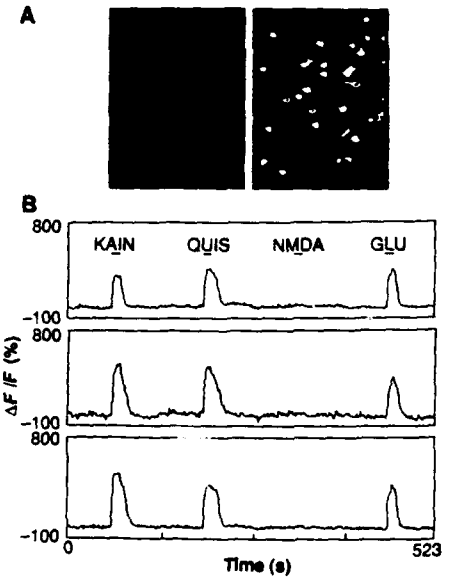

Fig. 2. Intracellular Ca^{2+} responses in cells from the neuroendocrine region of the mediobasal hypothalamus. The fluorescent Ca^{2+} indicator dye fluo-3 was used to study Ca^{2+} responses to the perfusion of glutamate and agonists in Hepes buffer (*12*). (**A**) Baseline fluorescence was subtracted from the video frame (*12*) before glutamate addition (left) and at the time of glutamate response (right). (**B**) Three cells responded to 10-s applications (short horizontal bars) of 10 μM kainate (KAIN), quisqualate (QUIS), and glutamate (GLU), but not to NMDA. All neurons (12 of 12) studied on this cover slip responded to glutamate, kainate, and quisqualate ($\Delta F/F$ range: 180 to 725%). Data are expressed as the percentage change in fluorescence over the baseline control fluorescence, with the baseline subsequently standardized as 0 for each neuron. At 100 μM, some cells responded to NMDA; this may in part be due to NMDA receptors or to binding of NMDA to a non-NMDA receptor. At 100 μM NMDA, hippocampal control neurons routinely responded to NMDA. Tetrodotoxin (1 μM) was used to block release of endogenous transmitter to ensure that only direct responses to glutamate agonists were detected. The data are presented as one averaged video frame per second. To avoid phototoxicity, a computer-controlled shutter blocked the light after each 350-ms recording. Sixty seconds after agonist application (vertical lines at bottom), cells were allowed to rest for 120 s in the dark with no recordings. Subsequent recording showed that the cells responded to 1 and 3 μM glutamate, and to an increase in extracellular K^+ (56 mM).

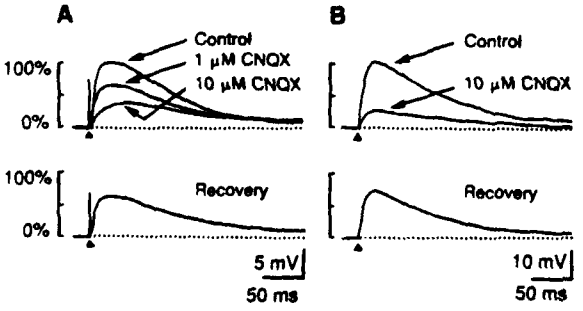

Fig. 3. Effect of the non-NMDA receptor antagonist CNQX on EPSPs in the (**A**) paraventricular nucleus (PVN) and (**B**) arcuate nucleus (ARC) in hypothalamic slices. Slices were cut with a Vibroslicer and transferred to a recording chamber where they were kept at 32°C, oxygenated with a mixture of 95% O_2 and 5% CO_2, and perfused with a standard artificial cerebrospinal fluid. Signals were amplified with an Axoclamp 2A and stored on videotape for subsequent analysis. The antagonists, bath-applied at 1 μM, decreased the EPSP amplitude by about 40% in PVN. At 10 μM, the EPSP amplitude was decreased by approximately 60% in PVN and 75% in ARC. Both cells were hyperpolarized to prevent action potentials. After more than 1 hour, recovery was obtained with 1 μM CNQX. Although nearly complete recovery could be obtained with low doses of CNQX (1 to 3 μM), total recovery from higher doses (10 to 30 μM) was never observed, even after washout periods of more than 90 min. The long-lasting effects of CNQX were probably due to its high binding affinity (*23*). Nonetheless, little or no change in resting potential or input resistance occurred during application of CNQX, even at the highest doses. To avoid the contamination of EPSP by a potential reversed inhibitory postsynaptic potential, the experiments were done in 50 μM picrotoxin. Each trace is an average of 20 responses. Stimulus intensity was 500 μA for PVN and 100 μA for ARC. Data from the two cells shown here are representative of data for 20 neurons from PVN and 6 from ARC examined in this study (▲, electrical stimulation).

REFERENCES AND NOTES

1. D. A. Poulain and J. B. Wakerly, *Neuroscience* **4**, 773 (1982); J. A. Silverman and G. E. Pickard, in *Chemical Neuroanatomy*, P. C. Emson, Ed. (Raven, New York, 1983), pp. 295–336; L. W. Swanson and P. E. Sawchenko, *Annu. Rev. Neurosci.* **6**, 269 (1983); L. W. Swanson, in *Handbook of Chemical Neuroanatomy: Integrated Systems of the CNS*, A. Bjorklund, T. Hokfelt, L. W. Swanson, Eds. (Elsevier, Amsterdam, 1987), pp. 1–124; C. D. Sladek and W. E. Armstrong, in *Vasopressin*, D. M. Gash and G. J. Boer, Eds. (Plenum, New York, 1987), p. 275; W. F. Ganong and L. Martini, *Front. Neuroendocrinol.* **11**, 1 (1990); T. Hokfelt *et al.*, *Acta Physiol. Scand. Suppl.* **583**, 105 (1989)
2. L. P. Renaud *et al.*, in *The Electrophysiology of the Secretory Cell*, A. M. Poisner and J. Trifaro, Eds. (Elsevier, Amsterdam, 1985), pp. 165–194.
3. Rabbit antisera against glutamate conjugated by glutaraldehyde to keyhole limpet hemocyanin were tested for specificity by enzyme-linked immunosorbent assay (ELISA) and immunodot blot. The antibody did not recognize any of 20 amino acids tested for cross-reactivity including aspartate, GABA, glycine, taurine, and glutamine, or the dipeptide *N*-acetylaspartylglutamate. On Western blots, the antibody did not bind to polyglutamate or to native

rat brain protein but did bind to glutamate cross-linked by glutaraldehyde to rat brain proteins. Solid-phase absorption of the antibody to glutamate conjugated to bovine serum albumin eliminated positive staining.
4. A. N. van den Pol, *Science* **228**, 332 (1985).
5. ———, *J. Microsc. (Oxford)* **155**, 27 (1989).
6. The identity of 18 neurons from the arcuate and paraventricular nuclei as neuroendocrine was confirmed in another experiment in which cells projecting to the vascular system were labeled by retrograde axonal transport of intravenous injections of horseradish peroxidase [R. D. Broadwell and M. W. Brightman *J. Comp. Neurol.* **166**, 257 (1976)]. Presynaptic glutamate-immunoreactive boutons were found on each cell (C. Decavel and A. N. van den Pol, *in preparation*).
7. The number of gold particles per bouton varied with the concentrations of antisera. The ratio of labeling of highly immunoreactive to less reactive structures was similar over several antisera concentrations. The presence of high levels of glutamate in presynaptic boutons supports, but does not prove, the possibility that it is released. All neurons probably contain some glutamate. Those cells that use glutamate as a neurotransmitter appear to maintain higher concentrations of glutamate in their axon terminals than other cells do (*8, 9, 19*), as shown ultrastructurally by ratios of immunogold particles over different cells.
8. P. Somogyi, K. Halasy, J. Somogyi, J. Storm-Mathisen, O. P. Ottersen, *Neuroscience* **19**, 1045 (1986).
9. O. P. Ottersen, *J. Chem. Neuroanat.* **2**, 57 (1989).
10. J. A. Connor *et al.*, *Science* **240**, 649 (1988); D. W. Choi, *Neuron* **1**, 623 (1988).
11. Hypothalamic neurons from late embryonic or early postnatal rats were plated on glass cover slips treated with polylysine and collagen [A. N. van den Pol, U. di Porzio, U. Rutishauser, *J. Cell Biol.* **102**, 2281 (1986)]. After 5 to 60 days in vitro, cells were incubated in fluo-3 acetoxymethyl ester (Molecular Probes) for 45 min in Hepes buffer (10 mM Hepes, 25 mM glucose, 137 mM NaCl, 5.3 mM KCl, 3 mM $CaCl_2$, 1 mM $MgCl_2$, 1 μM tetrodotoxin, pH 7.4), and placed in a microscope chamber where glutamate or its agonists could be serially perfused. For experiments involving NMDA, the same buffer without $MgCl_2$ was utilized. To reduce phototoxicity, we used neutral density filters which allowed only 1% of the normal fluorescent light emitted by the mercury arc lamp to reach the cells. Fluo-3 fluorescent cells could barely be detected without digital intensification of the video image.
12. A Zeiss IM35 inverted microscope with a ×20 Olympus ultraviolet objective (numerical aperture = 0.70) was fitted with a computer-controlled shutter to block fluorescent light when a video frame was not being recorded. A Hamamatsu SIT video camera was interfaced with an ITI 151 video processor driven by an IBM AT computer. Processed images were stored on a 2023F Panasonic laser disk recorder. Additional details are found in A. H. Cornell-Bell, S. M. Finkbeiner, M. S. Cooper, S. J. Smith, *Science* **247**, 470 (1990) A Bio-Rad confocal scanning laser microscope was also used to confirm our results.
13. Although our results indicate an important role of kainate and quisqualate receptors in excitatory transmission of hypothalamic neurons, these experiments do not rule out a contribution from the NMDA receptor. Under the appropriate conditions, such as depolarization to about −30 mV, glutamate could induce inward current flow through NMDA receptor–activated channels, and an NMDA component to the decay phase of the EPSP in some paraventricular nucleus neurons could be detected. Nonetheless, our data suggest that NMDA receptors contribute to synaptic transmission less in the hypothalamus than in other brain areas such as the cerebral cortex or hippocampus.
14. Several studies in the supraoptic and paraventricular nuclei have combined intracellular recording and staining with vasopressin and oxytocin-neurophysin immunocytochemistry, antidromic stimulation, Nissl counterstaining, or visual determination of location in slices or sections; the purpose of these multidisciplinary studies has been to identify the electrophysiological properties of the major groups of neurons and neuroendocrine cells in these nuclei [R. D. Andrew, B. A. MacVicar, F. E. Dudek, G. I. Hatton, *Science* **211**, 1187 (1981); P. Cobbet, K. G. Smithson, G. I. Hatton, *Brain Res.* **362**, 7 (1986); J. G. Tasker and F. E. Dudek, *J. Physiol. (London)*, in press; N. W. Hoffman, J. G. Tasker, F. E. Dudek, *Soc. Neurosci. Abstr.* **15**, 1088 (1989) (*2*). The 13 paraventricular cells had high input resistance (200 to 500 megohms), a regular or slowly adapting discharge of action potentials with no low-threshold potential to a depolarizing current pulse, and linear current-voltage relation to about −100 mV. Identical neurons in the paraventricular nucleus have been injected with Lucifer Yellow or biocytin and shown to be magnocellular (Tasker and Dudek) and neurophysin-positive (Hoffman *et al.*); therefore, this cell type has been identified as a neurosecretory cell. These electrophysiological properties are identical to those recorded in the supraoptic nucleus (*2*), which contains primarily neurosecretory cells. The other seven cells displayed low-threshold calcium spikes and strong time-dependent inward rectification [P. Poulain and B. Carette *Brain Res. Bull.* **19**, 453 (1987); Tasker and Dudek; Hoffman *et al.*] This latter cell type is neurophysin-negative and is probably not neurosecretory. EPSPs in all of these cells were blocked in a dose-dependent manner by CNQX.
15. V. K. Gribkoff and F. E. Dudek, *Brain Res.* **442**, 152 (1988); *J. Neurophysiol.* **63**, 60 (1990). Glutamate immunoreactivity has also been described in the supraoptic nuclei [R. B. Meeker, D. J. Swanson, J. N. Hayward, *Neuroscience* **33**, 157 (1989)].
16. D. T. Monaghan and C. W. Cotman, *Brain Res.* **252**, 91 (1982); T. C. Rainbow, C. M. Wieczorek, S. Halpain, *ibid.* **309**, 173 (1984); C. W. Cotman *et al.*, *Trends Neurosci.* **10**, 273 (1987).
17. J. P. Herman and S. J. Wiegand, *Brain Res* **383**, 367 (1986); G. M. Peterson and R. Y. Moore, *ibid.* **202**, 165 (1980).
18. A. N. van den Pol, *J. Comp. Neurol.* **204**, 65 (1982); *ibid.* **206**, 317 (1982).
19. J. Storm-Mathisen *et al.*, *Nature* **301**, 517 (1983).
20. M. L. Tappaz, *Psychoneuroendocrinology* **9**, 85 (1984); A. N. van den Pol, *J. Neurosci.* **5** 2940 (1985); J. C. R. Randle and L. P. Renaud, *J Physiol. (London)* **387**, 629 (1986).
21. C. Decavel and A. N. van den Pol, *Soc. Neurosci. Abstr.* **15**, 1086 (1989).
22. P. Somogyi *et al.*, *J. Neurosci.* **4**, 2590 (1984); B. Meister, T. Hokfelt, M. Geffard, W. Oertel, *Neuroendocrinology* **48**, 516 (1988); B. J. Everitt, T. Hokfelt, J. Y. Wu, M. Goldstein, *ibid.* **39**, 189 (1984). As with the excitatory transmitter glutamate, with serial ultrathin sections examined in the electron microscope we found dense-core vesicles in all boutons immunoreactive for the inhibitory transmitter GABA [C. Decavel and A. N. van den Pol, *J. Comp. Neurol.*, in press; (*21*)]. Dense-core vesicles are generally considered to contain neuroactive peptides or amines, suggesting extensive colocalization of amino acid transmitters with other neuroactive substances.
23. T. Honore, J. Drejer, E. O. Nielsen, M. Nielsen, *Biochem. Pharmacol.* **38**, 3207 (1989).
24. We thank W. Armstrong, A. Cornell-Bell, C. Decavel, S. Finkbeiner, N. Hoffman, S. Smith, and J. Tasker for helpful suggestions. Supported by NIH grants NS16296, NS10174, and DA05711 and the Air Force Office of Scientific Research.

5 June 1990; accepted 31 October 1990

A Borna Virus cDNA Encoding a Protein Recognized by Antibodies in Humans with Behavioral Diseases

SUSAN VANDEWOUDE, JUERGEN A. RICHT, MARY CHRISTINE ZINK, RUDOLF ROTT, OPENDRA NARAYAN, JANICE E. CLEMENTS

Borna disease virus (BDV) causes a rare neurological disease in horses and sheep. The virus has not been classified because neither an infectious particle nor a specific nucleic acid had been identified. To identify the genome of BDV, a subtractive complementary DNA expression library was constructed with polyadenylate-selected RNA from a BDV-infected MDCK cell line. A clone (B8) was isolated that specifically hybridized to RNA isolated from BDV-infected brain tissue and BDV-infected cell lines. This clone hybridized to four BDV-specific positive strand RNAs (10.5, 3.6, 2.1, and 0.85 kilobases) and one negative strand RNA (10.5 kilobases) in BDV-infected rat brain. Nucleotide sequence analysis of the clone suggested that it represented a full-length messenger RNA which contained several open reading frames. In vitro transcription and translation of the clone resulted in the synthesis of the 14- and 24-kilodalton BDV-specific proteins. The 24-kilodalton protein, when translated in vitro from the clone, was recognized by antibodies in the sera of patients (three of seven) with behavioral disorders. This BDV-specific clone will provide the means to isolate the other BDV-specific nucleic acids and to identify the virus responsible for Borna disease. In addition, the significance of BDV or a BDV-related virus as a human pathogen can now be more directly examined.

BORNA DISEASE IS AN INFECTIOUS neurological disease that occurs sporadically in horses and sheep in Central Europe (*1*). Brain homogenates from infected animals can be used to infect a large number of animal species, from rodents to nonhuman primates (*2–4*). Studies in rats have shown that the agent is highly neurovirulent and invades the brain from peripheral sites by axonal transport (*2*). It replicates in specific groups of neurons in the cerebral cortex and causes biphasic behavioral disease; the short-term effects of Borna disease include aggression and hyperactivity and the long-term effects include apathy and eating disorders (*3*). In tree shrews (*Tupaia*

Journal of Physiology (1991), **434**, pp. 271–293
With 13 figures
Printed in Great Britain

ELECTROPHYSIOLOGICAL PROPERTIES OF NEURONES IN THE REGION OF THE PARAVENTRICULAR NUCLEUS IN SLICES OF RAT HYPOTHALAMUS

BY JEFFREY G. TASKER AND F. EDWARD DUDEK

From the Mental Retardation Research Center and Brain Research Institute, University of California Los Angeles, Center for the Health Sciences, Los Angeles, CA 90024, USA

(*Received 22 February 1990*)

SUMMARY

1. Neurones in the region of the hypothalamic paraventricular nucleus (PVN) of the rat were studied with intracellular recording in the coronal slice preparation. Three types of hypothalamic neurones were distinguished according to their membrane properties and anatomical positions. Lucifer Yellow or ethidium bromide was injected intracellularly to determine the morphology of some recorded cells.

2. The most distinctive electrophysiological characteristic was the low-threshold depolarizing potentials which were totally absent in type I neurones, present but variable in type II neurones and very conspicuous in type III neurones. Type II neurones generally showed relatively small low-threshold depolarizations ($26{\cdot}5 \pm 2{\cdot}2$ mV) which generated at most one to two action potentials. Type III neurones, on the other hand, generated large low-threshold potentials ($40{\cdot}3 \pm 2{\cdot}8$ mV) which gave rise to bursts of three to six fast action potentials. Deinactivation of the low-threshold conductance in both type II and type III neurones was voltage- and time-dependent. Low-threshold potentials persisted in TTX (1–3 μM) but were blocked by solutions containing low Ca^{2+} (0·2 mM) and Cd^{2+} (0·5 mM), suggesting they were Ca^{2+}-dependent.

3. Type I neurones had a significantly shorter membrane time constant ($14{\cdot}5 \pm 1{\cdot}7$ ms) than those of type II ($21{\cdot}6 \pm 1{\cdot}7$ ms) and type III neurones ($33{\cdot}8 \pm 4{\cdot}4$ ms). Input resistance and resting membrane potential did not differ significantly among the cell groups.

4. Current–voltage (I–V) relations were significantly different among the three cell types. Type I neurones had linear I–V relations to -120 mV, while type III neurones all showed marked anomalous rectification. I–V relations among type II neurones were more heterogeneous, although most (75%) had linear I–V curves to about -90 to -100 mV, inward rectification appearing at more negative potentials.

5. Type I neurones generated fast action potentials of relatively large amplitude ($64{\cdot}2 \pm 1{\cdot}1$ mV, threshold to peak) and long duration ($1{\cdot}1 \pm 0{\cdot}1$ ms, measured at half-amplitude); the longer duration was due to a shoulder on the falling phase of the spike. Type II neurones had large spikes ($66{\cdot}5 \pm 1{\cdot}6$ mV) of shorter duration

(0·9 ± 0·1 ms) with no shoulder. Type III neurones had relatively small spikes (56·1 ± 2·2 mV) of short duration (0·8 ± 0·1 ms) with no shoulder.

6. The three cell populations showed different patterns of repetitive firing in response to depolarizing current pulses. Type I neurones often generated spike trains with a delayed onset and little spike-frequency adaptation. Type II neurones fired repetitive spikes which showed more marked adaptation and no delayed onset. Type III neurones generated repetitive fast spikes when activated from depolarized membrane potentials, but developed repetitive bursts of spikes when activated from hyperpolarized potentials. Type III neurones sometimes showed prolonged after-hyperpolarizations (1–4 s) following bursts.

7. Some cells in all three populations displayed repetitive bursting characteristics, although patterns of bursting differed between cell types. Repetitive trains of action potentials separated by periods of silence (i.e. phasic bursting) characterized bursting in type I neurones. Bursting in type II neurones varied, consisting of either single, isolated trains of action potentials in a few cells (7%), or anodal-break membrane oscillations, supporting one to two action potentials, in others (18%). Recurrent low-threshold potentials generated repetitive bursts in 37% of type III neurones.

8. Electrical stimulation near the fornix evoked excitatory and/or inhibitory postsynaptic potentials (EPSPs and IPSPs) in all three cell types. Type I neurones often showed multiple EPSPs. Type II neurones usually generated IPSPs or an EPSP-IPSP sequence. EPSPs and synaptically activated low-threshold potentials with bursts of spikes were seen in type III neurones.

9. Intracellular dye injection revealed different morphologies in the three cell types. Type I neurones had relatively large soma diameters (20–30 μm) and two to three sparsely branched primary dendrites that were oriented bidirectionally. Type II neurones were smaller (10–25 μm) and more highly branched than type I neurones, although they also usually had a bidirectional orientation. Type III neurones were small (11–25 μm) and had radially oriented, multipolar dendritic arbors.

10. Based on electrophysiological criteria, three distinct hypothalamic cell types could be identified in the region of the PVN. Type I neurones were located within the PVN and showed electrical properties similar to neurones of the supraoptic nucleus: they were probably PVN magnocellular neurones. Type II neurones were also located inside the PVN and showed heterogeneous electrophysiological properties, distinct from those of type I neurones: they were probably PVN parvocellular neurones. Type III neurones were located dorsal to the PVN and showed distinctive bursting characteristics.

INTRODUCTION

Two important neurosecretory centres of the hypothalamus are the supraoptic and paraventricular nuclei (SON and PVN). On the basis of immunohistochemical studies, it is generally thought that the SON is comprised exclusively of magnocellular neurones which contain the neurohypophyseal hormones oxytocin and vasopressin and project to the neurohypophysis (Swaab, Nijveldt & Pool, 1975; Vandesande & Dierickx, 1975). The PVN, on the other hand, is more complex in its cytoarchitectural organization, its chemical makeup, and its afferent and efferent

connections. It consists mainly of two types of neurones: (1) oxytocinergic and vasopressinergic magnocellular neurones, which are located primarily in ventral and lateral subdivisions, and (2) neurosecretory and preautonomic parvocellular neurones, situated generally in the dorsal and medial aspects of the nucleus (Armstrong, Warach, Hatton & McNeil, 1980; Swanson & Kuypers, 1980). The PVN magnocellular neurones, together with those of the SON, project to the neurohypophysis. Neurosecretory parvocellular neurones project to the median eminence where they secrete hypophysiotrophic hormones into the portal circulation. Preautonomic parvocellular neurones project to autonomic centres in the brain stem and spinal cord (Sawchenko & Swanson, 1982).

Magnocellular neurones are among the best-studied neurosecretory neurones in the mammalian brain. The sensory input, pattern of neuronal activation and hormonal output have been well characterized using extracellular electrophysiological and chemical assay techniques (see Poulain & Wakerley, 1982, for review). It is known, for example, that oxytocinergic magnocellular neurones respond to suckling with a synchronous, high-frequency burst of action potentials and a bolus release of oxytocin into the general circulation, resulting in milk ejection. Vasopressinergic magnocellular neurones generate asynchronous, phasic bursts of action potentials in response to dehydration and haemorrhage, thus causing increased vasopressin release, antidiuresis and vasoconstriction.

The electrophysiological properties of magnocellular neurones in the SON have been studied extensively with intracellular recording techniques. They have been shown to have linear current–voltage relations (Mason, 1983; Bourque & Renaud, 1985*a*) and to generate fast action potentials which are both Na^+- and Ca^{2+}-dependent (Andrew & Dudek, 1983, 1984*a*; Bourque & Renaud, 1985*a*). The Ca^{2+} component of the action potential causes a shoulder on the falling phase (Mason & Leng, 1984). The intrinsic mechanism in part responsible for the phasic bursting in vasopressinergic magnocellular neurones have also been characterized. Burst initiation is caused by Ca^{2+}-mediated, depolarizing after-potentials which sum to form a plateau potential and cause repetitive spiking (Andrew & Dudek, 1983, 1984*a*; Bourque, 1986). Burst termination involves an after-hyperpolarization (AHP) caused by a Ca^{2+}-activated K^+ conductance (Andrew & Dudek, 1984*b*; Bourque, Randle & Renaud, 1985).

Little is known about the cellular physiology of either magnocellular or parvocellular neurones in the PVN, due largely to the comparative complexity of this nucleus and the difficulty in selectively studying any one population of cells. Intracellular studies have relied on the visual placement of the recording electrode or intracellular dye injection to determine the type of neurone being studied, both of which are associated with potential problems since the cytoarchitectural and morphological distinctions between magnocellular and parvocellular neurones show some overlap (van den Pol, 1982). The few intracellular electrophysiological studies performed in the PVN have concentrated primarily on magnocellular neurones (Dudek, Hatton & MacVicar, 1980; MacVicar, Andrew, Dudek & Hatton, 1982; Hatton, Cobbett & Salm, 1985; Cobbett, Smithson & Hatton, 1986). The comparative electrical properties of parvocellular and magnocellular neurones of the PVN have not been determined.

Recently, another population of electrically and anatomically distinct hypothalamic neurones was described in the guinea-pig (Poulain & Carette, 1987). When activated from hyperpolarized membrane potentials, these neurones generated large, Ca^{2+}-dependent low-threshold potentials and short bursts of action potentials. They were situated lateral and ventrolateral to the PVN (i.e. outside the PVN) and were not neurophysin-immunoreactive, suggesting they were neither magnocellular nor parvocellular, but a third type of hypothalamic neurone.

The present work was undertaken to distinguish the different cell types in the PVN region of the hypothalamus on the basis of their electrophysiological properties. We have identified three electrophysiologically distinct populations of neurones which appear to correspond to magnocellular neurones, parvocellular neurones and non-PVN neurones, respectively. Some of these data have been presented previously in abstract form (Tasker & Dudek, 1987; Hoffman, Tasker & Dudek, 1989).

METHODS

Slice preparation

Adult Sprague–Dawley rats (150–250 g) were decapitated and their brains removed and immersed in cold (1–4 °C), oxygenated artificial cerebrospinal fluid (ACSF, see below) for 1 min. One to two coronal slices (400–500 μm) of the hypothalamus just caudal to the optic chiasm were sectioned on a tissue chopper or with a vibroslicer (Campden Instruments) and placed on filter paper on the ramp of a slice recording chamber. The ACSF contained (in mM): 124 NaCl, 3 KCl, 2·4 $CaCl_2$, 26 $NaHCO_3$, 1·3 $MgSO_4$, 1·4 NaH_2PO_4 and 11 glucose. Heated ACSF (32–34 °C) was pumped into the chamber and drawn up over the slices with threads of gauze. A gas mixture of 95% O_2, 5% CO_2 was humidified and directed over the surface of the slices. Slices were allowed to equilibrate in the recording chamber for approximately 2 h prior to the start of experiments.

Electrophysiological techniques

Recording electrodes were pulled from glass capillaries (1·0 mm o.d., 0·5 mm i.d., American Glass Co.) on a Flaming–Brown puller. They were filled with 4 M-potassium acetate (100–200 MΩ), 3 M-potassium chloride (75–150 MΩ), 5% Lucifer Yellow dissolved in 1 M-lithium acetate (150–250 MΩ) or 1% ethidium bromide in 1 M-potassium acetate (Aghajanian & VanderMaelen, 1982). Cell impalement was achieved by advancing electrodes through the slice in 4 μm steps with a piezoelectric microdrive (Nanostepper) and oscillating the negative capacitance feedback. Electrical signals were recorded through an intracellular amplifier with a bridge circuit (Neurodata Instruments or Axon Instruments) and stored on magnetic tape (Hewlett–Packard) or digitized (Neurocorder, Neurodata Instruments) and stored on videotape. Analog data were subsequently digitized (ISC67AVE system, RC Electronics) and traces were generated on an X–Y plotter or laser printer. Slow events were played out directly on a pen recorder.

Bipolar stimulating electrodes consisted of two tightly wound, insulated platinum–iridium wires (75 μm diameter). Constant-current electrical stimulation was applied near the fornix at a series of intensities to evoke a full range of synaptic responses (5–500 μA, 0·5 ms, 0·3 Hz).

Recordings done with Lucifer Yellow-filled electrodes were not included in the electrophysiological analyses. Ethidium bromide in the recording electrode had no noticeable effect on electrical recordings.

Drug application

In some experiments, tetrodotxin (TTX, 1·5–3 μM) was added to the perfusate to block Na^+-dependent action potentials. To block Ca^{2+}-dependent events, the phosphate-buffered ACSF was replaced with a solution containing (in mM): 125·5 NaCl, 3 KCl, 1·3 $MgCl_2$, 10 N-2-hydroxyethylpiperazine-N'-2-ethanesulphonic acid (HEPES), 11 glucose, 0·2 $CaCl_2$ and 0·25–0·5 $CdCl_2$.

RESULTS

The data presented here were obtained from stable intracellular recordings (duration 15 min–7 h) of sixty-eight neurones in the region of the hypothalamic PVN. Criteria for acceptance of all cells were a resting potential $\geqslant 50$ mV, an input resistance $\geqslant 100$ MΩ and an action potential amplitude $\geqslant 50$ mV (threshold to peak). Recorded neurones were divided into three cell types based on their electrical membrane properties. The main electrophysiological criterion used for classifying the cells was the absence/presence and burst-generating capacity of low-threshold potentials. The anatomical position of the recorded cells with respect to the PVN was also used to distinguish the different cell types. Other electrophysiological properties studied were current–voltage (I–V) relations, membrane time constants, action potential waveforms, repetitive firing properties, after-hyperpolarizations and synaptic inputs. The passive electrical properties of the three cell types are presented in Table 1. No significant differences were seen in the input resistances or resting membrane potentials of the different cell types. Input resistances were calculated in the linear portion of the I–V curve.

TABLE 1. Electrophysiological properties of three cell types

	Type I	Type II	Type III
Resting potential (mV)	64·1 ± 2·9 (11)	58·5 ± 2·0 (12)	66·7 ± 3·1 (9)
Input resistance (MΩ)	216·3 ± 22·3 (12)	241·2 ± 25·7 (13)	212·7 ± 21·6 (13)
Time constant (ms)	14·5 ± 1·7 (16)	21·6 ± 1·7 (19)	33·8 ± 4·4 (11)*
Spike amplitude (mV) (threshold to peak)	64·2 ± 1·1 (13)	66·5 ± 1·6 (13)	56·1 ± 2·2 (14)*
Spike duration (ms) (half-max. amplitude)	1·12 ± 0·08 (13)	0·90 ± 0·03 (13)	0·82 ± 0·05 (14)*

Values are stated as the mean ± standard error of the mean. Values in parentheses represent the numbers of cells included in the means. Statistically significant differences among the three cell types ($P < 0{\cdot}01$, ANOVA) are designated by an asterisk at the end of the row (see text for statistical differences between groups).

Low-threshold potentials

The most distinctive electrophysiological feature was the capacity of 67% of cells recorded in this study to generate low-threshold depolarizing potentials. Low-threshold potentials are generated by the deinactivation, at hyperpolarized membrane potentials, of a voltage-dependent Ca^{2+} conductance which is inactive at resting and depolarized potentials (Llinás & Yarom, 1981; Jahnsen & Llinás, 1984; Minami, Oomura & Sugimori, 1986). All neurones were tested extensively for the presence of low-threshold potentials by progressively hyperpolarizing the cell to different potentials with steady current injection and delivering a large range of depolarizing current pulses. Long hyperpolarizing current pulses (150–300 ms) of different intensities were also delivered at resting potentials as well as at hyperpolarized and depolarized membrane potentials to detect low-threshold potentials as anodal-break responses.

One population of neurones (type I) failed to generate low-threshold potentials

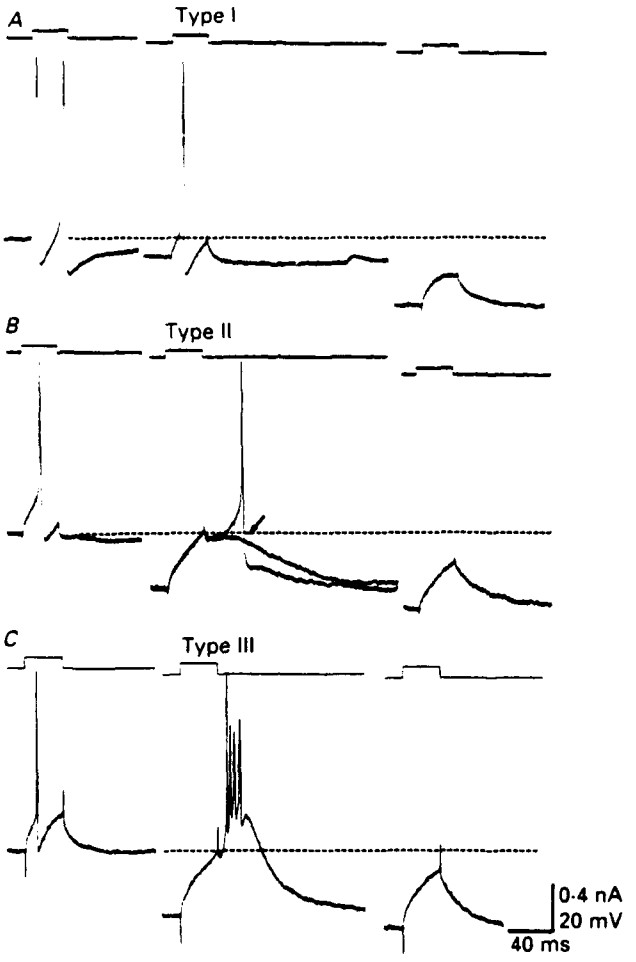

Fig. 1. Generation of low-threshold potentials. *A*, a type I neurone failed to generate a low-threshold potential when depolarized from hyperpolarized membrane potentials. This cell became less excitable with hyperpolarization. *B*, a type II neurone generated a small low-threshold potential (arrow) capable of causing a fast spike (superimposed trace) with depolarization from a hyperpolarized membrane potential. Further hyperpolarization with steady current injection caused the depolarizing current pulse to be subthreshold for both Na^+-spike and low-threshold potential generation. *C*, a type III neurone generated a large low-threshold potential, which outlasted the current pulse and gave rise to a burst of fast spikes, when depolarized from a hyperpolarized membrane potential. This cell became more excitable with hyperpolarization. The same depolarizing current pulse was subthreshold at a more hyperpolarized membrane potential. In this and the following figures, top traces represent current and bottom traces voltage recordings. Dashed lines represent resting membrane potential (-62 mV in *A*, -53 mV in *B* and -68 mV in *C*).

(Fig. 1*A*). These cells became less excitable (i.e. generated fewer fast action potentials in response to a given depolarization) when hyperpolarized with steady negative current injection. A second population of neurones (type II) showed a voltage-dependent, low-threshold depolarization which was relatively small in amplitude ($26{\cdot}5 \pm 2{\cdot}2$ mV, measured baseline to peak at maximum activation). The low-

threshold potentials in type II cells generated a maximum of one to two action potentials (Fig. 2*B*). The size and appearance of the low-threshold potentials in type II neurones varied from one cell to the next, but they never generated bursts of fast action potentials. A third cell group (type III) had large low-threshold potentials

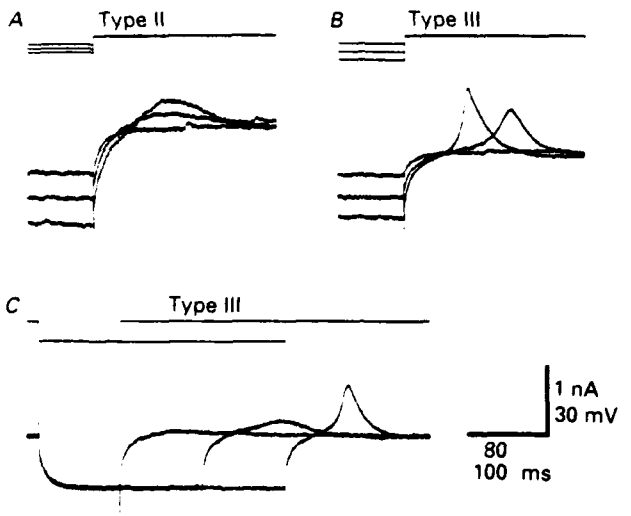

Fig. 2. Voltage and time dependence of low-threshold potentials. These recordings were made in perfusion medium containing 3 μM-TTX to block Na^+-dependent spikes. *A*, a type II neurone generated a small anodal-break low-threshold potential following membrane hyperpolarization with negative current injection. The amplitude of the potential increased in a graded fashion with stronger hyperpolarization. *B*, a similar protocol was applied to a type III neurone, which also showed a graded increase in the amplitude of the low-threshold potential with increased conditioning hyperpolarization. *C*, the same type III neurone as shown in *B* generated low-threshold potentials of increased amplitude as the duration of the conditioning hyperpolarization was increased. Note that the low-threshold potentials were graded, and not all-or-none. Upper time calibration refers to *A* and *B*, lower calibration to *C*.

(40·3 ± 2·8 mV) which generated bursts of three to six fast spikes (Fig. 1*C*). These cells became more excitable at hyperpolarized membrane potentials, presumably because of the deinactivation of a prominent low-threshold conductance.

The low-threshold potentials seen in type III neurones were significantly larger in amplitude than those seen in type II neurones ($P < 0{\cdot}01$, Student's t test). The large low-threshold potentials in type III neurones generated bursts of three or more fast spikes while the smaller ones of type II neurones produced a maximum of one to two spikes. This was the main distinguishing electrophysiological feature of these cells. Deinactivation of the low-threshold conductance depended on the amplitude as well as the duration of the membrane hyperpolarization in both cell types (Fig. 2). Activation of low-threshold potentials occurred in a graded fashion.

Low-threshold potentials in both type II and type III neurones were found to be Ca^{2+}-dependent. Bath application of the Na^+ channel blocker, tetrodotoxin (TTX, 1·5–3 μM), failed to reveal a latent low-threshold potential in type I neurones (Fig. 3*A*, $n = 2$) and had no apparent effect on the low-threshold potentials of type II (Fig. 3*B*, $n = 3$) and type III neurones (Fig. 3*C*, $n = 8$). In contrast, solutions containing

the Ca^{2+} channel antagonist Cd^{2+} (0·25–0·5 mM) and a lowered concentration of Ca^{2+} (0·2 mM) blocked the low-threshold potentials in both type II (Fig. 3*B*, $n = 2$) and type III neurones (Fig. 3*C*, $n = 3$). This block was reversible ($n = 2$).

Membrane time constants

Membrane time constants were taken from the charging portion of the averaged voltage transient ($n = 5$–50) elicited by weak hyperpolarizing current pulses (50–100 pA), which were delivered in the linear range of the current-voltage plot of each cell (Fig. 4). The charging portion of the voltage transient was used because the discharging curve was often associated with voltage-activated conductances in each cell type. Values of $(V_0 - V)/V_0$, taken at 0·3 ms intervals and integrated over ±0·1 ms, were plotted against time on a semilogarithmic scale, where V was the value of the voltage transient and V_0 was the maximum voltage deflection during the pulse. A straight line was fitted to the later, linear portion of the curve and the slope of the line calculated to determine the membrane time constant. Although the neurones of all three cell types were apparently not isopotential (Fig. 4), the first equalizing time constants were not calculated in the present analysis. The mean membrane time constants were significantly different among the three cell types (Table 1, $P < 0·01$, analysis of variance (ANOVA)). Type III neurones had a mean time constant which was significantly longer than that seen in type I ($P < 0·01$) and type II neurones ($P < 0·01$, Newman–Keuls test). The mean time constants of type I and type II neurones were also significantly different from each other ($P < 0·05$, Newman–Keuls test).

Current–voltage relations

Current–voltage (I–V) relations were calculated for thirty neurones ($n = 10$ for each cell type). A rectification ratio was calculated for each cell by dividing the input resistance of the cell measured with a weak current pulse (usually −50 or −100 pA) that hyperpolarized the cell 10 to 20 mV by the input resistance value measured with a strong current pulse that hyperpolarized the cell 50 to 60 mV; a ratio of 1·0 signified perfect linearity and a ratio ≥ 1·0 signified non-linearity. The mean rectification ratios, indicative of the degree of inward (anomalous) rectification, were found to differ significantly among cell groups ($P < 0·001$, ANOVA). All type I neurones showed approximately linear I–V relations between −65 and −120 mV (Fig. 5*A*), with a mean rectification ratio of 1·07 ± 0·03. Some type I neurones (20%) showed time-dependent inward rectification with longer current pulses. Type II neurones were heterogeneous in their I–V relations. Most type II neurones had linear I–V curves to approximately −90 to −100 mV, but showed inward rectification at more hyperpolarized potentials (Fig. 5*B*). Some type II neurones (38%) had linear I–V relations to potentials more negative than −120 mV. The mean rectification ratio of type II neurones was 1·19 ± 0·05. All type III neurones studied had non-linear I–V relations (Fig. 5*C*), showing pronounced inward rectification. They had a mean rectification ratio of 2·04 ± 0·17. The strong inward rectification in type III neurones is illustrated in Fig. 6 by a dramatic decrease in input resistance, as seen by the reduced voltage deflection to a fixed negative current pulse at hyperpolarized membrane potentials.

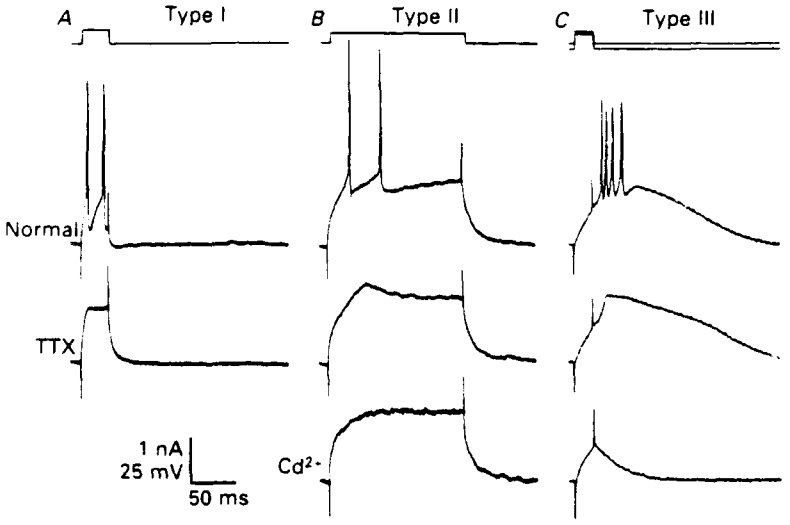

Fig. 3. Ca^{2+} dependence of low-threshold potentials. Bath application of TTX (3 μM) to block Na^+-dependent spikes, while not uncovering any low-threshold potential in a type I neurone (*A*), revealed a low-threshold potential in a type II neurone (*B*) and in a type III neurone (*C*). A bath-applied solution with low [Ca^{2+}] (0·2 mM) and containing cadmium (Cd^{2+}, 500 μM) blocked the low-threshold potentials in both the type II (*B*) and type III (*C*) neurones. The block was reversed in both cells (not shown). The type II and type III neurones were hyperpolarized from resting membrane potential (−63 mV in *A*, −55 mV in *B* and −60 mV in *C*) to reveal low-threshold potentials.

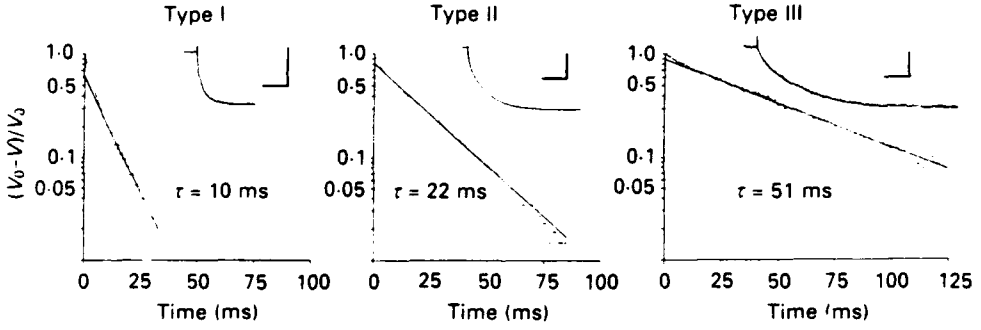

Fig. 4. Membrane time constants (τ). Semilogarithmic plots of $(V_0-V)/V_0$ *versus* time for voltage responses (insets) to weak current pulses in the three cell types (see text). The intensity of the current pulses was 50 pA for the type I and type III cells and 100 pA for the type II neurone. Charging curves represent averages of eight to fifty responses. The membrane time constant was calculated from the slope of a straight line fitted to the terminal part of the curve. Calibrations are 5 mV and 30 ms for the type I and III neurones and 10 mV and 30 ms for the type II neurone.

Fast action potentials

The three cell types generated fast, Na^+-dependent action potentials with different amplitudes and waveforms. Values for spike amplitudes and durations are presented in Table 1. Type I neurones had relatively large action potentials (measured from threshold to peak) that were of long duration (measured at half-maximum amplitude)

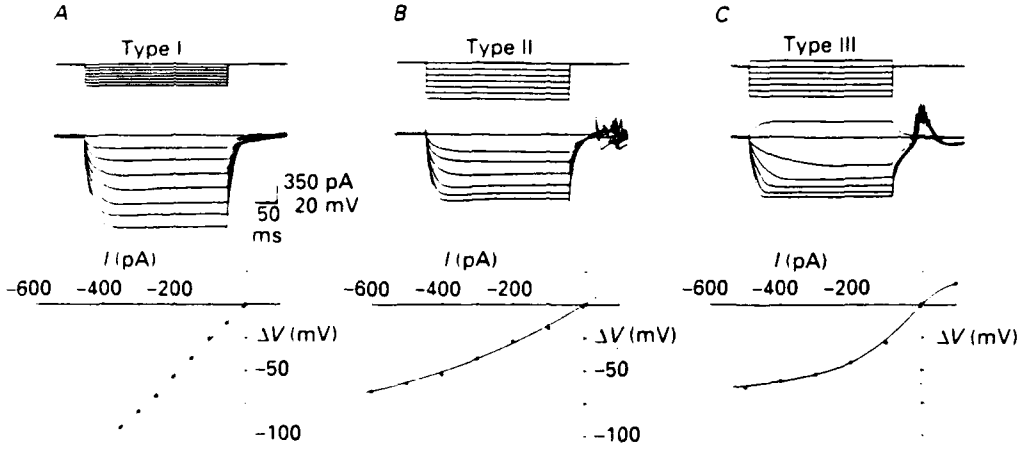

Fig. 5. Current–voltage (I–V) relations. Rectangular current pulses (300 ms) of increasing intensity were injected through the recording electrode and the voltage responses recorded in each cell type. A representative type I neurone had a linear I–V curve and showed no inward rectification to very negative membrane potentials (input resistance (R_N) = 300 MΩ, resting membrane potential (E_M) = −62 mV). A type II neurone had an I–V plot which gradually became non-linear at potentials negative to −90 mV, indicative of the progressive activation of inward rectifying currents (R_N = 170 MΩ, E_M = −52 mV). A type III neurone showed distinct membrane non-linearity and strong inward rectification (R_N = 250 MΩ, E_M = −70 mV). All traces are averages of ten to fifteen sweeps. Anodal-break spikes are truncated due to averaging.

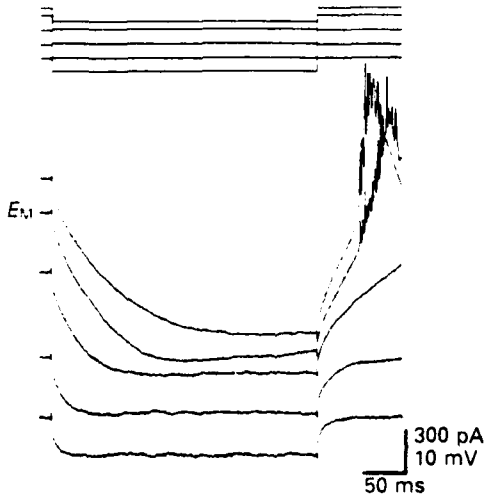

Fig. 6. Strong inward rectification in type III neurones. A 100 pA, 300 ms current pulse was delivered to a type III neurone while the membrane potential was depolarized and hyperpolarized to different levels with continuous current injection. Rectifying currents, which were activated with hyperpolarization from resting potential (E_M = −68 mV), were inactive when the membrane was hyperpolarized from a depolarized membrane potential (top voltage trace). The voltage response diminished substantially at more hyperpolarized potentials (bottom voltage traces). All traces are averages of ten sweeps. Anodal-break spikes are truncated due to averaging.

due to a small shoulder on the falling phase (Fig. 7*A*, arrow). Type II cells had action potentials of large amplitude and short duration that showed no shoulder. Type III neurones generated smaller action potentials of short duration with no shoulder, when recorded at depolarized potentials (i.e. when the low-threshold conductance

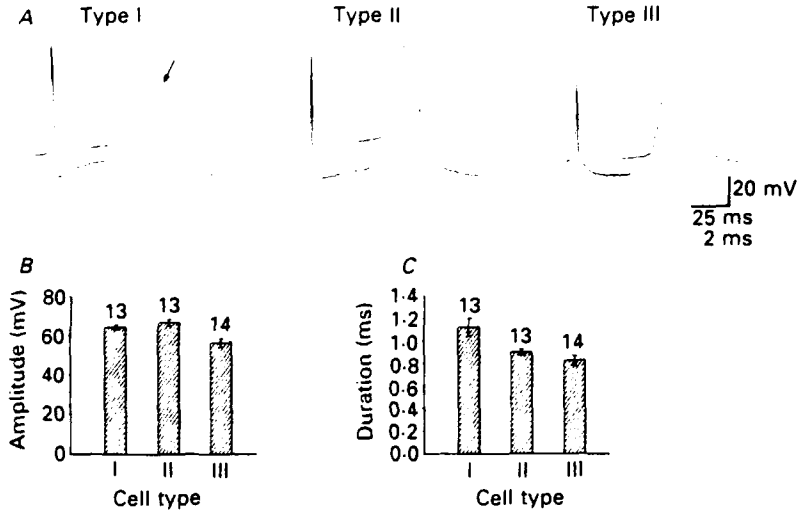

Fig. 7. Characteristics of fast, Na^+-dependent action potentials. *A*, spike waveforms differed among the three cell types. Type I neurones generated large-amplitude spikes which often showed a small shoulder on the falling phase (arrow). Type II neurones generated large spikes with no shoulder. Type III neurones showed relatively small-amplitude spikes with no shoulder (with low-threshold conductances inactivated). Upper time calibration applies to trace on the left and lower calibration to expanded trace on the right of each pair of sweeps. *B*, spikes in type III neurones were significantly smaller in amplitude (threshold to peak) than those of type I and II neurones ($P < 0{\cdot}01$, ANOVA). *C*, the average duration of spikes in type I neurones was significantly longer than those of type II and type III neurones (measured at half-maximum amplitude, $P < 0{\cdot}01$, ANOVA).

was inactive). The mean amplitudes of action potentials of the three cell types differed significantly ($P < 0{\cdot}01$, ANOVA). Action potentials of type I and type II neurones were significantly larger than those of type III neurones ($P < 0{\cdot}01$, Fig. 7*B*), but did not differ significantly from each other (Newman–Keuls test). Mean duration of action potentials also differed significantly among groups ($P < 0{\cdot}01$, ANOVA). The action potentials of type I neurones were significantly longer in duration than those of type II ($P < 0{\cdot}01$) and type III neurones ($P < 0{\cdot}01$, Newman–Keuls test, Fig. 7*C*), due to the shoulder on the repolarizing phase. The difference between type II and type III spike durations was not significant.

Repetitive firing properties

The repetitive firing characteristics were very different for the three cell types. Type I neurones responded to long depolarizing pulses with repetitive spikes which often showed a delayed onset caused by a 'notch' at the beginning of the pulse (Fig. 8*A*). The delay was accentuated at hyperpolarized potentials and was probably due

to a transient outward current (i.e. A-current, Randle, Bourque & Renaud, 1986*a*; Bourque, 1988). These cells showed a delayed return of the membrane potential to baseline following hyperpolarization pulses, also suggestive of an A-current. Type I neurones showed relatively little reduction of spike frequency during the spike train

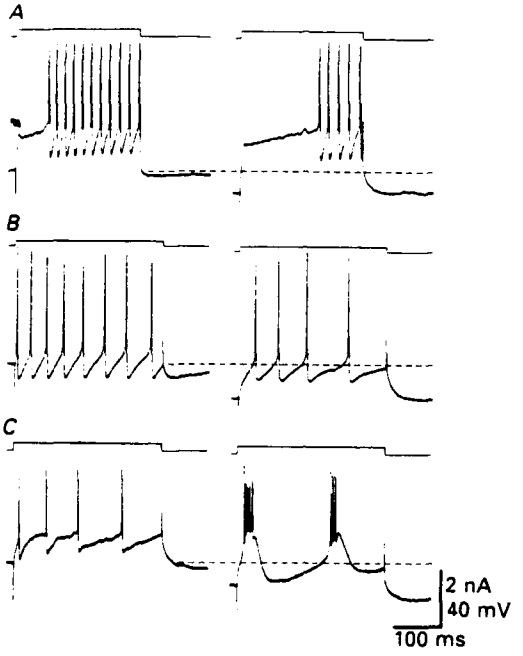

Fig. 8. Repetitive firing characteristics of the three cell types. *A*, in response to depolarizing current injection at resting membrane potential, a type I neurone generated repetitive spikes which showed only weak spike-frequency adaptation and a delayed onset following a 'notch' in the rising phase of the voltage transient (arrow, $E_M = -63$ mV). Hyperpolarization of the cell membrane with continuous negative current injection increased the onset delay (right). *B*, a type II neurone responded to a depolarizing current pulse at resting potential (-52 mV) with repetitive spikes which showed no delay and weak spike-frequency adaptation which increased at hyperpolarized membrane potentials (right). *C*, a type III neurone responded to a depolarizing current pulse with repetitive single spikes when it was held at a depolarized membrane potential with continuous positive current injection (left). The same current pulse caused regenerative low-threshold potentials and bursts of spikes at resting potential (-60 mV, right). The dashed lines represent resting membrane potential in *A* and *B* and the depolarized membrane potential at which the low-threshold Ca^{2+} conductance was inactivated in *C*.

(i.e. weak spike-frequency adaptation). Type II neurones generally displayed repetitive firing with little frequency adaptation at resting potential and increased frequency adaptation at hyperpolarized membrane potentials (Fig. 8*B*). Type III neurones showed repetitive firing when activated at depolarized membrane potentials but fired bursts with strong frequency adaptation when activated from hyperpolarized potentials (Fig. 8*C*).

After-hyperpolarizations

Pronounced after-hyperpolarizations (AHPs) were observed in all three cell types. Quantitative comparison of AHPs was not possible due to the different repetitive

firing properties of each cell type. However, type I and type II neurones showed AHPs which were usually 5–10 mV in amplitude and lasted 100–800 ms following spike trains (40–50 Hz for 300 ms). Type III neurones had post-burst AHPs of variable amplitude and duration. Some type III cells generated long AHPs, lasting

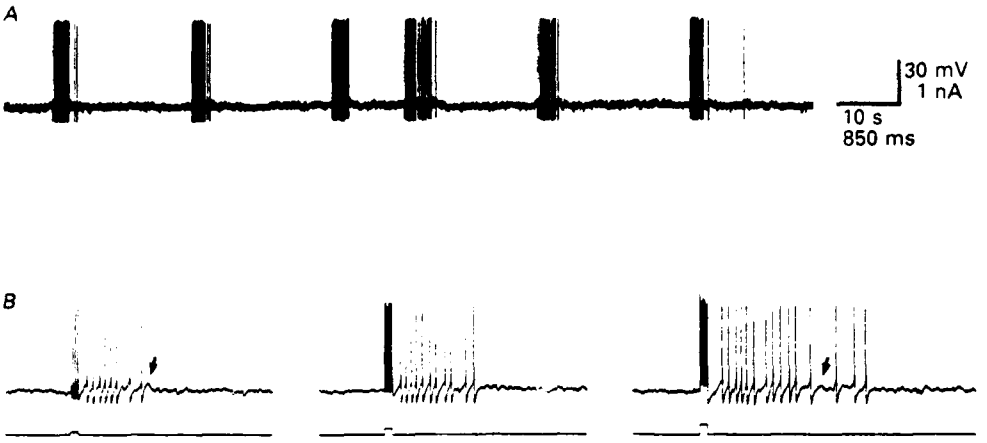

Fig. 9. Bursting in type I cells. *A*, this cell spontaneously generated repetitive trains of action potentials separated by periods of quiescence (i.e. phasic bursting). *B*, the same neurone responded to depolarizing current pulses (bottom traces) with trains of spikes during the pulse and after-discharges of spikes following each pulse. Increased numbers of spikes during the pulse caused spike after-discharges of increasing duration (four spikes fired during the pulse on the left, six spikes during the pulse in the middle and eight spikes during the pulse on the right). The membrane potential was maintained depolarized by 10 mV with continuous current injection in both *A* and *B* ($E_M = -62$ mV). Depolarizing after-potentials (see text) are designated by arrows in *B*. Upper time calibration refers to *A*, lower calibration to *B*.

1–4 s. It is likely that the ionic conductance responsible for AHPs was a Ca^{2+}-activated K^+ conductance, and not a Cl^- conductance, since AHPs were also present in experiments performed with recording electrodes containing KCl ($n = 7$), where the Cl^- equilibrium potential was shifted positive.

Bursting characteristics

All three cell types showed the capacity to generate bursts of action potentials, although bursting characteristics were different across cell groups. Though usually silent, three of six type I neurones which were depolarized with direct current injection showed repetitive trains of action potentials separated by silent periods (i.e. 'phasic' bursting, Fig. 9*A*). Single action potentials in these 'phasic' cells were often followed by depolarizing after-potentials (Fig. 9*B*), and small plateau-like depolarizations underlying the spike trains could be seen when voltage records were examined at high gain. Spike trains evoked by injection of positive current in these cells were often followed by after-discharges of spikes which long outlasted the current pulses (Fig. 9*B*). The duration of spike after-discharges was dependent on the number of action potentials which fired during the current pulse, suggesting the summation of depolarizing after-potentials following individual spikes.

Type II neurones were heterogeneous in their bursting behaviour, only six of

twenty-eight cells showing bursting properties. Two type II neurones showed isolated trains of action potentials (Fig. 10*A*), but these bursts occurred only sporadically and, unlike the 'phasic' bursts of some type I cells, could not be caused to occur repetitively with steady current injection. More frequently, type II neurones

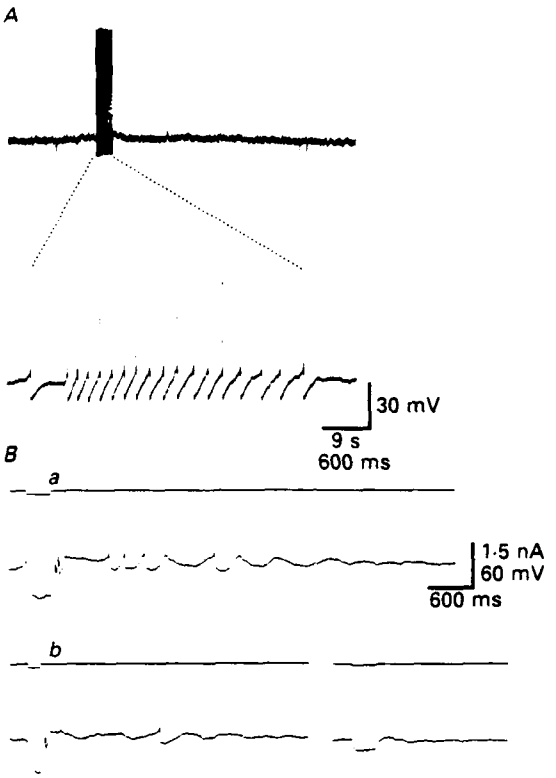

Fig. 10. Bursting in type II neurones. *A*, this type II neurone generated occasional trains of action potentials which were not repetitive. Upper time calibration applies to top trace and lower calibration to bottom, expanded trace. *Ba*, a different type II neurone developed, as a rebound response to membrane hyperpolarization induced by negative current injection, membrane potential oscillations generating up to two fast spikes at the peaks. *Bb*, a current pulse of shorter duration (left) or lower intensity (right) elicited less membrane oscillation.

($n = 5$) developed oscillations in their membrane potential following the offset of negative current injection (Fig. 10*B*). These oscillations consisted of an initial plateau depolarization with one to two superimposed action potentials, followed by a series of sinusoidal oscillations which could generate single action potentials. The amplitude and overall duration of the oscillations were dependent on the duration and the amplitude of the preceding hyperpolarization (Fig. 10*B*). One of the type II neurones which generated isolated trains of action potentials also showed membrane potential oscillations.

Type III neurones showed bursts of three to six action potentials superimposed on low-threshold Ca^{2+} potentials, as described above. Seven of nineteen type III

neurones generated repetitive bursts, either spontaneously or in response to continuous current injection (Fig. 11*A*). Membrane oscillations and repetitive bursts often occurred at resting potential following hyperpolarizing current pulses in these cells (Fig. 11*B*).

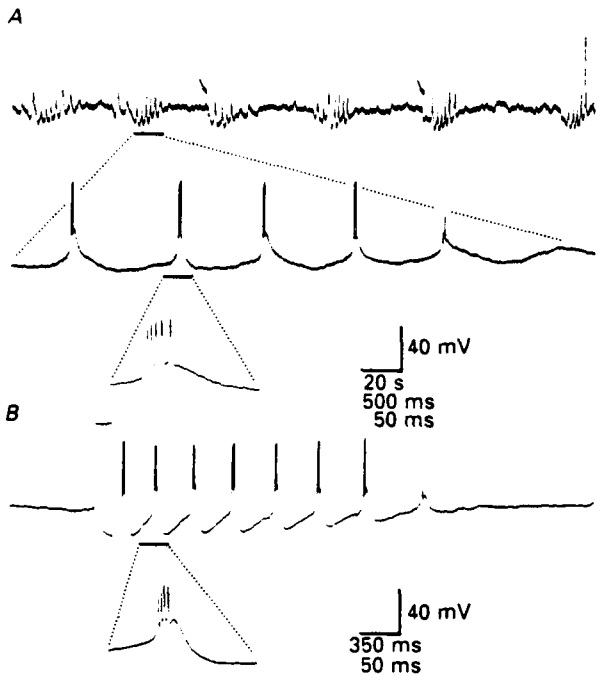

Fig. 11. Bursting in type III neurones. *A*, abrupt spontaneous hyperpolarizations (arrows) from a depolarized membrane potential in this type III neurone (membrane potential was maintained depolarized at approximately −55 mV with continuous current injection) led to the activation of spontaneous, repetitive low-threshold potentials and bursts of action potentials. *B*, a different type III cell showed regenerative low-threshold potentials and bursts of action potentials as an anodal-break response to a hyperpolarizing current pulse (upper bar) delivered at resting membrane potential (−60 mV). Upper time calibration refers to top trace, middle and lower calibrations to expanded traces below in both *A* and *B*.

Synaptic responses

Postsynaptic potentials could be evoked by electrical stimulation (50–500 μA) near the fornix in thirty-four of forty-four neurones tested. Both excitatory and inhibitory postsynaptic potentials (EPSPs and IPSPs) were seen in all three cell groups. Some type I cells (40%) responded to single electrical stimuli (50–100 μA) with multiple EPSPs (Fig. 12*A*). Both EPSPs and IPSPs in type I cells appeared to decay passively. Most type II cells (65%) responded to the same stimulation with IPSPs, half of those showing a combined EPSP–IPSP sequence (Fig. 12*B*). Low-threshold potentials could not be detected in these cells with extracellular stimulation. Most type III neurones (65%) showed EPSPs with a slow decay which did not follow passive electrotonic kinetics (Fig. 12*C*). Hyperpolarization of these

cells caused them to respond to extracellular stimulation with low-threshold potentials and bursts of spikes (Fig. 12*C*). Multiple EPSPs in response to single stimuli were not seen in type II and type III neurones.

Anatomical characteristics

The PVN was distinguished from surrounding tissue by its translucent appearance in the slice. Thus, the approximate location of each recorded cell with respect to the

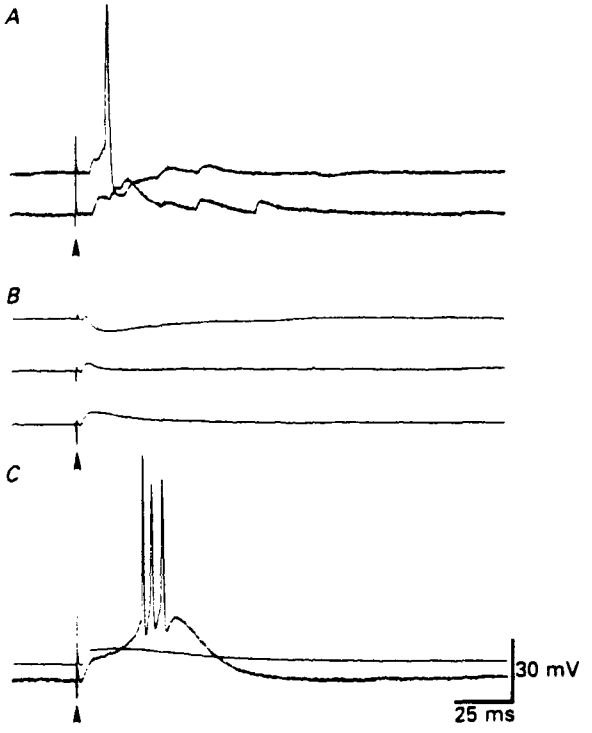

Fig. 12. Synaptic responses of the three cell types. *A*, a type I neurone responded to extracellular electrical stimulation (arrow, 100 μA, 0·5 ms) with EPSPs and a spike at resting membrane potential (−63 mV, top trace). Hyperpolarization of the cell membrane to −85 mV with continuous negative current revealed multiple evoked PSPs (EPSPs and possible reversed IPSPs) underlying the spike (bottom trace). *B*, a type II neurone responded to extracellular stimulation (arrow, 100 μA, 0·5 ms) with an EPSP–IPSP sequence at resting potential (−60 mV, top trace). The IPSP was reversed with membrane hyperpolarization (middle and bottom traces, all traces are averages of four to seven sweeps). The reversal potential for evoked IPSPs in this cell was between −75 and −80 mV. *C*, extracellular stimulation (arrow, 50 μA, 0·5 ms) of a type III neurone caused a long-lasting EPSP at resting potential (−70 mV, average of five sweeps). Stimulation at the same intensity evoked a low-threshold potential and a burst of fast spikes when the cell was hyperpolarized with continuous negative-current injection.

PVN was visually estimated from the placement of the recording electrode. Type I and type II neurones appeared from this estimation to be located within the PVN, while type III neurones appeared to be located just dorsal to the PVN.

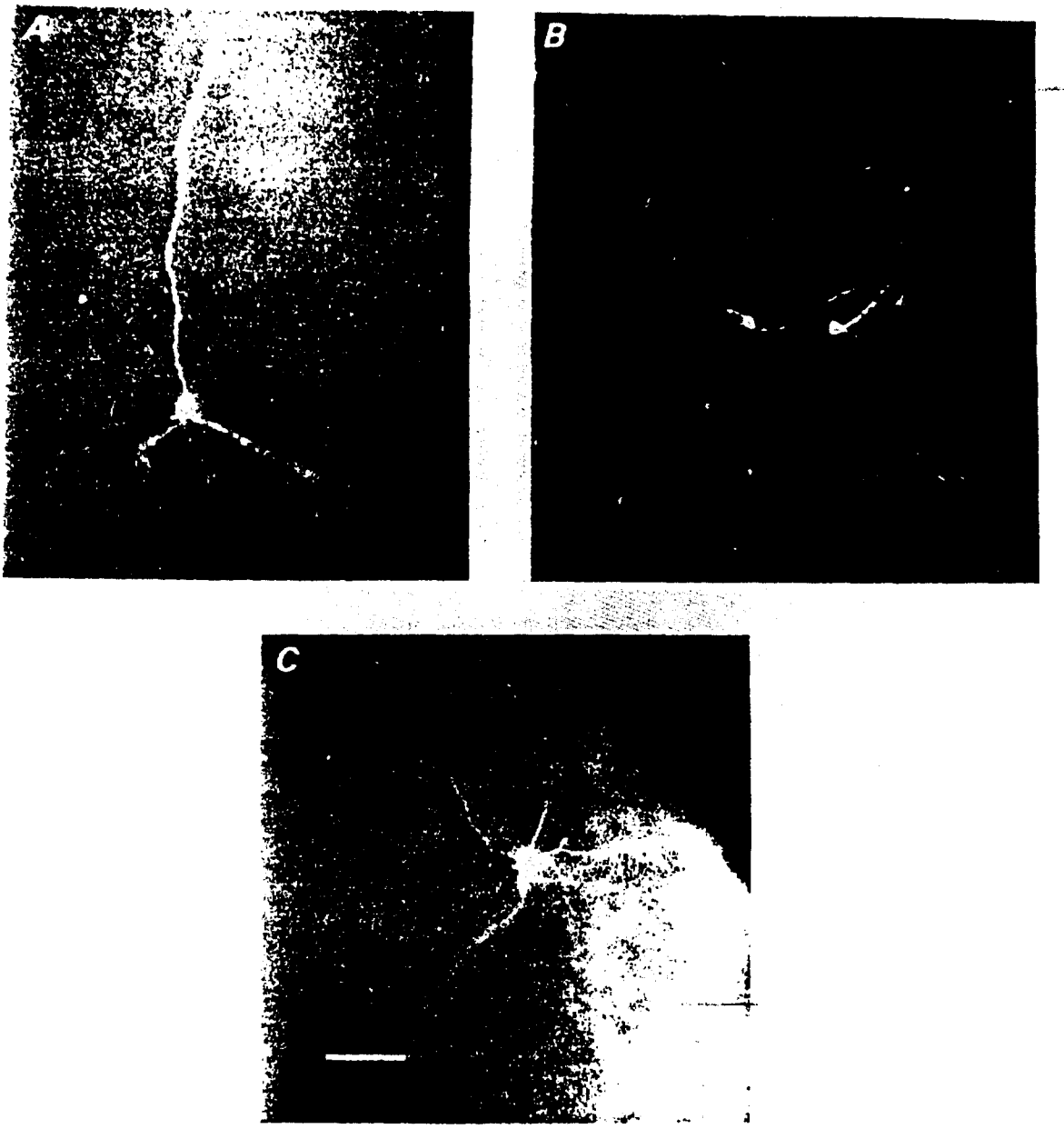

Fig. 13. Hypothalamic neurones labelled by intracellular injection of Lucifer Yellow. *A*, a type I neurone showing few, sparsely branched primary dendrites. *B*, two type II neurones which were smaller than the type I neurone. The cell on the left showed three primary dendrites giving rise to secondary processes. Each cell was recorded and injected with current. *C*, a type III neurone with a multipolar dendritic tree radiating out from the soma. It was located dorsal to the PVN, near the third ventricle (upper right), and had processes which terminated close to the ependymal cell layer of the ventricle. Calibration bar = 75 μm and applies to *A*, *B* and *C*.

A total of twenty five neurones were injected with Lucifer Yellow or ethidium bromide (Yagodaman & VanderMaelen, 1982) after electrophysiological characterization. Electrophysiological classification of cells with Lucifer Yellow electrodes was based on the presence or absence of low threshold potentials and, if present,

whether the low-threshold potentials generated bursts of action potentials. As described above, type I cells did not generate low-threshold potentials, while type II cells showed small low-threshold potentials which supported a maximum of one or two spikes, and type III neurones generated robust low-threshold potentials supporting bursts of up to six spikes. Because of the adverse effects on recorded neurones of the Lucifer Yellow (and/or the lithium acetate in which it was dissolved), recordings done with Lucifer Yellow-filled electrodes were not included in the electrophysiological analyses described above. Ethidium bromide did not have any noticeable effect on electrical recordings.

Twelve injected neurones (three type I, seven type II and five type III cells) were sufficiently labelled to determine their morphology. Preliminary morphological analysis indicated that type I neurones had relatively large soma diameters (20–30 μm, long axis) and only two to three sparsely branched, primary dendrites with dendritic spines (Fig. 13*A*). Type II neurones tended to have smaller soma diameters (10–25 μm) and more highly branched dendritic arbors, with two to four primary dendrites giving rise to secondary branches (Fig. 13*B*). Type III neurones had somata which were 11–25 μm in diameter, with four to six primary dendrites giving rise to secondary dendrites (Fig. 13*C*). Type I and type II neurones generally had elongated, bidirectional dendritic orientations. Cells were seen in all three groups that had dendrites which terminated very close to the third ventricle.

DISCUSSION

Our data indicate that at least three electrophysiologically distinct types of neurone are present in the PVN region of the hypothalamus. Based upon the locations of the three cell populations and comparisons between our electrophysiological observations and data from the SON, we suggest that type I cells are PVN magnocellular neurones, type II cells are PVN parvocellular neurones and type III cells are non-PVN neurones.

Type I neurones

Type I neurones were situated inside the PVN and had electrophysiological properties which were very similar to those of magnocellular neurones of the SON. They had linear I–V relations to very hyperpolarized membrane potentials, much like SON neurones (Mason, 1983; Bourque & Renaud, 1985*a*). A shoulder on the falling phase of the action potentials, similar to that of type I neurones in this study, has been described in SON neurones and has been attributed to a high-threshold Ca^{2+} conductance which contributes to the action potential (Mason & Leng, 1984) and is augmented during the spike broadening associated with repetitive firing in these cells (Andrew & Dudek, 1985; Bourque & Renaud, 1985*b*). Type I neurones often displayed, in response to depolarizing pulses, a delayed onset to spike firing caused by a hyperpolarizing 'notch' in the membrane potential, as well as a delayed return to baseline of the membrane potential following hyperpolarizing pulses; these properties closely resembled those associated with a putative A-current described in SON magnocellular neurones (Randle, Bourque & Renaud, 1986*a*; Bourque, 1988).

The bursting characteristics of some type I cells were similar to the phasic firing behaviour described for vasopressinergic magnocellular neurones *in vivo* and *in vitro* (see Poulain & Wakerley, 1982; Dudek, Tasker & Wuarin, 1989). Depolarizing after-potentials followed action potentials and appeared to sum to generate spike bursts, either as repetitive trains of action potentials or as long after-discharges. In the SON, the summation of Ca^{2+}-dependent depolarizing after-potentials to form plateau potentials has been described as the mechanism for phasic firing (Andrew & Dudek, 1984*a*; Bourque, 1986; Andrew, 1987). That phasic firing was seen in 50% of type I neurones tested is consistent with these neurones being magnocellular neurones comprised of both oxytocinergic (i.e. non-phasic) and vasopressinergic (i.e. phasic) neurones (Poulain & Wakerley, 1982; Cobbett *et al.* 1986).

Our preliminary anatomical data suggest morphological similarities (i.e. soma diameters of 20–30 μm with two to three sparsely branched, spiny dendrites) between labelled type I neurones and Lucifer Yellow-labelled magnocellular neurones of the SON (Randle, Bourque & Renaud, 1986*b*) and Golgi-stained magnocellular neurones of the PVN (Armstrong *et al.* 1980; van den Pol, 1982).

Type II neurones

Type II neurones were located within the PVN and showed electrophysiological properties which were distinct from those of type I neurones and SON magnocellular neurones. The principal distinguishing characteristic of these cells was their capacity to generate a small low-threshold potential, similar to that seen in some neurones of the neocortex (Friedman & Gutnick, 1987), the dorsal raphe nucleus (Burlhis & Aghajanian, 1987) and in dopamine-containing regions of the midbrain (Grace & Onn, 1989). The heterogeneity seen in the electrical properties of type II cells (e.g. low-threshold potentials of various amplitudes, inconsistent I–V relations across cells and differences in bursting behaviour) suggests that this group of neurones consists of more than one cell type. This electrophysiological heterogeneity is consistent with the diversity of anatomical and functional cell types that make up the parvocellular populations of the PVN (Armstrong *et al.* 1980; van den Pol, 1982; Swanson & Sawchenko, 1983).

Type II neurones were morphologically distinct from type I neurones. They were smaller in diameter and tended to have more complex dendritic arbors than type I cells. Anatomical studies of PVN parvocellular neurones indicate diverse cell morphologies. Thus, some parvocellular neurones have been described which show sparse dendritic branching (van den Pol, 1982), while putative catecholaminergic neurones have been shown in the parvocellular regions of the PVN to have bipolar dendritic arbors which give off numerous secondary branches (Chan-Palay, Zaborszky, Kohler, Goldstein & Palay, 1984). Multiple preautonomic neurones have also been described in the ventromedial parvocellular aspect of the PVN (Rho & Swanson, 1989). Type II neurones labelled with Lucifer Yellow in our study were multipolar and generally showed a bipolar orientation of their primary dendrites, often with abundant branching of secondary dendrites. Their size and pattern of dendritic aborization correlated closely with those of PVN parvocellular neurones.

Low-threshold potentials were not affected by bath application of TTX in three type II neurones, but were blocked by application of medium containing low

Ca^{2+} and Cd^{2+} in two type II neurones. This suggests that the low-threshold depolarizations in these cells were Ca^{2+}-dependent, although, in light of the small number of cells tested and the heterogeneity of the low-threshold potentials seen in these cells, it cannot be ruled out that a subthreshold, persistent Na^{+} conductance (Stafstrom, Schwindt, Chubb & Crill, 1985) may have contributed to the low-threshold potentials in some of the type II neurones which were not pharmacologically tested. Nevertheless, the apparent 'low-threshold' nature of these potentials (i.e. deinactivated when hyperpolarized from resting potential) in all the cells suggests that this is not the case.

If it is assumed that the low-threshold potentials in all type II cells were associated with a Ca^{2+} conductance, then the large variability in the appearance of low-threshold potentials in these cells suggests that they may not be a separate population of cells, but rather, type III neurones with varying degrees of deinactivation of their low-threshold Ca^{2+} channels. This is unlikely for two reasons: (1) low-threshold potentials in type III neurones, unlike those of type II neurones, were very distinctive in their large amplitude and their capacity to generate bursts of spikes, and (2) neurones showing low-threshold bursting characteristics (i.e. type III neurones) were all located outside the PVN (Tasker & Dudek, 1987) while neurones generating small low-threshold potentials (i.e. type II neurones) were situated within the PVN, suggesting that they are different populations of cells.

Type III neurones

Type III neurones were located just dorsal to the PVN (Tasker & Dudek, 1987). Poulain & Carette (1987) have described a population of neurones lateral and ventrolateral to the PVN in the guinea-pig that generate large low-threshold potentials and have bursting characteristics very similar to those seen in our type III cells. As the neurones described in these two studies probably belong to the same hypothalamic cell population, these cells would therefore appear to nearly surround the PVN. Preliminary results from our laboratory suggest that local inhibitory interneurones in this region project to magnocellular and parvocellular neurones in the PVN (Tasker & Dudek, 1988). Although further electrophysiological studies are required to confirm this, it is tempting to speculate that type III neurones may be inhibitory interneurones which relay information to PVN magnocellular and/or parvocellular neurones. Autoradiography and combined immunohistochemical/tracer studies have shown that projections from limbic structures terminate in a perinuclear fashion, forming a 'halo' around the SON and PVN (Sawchenko & Swanson, 1983; Silverman & Oldfield, 1984). The majority of magnocellular and parvocellular dendrites are contained within the nucleus (Armstrong *et al.* 1980; van den Pol, 1982). Recent immunohistochemical studies have revealed neurones immunopositive for γ-aminobutyric acid (GABA) and glutamic acid decarboxylase (GAD) in and around the SON (van den Pol, 1985; Theodosis, Paut & Tappaz, 1986) and PVN (Tappaz, Bosler, Paut & Berod, 1985; Kakucska, Tappaz, Gaal, Stoeckel & Makara, 1988; Meister, Hokfelt, Geffard & Oertel, 1988). Perinuclear inhibitory interneurones, therefore, could be the substrate by which such limbic structures as the lateral septum (Lebrun, Poulain & Theodosis, 1983) and the ventral subiculum (Ferreyra, Kannan & Koizumi, 1983) exercise their inhibitory effects on SON and PVN neurones.

The low-threshold bursting characteristics of type III neurones in this study resemble those of inferior olivary neurones (Llinás & Yarom, 1981) and thalamic neurones (Jahnsen & Llinás, 1984). The oscillatory behaviour in these neurones is implicated in the cerebellar climbing fibre system and in cortical spindle generation (Steriade and Deschênes, 1984), respectively. The question arises as to what function the oscillatory behaviour in bursting hypothalamic neurones may subserve. Although no data are yet available to answer this question, the periodicity of bursting in these cells seems to preclude a direct presynaptic involvement in the phasic firing of vasopressinergic magnocellular neurones (although see Poulain & Carette, 1987) or in the synchronous high-frequency discharge of oxytocinergic magnocellular neurones (see Poulain & Wakerley, 1982). The bursting periodicity of type III neurones seen in our experiments, however, may not directly reflect that which occurs *in vivo*, since many of the synaptic inputs which would modulate this behaviour may not be present in the slice preparation.

This study presents a detailed electrophysiological characterization of neurones in the PVN region of the rat hypothalamus. Our data suggest that electrophysiologically distinct neurones in the PVN correspond to magnocellular and parvocellular neurones. Further studies using intracellular injection of neuronal markers and immunohistochemical identification of neurotransmitters necessary to confirm this are currently underway (Hoffman *et al.* 1989).

We thank Dr Dorwin Birt for the data analysis software he kindly provided and Dr Neil Hoffman for anatomical assistance. This work was supported by a fellowship from the National Institute of Neurological Disorders and Stroke (NS08049) to J. G. T. and by a grant from the Air Force Office of Scientific Research (AFOSR 87-0361 and 90-0056) to F. E. D.

REFERENCES

AGHAJANIAN, G. K. & VANDERMAELEN, C. P. (1982). Intracellular identification of central noradrenergic and serotonergic neurons by a new double labeling procedure. *Journal of Neuroscience* **2**, 1786–1792.

ANDREW, R. D. (1987). Endogenous bursting by rat supraoptic neuroendocrine cells is calcium dependent. *Journal of Physiology* **384**, 451–465.

ANDREW, R. D. & DUDEK, F. E. (1983). Burst discharge in mammalian neuroendocrine cells involves an intrinsic regenerative mechanism. *Science* **221**, 1050–1052.

ANDREW, R. D. & DUDEK, F. E. (1984*a*). Analysis of intracellularly recorded phasic bursting by mammalian neuroendocrine cells. *Journal of Neurophysiology* **51**, 552–566.

ANDREW, R. D. & DUDEK, F. E. (1984*b*). Intrinsic inhibition in magnocellular neuroendocrine cells of rat hypothalamic slices. *Journal of Physiology* **353**, 171–185.

ANDREW, R. D. & DUDEK, F. E. (1985). Spike broadening in magnocellular neuroendocrine cells of rat hypothalamic slices. *Brain Research* **334**, 176–179.

ARMSTRONG, W. E., WARACH, S., HATTON, G. I. & MCNEILL, T. H. (1980). Subnuclei in the rat hypothalamic paraventricular nucleus: A cytoarchitectural, horseradish peroxidase and immunocytochemical analysis. *Neuroscience* **5**, 1931–1958.

BOURQUE, C. W. (1986). Calcium-dependent spike after-current induces burst firing in magnocellular neurosecretory cells. *Neuroscience Letters* **70**, 204–209.

BOURQUE, C. W. (1988). Transient calcium-dependent potassium current in magnocellular neurosecretory cells of the rat supraoptic nucleus. *Journal of Physiology* **397**, 331–347.

BOURQUE, C. W., RANDLE, J. C. R. & RENAUD, L. P. (1985). A calcium-dependent potassium conductance in rat supraoptic nucleus neurosecretory neurons. *Journal of Neurophysiology* **54**, 1375–1382.

BOURQUE, C. W. & RENAUD, L. P. (1985*a*). Calcium-dependent action potentials in rat supraoptic neurosecretory neurones recorded *in vitro*. *Journal of Physiology* **363**, 419–428.

BOURQUE, C. W. & RENAUD, L. P. (1985*b*). Activity dependence of action potential duration in rat supraoptic neurosecretory neurones recorded *in vitro*. *Journal of Physiology* **363**, 429–439.

BURLHIS, T. M. & AGHAJANIAN, G. K. (1987). Pacemaker potentials of serotonergic dorsal raphe neurons: Contribution of a low-threshold Ca^{2+} conductance. *Synapse* **1**, 582–588.

CHAN-PALAY, V., ZABORSZKY, L., KOHLER, C., GOLDSTEIN, M. & PALAY, S. L. (1984). Distribution of tyrosine-hydroxylase-immunoreactive neurons in the hypothalamus of rats. *Journal of Comparative Neurology* **227**, 467–496.

COBBETT, P., SMITHSON, K. G. & HATTON, G. I. (1986). Immunoreactivity to vasopressin- but not oxytocin-associated neurophysin antiserum in phasic neurons of rat hypothalamic paraventricular nucleus. *Brain Research* **362**, 7–16.

DUDEK, F. E., HATTON, G. I. & MACVICAR, B. A. (1980). Intracellular recordings from the paraventricular nucleus in slices of rat hypothalamus. *Journal of Physiology* **301**, 101–114.

DUDEK, F. E., TASKER, J. G. & WUARIN, J.-P. (1989). Intrinsic and synaptic mechanisms of hypothalamic neurons studied with slice and explant preparations. *Journal of Neuroscience Methods* **28**, 59–69.

FERREYRA, H., KANNAN, H. & KOIZUMI, K. (1983). Influences of the limbic-system on hypothalamo-neurohypophysial system. *Brain Research* **264**, 31–45.

FRIEDMAN, A. & GUTNICK, M. J. (1987). Low-threshold calcium electrogenesis in neocortical neurons. *Neuroscience Letters* **81**, 117–122.

GRACE, A. A. & ONN, S.-P. (1989). Morphology and electrophysiological properties of immunocytochemically identified rat dopamine neurons recorded in vitro. *Journal of Neuroscience* **9**, 3462–3481.

HATTON, G. I., COBBETT, P. & SALM, A. K. (1985). Extranuclear axon collaterals of paraventricular neurons in the rat hypothalamus: intracellular staining, immunocytochemistry and electrophysiology. *Brain Research Bulletin* **14**, 123–131.

HOFFMAN, N. W., TASKER, J. G. & DUDEK, F. E. (1989). Comparative electrophysiology of magnocellular and parvocellular neurons of the hypothalamic paraventricular nucleus. *Society for Neuroscience Abstracts* **15**, 1088.

JAHNSEN, H. & LLINÁS, R. (1984). Electrophysiological properties of guinea-pig thalamic neurones: an *in vitro* study. *Journal of Physiology* **349**, 205–226.

KAKUCSKA, I., TAPPAZ, M. L., GAAL, G., STOECKEL, M. E. & MAKARA, G. B. (1988). Gabaergic innervation of somatostatin-containing neurosecretory cells of the anterior periventricular hypothalamic area: A light and electron microscopy double immunolabelling study. *Neuroscience* **25**, 585–593.

LEBRUN, C. J., POULAIN, D. A. & THEODOSIS, D. T. (1983). The role of the septum in the control of the milk ejection reflex in the rat: effects of lesion and electrical stimulation. *Journal of Physiology* **339**, 17–31.

LLINÁS, R. & YAROM, Y. (1981). Electrophysiology of mammalian inferior olivary neurones *in vitro*. Different types of voltage-dependent ionic conductances. *Journal of Physiology* **315**, 549–567.

MACVICAR, B. A., ANDREW, R. D., DUDEK, F. E. & HATTON, G. I. (1982). Synaptic inputs and action potentials of magnocellular neuropeptidergic cells: intracellular recording and staining in slices of rat hypothalamus. *Brain Research Bulletin* **8**, 87–93.

MASON, W. T. (1983). Electrical properties of neurons recorded from the rat supraoptic nucleus in vitro. *Proceedings of the Royal Society* B **217**, 141–161.

MASON, W. T. & LENG, G. (1984). Complex action potential waveform recorded from supraoptic and paraventricular neurones of the rat: Evidence for sodium and calcium spike components at different membrane sites. *Experimental Brain Research* **56**, 135–143.

MEISTER, B., HOKFELT, T., GEFFARD, M. & OERTEL, W. (1988). Glutamic acid decarboxylase- and γ-aminobutyric acid-like immunoreactivities in corticotropin-releasing factor-containing parvocellular neurons of the hypothalamic paraventricular nucleus. *Neuroendocrinology* **48**, 516–526.

MINAMI, T., OOMURA, Y. & SUGIMORI, M. (1986). Ionic basis for the electroresponsiveness of guinea-pig ventromedial hypothalamic neurones *in vitro*. *Journal of Physiology* **380**, 145–156.

POULAIN, P. & CARETTE, B. (1987). Low-threshold calcium spikes in hypothalamic neurons recorded near the paraventricular nucleus in vitro. *Brain Research Bulletin* **19**, 453–460.

POULAIN, D. A. & WAKERLEY, J. B. (1982). Electrophysiology of hypothalamic magnocellular neurones secreting oxytocin and vasopressin. *Neuroscience* **7**, 773–808.

RANDLE, J. C. R., BOURQUE, C. W. & RENAUD, L. P. (1986*a*). α_1-Adrenergic receptor activation depolarizes rat supraoptic neurosecretory neurons in vitro. *American Journal of Physiology* **251**, 569–574.

RANDLE, J. C. R., BOURQUE, C. W. & RENAUD, L. P. (1986*b*). Serial reconstruction of Lucifer Yellow-labeled supraoptic nucleus neurons in perfused rat hypothalamic explants. *Neuroscience* **17**, 453–467.

RHO, J.-H. & SWANSON, L. W. (1989). A morphometric analysis of functionally defined subpopulations of neurons in the paraventricular nucleus of the rat with observations on the effects of colchicine. *Journal of Neuroscience* **9**, 1375–1388.

SAWCHENKO, P. E. & SWANSON, L. W. (1982). Immunohistochemical identification of neurons in the paraventricular nucleus of the hypothalamus that project to the medulla or to the spinal cord in the rat. *Journal of Comparative Neurology* **205**, 260–272.

SAWCHENKO, P. E. & SWANSON, L. W. (1983). The organization of forebrain afferents to the paraventricular and supraoptic nuclei of the rat. *Journal of Comparative Neurology* **218**, 121–144.

SILVERMAN, A.-J. & OLDFIELD, B. J. (1984). Synaptic input to vasopressin neurons of the paraventricular nucleus (PVN). *Peptides* **5**, 139–150.

STAFSTROM, C. E., SCHWINDT, P. C., CHUBB, M. C. & CRILL, W. E. (1985). Properties of persistent sodium conductance and calcium conductance of layer V neurons from cat sensorimotor cortex in vitro. *Journal of Neurophysiology* **53**, 153–170.

STERIADE, M. & DESCHÊNES, M. (1984). The thalamus as a neuronal oscillator. *Brain Research Reviews* **8**, 1–63.

SWAAB, D. F., NIJVELDT, F. & POOL, C. W. (1975). Immunofluorescence of vasopressin and oxytocin in the rat hypothalamo-neurohypophyseal system. *Journal of Neural Transmission* **36**, 195–215.

SWANSON, L. W. & KUYPERS, H. G. J. M. (1980). The paraventricular nucleus of the hypothalamus: Cytoarchitectonic subdivisions and organization of projections to the pituitary, dorsal vagal complex, and spinal cord as demonstrated by retrograde fluorescence double-labeling methods. *Journal of Comparative Neurology* **194**, 555–570.

SWANSON, L. W. & SAWCHENKO, P. E. (1983). Hypothalamic integration: Organization of the paraventricular and supraoptic nuclei. *Annual Review of Neuroscience* **6**, 269–324.

TAPPAZ, M. L., BOSLER, O., PAUT, L. & BEROD, A. (1985). Glutamate decarboxylase-immunoreactive boutons in synaptic contacts with hypothalamic dopaminergic cells: A light and electron microscopy study combining immunocytochemistry and radioautography. *Neuroscience* **16**, 111–122.

TASKER, J. G. & DUDEK, F. E. (1987). Low-threshold calcium spikes recorded in the region of the rat hypothalamic paraventricular nucleus. *Society for Neuroscience Abstracts* **13**, 1370.

TASKER, J. G. & DUDEK, F. E. (1988). Local circuit interactions between neurons in the region of the rat paraventricular nucleus. *Society for Neuroscience Abstracts* **14**, 1178.

THEODOSIS, D. T., PAUT, L. & TAPPAZ, M. L. (1986). Immunocytochemical analysis of the GABAergic innervation of oxytocin- and vasopressin-secreting neurons in the rat supraoptic nucleus. *Neuroscience* **19**, 207–222.

VAN DEN POL, A. N. (1982). The magnocellular and parvocellular paraventricular nucleus of the rat: Intrinsic organization. *Journal of Comparative Neurology* **206**, 317–345.

VAN DEN POL, A. N. (1985). Dual ultrastructure localization of two neurotransmitter-related antigens: Colloidal gold-labeled neurophysin-immunoreactive supraoptic neurons receive peroxidase-labeled glutamate decarboxylase- or gold-labeled GABA-immunoreactive synapses. *Journal of Neuroscience* **5**, 2940–2954.

VANDESANDE, F. & DIERICKX, K. (1975). Identification of the vasopressin-producing and of the oxytocin-producing neurones in the hypothalamic magnocellular system of the rat. *Cell and Tissue Research* **164**, 153–162.

Journal of Neuroscience Methods, 38 (1991) 129–143

NSM 01243

Comparison of three intracellular markers for combined electrophysiological, morphological and immunohistochemical analyses

Jeffrey G. Tasker, Neil W. Hoffman and F. Edward Dudek

Mental Retardation Research Center, UCLA School of Medicine, Los Angeles, CA (U.S.A.)

(Received 9 Ocotber 1990)
(Revised version received 14 January and 15 March 1991)
(Accepted 19 March 1991)

Key words: Lucifer yellow; Ethidium bromide; Biocytin; Hypothalamus; Slice; Paraventricular nucleus; Supraoptic nucleus

Hypothalamic paraventricular and supraoptic neurons were recorded intracellularly in coronal slices and injected with Lucifer yellow, ethidium bromide or biocytin. Electrical properties, morphological staining and neurophysin immunohistochemistry were compared among the 3 markers. Lucifer yellow electrodes had a high resistance and frequently blocked during experiments. Neurons recorded with Lucifer yellow electrodes had low input resistances and low-amplitude, broad spikes. Lucifer yellow labeling in whole mount was highly fluorescent, revealing distal dendrites and axons. Of cells injected with Lucifer yellow, 64% were recovered but were faint after immunohistochemical processing. Recordings with ethidium bromide electrodes were similar to controls, although electrode blockage sometimes occurred. Only somata and proximal dendrites of ethidium bromide-filled neurons were visible in whole-mount. Forty percent of cells injected with ethidium bromide were recovered after immunohistochemical processing; these were invariably faint. Recordings with biocytin-filled electrodes were similar to control recordings. Biocytin-filled, HRP-labeled cells showed distal dendrites and often dendritic spines and axons in 50–75-μm sections. Seventy percent of biocytin-injected cells labeled with fluorescent markers were recovered and remained strongly labeled after immunohistochemical processing. Biocytin had the best electrical and staining properties for combined electrophysiological and anatomical studies.

Introduction

Combining intracellular recording and staining provides the most direct link between cellular electrophysiology and anatomy in the study of the nervous system. Intracellular staining can be used to determine the location, morphology and often the immunohistochemical identity of electrophysiologically characterized neurons. While these anatomical analyses are not always necessary in relatively homogeneous structures, such as the hippocampus, they are important when studying more complex structures made up of diverse cell types. For example, in the hypothalamus, with its heterogeneous population of neurons, it is often necessary to determine the transmitter/hormone content of the recorded cell with immunohistochemical techniques in order to ascertain the type of neuron under study.

Several potential problems, often not treated in the literature, can be encountered in the electrophysiological recording and histological treatment of intracellularly recorded and stained neurons. Intracellular dyes often increase the resis-

Correspondence: F. Edward Dudek, Ph.D., Mental Retardation Research Center, NPI 58-258, UCLA School of Medicine, 760 Westwood Plaza, Los Angeles, CA 90024, U.S.A. Tel.: (213) 206-3622; Fax: (213) 206-5060.

tance of the recording electrode, making it difficult or impossible to inject current or dye. Under these conditions, electrode blockage increases the electrical noise to an unacceptably high level, often making electrical recordings impossible. Some intracellular stains or the vehicle in which they are dissolved can adversely affect the electrophysiological properties of the recorded cell. The level of technical difficulty and the time investment in histological procedures can also be a concern. An important consideration for any method of intracellular staining is whether a particular label will survive fixation, dehydration, sectioning and other histological procedures. Finally, the strength of the label is critical. During immunohistochemical studies, for example, it is important that the immunohistochemical reaction product not obscure the intracellular label and vice versa (Scharfman et al., 1989). Thus, the ideal intracellular marker would (a) confer excellent electrical properties to the recording electrode, (b) not alter the electrophysiological characteristics of the recorded neuron, (c) be visualized with relatively straight-forward histological techniques, and (d) provide a stable marker that is robust but compatible with other labels used in immunohistochemical procedures.

The purpose of this comparison was to assess which intracellular labeling techniques would yield optimal electrophysiology and anatomy. The limitations of certain intracellular labeling techniques make it difficult to combine electrophysiological analysis with detailed anatomical evaluation. For example, horseradish peroxidase (HRP) is a frequently used marker which provides a permanent stain (Kitai et al., 1989), but because of its large molecular weight (M_W = 40 000) and electrode-blocking characteristics, acceptable intracellular recording and dye injection are difficult to achieve without beveling or breaking the tip of the recording electrode. Other substances, such as carboxyfluorescein, cannot be fixed and thus have limited anatomical applications (Rao et al., 1986). Currently, three intracellular markers are most frequently used for the electrophysiological and anatomical study of intracellularly recorded neurons. Lucifer yellow has been the most common of the three and several studies that describe Lucifer yellow staining and associated immunohistochemical techniques have appeared (Kawata et al., 1983; Reaves et al., 1983; Smithson et al., 1984). Ethidium bromide is another marker that is compatible with both electrophysiological and immunohistochemical studies (Aghajanian and Vandermaelen, 1982; Mason et al., 1988; McCarthy and Lawson, 1988). Lastly, a method developed recently by Horikawa and Armstrong (1988) uses biocytin injection and application of avidin-conjugated markers to stain recorded cells. This method is gaining widespread recognition as a powerful tool for the combined electrophysiological and anatomical study of single neurons. A recent report has described its compatibility with immunohistochemical techniques (Rønnekleiv et al., 1990). The present study compared Lucifer yellow, ethidium bromide and biocytin to determine which of these intracellular markers is best for combined electrophysiological, morphological and immunohistochemical studies of intracellularly recorded neurons.

Methods

Slice preparation

Adult Sprague–Dawley rats (150–250 g) were decapitated and their brains rapidly removed and immersed for 1 min in cold (1–4°C), oxygenated artificial cerebrospinal fluid (ACSF). The ACSF contained (in mM): 124 NaCl, 3 KCl, 2.4 $CaCl_2$, 26 $NaHCO_3$, 1.3 $MgSO_4$, 1.4 NaH_2PO_4, and 11 glucose. The base of the brain was blocked on ice with a razor and the caudal end of the block was mounted on the chuck of a vibroslice (Campden Instr.) with cyanoacrylate. The chuck with the tissue block was quickly immersed in cold ACSF in the vibroslice chamber, and coronal slices (400–500 μm) containing the paraventricular and/or supraoptic nuclei were sectioned. One to 2 slices were placed on filter paper on the ramp of an interface recording chamber (Haas et al., 1979). The ACSF was heated to 32–34°C and pumped into the chamber, where it was drawn up over the slices by capillarity or, in some cases, with threads of gauze. A gas mixture of 95% O_2/5% CO_2 was humidified and continuously

directed over the surface of the slices in the chamber. Slices were allowed to equilibrate in the recording chamber for approximately 2 h prior to the start of experiments.

Electrical recording and dye injection

Recording electrodes were pulled from microfilament capillary glass (1.0 mm OD, 0.5 mm ID) on a Flaming-Brown puller. They were filled with (1) 2–5% Lucifer yellow dissolved in 0.5–1 M lithium acetate or 0.5–1 M lithium chloride, (2) 1% ethidium bromide in 1 M potassium acetate, or (3) 2% biocytin in 2 M potassium acetate or 2 M potassium chloride. Control electrodes contained 2–4 M potassium acetate only. Cell impalement was accomplished by advancing the electrodes through the slice in 4-μm steps with a piezoelectric microdrive and oscillating the negative capacitance feedback. Electrical signals were recorded through an intracellular amplifier with a bridge circuit and stored on magnetic tape or digitized and stored on videotape. Lucifer yellow and biocytin were injected with negative current pulses (0.2–2.5 nA, 200–500 ms, 1–2 Hz, 2–15 min for Lucifer yellow; 0.2–1.0 nA, 200–250 ms, 1–2 Hz, 5–30 min for biocytin). Ethidium bromide was injected using positive current pulses (0.2–1.0 nA, 200–500 ms, 1–2 Hz, 4–15 min). Larger currents were used to inject Lucifer yellow because of electrode blockage. Traces were generated by digitizing the data and printing them on a laser printer. All dyes were purchased from Sigma Chemical Co. or Molecular Probes, Inc. Electrophysiological data are expressed as the mean ± SEM.

Fixation and morphological examination

All slices were fixed by immersion for 12–14 h in 4% paraformaldehyde in 0.1 M sodium cacodylate buffer (pH 7.4) at 4°C. Slices that contained neurons injected with Lucifer yellow or ethidium bromide were processed for whole-mount examination. These slices were rinsed 3 times in 0.05 M Tris-buffered 0.15 M NaCl solution (TBS) and dehydrated in increasing concentrations of ethanol (50%, 70%, 95% and twice 100%, 20 min at each concentration), cleared in methyl salicylate (10 min), mounted and coverslipped. They were examined under the microscope with epifluorescence illumination using Nikon filters – B-excitation (495 nm) and 515W-absorption filters for the Lucifer yellow label and G-excitation (546 nm) and 580W-absorption filters for the ethidium bromide label.

Morphological and immunohistochemical analyses were not both performed on the same biocytin-injected neurons in this study. The cells that were used for immunohistochemistry were labeled with fluorescent markers, whereas those selected for morphological analysis were labeled using an avidin-biotinylated horseradish peroxidase (ABC-HRP) reaction, similar to the procedure described by Horikawa and Armstrong (1988). Briefly, after fixation, biocytin-injected slices for morphological analysis were rinsed several times in TBS and cryoprotected overnight in 30% sucrose in TBS. Sections of these slices were cut at a thickness (50–75 μm) sufficient to preserve much of the dendritic arbor and ensure adequate penetration of the avidin-biotinylated complex. Frozen sections were cut on a sliding microtome and then rinsed in TBS (3 × 10 min). Endogenous peroxidase activity was blocked by incubating sections for 5 min in a solution of 3% H_2O_2 and 10% methanol in TBS. Sections were then washed once in TBS and twice in 0.1 M phosphate-buffered saline (PBS) for 10 min each, followed by 2–4-h incubation at room temperature in the ABC-HRP complex (Vectastain-elite kit, Vector Laboratories) diluted 1:200 in PBS containing 0.5% Triton X-100. Sections were then washed 3 times for 10 min in PBS and stained using a chromogen solution containing 3,3'-diaminobenzidene · 4 HCl (DAB, Sigma, grade II) and glucose oxidase (GOD; Smithson et al., 1984). Neurons injected with biocytin and reserved for immunohistochemistry, on the other hand, were labeled using fluorescent markers. These slices were sectioned thinner (5 or 10 μm) to facilitate antibody penetration, to reduce false-positive double labeling due to immunostaining above or below the biocytin-filled neuron, and to standardize the immunohistochemical procedures for each intracellular marker as much as possible (see below). After sectioning, these cells were labeled by incubating sections in solutions containing

avidin conjugated either with rhodamine or with 7-amino-4-methyl-coumarin-3-acetic acid (AMCA, Vector Laboratories) for 4 h at room temperature (24°C). Both markers were diluted 1:200 in PBS containing 0.5% Triton X.

Immunohistochemistry

Slices containing cells labeled with Lucifer yellow and ethidium bromide, as well as those with biocytin-filled cells not used for morphological analysis (see above), were processed immunohistochemically according to the procedure described by Smithson et al. (1984). Those slices containing cells labeled with Lucifer yellow and ethidium bromide were first rehydrated in descending concentrations of ethanols. All slices, including biocytin-injected slices for immunohistochemical processing, were rinsed in TBS and post-fixed for 2 h in Bouin's solution at 4°C. They were then rinsed in TBS, dehydrated in the ascending series of ethanols, and embedded in polyethylene glycol (PEG, MW 1450, Sigma; see Smithson et al., 1983). The PEG blocks were sectioned at 5 or 10 μm on a rotary microtome. Tissue sections were rehydrated in the descending ethanol concentration series to TBS (3 washes of 5 min each). Biocytin-filled cells were labeled at this stage by incubating the sections in avidin-conjugated rhodamine or AMCA (see above). All sections were then scanned under epifluorescence microscopy for labeled cell bodies and processes. Cells labeled with Lucifer yellow and ethidium bromide were visualized using the filter combinations described above. The filters used for the rhodamine-labeled biocytin were G-excitation (546 nm) and 580W-absorption and those used for the AMCA-labeled biocytin were UV-excitation (365 nm) and 420K-absorption.

Neurophysin immunohistochemistry was performed on all sections containing labeled cell bodies and processes, as well as on immediately adjacent sections. Non-immune protein interactions were first blocked by a 30-min incubation in normal goat serum diluted in PBS (10% when applying the indirect immunofluorescence procedure and 1% when using the ABC technique). Triton X-100 (0.2%) was added to the solution for the ABC technique but omitted in the immunofluorescence procedure since it had been applied previously to enhance penetration of the avidin-conjugated biocytin marker (see above). Sections were then rinsed in PBS (3 × 5 min) and incubated for 12–14 h at 4°C and for an additional 2 h at room temperature in a polyclonal antiserum generated in rabbit against general neurophysin (Seif et al., 1977), or in a monoclonal mouse antiserum directed against vasopressin-associated neurophysin (PS 41; Ben-Barak et al., 1985; Whitnall et al., 1985). The rabbit polyclonal antibody was diluted at 1:200 (for indirect immunofluorescence) or 1:2000 (for the ABC-HRP procedure) in 0.1 M PBS containing 1% normal goat serum and 0.05% NaN_3. Triton X-100 (0.2%) was added to the antiserum dilution in initial experiments but was omitted subsequently. This did not affect levels of immunoreactivity. The mouse monoclonal antiserum was diluted at 1:500 in 0.05 M TBS with 0.2% Triton X-100 and used with the ABC-HRP procedure only. Replacement of the immunized sera with the same dilution of non-immunized serum resulted in a complete absence of immunoreactivity.

After incubation in the primary antiserum, sections were washed in PBS (3 × 5 min). For cells injected with Lucifer yellow or ethidium bromide, neurophysin immunohistochemistry was performed using the ABC-HRP procedure. The DAB-GOD reaction was used as the chromogen (see above), as described in detail by Smithson et al. (1984). Sections were mounted and coverslipped with methyl salicylate, then examined and photographed under epifluorescence and bright-field microscopy. For biocytin-injected neurons labeled with avidin-conjugated AMCA or avidin-conjugated rhodamine, the indirect immunofluorescence procedure (Sternberger, 1974) was used. These sections were incubated for 1 h at room temperature in goat anti-rabbit IgG conjugated with fluorescein isothiocyanate (FITC, Boehringer Mannheim) in PBS (1:50). Sections were then rinsed in PBS (3 × 5 min), mounted onto slides and coverslipped using glycerol/PBS (1:4) as the mounting medium. *N*-Propyl gallate (1%) was added to the mounting medium to retard photobleaching of fluorescence for about 75% of the cells double-labeled with biocytin (Giloh and Se-

dat, 1982). Sections were immediately examined and photographed under epifluorescence microscopy using the B-excitation and 515W-absorption filter combination for FITC and the appropriate filter combinations for AMCA and rhodamine (see above). Some sections were counterstained with cresyl violet.

Results

Lucifer yellow, ethidium bromide and biocytin were evaluated and compared on the basis of qualitative and quantitative electrophysiological and anatomical criteria. The electrical properties evaluated were electrode resistance and current-passing capacity, stability of recording, resting potentials, input resistances and action potential characteristics. The anatomical criteria compared were whole-mount morphological characteristics, complexity of histological procedures, stability of the intracellular label and its compatibility with immunohistochemical double-labeling.

Electrophysiological properties

The electrophysiological properties of hypothalamic neurons recorded with electrodes filled with the different intracellular markers and potassium acetate (controls) are summarized in Table I.

Lucifer yellow

Electrodes containing Lucifer yellow dissolved in LiAc or LiCl characteristically had resistances which were 30–300% higher than the same electrodes filled with potassium acetate. The fine electrodes needed for the impalement of hypothalamic neurons had resistances of 80–120 MΩ filled with 2 M potassium acetate, but the same electrodes had resistances of 150–250 MΩ when filled with Lucifer yellow. Reducing electrode resistance with blunter electrode tips made impalement of these cells much more difficult. Passing continuous negative current through the recording electrode is a commonly used and effective method of stabilizing electrical recordings after impalement of a neuron. Because of the high resistance of electrodes containing Lucifer yellow, current was difficult to pass and it was often difficult to obtain stable intracellular recordings. In addition, because Lucifer yellow is ejected iontophoretically using negative current, staining of neurons that failed to stabilize sufficiently for electrophysiological recording (i.e., temporarily impaled cells) sometimes occurred.

TABLE I

ELECTRICAL PROPERTIES OF HYPOTHALAMIC NEURONS RECORDED WITH ELECTRODES CONTAINING POTASSIUM ACETATE (CONTROL), LUCIFER YELLOW, ETHIDIUM BROMIDE AND BIOCYTIN

	Control	Lucifer yellow	Ethidium bromide	Biocytin
Resting potential (mV)	61.3 ± 2.3 (13)	60.0 ± 2.2 (6)	60.0 ± 2.6 (6)	58.9 ± 1.4 (12)
Input resistance (MΩ)	197.8 ± 24.6 (15)	145.5 ± 22.2 (10)	255.4 ± 14.9 (12)	223.9 ± 19.7 (14)
Spike amplitude (mV threshold-peak)	62.5 ± 1.1 (11)	48.2 ± 1.6 (9) **	61.9 ± 1.5 (8)	66.4 ± 2.2 (10)
Spike duration (ms @ 1/2 amplitude)	0.86 ± 0.04 (10)	2.12 ± 0.29 (9) **	1.01 ± 0.06 (11)	0.88 ± 0.08 (12)

Values are expressed as the mean ± SE (*n*). Resting membrane potentials were calculated after withdrawal from the cell. Input resistances were calculated in the linear portion of I–V curves. Values for resting potential and input resistance were taken from putative magnocellular, parvocellular and peri-PVN bursting neurons since no significant difference was found in these properties among the three cell types in previous studies (Tasker and Dudek, 1991; Hoffman et al., 1991). Values of spike amplitude were taken from putative magnocellular and parvocellular neurons only since spike amplitudes were not found to differ significantly among these PVN cell populations. Spike-duration values were taken only from putative parvocellular and peri-PVN bursting neurons since spike durations were not found to differ signficantly among these cells. Statistical differences among groups were first determined using analyses of variance (ANOVA). Where the ANOVA revealed a significant difference, the experimental groups were compared to the control groups with Dunnet's test. $P < 0.05$ was considered significant. ** Designates groups which differed significantly from controls at $P < 0.01$.

Clogging of the electrode tip, as evidenced by a substantial increase in the electrode resistance with time, was also common during the course of experiments.

The electrical properties of 16 cells were recorded with electrodes filled with Lucifer yellow. The quality of intracellular recordings made with these electrodes was generally poor compared to recordings with potassium-acetate electrodes (Table I). High electrode resistance often made it difficult to balance the bridge and caused high levels of baseline electrical noise. Recordings were often electrically unstable and tended to degenerate relatively quickly with time. As indicated in Table I, cells recorded with Lucifer yellow electrodes tended to have lower input resistances than cells recorded with control electrodes, although the difference was not statistically significant. Action potentials of cells recorded with Lucifer yellow electrodes were significantly smaller in amplitude (measured threshold to peak) and longer in duration (measured at half-maximum amplitude) than those of cells recorded with electrodes containing potassium acetate (Table I and Fig. 1B). Current–voltage (I–V) relations were difficult to calculate with Lucifer yellow electrodes due to clogging of the tip with current injection (Fig. 1B). Resting membrane potentials usually decreased and spikes became smaller and broader as Lucifer yellow and/or the lithium vehicle diffused into the cell during the course of recording. The high resistance of the electrodes and high incidence of electrode blockage often necessitated passage of

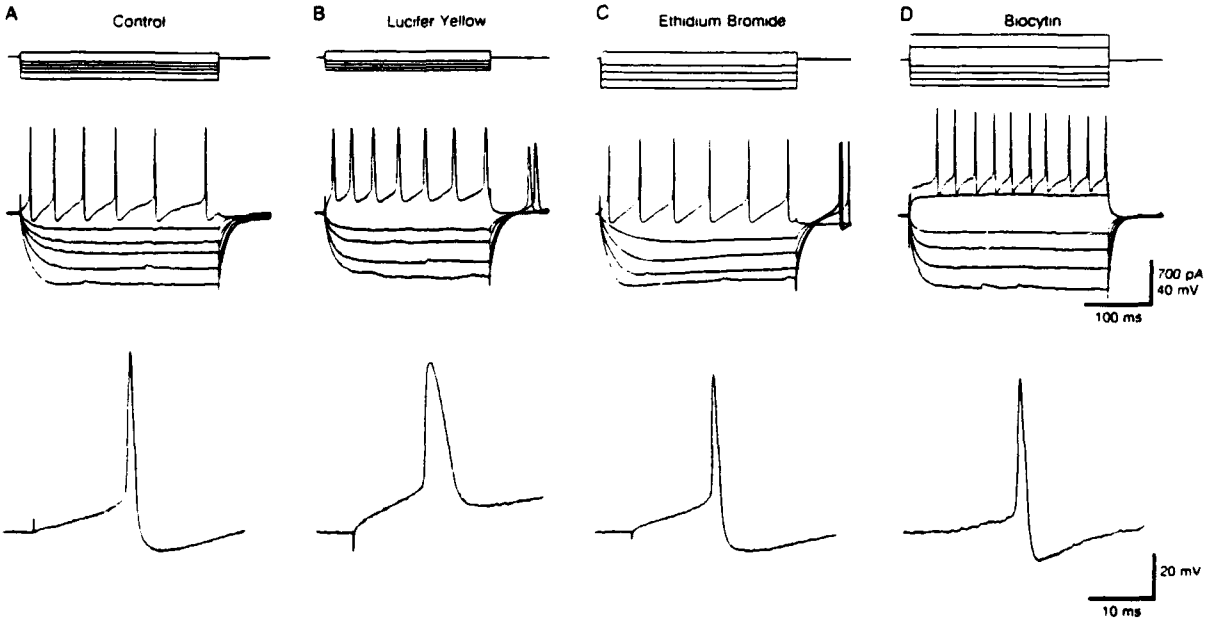

Fig. 1. Electrical properties of intracellular recordings with dye-filled electrodes. The voltage responses to a series of rectangular pulses of injected current, or current-voltage (I–V) series, are shown for each intracellular marker and for controls. Top traces are current recordings, middle traces are voltage responses and lower traces are expanded sweeps of the first spike of each spike train. A: control recording of a putative magnocellular neuron (Tasker and Dudek, 1991) with an electrode filled with potassium acetate (4 M). B: I–V series in a putative magnocellular neuron with an electrode filled with Lucifer yellow (5% in 1 M lithium acetate). Note the artifactual fluctuation in the most negative voltage deflection, caused by electrode blockage with relatively low-intensity current injection (−200 pA). The current-evoked spike is substantially broader than that seen in the control recording. C: I–V series in a putative parvocellular neuron with a recording electrode filled with ethidium bromide. The electrical properties of this recording are comparable to those of the control recording. D: I–V series recorded in a putative magnocellular neuron with a biocytin-filled electrode. Current injection and the morphology of the current-evoked spike in this recording were also qualitatively similar to those seen in the control recording. Spontaneous postsynaptic potentials are present in some traces from all recordings but are distinguishable from electrical noise caused by electrode blockage.

strong currents (up to 2.5 nA, see Methods) in order to inject a sufficient quantity of dye to label the cells. The recording electrodes invariably clogged during dye injection and any subsequent electrical analysis of the neuron was impossible.

Ethidium bromide

Twelve cells were recorded with electrodes filled with ethidium bromide. The quality of the intracellular recordings with ethidium bromide was good. Electrode resistances with ethidium bromide were 80–160 MΩ. Although the resistance of these electrodes was up to 35% higher than that of controls, they provided relatively noise-free recordings which remained stable for long periods of time. Injection of strong currents sometimes caused electrode blockage. The electrical properties of cells recorded with ethidium bromide electrodes were not significantly different from those of cells recorded with electrodes filled with potassium acetate (Table I). Fast action potentials and I–V relations were qualitatively similar to those in control recordings (Fig. 1C). The unwanted labeling of temporarily impaled cells was less of a problem since the dye is positively charged and was not iontophoresed from the electrode with the passage of negative current to stabilize the impalement. Electrode blockage occurred occasionally with prolonged recordings and sustained current injection. Dye injection (see Methods) usually caused blockage of the electrode tip.

Biocytin

A total of 27 neurons were recorded with biocytin-filled electrodes. No significant differences were found in the electrical properties of cells recorded with biocytin electrodes and those recorded with electrodes containing potassium acetate (Table I). Action potentials and I–V relations recorded with biocytin-filled electrodes were qualitatively similar to those seen in control recordings (Fig. 1D). Biocytin electrodes were 5–20% higher in resistance than the same electrodes containing 2 M potassium acetate, but were low enough in resistance to permit passage of strong currents, either positive or negative, without clogging. It was rare for electrode blockage to occur and often experiments could be continued or extended after dye injection was completed. Dye injection could be accomplished by passing either positive or negative current (see Horikawa and Armstrong, 1988) and, as with Lucifer yellow, staining of only temporarily impaled cells (i.e., cells that were lost due to partial impalement) was a potential problem. Recording for over 10 min without performing the injection protocol or dye injection for $\geqq 5$ min (see Methods) was usually sufficient to label recorded neurons.

Anatomical properties

As described in Methods, slices containing neurons labeled with Lucifer yellow and ethidium bromide were all examined initially in the whole-mount preparation and then sectioned at 5 or 10 μm and processed immunohistochemically according to the technique described by Smithson et al. (1984). Slices containing biocytin-filled cells were divided into 2 groups: those slices that were sectioned at 50–75 μm and histologically processed for morphological examination with procedures modified from Horikawa and Armstrong (1988), and those that were sectioned at 5 or 10 μm and immunohistochemically processed with methods modified from Smithson et al. (1984).

Lucifer yellow

Intracellular labeling with Lucifer yellow provided a simple (see Methods), detailed whole-mount visualization of the injected neuron (Fig. 2A and B). Successful injections were characterized by brightly labeled neurons, of which much of the dendritic arbor and often the dendritic spines and axon were stained. Successful labeling was dependent on the duration of the injection and on the degree and rapidity of electrode blockage during dye injection.

After whole-mount examination, neurophysin immunohistochemistry using the ABC-HRP reaction was performed on slices containing neurons filled with Lucifer yellow. This opaque reaction product obscured the Lucifer yellow label in the cytoplasmic compartment but not in the nucleus of injected cells (Smithson et al., 1984). There-

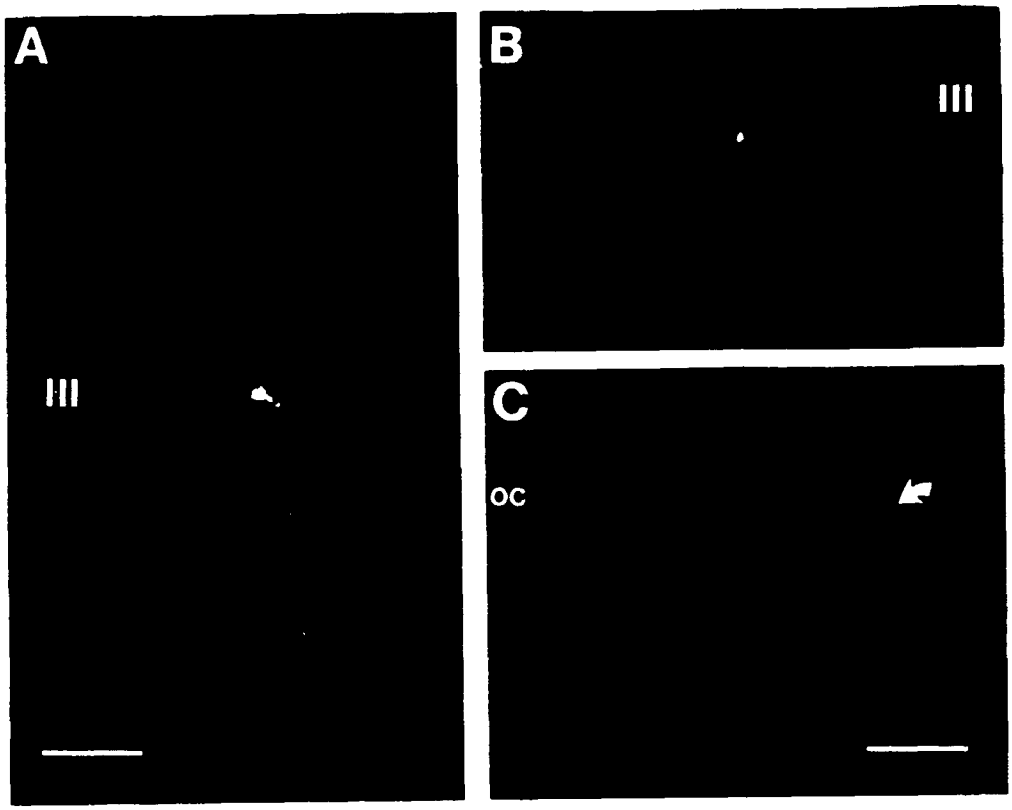

2

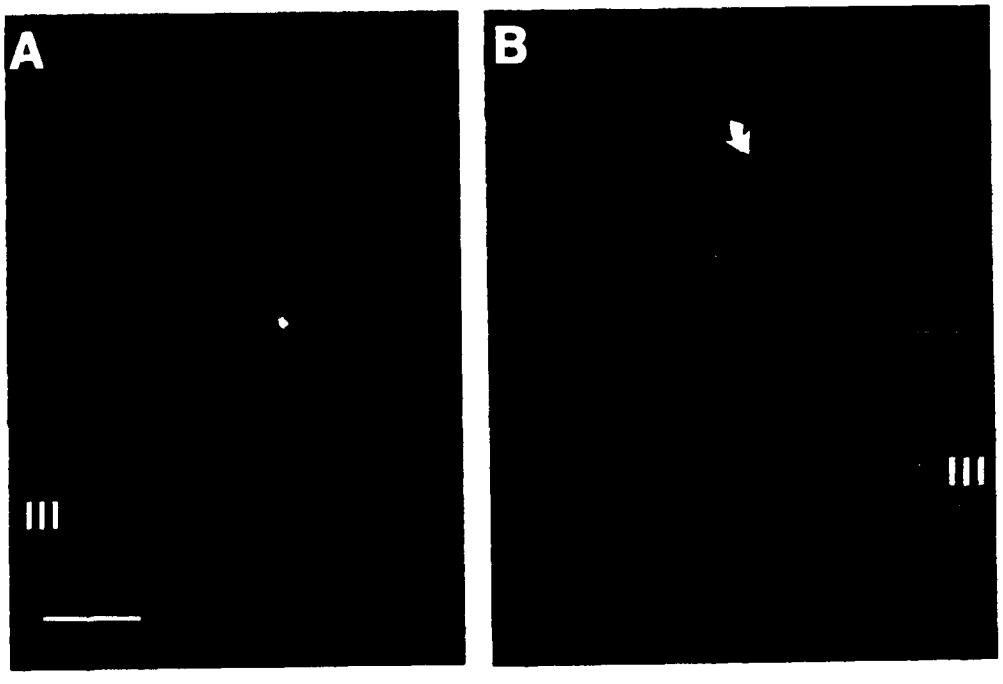

3

fore, in order to visualize both markers in the same cell, it was necessary to cut sections sufficiently thin (5–10 μm) to obtain a nuclear profile of the injected neuron (Fig. 2C). The Lucifer yellow fluorescence was relatively labile before the slices were embedded but remained stable for months in slices embedded in PEG and protected from light (Smithson et al., 1983). Approximately 64% of the total neurons injected with Lucifer yellow were recovered after sectioning and neurophysin immunohistochemistry. Cells recovered at this stage were often faint.

Ethidium bromide

Ethidium bromide fluorescence was less bright and labeled less of the injected neuron in the whole-mount preparation than either Lucifer yellow or biocytin. Although somata fluoresced fairly brightly, only proximal segments of dendrites and rarely axons or dendritic spines were visible with ethidium bromide (Fig. 3A). The ethidium bromide label was not as stable as Lucifer yellow or biocytin when embedded and stored in PEG or through the immunohistochemical processing. Only 40% of neurons injected with ethidium bromide were recovered after neurophysin immunohistochemistry. These labeled cells were always very faint (Fig. 3B).

Biocytin

Neuronal labeling with biocytin did not permit true whole-mount visualization of filled cells because slices containing biocytin-injected cells were sectioned (50–75 μm) to allow penetration of the avidin-biotinylated HRP complex. However, most of the morphological features of the hypothalamic neurons examined in this study were preserved in sections within this thickness range, and reconstruction of the labeled neuron from serial sections was possible when the cell was not contained entirely in a single section. This biocytin histochemical procedure provided Golgi-like staining of the dendrites and often revealed dendritic spines and axons of injected neurons (Fig. 4; Horikawa and Armstrong, 1988). Biocytin was very stable in injected neurons as slices were sometimes stored in chilled fixative for weeks or in PEG blocks for months prior to histochemical processing without any apparent decrement in neuronal labeling.

Rhodamine and 7-amino-4-methylcoumarin-3-acetic acid (AMCA) were the fluorescent markers used to label the biocytin-filled cells that were immunohistochemically processed. Fluorescein isothiocyanate (FITC) was always used as the immunohistochemical label in sections containing biocytin-filled cells. The brightest intracellular fluorescent marker that we used was rhodamine (Fig. 5A); however, it was excited by the fluorescein excitation light band, albeit at reduced efficiency, and thus partially obscured the FITC immunohistochemical label (Fig. 5B and C). The blue-fluorescing AMCA marker, on the other hand, although not as bright as the rhodamine (Fig. 6), was only excited by light in the ultraviolet range and not by the fluorescein excitation band; this allowed for good separation of the intracellular and immunohistochemical labels. The combi-

◀Fig. 2. Labeling with Lucifer yellow. A: whole-mount photomicrograph of a putative parvocellular neuron in the PVN labeled with Lucifer yellow. B: peri-PVN neuron filled with Lucifer yellow and photographed in whole mount. Somata and proximal and distal processes were brightly labeled with Lucifer yellow. C: combined transmitted-light/epifluorescence photomicrograph of a double-labeled magnocellular neuron (curved arrow) in the SON after immunohistochemistry for vasopressin-associated neurophysin. The Lucifer yellow label was contained within the nucleus while the immunostain was restricted to the cytoplasmic compartment of the injected cell. Calibration bar in A = 100 μm and applies to A and B; calibration in C = 50 μm; III, third ventricle; OC, optic chiasm.

Fig. 3. Ethidium bromide labeling. A: fluorescent label was only visible in the somata and proximal dendrites of these peri-PVN cells injected with ethidium bromide and viewed in whole mount. Recording and dye injection was performed in only one cell, suggesting dye coupling. B: combined transmitted-light/epifluorescence photomicrograph of a PVN cell labeled with ethidium bromide (curved arrow) and immunohistochemically processed for neurophysin using the ABC-HRP immunostain. The ethidium bromide fluorescence was very faint despite the immunonegativity of the cell. Calibration bar = 50 μm and is the same for A and B; III, third ventricle.

4

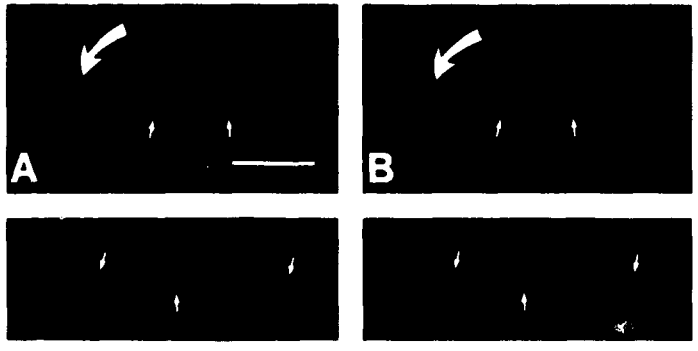

6

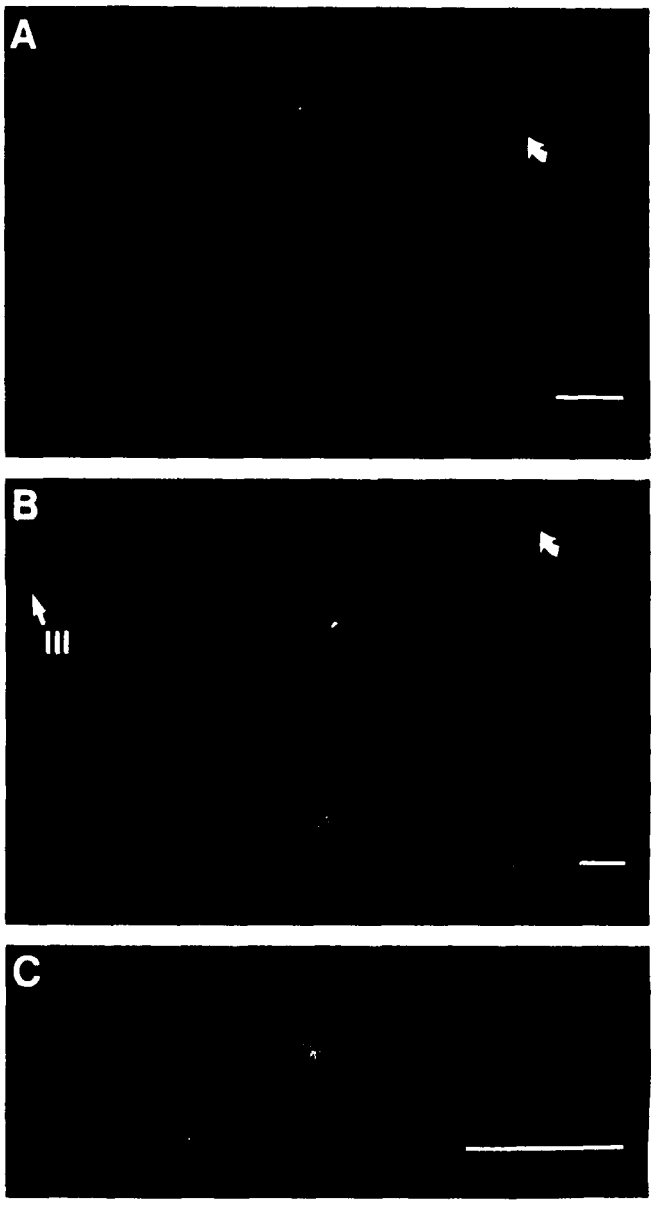

5

nation of AMCA-biocytin and FITC-neurophysin labeling sometimes permitted the identification of immunoreactive dendrites and axonal processes (Fig. 6). Of the neurons injected with biocytin, 70% were recovered and remained brightly labeled after sectioning and immunohistochemical staining.

Discussion

The primary purpose of an intracellular marker is to combine electrophysiological experiments with anatomical analyses of recorded cells; the ideal marker should therefore provide a strong, stable intracellular label without compromising the electrophysiological properties of the intracellular recording. This study evaluated three intracellular markers, Lucifer yellow, ethidium bromide and biocytin, based on the degree to which these markers permit the combination of electrophysiological, morphological and immunohistochemical analyses of intracellularly recorded hypothalamic neurons.

Lucifer yellow

Electrophysiology

Lucifer yellow is widely used as a lithium salt and as a potassium salt. The low solubility of the potassium salt of Lucifer yellow (1.25% in water and less in potassium salt solutions) limits the concentration of dye in the electrode solution and thus reduces the intensity of labeling possible. The potassium salt is useful in whole-cell patch-clamp recordings in which lower concentrations of the dye are required to label recorded cells because of the large tip diameter of the electrode and resultant dialysis of the intracellular milieu with the electrode contents. The lithium salt of Lucifer yellow is more highly soluble (about 5% in water) and is the most commonly used form of Lucifer yellow in experiments performed with sharp intracellular electrodes (Stewart, 1978). However, lithium may have adverse effects on cell electrical properties. For example, it may affect postsynaptic second messenger function. It has been reported to block inositol phosphate metabolism and thus, with time, deplete intracellular inositol (Berridge et al., 1989). Similarly, intracellular lithium may inhibit adenylate cyclase activity (Ebstein et al., 1989), which could affect cyclic AMP-dependent sodium, calcium or potassium channels (Kaczmarek and Levitan, 1987). Lithium leakage into the cytosol may also enhance calcium conductance and/or partially block potassium conductance, which would affect the resting membrane potential and spike-firing characteristics of the recorded cell (Mayer et al., 1984).

◀Fig. 4. Morphological labeling with biocytin. A 50-μm section containing a cell recorded in the region of the PVN, injected with biocytin and stained with the ABC-HRP reaction (see text). Distal dendrites and the axon (arrow) of this cell were visible with the opaque biocytin label. Calibration bar = 100 μm; Fx, fornix; III, third ventricle.

Fig. 5. Immunohistofluorescence of a biocytin-filled, rhodamine-labeled neuron. A: fluorescence photomicrograph under rhodamine filters of a 10-μm section containing a PVN magnocellular neuron labeled with rhodamine/biocytin (curved arrow) before immunohistochemical processing. B: the same section (at lower magnification) under fluorescein filters after neurophysin immunohistochemistry using a FITC immunolabel. The strongly labeled cell (curved arrow) fluoresces in the range of frequencies detected by the fluorescein filters making double labeling difficult to detect. C: at high-magnification, the faint yellow halo of immunofluorescence surrounding the nucleus of the rhodamine/biocytin-labeled cell was apparent, indicating that this cell was immunoreactive for neurophysin. Calibration bars = 50 μm in A and B, and 25 μm in C; III, third ventricle.

Fig. 6. Immunohistochemical labeling of a biocytin-filled, AMCA-stained cell. A: fluorescence photomicrographs of 10-μm sections containing a biocytin/AMCA-labeled PVN cell (curved arrow) seen under ultraviolet filters after neurophysin immunohistochemistry. Only the injected cell and its processes (small arrows in top and bottom photomicrographs) showed the blue AMCA fluorescence. B: the same sections seen under fluorescein filters. The biocytin/AMCA stained cell soma and processes (small arrows in top and bottom photomicrographs) were double labeled with the FITC immunolabel, indicating that the cell was immunopositive for neurophysin. Calibration bar in A = 25 μm and applies to top and bottom photomicrographs in A and B.

In terms of electrical properties, Lucifer yellow was the least acceptable of the 3 intracellular markers tested. It increased the resistance of the recording electrode approximately 2-fold (compared to the same electrodes filled with potassium acetate) and caused a low signal-to-noise ratio and blockage of the electrode tip. Cells recorded with Lucifer yellow electrodes were unstable and had relatively low resting membrane potentials and low amplitude, broad action potentials. Increased Ca^{2+} conductance or decreased K^+ conductance caused by leakage of the lithium into the cell may partially account for the low membrane potentials and altered spikes in these recordings (Mayer et al., 1984), especially since these effects became progressively more pronounced with time. It is still unclear what effect Lucifer yellow and/or lithium have on cells that reduces the likelihood of stable impalements, but this, as well as the altered electrophysiological properties probably contributes to the poor quality of recording. It is important to note that cell impalement with sharp electrodes (i.e., non-patch electrodes) appears, even under the best conditions, to irreparably damage the cell membrane, since input resistances increase nearly 10-fold in recordings with patch electrodes (Blanton et al., 1989), suggesting that less current leak occurs around the electrode tip. Therefore, when dissolved in LiAc or LiCl at the concentrations used here, Lucifer yellow appears to further compromise intracellular recordings with sharp electrodes. An accurate analysis of the electrophysiological properties of recorded neurons was thus impossible in the present experiments using electrodes filled with the lithium salt of Lucifer yellow (see also Tseng and Haberly, 1989; Tasker and Dudek, 1991; Hoffman et al., 1991). It is possible that at lower concentrations and in a potassium salt solution, Lucifer yellow would have less deleterious effects on recorded cells, but this would reduce the intensity of intracellular staining.

Anatomy

The relative ease with which whole-mount visualization could be accomplished (see Methods) and the bright fluorescence of the label (in strongly labeled neurons) made Lucifer yellow an effective intracellular marker for quick morphological screening and photomicrography of recorded cells. The Lucifer yellow label, however, was not permanent, and prolonged exposure to epifluorescent illumination caused photobleaching of the fluorescence. Therefore, further processing of the tissue to render the Lucifer label permanent (e.g., photooxidation; see Maranto, 1982; or immunohistochemical labeling; see Taghert et al., 1982) would be necessary to perform extensive morphological analyses under the microscope.

The stability of the Lucifer yellow label through sectioning and immunohistochemistry was greater than that of the ethidium bromide and slightly lower than that of the biocytin labels. Although 64% of Lucifer-injected cells were recovered, the intensity of staining after immunohistochemical processing tended to be weaker than that of the biocytin labels.

The procedure for the double labeling of neurons injected with Lucifer yellow used in this study employed the HRP-DAB immunolabel. This reaction product obscures Lucifer yellow in the cytoplasmic compartment and requires that the nucleus of the stained cell be cross-sectioned in order that Lucifer yellow and immunolabeling be observable in the same cell (Smithson et al., 1984). It may be possible to simplify this procedure and achieve a higher recovery rate of Lucifer-stained cells by using thicker sections and substituting a fluorescent immunolabel for the HRP-DAB label, although this might decrease sensitivity and increase the incidence of false-positive results (see Smithson et al., 1984). Nevertheless, regardless of the histochemical procedures used, we found the electrical properties of recordings performed with Lucifer yellow electrodes unacceptable for studies requiring rigorous electrophysiological analyses.

Ethidium bromide

A notable limitation of ethidium bromide is its known high carcinogenicity, requiring that particular caution be exercised in its handling.

Electrophysiology

Electrodes containing ethidium bromide were generally characterized by electrical properties that were comparable to those of control electrodes. They allowed stable, relatively noise-free recordings and had no apparent effect on the electrophysiological characteristics of recorded neurons. The only adverse effect of ethidium bromide on intracellular recordings was the tendency occasionally for electrodes to become blocked with sustained current injection.

Anatomy

Labeling with ethidium bromide was restricted to the cell body and proximal dendrites in the whole-mount preparation. We had a low recovery rate (40%) of labeled cells after sectioning and immunohistochemical double-labeling; those cells recovered at this point were very faint, making photographic documentation of results difficult (although see McCarthy and Lawson, 1988). Therefore, the most reliable procedure for combining intracellular staining and immunohistochemical labeling using ethidium bromide requires superimposing profiles of ethidium bromide labeled neurons photographed before immunohistochemistry and immunoreactive profiles obtained after immunohistochemical processing. This procedure is obviously less definitive for determining the immunoreactivity of a recorded neuron than simultaneously observing both the intracellular and the immunohistochemical labels. As is the case with Lucifer yellow labeling (see above), indirect immunofluorescence might be more compatible with ethidium bromide staining than is ABC-HRP immunohistochemistry. Nonetheless, the labile nature of ethidium bromide made it the least anatomically reliable of the three intracellular markers we studied.

Biocytin

Electrophysiology

Biocytin consistently conferred the best electrical properties on recording electrodes; intracellular recordings with biocytin electrodes were nearly identical to those performed with electrodes filled with potassium acetate. Current injection was possible over a wide range of intensities without any significant decrease in the stability of the recording or increase in electrical noise. Confirming earlier observations by Horikawa and Armstrong (1988), we found that biocytin had no perceptible effect on the electrophysiological characteristics of recorded neurons. Biocytin-filled electrodes can be used, therefore, in nearly all intracellular electrophysiological studies, including those requiring technically difficult recordings and rigorous analyses. Indeed, recent studies in hypothalamic (Erickson et al., 1990) and neocortical slices (Tasker et al., 1990) have used biocytin electrodes for single-electrode voltage-clamp experiments.

Anatomy

For the purpose of morphological analysis, we used the HRP-DAB chromogenic reaction in 50–75 μm sections to provide a nearly permanent, Golgi-like intracellular stain. This technique was sensitive enough to label dendrites, dendritic spines and axons. Although not used in the present experiments, higher sensitivity could probably be obtained by nickel or silver intensification of the DAB reaction product. For morphological analysis, this procedure was not as simple as the whole-mount preparation for observing cells labeled with Lucifer yellow or ethidium bromide due to the additional histochemical steps involved.

Double labeling of biocytin-filled neurons and immunoreactive cells was achieved with fluorescent markers. The recovery rate of 70% of biocytin-injected cells after sectioning and immunohistochemistry was the highest of the three intracellular markers. This suggests that biocytin and the fluorescent labels for biocytin are less labile than Lucifer yellow and ethidium bromide. However, the avidin-conjugated AMCA and rhodamine labels for biocytin were applied after tissue sectioning, hence their stability was required for a shorter period of time than that of Lucifer yellow or ethidium bromide. The relatively short excitation wavelength and the lower intensity of fluorescence of AMCA made it an intracellular label which was more suitable for double-labeling (using FITC as the immunolabel)

than the highly fluorescent rhodamine. Unlike AMCA, rhodamine is partially excited by the fluorescein excitation band and it therefore tended to obscure the immunofluorescence of double-labeled cells.

One potential limitation of this double-labeling procedure centers on the use of indirect immunofluorescence, which can be less sensitive than protocols that provide an opaque reaction product. Therefore, although similar patterns of neurophysin immunoreactivity are obtained with both indirect immunofluorescence and ABC-HRP staining, other transmitter systems may require modification of this procedure to increase sensitivity. The main limitation of the biocytin technique employed here was that morphological and immunohistochemical analyses could not be performed on the same cell. However, this was not necessarily a limitation of biocytin as an intracellular marker since, with modifications of this technique, it should be possible to combine the two procedures. Unlike Lucifer yellow or ethidium bromide, sectioning of the slice and histochemical treatment of the injected cell are required to reveal the intracellular biocytin. Although potentially a limitation of the technique because of the added steps involved, this may also be regarded as one of the strengths of this method since it allows the flexibility to choose the histochemical marker best suited for the purposes of a given double-labeling study (Horikawa and Armstrong, 1988). Although we have not attempted to extend this procedure beyond the light microscope level, electron microscopic analysis of injected cells may be possible using a modified version of the technique (e.g., with a reduced Triton-X concentration) and an electron-dense histochemical marker.

We have found that, of the three intracellular markers tested, biocytin provided the best overall combination of electrical and anatomical properties. Limitations of biocytin as an intracellular label (e.g., the lack of a true whole-mount and occasional necessity to reconstruct labeled cells, as well as the increased number of histochemical steps involved) were far outweighed by its electrophysiological and anatomical advantages. Biocytin also has the greatest potential for extending the anatomical study of recorded neurons to include both multiple immunohistochemical labeling and ultrastructural analysis.

Acknowledgments

We would like to thank Drs. K.G. Smithson for helping to initiate immunohistochemical double-labeling experiments in our laboratory, W.E. Armstrong for his invaluable advice on the use of biocytin, J.-P. Wuarin for contributing a labeled cell to this report and J.P. Walsh for his constructive comments on the manuscript. We thank C. Kinney for typing the manuscript, S. Sampogna for technical assistance and S. Belkin and C. Gray for their help in preparing figures. We would also like to acknowledge the generous gifts of antisera from Dr. A.G. Robinson (supported by NIH grant AM16166) and from Drs. M.H. Whitnall and H. Gainer. This work was supported by NINDS fellowships to J.G.T. (NS08049) and N.W.H. (NS08233) and grants from the Air Force Office of Scientific Research (87-0361 and 90-0056) to F.E.D.

References

Aghajanian, G.K. and VanderMaelen, C.P. (1982) Intracellular identification of central noradrenergic and serotonergic neurons by a new double labeling procedure. J. Neurosci., 2: 1786–1792.

Ben-Barak, Y., Russell, J.T., Whitnall, M.H., Ozato, K. and Gainer, H. (1985) Neurophysin in the hypothalamo-neurohypophysial system. I. Production and characterization of monoclonal antibodies. J. Neurosci., 5(1): 81–97.

Berridge, M.J., Downes, C.P. and Hanley, M.R. (1989) Neural and developmental actions of lithium: a unifying hypothesis. Cell, 59: 411–419.

Blanton, M.G., Lo Turco, J.J. and Kriegstein, A.R. (1989) Whole cell recording from neurons in slices of reptilian and mammalian cerebral cortex. J. Neurosci. Methods, 30: 203–210.

Ebstein, R.P., Newman, M.E., Bennett, E.R. and Lerer, B. (1989) Mechanism of lithium and ECS action in affective disorder: modulation of post-receptor second messenger function. In K.F. Tipton and M.B.H. Youdim (Eds.), Biochemical and Pharmacological Aspects of Depression, vol. 3, Topics in Neurochemistry and Neuropharmacology, Taylor & Frances, London, pp. 123–141.

Erickson, K.R., Rønnekleiv, O.K. and Kelly, M.J. (1990) Inward rectification (I_h) in immunocytochemically-identified vasopressin and oxytocin neurons of guinea-pig supraoptic nucleus, J. Neuroendocrinol., 2: 261–265.

Giloh, H. and Sedat, J.W. (1982) Fluorescence microscopy: reduced photobleaching of rhodamine and fluorescein protein conjugates by *n*-propyl gallate, Science, 217: 1252–1255.

Haas, H.L., Schaerer, B. and Vosmansky, M. (1979) A simple perfusion chamber for the study of nervous tissue slices in vitro, J. Neurosci. Methods, 1: 323–325.

Hoffman, N.W., Tasker, J.G. and Dudek, F.E. (1991) Immunohistochemical differentiation of electrophysiologically defined neuronal populations in the region of the rat hypothalamic paraventricular nucleus, J. Comp. Neurol., 307: 405–416.

Horikawa, K. and Armstrong, W.E. (1988) A versatile means of intracellular labeling: injection of biocytin and its detection with avidin conjugates, J. Neurosci. Methods, 25: 1–11.

Kaczmarek, L.K. and Levitan, I.B. (1987) Neuromodulation: The Biochemical Control of Neuronal Excitability, Oxford University Press, Inc., New York, NY.

Kawata, M., Sano, Y., Inenaga, K. and Yamashita, H. (1983) Immunohistochemical identification of Lucifer yellow-labeled neurons in the rat supraoptic nucleus, Histochemistry, 78: 21–26.

Kitai, S.T., Penny, G.R. and Chang, H.T. (1989) Intracellular labeling and immunocytochemistry. In L. Heimer and L. Zaborsky (Eds.), Neuroanatomical Tract-Tracing Methods 2, Plenum Press, New York, NY, pp. 173–199.

Maranto, A.R. (1982) Neuronal mapping: A photooxidation reaction makes Lucifer yellow useful for electron microscopy, Science, 217: 953–955.

Mason, P., Strassman, A. and Maciewicz, R. (1988) Serotonin immunocytochemistry of physiologically characterized raphe magnus neurons, Exp. Brain Res., 73: 1–7.

Mayer, M.L., Crunelli, V. and Kemp, J.A. (1984) Lithium ions increase action potential duration of mammalian neurons, Brain Res., 293: 173–177.

McCarthy, P.W. and Lawson, S.N. (1988) Differential intracellular labelling of identified neurones with two fluorescent dyes, Brain Res. Bull., 20: 261–265.

Rao, G., Barnes, C.A. and McNaughton, B.L. (1986) Intracellular fluorescent staining with carboxyfluorescein: a rapid and reliable method for quantifying dye-coupling in mammalian central nervous system, J. Neurosci. Methods, 16: 251–263.

Reaves, T.A., Jr., Hou-Yu, A., Zimmerman, E.A. and Hayward, J.N. (1983) Supraoptic neurons in the rat hypothalamo-neurohypophysial explant: double-labeling with Lucifer yellow injection and immunocytochemical identification of vasopressin- and neurophysin-containing neuroendocrine cells, Neurosci. Lett., 37: 137–142.

Rønnekleiv, O.K., Loose, M.D., Erickson, K.R. and Kelly, M.J. (1990) A method for immunocytochemical identification of biocytin-labeled neurons following intracellular recording, Biotechniques, 9: 432–438.

Scharfman, H.E., Kunkel, D.D. and Schwartzkroin, P.A. (1989) Intracellular dyes mask immunoreactivity of hippocampal interneurons, Neurosci. Lett., 96: 23–28.

Seif, S.M., Huellmantel, A.B., Platia, M.P., Haluszczak, C. and Robinson, A.G. (1977) Isolation, radioimmunoassay and physiologic secretion of rat neurophysins, Endocrinology, 100: 1317–1326.

Smithson, K.G., Cobbett, P., MacVicar, B.A. and Hatton, G.I. (1984) A reliable method for immunocytochemical identification of Lucifer Yellow injected, peptide-containing mammalian central neurons, J. Neurosci. Methods, 10: 59–69.

Smithson, K.G., MacVicar, B.A. and Hatton, G.I. (1983) Polyethylene glycol embedding: a technique compatible with immunocytochemistry, enzyme histochemistry, histofluorescence and intracellular staining, J. Neurosci. Methods, 7: 27–41.

Sternberger, L.A. (1974) Immunocytochemistry, Prentice-Hall, Englewood Cliffs, NJ.

Stewart, W.W. (1978) Functional connections between cells as revealed by dye-coupling with a highly fluorescent naphthalimide tracer, Cell, 14: 741–759.

Taghert, P.H., Bastiani, M.J., Ho, R.K. and Goodman, C.S. (1982) Guidance of pioneer growth cones: filopodial contacts and coupling revealed with an antibody to Lucifer yellow, Dev. Biol., 94: 391–399.

Tasker, J.G. and Dudek, F.E. (1991) Electrophysiological properties of neurones in the region of the paraventricular nucleus in slices of rat hypothalamus, J. Physiol., 434: 271–293.

Tasker, J.G., Obenaus, A., Peacock, W.J. and Dudek (1990) Analysis of synaptic inhibition in neocortical slices from pediatric patients with intractable epilepsy, Epilepsia, 31: 691.

Tseng, G. and Haberly, L.B. (1989) Deep neurons in piriform cortex. II. Membrane properties that underlie unusual synaptic responses, J. Neurophysiol., 62: 386–400.

Whitnall, M.H., Key, S., Ben-Barak, Y., Ozato, K. and Gainer, H. (1985) Neurophysin in the hypothalamo-neurohypophysial system. II. Immunocytochemical studies of the ontogeny of oxytocinergic and vasopressinergic neurons, J. Neurosci., 5(1): 98–109.

THE JOURNAL OF COMPARATIVE NEUROLOGY 307:405–416 (1991)

Immunohistochemical Differentiation of Electrophysiologically Defined Neuronal Populations in the Region of the Rat Hypothalamic Paraventricular Nucleus

N.W. HOFFMAN, J.G. TASKER, AND F.E. DUDEK
Mental Retardation Research Center, UCLA Center for the Health Sciences, Los Angeles, California 90024

ABSTRACT

Intracellular recording and labeling were combined with neurophysin immunohistochemistry to study neurons in the paraventricular nucleus region of the rat hypothalamus. Neuronal membrane properties were examined in hypothalamic slices, and cells were labeled by injecting biocytin or Lucifer yellow. Slices were then embedded, sectioned, and immunohistochemically processed for neurophysin. Immunoreactivity patterns, and in some cases counterstaining, enabled determinations of the cytoarchitectonic positions of recorded cells to be made. Recorded cells were divided into three types according to their electrophysiological characteristics. The first type lacked low-threshold Ca^{2+} spikes and displayed linear current-voltage relations, a short time constant, and evidence for an A current. These were relatively large cells that were typically immunoreactive for neurophysin and were situated near other neurophysin-positive neurons. The second type had relatively small low-threshold potentials that did not generate bursts of Na^+ spikes. These cells had heterogeneous current-voltage relations and intermediate time constants. They did not label for neurophysin, and most were located in the parvicellular subregion of the paraventricular nucleus. The third type had large low-threshold Ca^{2+} spikes that generated bursts of Na^+ spikes, and these cells had nonlinear current-voltage relations and long time constants. These neurons were dorsal or dorsolateral to the paraventricular nucleus and were not immunoreactive for neurophysin. These results indicate that paraventricular magnocellular neurons lack low-threshold potentials, whereas paraventricular parvicellular neurons display low-threshold potentials that generate one or two action potentials. Neurons that fire spike bursts from low-threshold potentials are adjacent to the paraventricular nucleus, confirming earlier reports.

Key words: magnocellular neurons, parvicellular neurons, intracellular recording, neurophysin, oxytocin, vasopressin

The hypothalamic paraventricular nucleus (PVN) is an important central neuroendocrine regulatory region. It, along with the supraoptic nucleus (SON), contains magnocellular neurosecretory neurons that synthesize and release into the general circulation the hormones, oxytocin, and vasopressin (Swaab et al., '75; Vandesande and Dierickx, '75; see Silverman and Pickard, '83). Among other important physiological functions, these peptidergic substances regulate milk ejection and fluid-volume homeostasis, respectively. Vasopressin and oxytocin are both packaged in secretory granules along with their respective neurophysins, fragments of the common precursor molecules from which the hormone peptide sequences are derived (see Silverman and Pickard, '83; Sofroniew, '85 for reviews). Vasopressin, oxytocin, and associated neurophysins are secreted from terminals of axons that project from the PVN and SON to the neural lobe of the pituitary gland.

Unlike the SON, which only contains magnocellular neuroendocrine cells, the PVN is a heterogeneous aggregate of neuronal types (Armstrong et al., '80; Swanson and Kuypers, '80; van den Pol, '82; Swanson and Sawchenko, '83). Magnocellular neurons primarily reside in specific PVN subregions. Those located in the posterior magnocellular subdivision (Swanson and Kuypers, '80; Swanson and Sawchenko, '83), also known as the medial and lateral magnocellular subdivisions (Armstrong et al., '80), are neurosecretory. The posterior magnocellular subdivision is the classic site of neurosecretory PVN cells that project to

Accepted January 25, 1991.

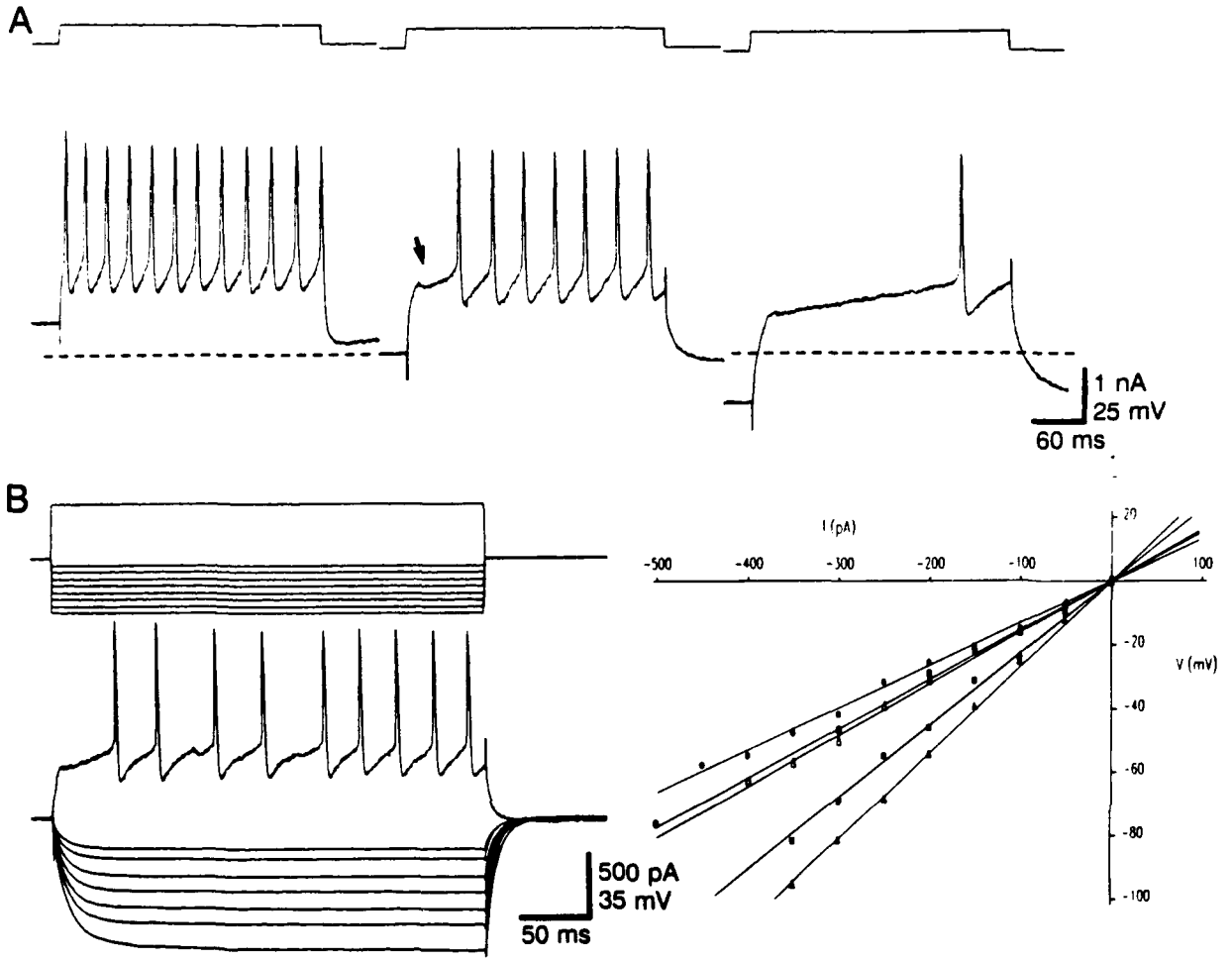

Fig. 1. Main electrical properties of non-LTS (type-I) neurons. **A:** When activated from resting membrane potential with a depolarizing current pulse, this cell showed a "notch" in its charging curve (arrow) and a delayed onset of action-potential generation (middle). The same depolarizing current pulse caused tonic firing when the cell was held depolarized (left) and augmented the delay to spike generation when it was hyperpolarized with direct current (right). Hyperpolarization did not reveal a low-threshold potential. Dashed lines represent resting membrane potential in this and the following figures. **B:** Current-voltage (I-V) relations. Intracellular injection of negative current pulses of increasing intensity caused graded voltage deflections. Positive current injection caused a spike train with a delayed onset (recordings in A and B are from different cells). Negative current and voltage traces in this and the following figures are averaged (n = 6–12). Top traces are injected current and the bottom traces voltage responses in this and the following figures. The I-V relations of non-LTS neurons were linear, as shown by I-V plots obtained from this and four other representative non-LTS neurons (right).

polarizing current pulses (0.5–2.5 nA, 250 ms, 2 Hz, 5–15 minutes). Slices were immersion-fixed overnight at 5°C in 4% paraformaldehyde solubilized in 0.1 M sodium cacodylate buffer. Slices were then dehydrated in an ascending series of ethanol concentrations (50, 75, 95, and 100%) and cleared in methyl salicylate. Whole-mount photomicrographs of Lucifer yellow-filled neurons were taken under epifluorescence using Nikon filters (excitation filter: B/absorption filter: 515W), and then slices were rehydrated (100, 95, 75, and 50% ethanols) and post-fixed in chilled (5°C) Bouin's solution for 2 hours. Thereafter they were rinsed in 0.05 M Tris-buffered saline (TBS), dehydrated in ascending ethanols, and embedded in polyethylene glycol (PEG, MW = 1450, Sigma Chemical Co., St. Louis, MO), as previously described (Smithson et al., '83, '84).

In other cases (n = 11) biocytin was iontophoresed with negative current pulses into recorded neurons (Horikawa and Armstrong, '88). These cells were not examined in whole mount; rather, tissue slices were fixed as described above and embedded in PEG. All PEG-embedded slices were sectioned at 5 or 10 μm on a rotary microtome for neurophysin immunohistochemistry. This was done to ensure adequate antibody penetration to recorded neurons (i.e., to reduce the possibility of false-negative determinations) and to reduce the likelihood of false-positive judgments due to immunoreactive neurons situated above or below the recorded cells. After sectioning, the tissue was rehydrated in descending ethanol concentrations (100, 95, 75, and 50%) to TBS. Biocytin-injected cells were labeled by incubating the sections in avidin conjugated with either 7-amino-4-methyl-coumarin-3-acetic acid (AMCA) or rhodamine (Vector Laboratories, Burlingame, CA). Both markers were diluted (1:200) in 0.1 M phosphate-buffered saline (PBS) containing 0.5% Triton X. Sections were scanned under an epifluorescence microscope equipped with the appropriate filter combinations (for avidin-

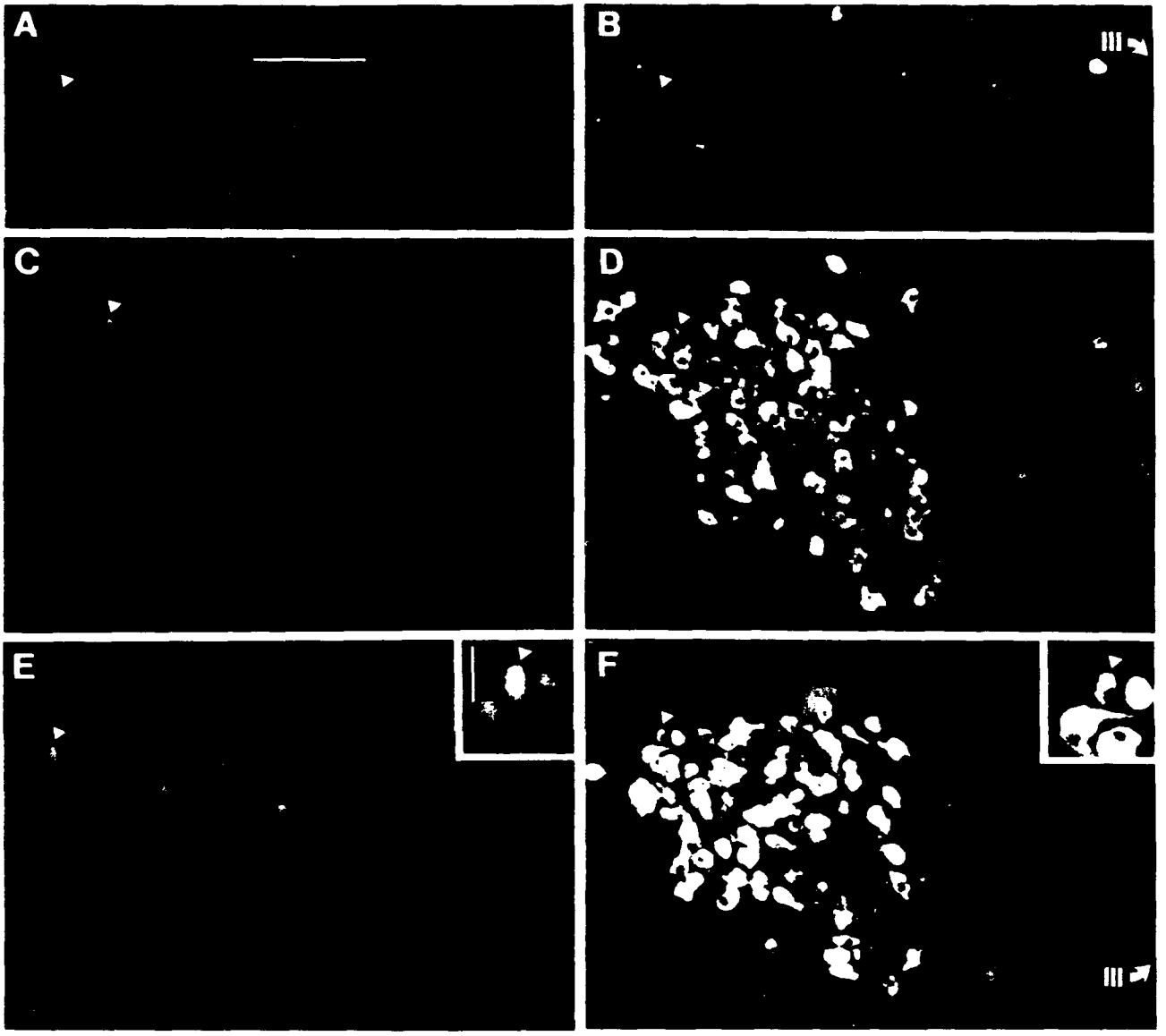

Fig. 2. Most rat LVS neurons were immunoreactive for both biocytin (PVN neuron that was recorded intracellularly injected with biocytin and immunohistochemically labeled for both). Photomicrographs are of 20-μm sections. Arrowheads point to the blue AMCA biocytin-labeled cell and arrows point to the yellow-green neurophysin immunoreactivity. **A:** The biocytin-filled neuron (AMCA-labeled neuron is also present in neurophysin immunohistochemistry). Calibration bar = 100 μm, and applies to all micrographs except insets. **B:** At this [illegible] was not visible with fluorescein filters (arrowhead [illegible] showing that AMCA is not visible under the excitation light band for fluorescein. After immunohistochemistry the neuron was visible under both AMCA (**C**) and fluorescein filter combinations (**D**) indicating that it was labeled for both biocytin and neurophysin. Part of its soma in an adjacent section was likewise double labeled for biocytin (**E**) and neurophysin (**F**) (insets show this portion of the soma at higher magnification; calibration bar = 25 μm), suggesting that this neuron was vasopressinergic or oxytocinergic. Note that under the AMCA excitation band, fluorescein is weakly excited, but its faint green color is easily distinguishable from the stronger blue fluorescence of AMCA (C and E). III denotes third ventricle.

conjugated AMCA, UV 420K, for avidin-conjugated rhodamine, G 580W, for Lucifer yellow, B 515W, to detect the presence of labeled neurons. Labeled cells were typically photographed at this time.

Neurophysin immunohistochemistry

Sections containing labeled cell bodies and processes, as well as immediately adjacent sections, were incubated in an antiserum generated in rabbit against both oxytocin- and vasopressin-associated neurophysins of the rat. This general neurophysin antiserum (7 17 73) was kindly provided by Dr. A. Robinson of the University of Pittsburgh and has been characterized by radioimmunoassay (Sofroniew et al., 1977). In our hands, immunoreactive somata were selectively concentrated in the SON, suprachiasmatic nucleus, magnocellular portions of the PVN, and accessory magnocellular regions. This distribution has been described by others (see Sofroniew, 1985) and provides a further anatomical control

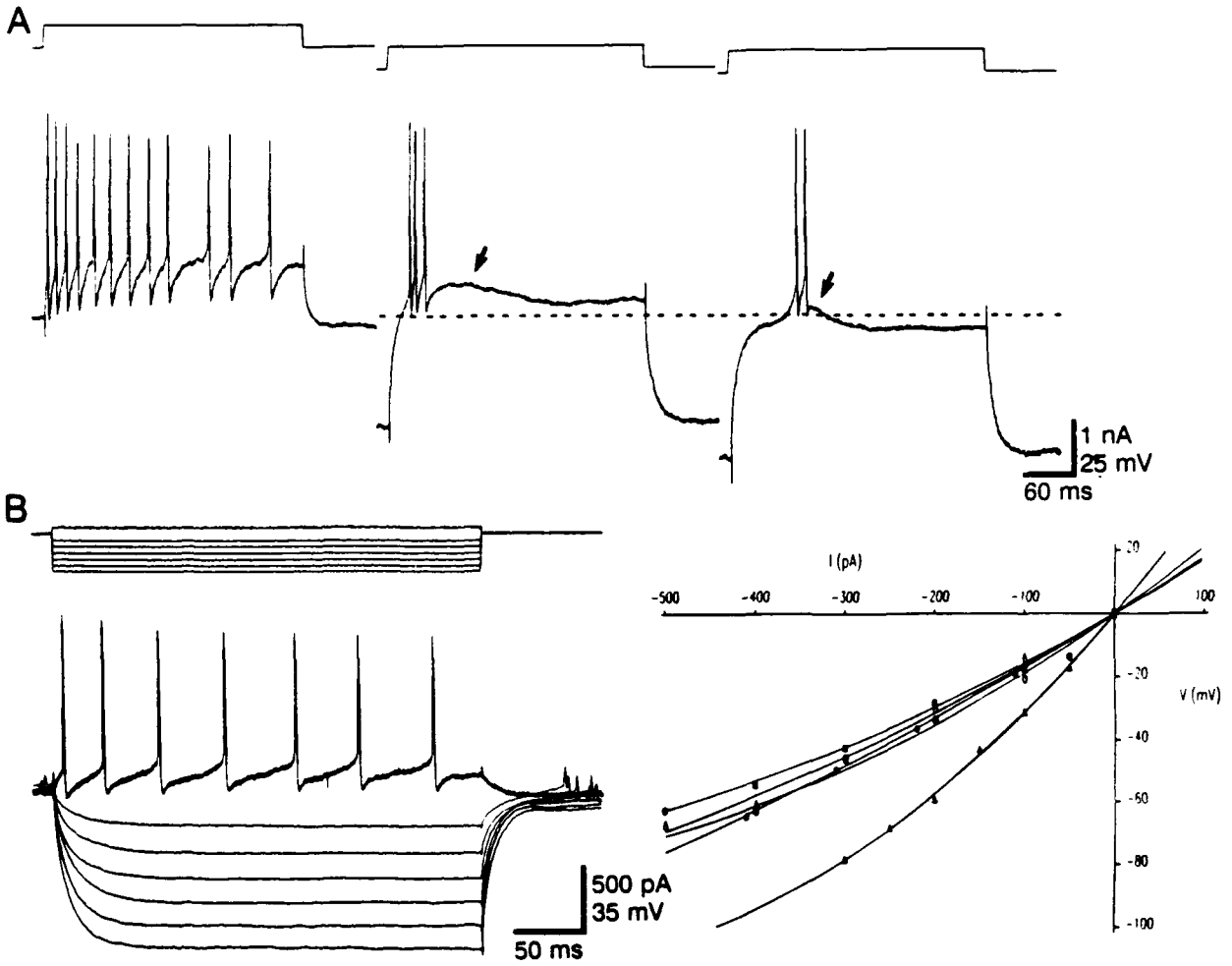

Fig. 3. Electrophysiological characteristics of non-bursting LTS (type-II) neurons. **A:** Activation of a representative cell with a positive current pulse caused tonic firing of action potentials at resting membrane potential (left) and the generation of a progressively deinactivated low-threshold potential (arrows) as the cell was hyperpolarized with continuous intracellular injection of negative current (middle and right). **B:** Current-voltage (I-V) relations of non-bursting LTS neurons. A representative non-bursting LTS neuron (left) showed slight inward rectification with large negative voltage deflections. The I-V relations of cells of this category varied from linear to weakly curvilinear, as shown by I-V plots from this and four other non-bursting LTS neurons (right).

for antiserum specificity. Replacement of the primary antiserum with the same dilution of nonimmunized rabbit serum resulted in a complete absence of immunostaining.

Sections containing cells that were injected with biocytin and labeled with avidin-conjugated AMCA or avidin-conjugated rhodamine were placed in 10% normal goat serum in PBS for 30 minutes. Next they were incubated in the primary antiserum (1:200 in PBS + 1% normal goat serum and 0.05% Na azide) overnight at 5°C and then for an additional 2 hours at room temperature. Following PBS rinses the sections were incubated for 1 hour in goat anti-rabbit IgG conjugated with fluorescein isothiocyanate (FITC, Boehringer Mannheim, Indianapolis, IN) (1:50 in PBS). Sections were again rinsed in PBS then mounted and coverslipped with glycerol:PBS (1:4), typically with the antioxidant, N-propyl gallate (1%) added to the mounting medium to retard photobleaching (Horikawa and Armstrong, '88; Rao et al., '86). Sections were then examined under epifluorescence microscopy for the presence of both neurophysin immunoreactivity and biocytin labeling, using the B/515W filter combination for FITC and the appropriate filter combinations for AMCA and rhodamine (see above).

Cells injected with Lucifer yellow were processed as described by Smithson et al. ('84). Briefly, slices were incubated in a 1:2,000 concentration of primary antiserum, as described above, and neurophysin immunohistochemistry was performed according to the avidin-biotinylated horseradish peroxidase (ABC) procedure (Vectastain-elite kit, Vector Laboratories, Burlingame, CA). An opaque, brown reaction product was formed from the chromogen, diaminobenzidine-tetrahydrochloric acid (Sigma Chemical Co., St. Louis, MO), via the glucose oxidase procedure of Smithson et al. ('84). Sections were mounted and coverslipped with methyl salicylate then microscopically examined and photographed under epifluorescence (B/515W) and bright-field illumination.

In the course of this investigation, we found that the biocytin/neurophysin double-labeling procedure was more useful than that combining Lucifer yellow with opaque

Fig. 4. None of the non-bursting (type-II) LTS neurons in PVN displayed neurophysin immunoreactivity. **A,B:** Photomicrographs of a 10 μm section under filters for the AMCA biocytin label (blue). A non-bursting LTS neuron filled with biocytin is shown before (A) and after (B) neurophysin immunohistochemistry. **C:** The same section under the fluorescein filter combination for the neurophysin immunolabel (yellow-green). After immunohistochemistry, the cell was not visible under fluorescein filters (arrowhead indicates position of soma). Note that this neuron was situated medial to most neurophysin labeled neurons in this portion of the PVN. Calibration bar = 100 μm; III denotes third ventricle.

staining of neurophysin (see Tasker et al., in press). Thus, the biocytin intracellular marker was preferentially employed. The avidin-AMCA label for biocytin was not visible under FITC filters while the avidin-rhodamine label was; therefore, the avidin-AMCA biocytin label was used more often than the avidin-rhodamine label ($n = 7$ vs. $n = 4$). Note that immunoreactivity was detectable in one rhodamine-labeled neuron and that equal numbers ($n = 2$) of rhodamine-labeled non-LTS and non-bursting LTS neurons were included in statistical analyses of PVN cell types (below). A detailed description of the biocytin procedure and comparison of all the procedures used in this study is provided elsewhere (Tasker et al., in press).

The pattern of immunoreactivity was usually sufficient for determining whether or not a recorded and labeled neuron was contained in the PVN. When neuronal position was ambiguous on the basis of neurophysin immunoreactivity, nissl preparations were made with either ethidium bromide (Schmued et al., '82) to counterstain sections containing biocytin-filled, immunofluorescence-labeled neurons or cresyl violet to counterstain sections with Lucifer yellow-filled, diaminobenzidine-immunostained cells.

Statistical analyses

Whether or not the three electrophysiologically defined cell categories differ in their expression of neurophysin was evaluated statistically, using Fisher's exact contingency table test (see Krauth, '88). Whether non-LTS, non-bursting LTS and bursting LTS neurons differ in size was tested by submitting diameter measurements (longest soma axis) of labeled neurons to analysis of variance followed by Newman-Keuls range tests. Statistical type-I error probabilities less than 0.05 were taken to indicate statistical significance.

RESULTS

Three populations of hypothalamic neurons in the PVN region were identified on the basis of their electrophysiological properties. These electrophysiologically defined categories were also differentiated on the basis of neurophysin immunoreactivity, soma size, and neuronal location with respect to the PVN. Non-LTS neurons conformed to the previous type-I classification (Tasker and Dudek, '91), since they lacked low-threshold potentials, had linear I-V relations and showed evidence for a pronounced A current (Fig. 1). Four of five non-LTS neurons, all situated in the PVN, were immunoreactive for neurophysin (Fig. 2). Two neurons with type-I electrophysiological characteristics were also recorded in the SON. One of these cells was histochemically processed and found to be neurophysin positive. Therefore, a total of five of six immunohistochemically tested hypothalamic neurons with non-LTS, type-I electrical properties stained positively for neurophysin.

Another PVN neuronal population was composed of non-bursting LTS cells; these conformed with type-II electrophysiological criteria (Tasker and Dudek, '91) by having relatively small low-threshold potentials that usually generated only one or two action potentials (Fig. 3A). Also consistent with this classification, non-bursting LTS cells were more heterogeneous in their electrophysiological properties than the other two cell types. Thus non-bursting LTS neurons displayed I-V relations that were linear or weakly nonlinear (Fig. 3B). Of nine non-bursting LTS

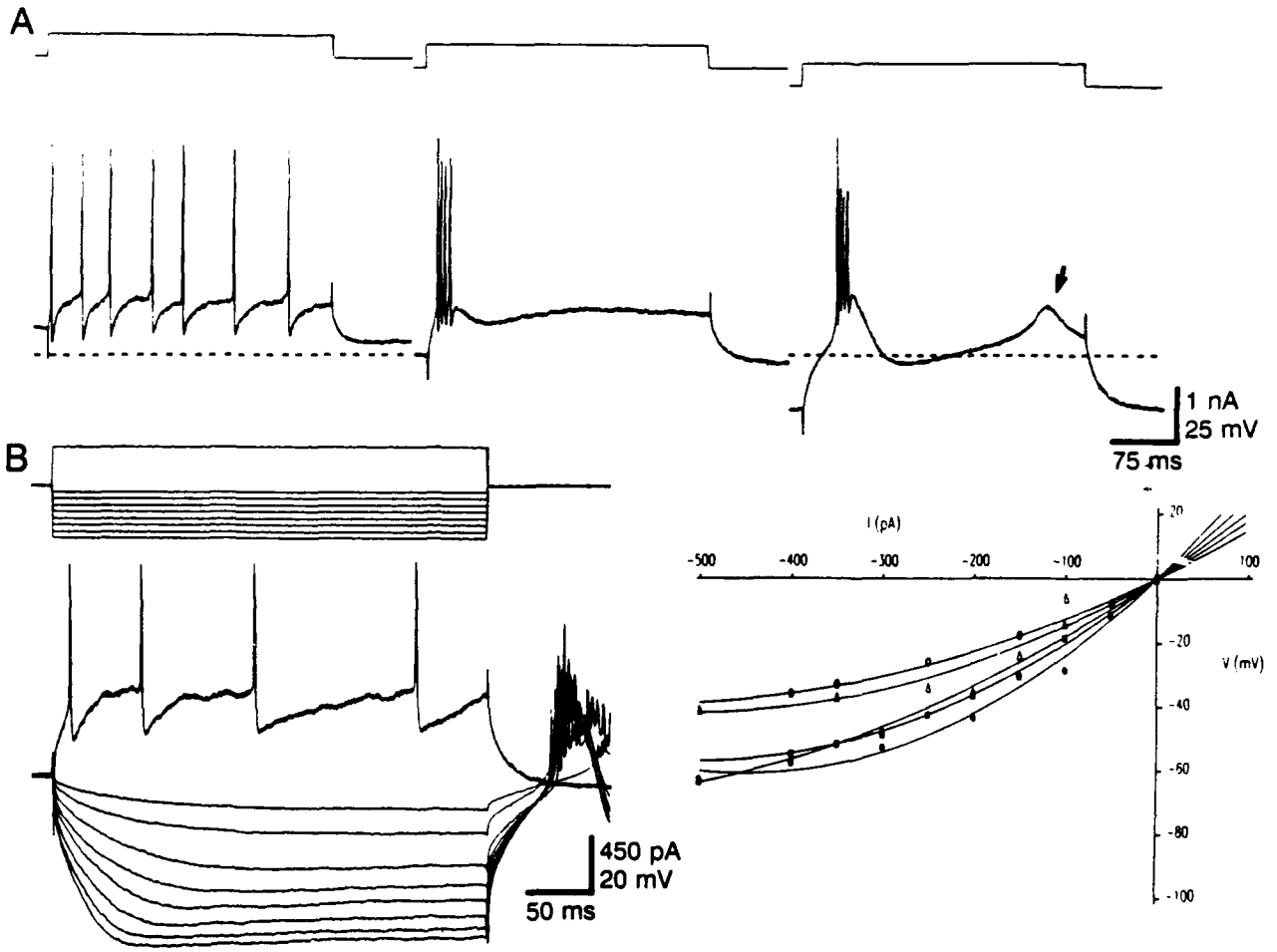

Fig. 5. Electrophysiology of bursting LTS (type-III) neurons. **A:** Depicted is a cell that showed partial deinactivation of the low-threshold conductance at resting membrane potential and generated a small burst in response to a depolarizing current pulse (middle). The low-threshold conductance was inactivated and the cell responded to the same pulse with tonic firing of action potentials when it was held at a depolarized membrane potential with positive direct current injection (left). The low-threshold conductance was fully deinactivated and generated a robust low-threshold potential and a burst of action potentials when the cell was depolarized from a more hyperpolarized membrane potential (right). The generation of a second low-threshold potential (arrow), subthreshold for action-potential generation, suggested an oscillatory behavior of the membrane potential. **B:** Plots of I-V relations of bursting LTS neurons. The low-threshold conductance was inactivated at resting membrane potential in this cell (left). It and four other representative bursting LTS neurons had I-V plots that were usually very curvilinear (right).

neurons recorded in this study, none stained positively for neurophysin (Fig. 4).

The third type of neuron encountered in this region conformed with type-III criteria (Tasker and Dudek, '91). These were referred to as bursting LTS cells since they invariably had large LTS potentials that generated bursts of three or more Na^+ spikes (Fig. 5A). They also displayed strong inward rectification in response to hyperpolarizing current pulses (Fig. 5B). None of the five bursting LTS neurons was immunoreactive for neurophysin (Fig. 6).

Figure 7 shows other salient electrophysiological properties of the three cell types. The anode-break response of each type usually differed markedly. Non-LTS neurons displayed a delayed return to baseline that suggested activation of an A current. Non-bursting LTS cells typically generated one or two anode-break spikes, or occasionally a low-threshold potential that was subthreshold for Na^+ spike generation. Bursting LTS neurons generated obvious low-threshold potentials and robust bursts of anode-break spikes (Fig. 7A). The membrane time constants were also calculated for most cells that were analyzed anatomically in this study. Lucifer-yellow recordings were not included in these calculations due to the adverse effects of the dye on the electrophysiological properties of the recorded cells (Tasker et al., in press), resulting in relatively small sample sizes. Nevertheless, the time constant values were consistent with those described by Tasker and Dudek ('91) and differed significantly among the three groups ($P < 0.05$, analysis of variance). Non-LTS (type-I) neurons displayed a short time constant (10.3 ± 1.4 ms, n = 3), that of non-bursting LTS (type-II) neurons was of intermediate duration (17.4 ± 2.3 ms, n = 6), and bursting LTS (type-III) neurons had a relatively long time constant (34.8 ± 10.5 ms, n = 3, Fig. 7B).

As indicated above, 80% of the non-LTS neurons recorded in the PVN stained positively for neurophysin, whereas 100% of the non-bursting LTS and bursting LTS

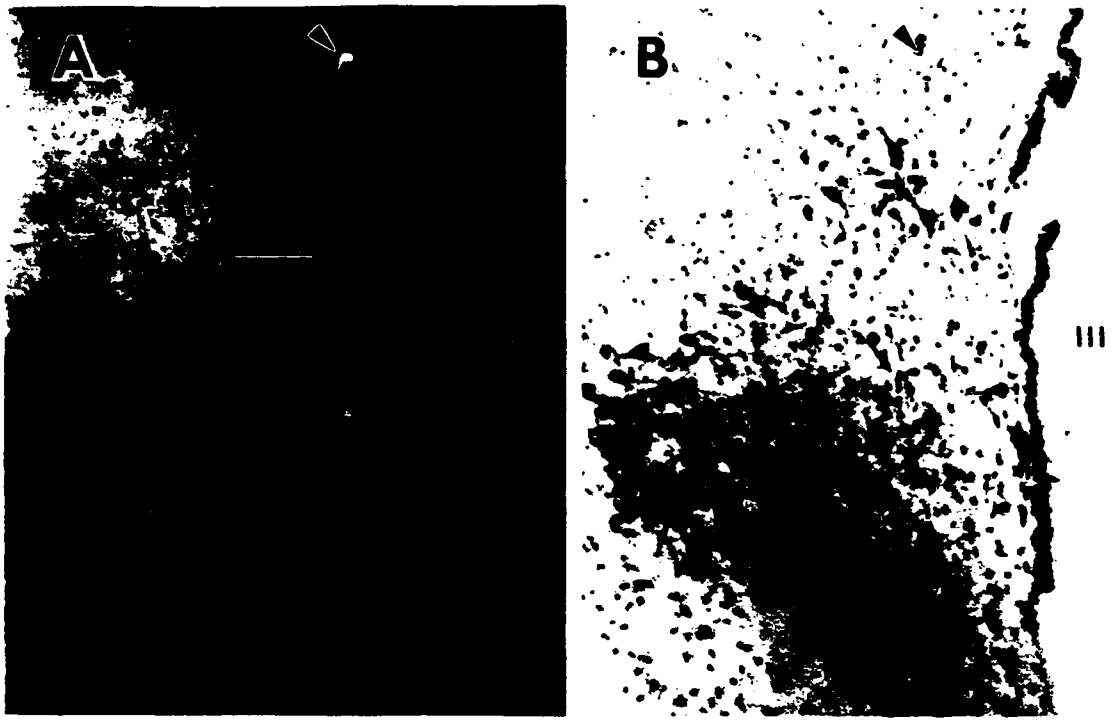

Fig. 6. Bursting LTS (type-III) neurons did not stain for neurophysin and all resided near the dorsal or dorsolateral border of the paraventricular nucleus. **A:** Combined bright-field/epifluorescence photomicrograph of a 5 μm section containing a bursting LTS neuron that was injected with Lucifer yellow (arrowhead). This cell was situated dorsal to the neurophysin-expressing neurons of the PVN. **B:** A bright-field photomicrograph of the same section showing the position of the injected cell (arrowhead), which appears outside of the paraventricular nucleus, as indicated by the distribution of neurophysin-stained neurons and cresyl-violet counterstaining. Calibration bar = 100 μm; III denotes third ventricle.

cells did not. This difference in neurophysin immunoreactivity between the cell categories was statistically significant ($P < 0.005$). Average soma diameter (longest axis) also differed significantly among the cell types ($P < 0.01$). This was due to the large size of the non-LTS neurons in comparison with the smaller non-bursting LTS and bursting LTS cells ($P < 0.05$, respectively). No statistically significant difference in soma size was observed between non-bursting LTS and bursting LTS neurons (Fig. 8).

The approximate cytoarchitectonic locations of the recorded neurons in and adjacent to the PVN were determined and compared schematically (Fig. 9). Four of five non-LTS neurons resided in the posterior magnocellular region of the PVN. One neurophysin-positive non-LTS neuron, which was also magnocellular (longest axis diameter = 30 μm), was observed on a partial tissue section that included much of but not the entire PVN. Based on the apparent PVN shape, as indicated by the distribution of other neurophysin- and nissl-stained magnocellular neurons, we determined that the cell was contained in the PVN portion just caudal to the posterior magnocellular subdivision. Of eight non-bursting LTS neurons six were clearly in PVN parvicellular regions, whereas one was situated near the ventral border and another near the lateral border of the nucleus. Of five bursting LTS neurons three were beyond the dorsal PVN border, and two resided near the dorsomedial border of the nucleus.

DISCUSSION

Findings of this study show that in the region of the PVN, neurons that can be differentiated according to their electrophysiological properties (Tasker and Dudek, '91) are also anatomically distinct. Neurons in the PVN lacking detectable LTS potentials (non-LTS neurons) were typically neurophysin-positive and larger than cells of the other two categories. This size characteristic held for the single non-LTS neuron that did not stain positively for neurophysin, its soma diameter (longest axis = 25 μm) being well within the range of other non-LTS cells measured in this study. Most of the non-LTS neurons, including the one not labeled for neurophysin, were recorded in the area generally described by Swanson and Kuypers ('80) as the posterior magnocellular subdivision and compartmentalized by Armstrong et al. ('80) as the medial and lateral magnocellular subdivisions of the PVN. Although some neurons of this area terminate in regions such as the external lamina of the median eminence for vasopressin or oxytocin release (Vandesande et al., '77; Weigand and Price, '80), most project to the neurohypophysis and thus constitute the well-established magnocellular neuroendocrine portion of the PVN. Therefore, given the likelihood of less than 100% antigen-detection sensitivity and the preponderance of the neurohypophysis-projecting cells in this portion of the PVN, it is probably this set of neurosecretory magnocellular neurons that was sampled.

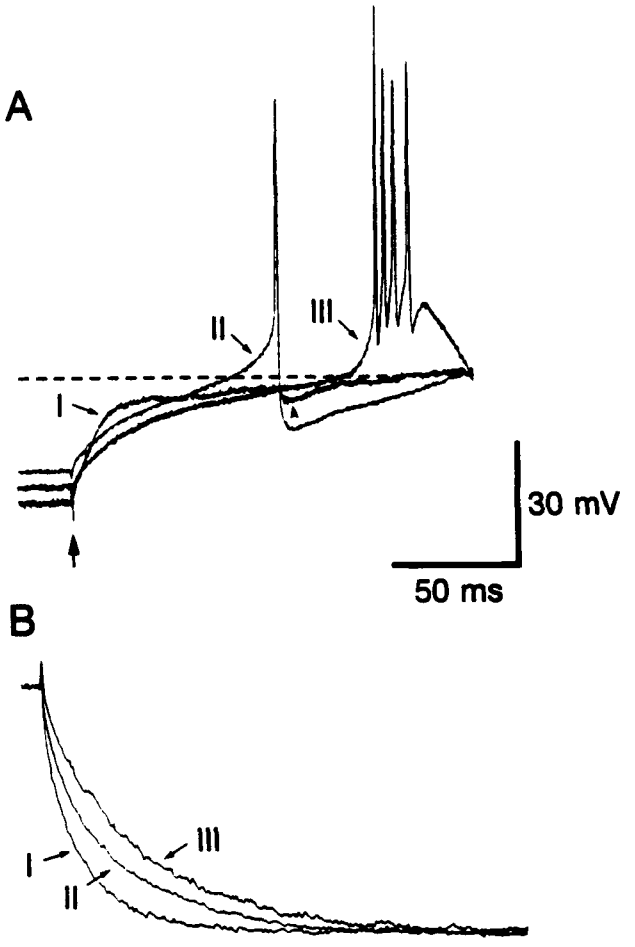

Fig. 7. Other electrophysiological characteristics of non-LTS (type-I), non-bursting LTS (type-II) and bursting LTS (type-III) neurons. **A:** Anodal break responses to the offset of a hyperpolarizing current pulse (large arrow). Following hyperpolarization non-LTS cells showed a delayed return of the membrane potential to baseline (dashed line), suggesting activation of an A current (I). Spontaneous IPSPs (arrowhead) were sometimes observed. Non-bursting LTS neurons frequently generated a single spike followed by a hyperpolarizing afterpotential that masked the small low-threshold potential (II). Bursting LTS neurons often responded to hyperpolarization with an anode-break low-threshold potential and a burst of action potentials (III), the amplitude of which depended on the duration and intensity of the preceding hyperpolarization. **B:** Membrane time constants. Non-LTS (I), nonbursting LTS (II), and bursting LTS (III) had relatively short, intermediate, and long time constants, respectively. Each trace is the charging phase of the membrane potential in response to 100 or 150 pA negative current pulses delivered in the linear range of each cell's I-V curve. The three voltage responses are averages of 5–10 sweeps and are normalized for comparative purposes.

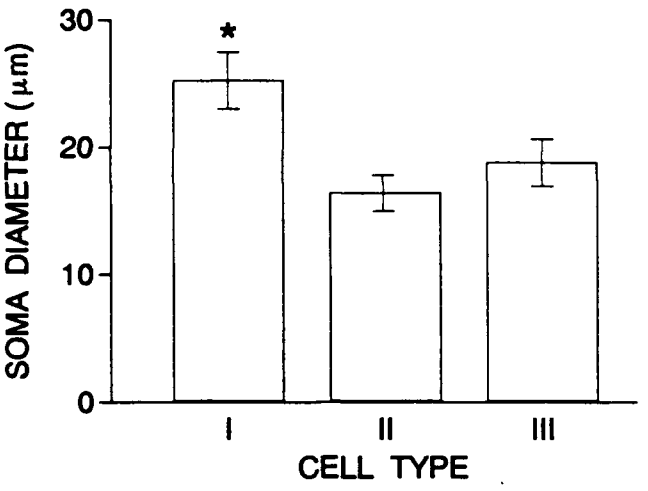

Fig. 8. A comparison of the soma diameters (longest axis) of non-LTS (type-I), non-bursting LTS (type-II), and bursting LTS (type-III) neurons in the region of the PVN. As illustrated in the above bar graph, non-LTS neurons (I) (n = 5) were larger than either non-bursting LTS (II) (n = 8) or bursting LTS (III) (n = 5) neurons, a size difference that was statistically significant in both cases (analysis of variance followed by Newman-Keuls range tests). Non-bursting LTS neurons (II) did not significantly differ from bursting LTS cells (III) in size. Mean (±SEM) soma diameters (in μm) of non-LTS, non-bursting LTS and bursting LTS neurons were 25 ± 2.2, 16 ± 1.4, and 19 ± 1.9, respectively. $^*P \leq 0.05$.

All non-LTS neurons were of the previously defined type-I neuronal category (Tasker and Dudek, '91). Such properties as action potential waveform, linear current-voltage relations and apparent A current are expressed by PVN neurons of this category and are shared by SON cells (Mason, '83; Mason and Leng, '84; Andrew and Dudek, '83, '84a,b; Bourque and Renaud, '85; Bourque, '86; Randle et al., '86). In the present study two SON neurons were recorded, one of which was histochemically processed and found to be neurophysin positive. Both cells also lacked LTS potentials and conformed with the other electrophysiological characteristics of the type-I PVN classification (Tasker and Dudek, '91). Therefore, this classification may pertain to magnocellular neurons in both the PVN and SON neurosecretory regions of the hypothalamus.

One non-LTS neuron that was immunoreactive for neurophysin appeared to reside in a portion of the PVN just caudal to the posterior magnocellular subdivision, a region described by Armstrong et al. ('80) as the posterior subnucleus of the PVN. This subdivision contains some neurosecretory cells but many other neurons that project to preganglionic autonomic cell groups in the brain stem and spinal cord (Saper et al., '76; Hosoya and Matsushita, '79; Armstrong et al., '80; Swanson and Sawchenko, '83). Many of these neurons also stain positively for neurophysin (Armstrong et al., '80). The size of the posterior subnuclear non-LTS cell recorded in the present study (longest axis = 30 μm) was clearly within the range of other non-LTS neurons and indicates that it was magnocellular. Some authors have reported that the set of oxytocin- and vasopressin-labeled neurons that project to autonomic centers consists of smaller neurons (Hosoya and Matsushita, '79; Swanson and Kuypers, '80; see Swanson and Sawchenko, '83; Rho and Swanson, '89), suggesting that this neurophysin-positive, non-LTS neuron was instead neurosecretory. However, Armstrong et al. ('80) noted that many brain stem-projecting cells in the posterior subnucleus are of comparable size to magnocellular neurons situated elsewhere in the PVN. Thus, while our findings suggest that neurosecretory magnocellular neurons display type-I (non-LTS) electrophysiological properties, the possibility that other large PVN neurons that express neurophysin do so as well cannot be excluded. Future studies could combine

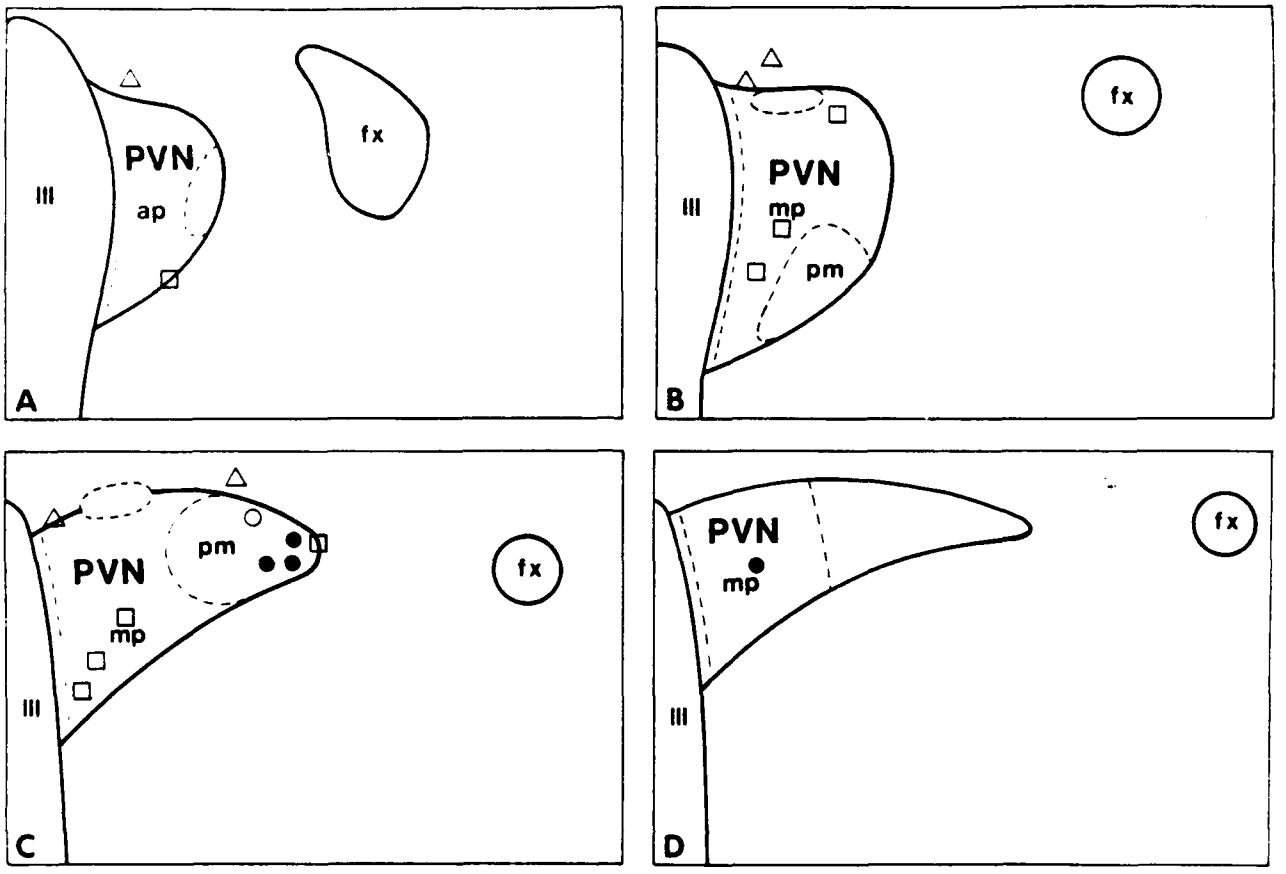

Fig. 9. Relative positions with respect to the paraventricular nucleus (PVN) of non-LTS (type-I), non-bursting LTS (type-II), and bursting LTS (type-III) neurons. **A–D:** A rostral-caudal progression through the PVN. Filled symbols indicate recorded and intracellularly labeled cells that stained positively for neurophysin, and open symbols indicate those that did not. Four of five non-LTS neurons (circles) recorded in the PVN resided in the posterior magnocellular su region (pm). Six of eight non-bursting LTS neurons (squares) were in the medial parvicellular subregion (mp), and one was near the ventral and another the lateral boundary of the PVN. All of the five bursting LTS neurons (triangles) were near or beyond the dorsal or dorsolateral boundary of the PVN. ap, anterior parvicellular subregion; fx, fornix; III, third ventricle.

retrograde labeling with intracellular recording and dye injection to address this question more extensively.

Neurons with LTS potentials that only generated one or two action potentials (non-bursting LTS cells) were identified in the present study; these cells also displayed other electrophysiological properties characteristic of the type-II classification (Tasker and Dudek, '91). Non-bursting LTS (type-II) cells were generally smaller than non-LTS (type-I) neurons and were never immunoreactive for neurophysin. Although the interpretation of negative immunohistochemical data is often problematic, our use of 5 or 10 μm sections reduced the possibility that poor antibody penetration contributed to these cells not staining for neurophysin. Most non-bursting LTS neurons clearly were situated in the PVN, for the most part in the medial parvicellular subregion. These findings support the hypothesis that non-bursting LTS neurons are parvicellular, which suggests that at least some may synthesize pituitary releasing factors. Therefore, the secretory actions of both non-LTS and non-bursting LTS neurons in the PVN may in part determine or regulate hormonal output of the pituitary, the former by directly secreting hormonal substances from the neural lobe and the latter by secreting releasing factors into the hypothalamo-hypophyseal portal circulation. This possibility could also be addressed by combining the techniques of intracellular recording, dye injection, and retrograde labeling.

Although having characteristic low-threshold potentials, it should be noted that the non-bursting LTS cells were more heterogeneous, electrophysiologically, than were the other two PVN cell types examined. In addition to showing variability in the size and appearance of the low-threshold potentials, which supported zero, one, or two Na^+ spikes, non-bursting LTS neurons had both rectifying and non-rectifying I-V relations. It is therefore possible that with further investigation, this class of cells will be found to form separate electrophysiological and functional categories corresponding to different populations of parvicellular neurons. It is also noteworthy that two non-bursting LTS neurons were respectively positioned near the ventral and the lateral PVN borders. These cells could not be definitively categorized as residing either within or outside of the nucleus, and thus it is possible that non-bursting, type-II electrical properties are not exclusive to parvicellular neurons situated in the PVN.

The final category, bursting LTS-neurons, consisted of cells with large LTS potentials that generated robust bursts of Na^+ spikes. These neurons conformed to the type-III

category (Tasker and Dudek, '91), and on the basis of their LTS potentials, burst firing, and lack of staining for neurophysin, they appear to be of the same type of peri-PVN LTS neuron first described by Poulain and Carette ('87) in guinea pig. Thus the bursting LTS neurons that we recorded and labeled were all neurophysin-negative and occupied positions adjacent to the PVN. They had somata similar in size to those of non-bursting LTS cells located in parvicellular PVN subregions. Unlike the earlier report (Poulain and Carette, '87), however, where identified LTS neurons had linear I-V relations and were lateral to the PVN, the bursting LTS cells that we encountered had rectifying I-V relations and were situated just dorsal or dorsolateral to the nucleus. Whether this represents a species or sampling difference is not known at this time. It is also not certain that all of the bursting LTS neurons of the present study were hypothalamic and not thalamic cells. All bursting LTS neurons were situated ventral to the dorsal tip of the third ventricle and proximal to the PVN, suggesting that they were hypothalamic (see Paxinos and Watson, '86). However, the precise border between the hypothalamus and thalamus is unclear.

In conclusion, our findings support previous hypotheses that non-LTS (type-I) and non-bursting LTS (type-II) PVN cells are magnocellular and parvicellular neurons, respectively, and that bursting LTS (type-III) neurons are situated at or beyond the PVN border. Although it is possible that this correlation between these PVN electrophysiological and anatomical cell classifications is not absolute, our data indicate that it is significant. This suggests separate physiological functions for non-LTS and non-bursting LTS cells. Further research is necessary to 1) determine if only magnocellular neurons that are neurosecretory display type-I electrophysiological properties, 2) electrophysiologically characterize functional and anatomical subsets of PVN parvicellular neurons, and 3) elucidate the functional importance of the bursting LTS (type-III) cells. Finally, how these electrophysiological properties promote the regulatory activities of the different PVN neuronal populations remains to be determined.

ACKNOWLEDGMENTS

This research was supported by a grant from the Air Force Office of Scientific Research (87-0361 and 90-0056) to F.E. Dudek and National Institutes of Health postdoctoral fellowships to N.W. Hoffman and J.G. Tasker (NS08233 and NS08049, respectively). We thank Dr. K. Smithson, Dr. R. Fisher, Dr. C. Houser, and Dr. P. Micevych for critical advice and Dr. A. Robinson for supplying the neurophysin antiserum (NIH AM16166). The technical assistance of S. Sampogna and D. Smith is gratefully acknowledged, as is that of S. Belkin and C. Gray in preparing figures.

LITERATURE CITED

Andrew, R.D., and F.E. Dudek (1983) Burst discharge in mammalian neuroendocrine cells involves an intrinsic regenerative mechanism. Science *221*:1050–1052.

Andrew, R.D., and F.E. Dudek (1984a) Analysis of intracellularly recorded phasic bursting by mammalian neuroendocrine cells. J. Neurophysiol. *51*:552–566.

Andrew, R.D., and F.E. Dudek (1984b) Intrinsic inhibition in magnocellular neuroendocrine cells of rat hypothalamus. J. Physiol. (Lond.) *353*:171–185.

Armstrong, W.E., S. Warach, G.I. Hatton, and T.H. McNeill (1980) Subnuclei in the rat hypothalamic paraventricular nucleus: A cytoarchitectural, horseradish peroxidase and immunocytochemical analysis. Neuroscience *5*:1931–1958.

Bourque, C.W. (1986) Calcium-dependent spike after-current induces burst firing in magnocellular neurosecretory cells. Neurosci. Lett. *70*:204–209.

Bourque, C.W., J.C.R. Randle, and L.P. Renaud (1985) Calcium-dependent potassium conductance in rat supraoptic nucleus neurosecretory neurons. J. Neurophysiol. *54*:1375–1382.

Bourque, C.W., and L.P. Renaud (1985) Calcium-dependent action potentials in rat supraoptic neurosecretory neurones recorded *in vitro*. J. Physiol. *363*:419–428.

Cobbett, P., K.G. Smithson, and G.I. Hatton (1986) Immunoreactivity to vasopressin- but not oxytocin-associated neurophysin antiserum in phasic neurons of rat hypothalamic paraventricular nucleus. Brain Res. *362*:7–16.

Dudek, F.E., J.G. Tasker, and J.-P. Wuarin (1989) Intrinsic and synaptic mechanisms of hypothalamic neurons studied with the slice and explant preparations. J. Neurosci. Methods *28*:59–69.

Harris, G.W. (1948) Neural control of the pituitary gland. Physiol. Rev. *28*:139–179.

Hoffman, N.W., J.G. Tasker, and F.E. Dudek (1988) Immunohistochemical differentiation of electrophysiologically distinct neurons in the region of the rat paraventricular nucleus. Soc. Neurosci. Abst. *14*:1178.

Hoffman, N.W., J.G. Tasker, and F.E. Dudek (1989) Comparative electrophysiology of magnocellular and parvocellular neurons of the hypothalamic paraventricular nucleus. Soc. Neurosci. Abstr. *15*:1088.

Horikawa, K., and W.E. Armstrong (1988) A versatile means of intracellular labeling: Injection of biocytin and its detection with avidin conjugates. J. Neurosci. Methods *25*:1–11.

Hosoya, Y., and M. Matsushita (1979) Identification and distribution of the spinal and hypophyseal projection neurons in the paraventricular nucleus of the rat: A light and electron microscopic study with the horseradish peroxidase method. Exp. Brain Res. *35*:315–331.

Jahnsen, H., and R. Llinás (1984) Electrophysiological properties of guinea-pig thalamic neurones: An *in vitro* study. J. Physiol. *349*:205–226.

Krauth, J. (1988) Distribution-Free Statistics: An Applications-Oriented Approach. New York: Elsevier, pp. 83–91.

Mason, W.T. (1983) Electrical properties of neurons recorded from the rat supraoptic nucleus in vitro. Proc. R. Soc. London B *217*:141–161.

Mason, W.T., and G. Leng (1984) Complex action potential waveform recorded from supraoptic and paraventricular neurones of the rat: Evidence for sodium and calcium spike components at different membrane sites. Exp. Brain Res. *56*:135–143.

Paxinos, G., and C. Watson (1986) The Rat Brain in Stereotaxic Coordinates. New York: Academic Press.

Poulain, P., and B. Carette (1987) Low-threshold calcium spikes in hypothalamic neurons recorded near the paraventricular nucleus *in vitro*. Brain Res. Bull. *19*:453–460.

Poulain, D.A., and J.B. Wakerley (1982) Electrophysiology of hypothalamic magnocellular neurons secreting oxytocin and vasopressin. Neuroscience *7*:773–808.

Randle, J.C.R., C.W. Bourque, and L.P. Renaud (1986) Alpha$_1$-adrenergic receptor activation depolarizes rat supraoptic neurosecretory neurons in vitro. Am. J. Physiol. *251*:R569–R574.

Rao, G., C.A. Barnes, and B.L. McNaughton (1986) Intracellular fluorescent staining with carboxyfluorescein: A rapid and reliable method for quantifying dye-coupling in mammalian central nervous system. J. Neurosci. Methods *16*:251–263.

Renaud, L.P. (1987) Magnocellular neuroendocrine neurons: Update on intrinsic properties, synaptic inputs and neuropharmacology. TINS *10*:498–502.

Rho, J.-L., and L.W. Swanson (1989) A morphometric analysis of functionally defined subpopulations of neurons in the paraventricular nucleus of the rat with observations on the effects of colchicine. J. Neurosci. *9*:1377–1388.

Saper, C.B., A.D. Loewy, L.W. Swanson, and W.M. Cowan (1976) Direct hypothalamo-autonomic connections. Brain Res. *117*:305–312.

Sawchenko, P.E., and L.W. Swanson (1982) Immunohistochemical identification of neurons in the paraventricular nucleus of the hypothalamus that project to the medulla or to the spinal cord in the rat. J. Comp. Neurol. *205*:260–272.

Sawchenko, P.E., L.W. Swanson, and W.W. Vale (1984) Corticotropin-releasing factor: Co-expression within distinct subsets of oxytocin-, vasopressin-, and neurotensin-immunoreactive neurons in the hypothalamus of the male rat. J. Neurosci. *4*:1118–1129.

Schmued, L.C., L.W. Swanson, and P.E. Sawchenko (1982) Some fluorescent counterstains for neuroanatomical studies. *J. Histochem. Cytochem. 30:*123–128.

Seif, S.M., A.B. Huellmantel, M.P. Platia, C. Haluszczak, and A.G. Robinson (1977) Isolation, radioimmunoassay and physiologic secretion of rat neurophysins. Endocrinology *100:*1317–1326.

Silverman, A.-J., and G.E. Pickard (1983) The hypothalamus. In P.C. Emson (ed): Chemical Neuroanatomy. New York: Raven Press, pp. 295–336.

Smithson, K.G., P. Cobbett, B.A. MacVicar, and G.I. Hatton (1984) A reliable method for immunocytochemical identification of *Lucifer yellow* injected, peptide-containing mammalian central neurons. J. Neurosci. Methods *10:*59–69.

Smithson, K.G., B.A. MacVicar, and G.I. Hatton (1983) Polyethylene glycol embedding: A technique compatible with immunocytochemistry, enzyme histochemistry, histofluorescence and intracellular staining. J. Neurosci. Methods. *7:*27–41.

Sofroniew, M.V. (1985) Vasopressin, oxytocin and their related neurophysins. In A. Bjorklund and T. Hokfelt (eds): Handbook of Chemical Neuroanatomy. Vol 4: GABA and Neuropeptides in the CNS, Part I. New York: Elsevier, pp. 93–165.

Swaab, D.F., C.W. Pool, and F. Nijveldt (1975) Immunofluorescence of vasopressin and oxytocin in the rat hypothalamo-neurohypophyseal system. J. Neural Transmission *36:*195–215.

Swanson, L.W., and P.E. Sawchenko (1983) Hypothalamic integration: Organization of the paraventricular and supraoptic nuclei. Annu. Rev. Neurosci. *6:*269–324.

Swanson, L.W., and H.G.J.M. Kuypers (1980) The paraventricular nucleus of the hypothalamus: Cytoarchitectonic subdivisions and organization of projections to the pituitary, dorsal vagal complex, and spinal cord as demonstrated by retrograde fluorescence double-labeling methods. J. Comp. Neurol. *194:*555–570.

Tasker, J.G., and F.E. Dudek (1987) Low-threshold calcium spikes recorded in the region of the rat paraventricular nucleus. Soc. Neurosci. Abst. *13:*1370.

Tasker, J.G., and F.E. Dudek (1991) Electrophysiological properties of neurons in the region of the paraventricular nucleus in slices of rat hypothalamus. J. Physiol. (Lond.) *434:*271–293.

Tasker, J.G., N.W. Hoffman, and F.E. Dudek (in press) A comparison of three intracellular markers for combined electrophysiological, morphological and immunohistochemical analyses. J. Neurosci. Methods.

van den Pol, A.N. (1982) The magnocellular and parvocellular paraventricular nucleus of the rat: Intrinsic organization. J. Comp. Neurol. *206:*317–345.

Vandesande, F., and K. Dierickx (1975) Identification of the vasopressin producing and oxytocin producing neurons in the hypothalamic magnocellular neurosecretory system of the rat. Cell Tissue Res. *164:*153–162.

Vandesande, F., K. Dierickx, and J. De Mey (1977) The origin of the vasopressinergic and oxytocinergic fibres of the external region of the median eminence of the rat hypophysis. Cell Tissue Res. *180:*443–452.

Weigand, S.J., and J.L. Price (1980) Cells of origin of the afferent fibers to the median eminence in the rat. J. Comp. Neurol. *192:*1–19.

JOURNAL OF NEUROPHYSIOLOGY
Vol. 65, No. 4, April 1991. Printed in U.S.A.

Excitatory Amino Acid Antagonists Inhibit Synaptic Responses in the Guinea Pig Hypothalamic Paraventricular Nucleus

JEAN-PIERRE WUARIN AND F. EDWARD DUDEK
Mental Retardation Research Center and the Laboratory of Neuroendocrinology of the Brain Research Institute, School of Medicine, University of California, Los Angeles, California 90024

SUMMARY AND CONCLUSIONS

1. The effects of specific excitatory amino acid (EAA) antagonists on evoked excitatory synaptic responses were studied in the hypothalamic paraventricular nucleus (PVN) of the guinea pig, by the use of the in vitro slice preparation. Intracellular recordings were obtained from paraventricular neurons, and excitatory postsynaptic potentials (EPSPs) and currents (EPSCs) were induced by perifornical electrical stimulation. To reduce the influence of a potential γ-aminobutyric acid$_A$ ($GABA_A$) inhibitory component on the synaptic responses, all experiments were performed in the presence of 50 μM picrotoxin.

2. Of 20 cells tested, 13 had electrophysiological characteristics similar to magnocellular neuropeptidergic cells (MNCs) and 7 displayed low-threshold Ca^{2+} spikes (LTSs). No difference was detected in the effect of the antagonists on the synaptic responses of cells with or without LTS potentials.

3. The broad-spectrum EAA antagonist kynurenic acid decreased the amplitude of the EPSPs and EPSCs in a dose-dependent manner: the mean decrease was 5% for 100 μM, 43% for 300 μM, and 70% for 1 mM.

4. The quisqualate/kainate-receptor–selective antagonist 6-cyano-2,3-dihydroxy-7-nitroquinoxaline (CNQX) induced a dose-dependent decrease of the EPSPs and EPSCs: 1 μM had no detectable effect, 3 and 10 μM caused 30 and 70% decreases, respectively, and 30 μM blocked the response almost completely. This effect was not accompanied by a change in resting membrane potential or input resistance and was slowly reversible.

5. The *N*-methyl-D-aspartate (NMDA)-receptor–selective antagonist DL-2-amino-5-phosphonopentanoic acid (AP5), applied at 30 and 300 μM, reduced slightly the amplitude of the decay phase of the EPSP but did not significantly affect the peak amplitude. In some cells, the current-voltage relationship of the decay phase of the EPSC revealed a region of negative slope conductance between −70 and −40 mV.

6. These results suggest that *1*) glutamate or a related EAA is responsible for the fast excitatory input to magnocellular and parvocellular neurons in the PVN and probably also for cells around PVN, *2*) a quisqualate/kainate receptor type is responsible for the rising phase and peak amplitude of the synaptic current, and *3*) an NMDA receptor contributes to the late part of the synaptic response.

INTRODUCTION

The mammalian hypothalamic paraventricular nucleus (PVN) is composed of a heterogeneous cell population that has been divided into two major groups: the magnocellular neuropeptidergic cells (MNCs) and the parvocellular neurons. The paraventricular MNCs are part of the magnocellular neuroendocrine system. They synthesize and secrete the two neuropeptide hormones, vasopressin and oxytocin. Their axons terminate on capillaries in the neural lobe of the hypophysis, and vasopressin and oxytocin are released directly into the general circulation (for reviews of the electrophysiology of this system, see Dudek et al. 1989; Poulain and Wakerley 1982; Renaud et al. 1985). The parvocellular neurons are responsible for the secretion of releasing factors in the hypophyseal portal circulation. These releasing factors participate in the regulation of the secretion of the anterior pituitary hormones (for reviews see Swanson and Sawchenko 1983; van den Pol 1982). The PVN also contains a distinct population of cells that send axons to the brain stem and spinal cord (Rho and Swanson 1989). These descending neurons are probably involved in autonomic and motor functions. Although numerous substances have been proposed as neurotransmitter candidates in the PVN, glutamate and related excitatory amino acids (EAAs) have received little attention.

The supraoptic nucleus is the other important nucleus containing MNCs. It is composed almost exclusively of MNCs. Recent electrophysiological studies in this nucleus have provided evidence that the primary mediator of fast excitatory transmission in the MNCs is glutamate or a related amino acid (Gribkoff and Dudek 1988, 1990). In the present study we tested the hypothesis that EAAs contribute to most of the excitatory neurotransmission in the PVN. We examined the effects of EAA antagonists on electrically induced synaptic responses in the guinea pig PVN. Morphological studies have shown that the PVN cell population is heterogeneous; we made an initial attempt to determine whether electrophysiological characteristics could reflect this morphological variety (Hoffman et al. 1988), and we tried to correlate these characteristics with the effects of EAA antagonists. We first tested a broad-spectrum antagonist, then we applied antagonists selective for the quisqualate/kainate receptor or for the *N*-methyl-D-aspartate (NMDA) receptor in an attempt to determine the functional relevance of each type of receptor in the synaptic responses.

The importance of γ-aminobutyric acid$_A$ ($GABA_A$) receptors as mediators of the fast inhibitory component of the synaptic response in the supraoptic nucleus is firmly established. Synaptic boutons immunostained with GABA make synaptic contact with MNCs (van den Pol 1985), and spontaneous and induced inhibitory postsynaptic potentials (IPSPs) are blocked by bicuculline (Randle et al. 1986). Therefore, to avoid a potential $GABA_A$-receptor–mediated component in the electrically induced synaptic response, we carried out all experiments with picrotoxin (50 μM) in the perfusion medium.

The aims of the present study were *1*) to test the hypothesis that EAAs are the primary neurotransmitter system for fast excitatory synaptic transmission in the PVN and *2*) to compare their contribution to excitatory transmission in the magnocellular system and in the parvocellular cell population. We assessed the effects of three amino acid receptor antagonists on the electrically induced synaptic responses: *1*) a broad-spectrum antagonist, kynurenic acid; *2*) a quisqualate/kainate-receptor antagonist, 6-cyano-2,3-dihydroxy-7-nitroquinoxaline (CNQX); and *3*) an NMDA-receptor antagonist, DL-2-amino-5-phosphonopentanoic acid (AP5). We used intracellular recording techniques and obtained synaptic activation with electrical stimulation of the region dorsal to fornix. Some of the experiments were done using the single-electrode voltage-clamp technique to decrease the influence of voltage-dependent conductances on the synaptic responses. Brief reports of some of these data have been presented (Dudek et al. 1989; Wuarin and Dudek 1988, 1989).

METHODS

Male guinea pigs weighing 300–400 g were anesthetized with pentobarbital sodium (100 mg/kg). Coronal slices (500 μm) were cut with a vibrating microtome from a block of hypothalamus. One to two slices containing the PVN were rapidly transferred to a thermoregulated (32–34°C) ramp chamber (Haas et al. 1979) and perfused at 2 ml/min with artificial cerebrospinal fluid containing (in mM) 124 NaCl, 26 $NaHCO_3$, 3 KCl, 1.3 $MgSO_4$, 1.4 NaH_2PO_4, 2.4 $CaCl_2$, and 10 glucose. The preparation was oxygenated with 95% O_2-5% CO_2, and pH was kept in the range 7.35–7.45.

For current-clamp experiments, micropipettes were filled with 4 M K acetate (tip resistance 80–130 MΩ) or 3 M KCl (tip resistance 60–80 MΩ). Voltage-clamp experiments were done using electrodes filled with 2 M CsCl and 100 mM QX 314 (tip resistance 60–80 MΩ). As previously described (Brown and Johnston 1983), Cs^+ nearly doubled the input resistance within the first 10 min of recording. Signals were recorded with a single-electrode voltage-clamp amplifier (Axoclamp-2A). During voltage-clamp experiments, the headstage potential was monitored on a separate oscilloscope to ensure that electrode capacitance was completely neutralized and headstage potential stable before the voltage was sampled for the next cycle. Sampling rate was 4–6 kHz and output bandwidth 0.3–1 kHz. Filling the recording electrodes with a K^+ channel blocker (Cs^+) and a Na^+ channel blocker (QX 314) allowed us to "linearize" the cell membrane, to reduce to some extent the space-clamp problem, and also to be able to study the induced synaptic responses at depolarized levels without Na^+ spikes. Spontaneous synaptic currents, however, could not be studied because they were too small to be clearly defined from the background noise. Signals were stored on a video cassette recorder.

Extracellular stimulation was obtained with a bipolar electrode of Teflon-insulated, platinum-iridium wire. In all experiments, the stimulation electrode was positioned ~1 mm dorsal to the fornix column. Pulses of constant current (0.5 ms) were applied at intensities ranging from 50 to 500 μA. For each cell, the stimulus intensity was adjusted to be supramaximal. Because extracellular stimuli of the same intensity induced excitatory postsynaptic potentials (EPSPs) and currents (EPSCs) of variable amplitude, the responses were averaged (n = 20 in most cases) for each cell. During voltage-clamp experiments, the stimulation artifact was partially blanked by the amplifier. In all experiments, picrotoxin (50 μM) was added in the perfusion medium. In hippocampal neurons, 5–10 μM picrotoxin has been demonstrated to block most of the $GABA_A$-induced Cl^- current (Brown and Johnston 1983); 50 μM was used to ensure that almost all of the $GABA_A$ component of the synaptic potential would be blocked.

All drugs were applied in the perfusion bath for ≥20 min to ascertain that the EPSP and EPSC amplitude measurements were done in steady state. The following drugs were used: picrotoxin (50 μM), kynurenic acid (100 and 300 μM and 1 mM), AP5 (30 and 300 μM), and CNQX (3, 10, and 30 μM). CNQX was obtained from Tocris Neuramin (Buckhurst Hill, UK); the other drugs were obtained from Sigma (St. Louis, MO). Results are expressed as mean ± SE.

RESULTS

In total, 20 cells were recorded. The mean resting membrane potential was −67 ± 3 mV and input resistance was 279 ± 25 MΩ. Out of 10 cells recorded in the bridge mode with K acetate–containing microelectrodes, 2 were silent and 8 were spontaneously firing action potentials at a frequency ranging from 1 to 5 Hz. All cells in this study responded to extracellular stimulation with a compound EPSP that, in most cells, reached threshold for Na^+ spikes when the stimulus was delivered at resting membrane potential. To better reveal the underlying synaptic response and avoid Na^+ spikes, we hyperpolarized the cells by 10–25 mV. Picrotoxin, added to the perfusion medium to reduce the potential influence of a reversed IPSP on the synaptic response, did not modify the values of resting membrane potential and input resistance.

On the basis of their electrophysiological properties, the neurons were classified in two categories: cells that were putative MNCs and cells displaying low-threshold Ca^{2+} spikes (LTSs) (Hoffman et al. 1989; Llinàs and Jahnsen 1982; Llinàs and Yarom 1981; Poulain and Carette 1987). The cells in the first group (n = 13) resembled supraoptic MNCs (Renaud 1987). They responded to a depolarizing current pulse with a regular discharge of action potentials and had linear current-voltage (I-V) relations. LTS potentials were completely absent in these neurons (Tasker and Dudek 1991). The LTS cells (n = 7) typically showed a slow (100–200 ms) depolarizing potential when briefly depolarized from a hyperpolarized potential with an intracellular current pulse (Fig. 1*B*). In each case, the LTS triggered a burst of action potentials. In contrast to MNCs, they consistently displayed a strong time-dependent inward rectification (Tasker and Dudek 1991).

Effect of kynurenic acid and CNQX on EPSPs

Kynurenic acid applied in the perfusion bath decreased the amplitude of the electrically induced EPSPs in all of the eight cells tested. The mean decrease was 5 ± 2.8% (n = 4) for 100 μM, 43 ± 1.3% (n = 3) for 300 μM, and 70 ± 1.3% (n = 4) for 1 mM. For a given concentration, the decrease in amplitude of the EPSP was similar in MNCs and LTS cells (n = 4 for each type of cell; Fig. 1). The inhibition was dose dependent and reversible (see Dudek et al. 1989). The estimated concentration of kynurenic acid that inhibited the EPSP amplitude by 50% (IC_{50}) was ~500 μM. When CNQX became available, we stopped using kynurenic acid and switched to this new antagonist because it has been shown to be much more potent and selective for the quisqualate and kainate receptor subtypes (Honoré et al. 1988). CNQX also inhibited EPSPs in a dose-dependent manner: the smallest detectable effect was obtained with 1 μM, and 3

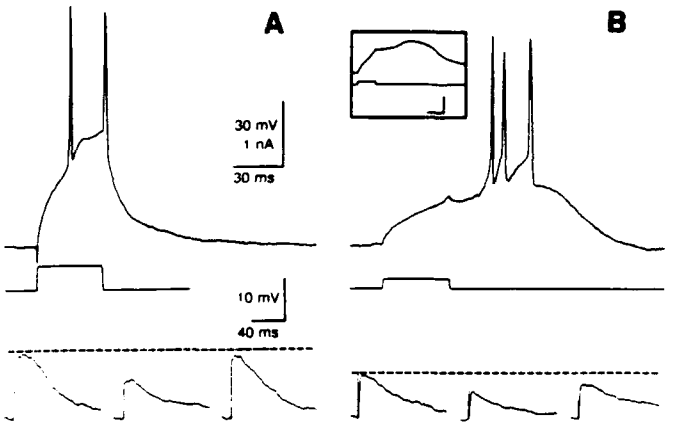

FIG. 1. Kynurenic acid decreased EPSP amplitude in 2 types of PVN cells. *Top traces in A* show the response of an MNC to a brief depolarizing current pulse. A current pulse of the same duration triggered an LTS potential in another cell (*B*). *B, inset*: cell shown was recorded with an electrode containing CsCl (2 M) and QX 314 (100 mM). This cell was current-clamped at −90 mV and had an input resistance of 400 MΩ. Each of the 7 cells considered to have LTS potentials showed a similar depolarizing potential. The decrease in EPSP amplitude for 300 μM kynurenic acid was similar in both cell types (*bottom traces*). Calibration for the inset is 40 ms, 30 mV, and 1 nA. *Bottom traces* are examples of individual sweeps.

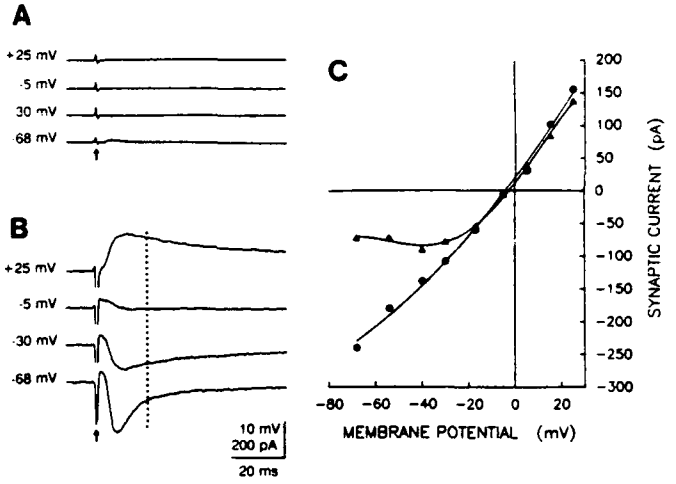

FIG. 3. Voltage dependence of the EPSC. Cell was recorded with a microelectrode containing CsCl (2 M) and QX 314 (100 mM). Voltage recordings at 4 different holding potentials (*A*) and corresponding synaptic current recordings (*B*). Traces are an average of 5 sweeps. Stimulus artifact is indicated by arrow, stimulus intensity was 500 μA. *C*: plot of peak synaptic current amplitude (●) and amplitude 10 ms after peak (▲ in *C*; vertical dotted line in *B*) as a function of membrane potential. This cell was an MNC.

μM decreased the amplitude of induced EPSPs by >50% (n = 3: 2 MNCs and 1 LTS cell; Fig. 2).

Effect of CNQX on EPSCs

To decrease the influence of voltage-dependent conductances on the synaptic responses, we investigated the effects of CNQX with the single-electrode voltage-clamp technique. The amplitude of the EPSCs at a holding potential equal to resting membrane potential was in the range of 200–600 pA. The *I-V* relationship of the peak amplitude of the EPSC was almost linear (Fig. 3). In some cells (e.g., see cell in Fig. 3), the *I-V* relation showed a region of negative slope conductance between −40 and −70 mV when the synaptic current was measured 10 ms after the peak. The reversal potential for both peak and late phase currents was between −10 and 0 mV.

In a manner similar to the effects on EPSPs, CNQX reduced the amplitude of evoked EPSCs (Fig. 4*A*). At the

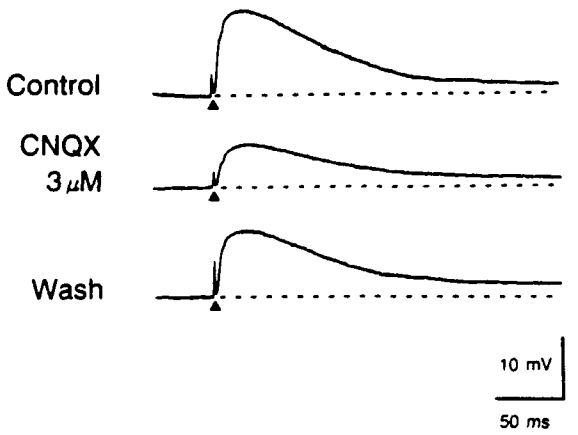

FIG. 2. CNQX reduced the amplitude of evoked EPSPs. The antagonist, bath applied at 3 μM, reduced the EPSP amplitude by ~50%. Cell was hyperpolarized by 20 mV to keep it from firing action potentials and to reveal synaptic response. Resting membrane potential was −65 mV. Stimulus intensity was 500 μA, 0.1 Hz. Each trace is average of 20 responses. Stimulus artifact is indicated by triangle. This cell was an MNC, firing action potentials regularly at 3–4 Hz.

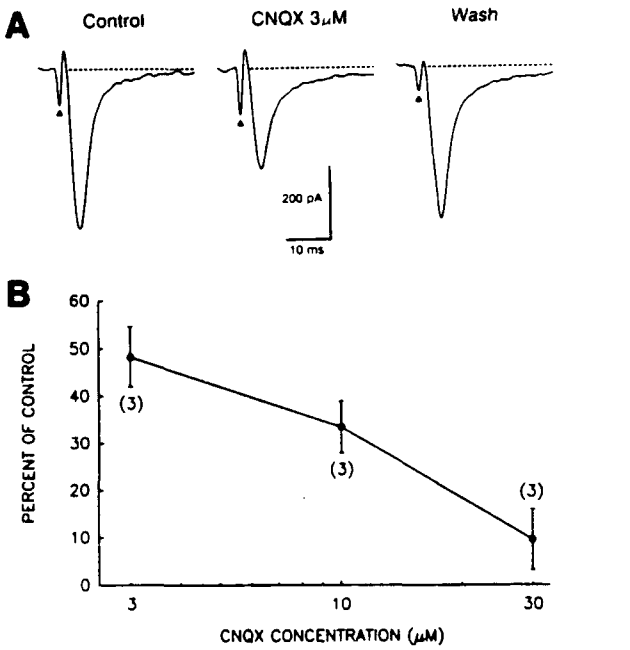

FIG. 4. CNQX reduced the amplitude of evoked EPSCs in a dose-dependent manner. *A*: synaptic current amplitude was reduced by 50% after 20 min in the presence of 3 μM CNQX. Holding potential was the same as resting membrane potential (−63 mV). Traces are average of 20 responses. Stimulus artifact is indicated by triangle. This cell was an MNC. *B*: concentration-response curve showing the effect of CNQX on EPSC amplitude. Each point shows mean percentage (±SE) of EPSC amplitude remaining after bath application of CNQX. Values in parentheses are number of cells tested. Each EPSC amplitude measurement was made >15 min after the start of antagonist application.

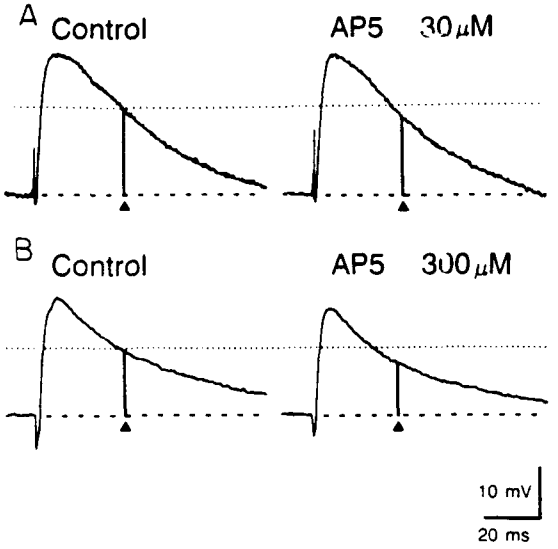

FIG. 5. Effect of the NMDA antagonist AP5 on evoked EPSPs. AP5 decreased slightly the amplitude of the decay phase of the EPSP measured 25 ms after the peak (▲). Antagonist was applied for 30 min before its effect was recorded. *A*: cell was an MNC, firing bursts of action potentials; membrane potential was hyperpolarized by 20 mV, resting membrane potential was −68 mV, and input resistance was 250 MΩ. *B*: cell was also an MNC, firing action potentials regularly at 0.2 Hz; membrane potential was hyperpolarized by 15 mV, resting membrane potential was −67 mV, and input resistance was 420 MΩ. Stimulus intensity was 500 μA in *A* and 450 μA in *B*; stimulation frequency was 0.1 Hz for both cells. Traces are averages of 10 (*A*) and 20 (*B*) sweeps.

lowest concentration used in these experiments (1 μM), the CNQX-induced inhibition was almost completely reversible, even after bath applications longer than 25 min. At higher concentrations (10 and 30 μM), we never observed a complete recovery of the control EPSP or EPSC amplitude after bath application of ≥15 min. The CNQX effect was concentration dependent, with an estimated IC_{50} value of 3 μM (Fig. 4*B*). No difference was observed in the effect of CNQX on the EPSPs and EPSCs between MNCs (n = 8) and LTS cells (n = 3).

Effects of AP5 on EPSPs

The NMDA-selective antagonist AP5 was tested in three cells, at 30 (n = 1) and 300 μM (n = 2). No effect on the peak amplitude of the synaptic response was detected at 30 μM (Fig. 5). The amplitude of the synaptic potential measured 25 ms after the peak was slightly decreased. Approximately 10% decrease of the EPSP amplitude was observed at 300 μM. Neither concentration affected the raising phase of the EPSPs. The higher concentration (300 μM) was tested on one LTS cell and on one MNC, and a similar inhibition was observed on both cell types.

DISCUSSION

Comparison with the supraoptic nucleus

The results obtained in the present study on the PVN support earlier research showing that kynurenic acid and γ-d-glutamylglycine decreased the amplitude of spontaneous and evoked EPSPs in the rat supraoptic nucleus (Gribkoff and Dudek 1990). On the basis of the observation that these broad-spectrum antagonists, but not AP5, depressed EPSPs in supraoptic neurons, it was proposed that non-NMDA receptors mediate fast excitatory synaptic transmission. We have confirmed these results and have also shown that the selective non-NMDA antagonist CNQX inhibits EPSPs and EPSCs in all of the PVN neurons tested. Because this antagonist has a higher affinity for non-NMDA receptors than does kynurenic acid, it was possible to use concentrations of CNQX two orders of magnitude lower than kynurenic acid to obtain the same inhibition. In the previous work on the supraoptic nucleus (Gribkoff and Dudek 1990), several doses of kynurenic acid were used, but it was difficult to obtain precise dose-response data because of the variable amplitude of individual EPSPs. Averaging of the evoked responses eliminated this problem and allowed quantitative evaluation of the dose-response data and calculation of IC_{50} (for comparison, see Blake et al. 1988; Honoré et al. 1988; McBain et al. 1988; Neuman et al. 1988; Yamada et al. 1989). Another potential problem with the previous results concerned the extensive GABA input to the supraoptic nucleus (Randle et al. 1986). Bicuculline partially antagonized some of the positive-going PSPs recorded when supraoptic neurons were hyperpolarized, which implied that the effect of kynurenic acid was underestimated. Nonetheless, kynurenic acid still depressed the PSPs in the presence of bicuculline. In the present study, all experiments were performed in picrotoxin to eliminate any possible contribution of $GABA_A$ receptors to our analyses of the effects of the EAA antagonists on synaptic potentials. Therefore our experiments, under conditions where it was possible to improve the isolation and resolution of excitatory synaptic events, corroborate the results previously observed in the supraoptic nucleus (Gribkoff and Dudek 1990).

Excitatory synaptic inputs to PVN

Perifornical stimulation activated one group of afferents to PVN, but many others probably exist. Spontaneous PSPs are another measure of synaptic inputs to PVN neurons. Gribkoff and Dudek (1990) showed that kynurenic acid reduced the amplitude of spontaneous EPSPs in the supraoptic nucleus and, in particular, eliminated the largest ones. This suggests that, in addition to possibly decreasing presynaptic firing, kynurenic acid produced a postsynaptic block of EAA receptors and caused a reduction of the amplitude of spontaneous EPSPs. Our results with kynurenic acid were qualitatively similar. Most of our experiments aimed at testing the effects of CNQX were done in voltage-clamp, which precluded a study of the spontaneous EPSCs (see METHODS); however, in two cells recorded in current-clamp, CNQX (3 μM) blocked most of the spontaneous EPSPs. When combined with the larger body of data from perifornical stimulation, this suggests that EAAs mediate many fast excitatory inputs to the PVN, as in the supraoptic nucleus.

The highest concentrations of kynurenic acid (1 mM) and CNQX (30 μM) inhibited the synaptic response by ~70 and 90%, respectively. Although it is possible that some inputs were completely blocked while others were unaffected, it seems more likely that the antagonists exerted an incomplete block of all the glutamatergic inputs and that higher concentrations such as 3 mM kynurenic acid and

100 μM CNQX would have blocked the synaptic response completely. We did not test these concentrations because the time for recovery from the inhibition was already very long for the highest concentrations and because of potential nonspecific effects.

Heterogeneity of cell types in the PVN

The previous studies in the supraoptic nucleus provided data primarily, if not exclusively, on the vasopressinergic and oxytocinergic neurons of the magnocellular neuroendocrine system. Although these two types of neuroendocrine cells certainly have different synaptic inputs, they probably have very similar intrinsic electrophysiological properties. Numerous anatomic and immunohistochemical studies of the PVN, however, have shown that this nucleus is much more heterogeneous in terms of cell types than the supraoptic nucleus. Not only does it have the same classes of magnocellular neuroendocrine cells that project to the neurohypophysis, it also contains vasopressinergic and oxytocinergic cells that project to other areas in the CNS. The parvocellular neuroendocrine system, which secretes such substances as corticotropin-releasing hormone at the median eminence, is also within this nucleus. Finally, recent studies on neurons located at the periphery of the PVN have revealed a different cell type, which fires LTS potentials (Poulain and Carette 1987). Ongoing studies in the PVN combining intracellular recording and staining have begun to classify these cell types (Hoffman et al. 1988, 1989), and on the basis of these criteria we have recorded from several types of PVN neurons. Because the same effects of EAA antagonists were obtained in all the different PVN cells, the pattern of the excitatory synaptic activation induced by glutamate is probably similar in every cell type in the PVN. Because the PVN contains many types of neuroendocrine cells and nonneuroendocrine hypothalamic neurons, these data support the hypothesis that glutamate is the primary fast excitatory transmitter at excitatory synapses throughout the hypothalamus. This hypothesis is consistent with recent work on hypothalamic neurons in the suprachiasmatic nucleus, which has shown that kynurenic acid (Cahill and Menaker 1989a,b) and the quinoxalinedione DNQX (Kim and Dudek 1989) block both retinal and nonretinal input to this nucleus, further indicating that glutamate is the major fast excitatory transmitter throughout the hypothalamus.

NMDA component of the synaptic response

The NMDA antagonist AP5 only slightly affected the induced EPSPs, even when tested at a very high concentration. This result was expected, because the effects of AP5 were examined at hyperpolarized membrane potentials, and the ionic channel linked to the NMDA receptor is known to be gradually blocked by Mg^{2+} in the hyperpolarized range (Mayer et al. 1984, Nowak et al. 1984). In many of our initial experiments, the cell membrane potential was maintained at 10–20 mV below resting membrane potential by injecting negative current in the cell. At such hyperpolarized potentials, the NMDA current is likely to be almost completely blocked. In voltage-clamp, we found in some cells a voltage-dependent component to the decay phase of EPSCs, which showed characteristics generally attributed to the NMDA current: a negative slope conductance region between −70 and −40 mV and a reversal potential near 0 mV. This component of the EPSC is clearly reminiscent of an NMDA current such as reported in hippocampal CA1 (Collingridge et al. 1988; Hestrin et al. 1990) and cultured neurons (Forsythe and Westbrook 1988). However, we did not detect this voltage-dependent component to the late phase of EPSCs in all PVN cells tested. Space-clamp problems may have prevented the decay phase of the EPSC from being adequately controlled in all cells. The single-electrode voltage-clamp with conventional microelectrodes has limitations that make it inappropriate for a quantitative study of small currents and of currents generated at synapses distant from the soma (for a detailed discussion see Johnston and Brown 1983). Whole-cell recordings with patch pipettes (Blanton et al. 1989) will allow a better resolution of the NMDA current in PVN cells. A recent study using this technique (Hestrin et al. 1990) showed that, at the excitatory synapse between the Schaffer collateral fibers and CA1 pyramidal neurons of rat hippocampus, AP5 blocked a slow, voltage-dependent component to the EPSC without affecting the peak amplitude.

Glycine is known to activate the NMDA receptor (Johnson and Ascher 1987). We did not add glycine in the perfusion bath on the assumption that the subsynaptic concentration of glycine in the slice would be sufficient to modulate the NMDA receptor activity (Thomson 1989). If the glycine concentration were not high enough in our preparation, we might have underestimated the amplitude of the NMDA current. Furthermore, CNQX has been shown to antagonize NMDA responses in the absence of glycine (Birch et al. 1988; Lester et al. 1989); therefore, if the concentration of glycine were too low in the slice, CNQX may have blocked the NMDA current in addition to blocking the non-NMDA current, and its effects may have been overestimated. However, preliminary results from our laboratory showed no modification of the NMDA current in the neocortex with 3 μM glycine, suggesting that the concentration of glycine in the slice is sufficient to activate most of the NMDA current.

EAAs as transmitters in the hypothalamus

Our results support and extend recent data (van den Pol et al. 1990) suggesting that glutamate plays a major role in the control of the mammalian neuroendocrine system. They strengthen the evidence that EAAs are the primary mediator of fast excitatory transmission in the mammalian hypothalamus and indicate that EAAs generate fast EPSPs in PVN neurons, primarily through activation of non-NMDA receptors. However, NMDA receptors are probably activated under depolarized conditions, and additional research is necessary to evaluate more rigorously the voltage dependence and magnitude of NMDA-receptor–mediated synaptic currents in the different types of hypothalamic neurons.

We thank C. Kinney for secretarial assistance.

This research was supported by National Institute of Drug Abuse Grant DA-05711 and by the Air Force Office of Scientific Research Grants 87-0361 and 90-0056 to F. E. Dudek and by a fellowship from the Swiss National Science Foundation to J.-P. Wuarin.

Address for reprint requests: F. E. Dudek, Mental Retardation Research Center, University of California at Los Angeles School of Medicine, 760 Westwood Plaza, NPI 58-258, Los Angeles, CA 90024.

Received 11 July 1990; accepted in final form 5 December 1990.

REFERENCES

BIRCH, P. J., GROSSMAN, C. J., AND HAYES, A. G. 6,7-Dinitro-quinoxaline-2,3-dion and 6-nitro,7-cyano-quinoxaline-2,3-dion antagonise responses to NMDA in the rat spinal cord via an action at the strychnine-insensitive glycine receptor. *Eur. J. Pharmacol.* 156: 177–180, 1988.

BLAKE, J. F., BROWN, M. W., AND COLLINGRIDGE, G. L. CNQX blocks acidic amino acid induced depolarizations and synaptic components mediated by non-NMDA receptors in rat hippocampal slices. *Neurosci. Lett.* 89: 182–186, 1988.

BLANTON, M. G., LO TURCO, J. J., AND KRIEGSTEIN, A. R. Whole cell recording from neurons in slices of reptilian and mammalian cerebral cortex. *J. Neurosci. Methods* 30: 203–210, 1989.

BROWN, T. H. AND JOHNSTON, D. Voltage-clamp analysis of mossy fiber synaptic input to hippocampal neurons. *J. Neurophysiol.* 50: 487–507, 1983.

CAHILL, G. M. AND MENAKER, M. Responses of the suprachiasmatic nucleus to retinohypothalamic tract volleys in a slice preparation of the mouse hypothalamus. *Brain Res.* 479: 65–75, 1989a.

CAHILL, G. M. AND MENAKER, M. Effects of excitatory amino acid antagonists on suprachiasmatic nucleus responses to retinohypothalamic tract volleys. *Brain Res.* 479: 76–82, 1989b.

COLLINGRIDGE, G. L., HERRON, C. E., AND LESTER, R. A. Synaptic activation of *N*-methyl-D-aspartate receptors in the Schaffer collateral–commisural pathways of rat hippocampus. *J. Physiol. Lond.* 399: 283–300, 1988.

DUDEK, F. E., TASKER, J. G., AND WUARIN, J.-P. Intrinsic and synaptic mechanisms of hypothalamic neurons studied with slice and explant preparations. *J. Neurosci. Methods* 28: 59–69, 1989.

DUDEK, F. E., WUARIN, J.-P., AND KIM, Y. I. Excitatory amino acids mediate fast synaptic transmission in the hypothalamus. *Biomed. Res. 10, Suppl.* 3: 13–20, 1989.

FORSYTHE, I. D. AND WESTBROOK, G. L. Slow excitatory postsynaptic currents mediated by *N*-methyl-D-aspartate receptors on cultured mouse central neurons. *J. Physiol. Lond.* 396: 515–533, 1988.

GRIBKOFF, V. K. AND DUDEK, F. E. The effects of the excitatory amino acid antagonist kynurenic acid on synaptic transmission to supraoptic neuroendocrine cells. *Brain Res.* 442: 152–156, 1988.

GRIBKOFF, V. K. AND DUDEK, F. E. Effects of excitatory amino acid antagonists on synaptic responses of supraoptic neurons in slices of rat hypothalamus. *J. Neurophysiol.* 63: 60–71, 1990.

HAAS, H. L., SCHAERER, B., AND VOSMANSKY, M. A simple perfusion chamber for the study of nervous tissue slices in vitro. *J. Neurosci. Methods* 1: 323–325, 1979.

HESTRIN, S., NICOLL, R. A., PERKEL, D. J., AND SAH, P. Analysis of excitatory synaptic action in pyramidal cells using whole-cell recording from rat hippocampal slices. *J. Physiol. Lond.* 422: 203–225, 1990.

HOFFMAN, N. W., TASKER, J. G., AND DUDEK, F. E. Immunohistochemical differentiation of electrophysiologically distinct neurons in the region of the rat paraventricular nucleus. *Soc. Neurosci. Abstr.* 14: 1178, 1988.

HOFFMAN, N. W., TASKER, J. G., AND DUDEK, F. E. Comparative electrophysiology of magnocellular neurons of the hypothalamic paraventricular nucleus. *Soc. Neurosci. Abstr.* 15: 1088, 1989.

HONORÉ, T., DAVIES, S. N., DREJER, J., FLETCHER, E. J., JACOBSEN, P., LODGE, D., AND NIELSEN, F. E. Quinoxalinediones: potent competitive non-NMDA glutamate receptor antagonists. *Science Wash. DC* 241: 701–703, 1988.

JOHNSON, J. W. AND ASCHER, P. Glycine potentiates the NMDA response in cultured mouse brain neurons. *Nature Lond.* 325: 529–531, 1987.

JOHNSTON, D. AND BROWN, T. H. Interpretation of voltage-clamp measurements in hippocampal neurons. *J. Neurophysiol.* 50: 464–486, 1983.

KIM, Y. I. AND DUDEK, F. E. Antagonism of fast excitatory postsynaptic potentials in suprachiasmatic nucleus neurons by excitatory amino acid antagonists. *Soc. Neurosci. Abstr.* 15: 1088, 1989.

LESTER, R. J., QUARUM, M. L., PARKER, J. D., WEBER, E., AND JAHR, C. E. Interaction of 6-cyano-7-nitroquinoxaline-2,3-dione (CNQX) with the *N*-methyl-D-aspartate (NMDA) receptor–associated glycine binding site. *Mol. Pharmacol.* 35: 565–570, 1989.

LLINÀS, R. AND JAHNSEN, H. Electrophysiology of mammalian thalamic neurones in vitro. *Nature Lond.* 297: 406–408, 1982.

LLINÀS, R. AND YAROM, Y. Properties and distribution of ionic conductances generating electroresponsiveness of mammalian inferior olivary neurons in vitro. *J. Physiol. Lond.* 315: 569–584, 1981.

MAYER, M. L., WESTBROOK, G. L., AND GUTHRIE, P. B. Voltage-dependent block by Mg^{2+} of NMDA responses in spinal cord neurones. *Nature Lond.* 309: 261–263, 1984.

MCBAIN, C. J., BODEN, P., AND HILL, R. G. The kainate/quisqualate receptor antagonist, CNQX, blocks the fast component of spontaneous epileptiform activity in organotypic cultures of rat hippocampus. *Neurosci. Lett.* 93: 341–345, 1988.

NEUMAN, R. S., BEN-ARI, Y., GHO, M., AND CHERUBINI, E. Blockade of excitatory synaptic transmission by 6-cyano-7-nitroquinoxaline-2,3-dione (CNQX) in the hippocampus in vitro. *Neurosci. Lett.* 92: 64–68, 1988.

NOWAK, L., BREGESTOVSKI, P., ASHER, P., HERBET, A., AND PROCHIANTZ, A. Magnesium gates glutamate-activated channels in mouse central neurons. *Nature Lond.* 307: 462–465, 1984.

POULAIN, D. A. AND WAKERLEY, J. B. Electrophysiology of hypothalamic magnocellular neurones secreting oxytocin and vasopressin. *Neuroscience* 7: 773–808, 1982.

POULAIN, P. AND CARETTE, B. Low-threshold calcium spikes in hypothalamic neurons recorded near the paraventricular nucleus in vitro. *Brain Res. Bull.* 19: 453–460, 1987.

RANDLE, J. C. R., BOURQUE, C. W., AND RENAUD, L. P. Characterization of spontaneous and evoked inhibitory postsynaptic potentials in rat supraoptic neurosecretory neurons in vitro. *J. Neurophysiol.* 56: 1703–1717, 1986.

RENAUD, L. P. Magnocellular neuroendocrine neurons: update on intrinsic properties, synaptic inputs and neuropharmacology. *Trends Neurosci.* 10: 498–502, 1987.

RENAUD, L. P., BOURQUE, C. W., DAY, T. A., FERGUSON, A. V., AND RANDLE, J. C. R. Electrophysiology of mammalian hypothalamic supraoptic and paraventricular neurosecretory cells. In: *The Electrophysiology of the Secretory Cell*, edited by A. M. Poisner and J. Trifaro. Amsterdam: Elsevier, 1985, p. 165–194.

RHO, J.-H. AND SWANSON, L. W. A morphometric analysis of functionally defined subpopulations of neurons in the paraventricular nucleus of the rat with observations on the effects of colchicine. *J. Neurosci.* 9: 1375–1388, 1989.

SWANSON, L. W. AND SAWCHENKO, P. E. Hypothalamic integration: organization of the paraventricular and supraoptic nuclei. *Annu. Rev. Neurosci.* 6: 269–324, 1983.

TASKER, J. G. AND DUDEK, F. E. Electrophysiological properties of neurones in the region of the paraventricular nucleus in slices of rat hypothalamus. *J. Physiol. Lond.* 434: 271–293, 1991.

THOMSON, A. M. Glycine modulation of the NMDA receptor/channel complex. *Trends Neurosci.* 12: 349–353, 1989.

VAN DEN POL, A. N. The magnocellular and parvocellular paraventricular nucleus of rat: intrinsic organization. *J. Comp. Neurol.* 206: 317–345, 1982.

VAN DEN POL, A. N. Dual ultrastructural localization of two neurotransmitter-related antigens: colloidal gold-labeled neurophysin-immunoreactive supraoptic neurons receive peroxidase-labeled glutamate decarboxylase- or gold-labeled GABA-immunoreactive synapses. *J. Neurosci.* 5: 2940–2954, 1985.

VAN DEN POL, A. N., WUARIN, J.-P., AND DUDEK, F. E. Glutamate, the dominant excitatory transmitter in neuroendocrine regulation. *Science Wash. DC.* 250: 1276–1278, 1990.

WUARIN, J.-P. AND DUDEK, F. E. Kynurenate antagonism of fast EPSPs in paraventricular neurons. *Soc. Neurosci. Abstr.* 14: 1178, 1988.

WUARIN, J.-P. AND DUDEK, F. E. Contrasting effects of NMDA and non-NMDA antagonists on fast EPSPs in neurons of the paraventricular nucleus. *Soc. Neurosci. Abstr.* 15: 1088, 1989.

YAMADA, K. A., DUBINSKY, J. M., AND ROTHMAN, S. M. Quantitative physiological characterization of a quinoxalinedione non-NMDA receptor antagonist. *J. Neurosci.* 9: 3230–3236, 1989.

INTRACELLULAR MEMBRANE AND SYNAPTIC PROPERTIES IN MEDIAL PREOPTIC SLICES CONTAINING THE SEXUALLY DIMORPHIC NUCLEUS OF THE RAT

Neil W. Hoffman, Yang I. Kim, Roger A. Gorski and F. Edward Dudek[1]

Mental Retardation Research Center
and
Laboratory of Neuroendocrinology
Brain Research Institute

UCLA Center for the Health Sciences
760 Westwood Plaza
Los Angeles, CA 90024-1759

Running Head: Electrophysiology of medial preoptic neurons

Key Words: Medial Preoptic Area, Medial Preoptic Nucleus, Sexually Dimorphic Nucleus of Preoptic Area, Intracellular Recording, Biocytin, Low-threshold Ca^{2+} spikes, Gamma-Amino Butyric Acid

[1] To whom correspondence should be addressed. Present address: Department of Anatomy and Neurobiology, Colorado State University, Fort Collins, CO 80523.

SUMMARY AND CONCLUSIONS

1. Passive and active electrophysiological properties of neurons (n=46) in the medial preoptic area (MPOA) were studied in hypothalamic slices from rats (primarily males). This investigation compared electrical properties between neurons in the sexually dimorphic nucleus of the preoptic area (SDN-POA) with those situated in other parts of the MPOA. We evaluated whether the MPOA contains a markedly heterogeneous population of cell types, defined on the basis of electrophysiological properties such as low-threshold Ca^{2+} spikes (LTS) and current-voltage (I-V) relations. Evoked and spontaneous synaptic potentials were also studied.

2. Neurons in the SDN-POA shared a common set of intrinsic membrane properties with other medial preoptic cells. In response to depolarization from a hyperpolarized condition, medial preoptic cells were uniformly capable of producing Ni^{2+}-sensitive (500 μM in a low Ca^{2+} buffer) LTS potentials (mean amplitude at maximum activation $\pm$ SEM = 29 $\pm$ 1.8 mV) that generated one or more action potentials. Most neurons (92%) displayed linear I-V relations in the hyperpolarizing direction (-40 mV or more from resting potential = 61.1 $\pm$ 1.6 mV of tested neurons). Only two cells showed evidence for weak anomalous inward rectification at hyperpolarized membrane potentials. Mean resting potential for medial preoptic neurons ($\pm$ SEM) was -60.7 $\pm$ 2.2 mV, input resistance was 196 $\pm$ 20 MΩ, and membrane time constant was 15.2 $\pm$ 2.5 ms. Most neurons displayed moderate Na^{+}-spike frequency adaptation, and afterhyperpolarizations typically followed spike trains.

3. Spontaneous postsynaptic potentials (PSPs), most of which were inhibitory, were

frequently recorded. In most medial preoptic neurons (83%), extracellular stimulation of the dorsal preoptic region evoked a fast EPSP closely followed by an IPSP. In some neurons, evoked EPSPs were not observed unless the evoked IPSPs were blocked with 10-50 μM bicuculline. The IPSPs reversed at -71 $\pm$ 5 mV (i.e., near E_{Cl^-} reported for other hypothalamic neurons).

4. Biocytin-injected neurons (n = 24) were found in the SDN-POA, as well as other parts of the medial preoptic nucleus and MPOA. Stained neurons had 1 or 2 primary dendrites (46% of stained cells) or had multipolar dendritic arrays (54% of cells); dendrites were aspiny or sparsely spiny and displayed limited branching. Morphologically definable cell types were similar electrophysiologically and were not specific to medial preoptic subdivisions.

5. These findings indicate that SDN-POA neurons share similar electrophysiological properties with surrounding medial preoptic cells. They also suggest that when compared with such hypothalamic nuclei as the paraventricular nucleus, the MPOA is *relatively* homogeneous in terms of sets of intrinsic membrane properties examined under constant temperature conditions. This is despite the differing morphology of these neurons and other heterogeneities apparent at different levels of analyses.

INTRODUCTION

The medial preoptic area (MPOA) is a hypothalamic region with a role in regulating diverse physiological processes, including fluid volume (Swanson and Mogenson 1981; van Gemert et al. 1975), core temperature (Boulant 1980), and reproduction (Giantonio et al. 1970; see Gorski 1985). The firing rates of medial preoptic neurons are sensitive to osmotic stimuli, glucose, temperature changes, and gonadal steroids (Boulant and Silva 1989). Lesions of the MPOA prevent phasic patterns of gonadotropic hormonal activity that promote ovulation in rodents (see Gorski 1985), and these also reduce male sexual (Giantonio et al. 1970) and maternal (Cohn and Gerall, 1989; Jacobson et al., 1980) behaviors. The adult expression of these reproductive activities depends on the presence of gonadal steroids during development (see Gorski 1985). Steroid hormones also alter synaptic morphology (Raisman and Field 1973) and cytoarchitectural subdivisions within the MPOA. The male version of the sexually dimorphic nucleus of the preoptic area (SDN-POA), which is larger than that of the female (Gorski et al. 1980), requires circulating androgens perinatally (Jacobson et al. 1981).

Anatomical and neurochemical techniques have been used extensively to study the MPOA from neuroendocrine and developmental perspectives. The animal model for most of this work has been the rat. In this species the MPOA is anatomically complex and has several subdivisions, including three subdivisions of the medial preoptic nucleus, the largest and most pronounced cell-dense region of the MPOA. One of these subdivisions, the medial preoptic nucleus centralis, largely corresponds with the posterior SDN-POA (Bloch and

Gorski 1988; Simerly and Swanson 1986). The MPOA also contains neurons that synthesize a variety of neurotransmitters and peptides (Simerly et al. 1986). Whether neurons in the SDN-POA have unique electrical properties when compared with other medial preoptic neurons is presently unknown. It is also not known whether the marked anatomical and neurochemical heterogeneity within the MPOA is associated with a similar degree of heterogeneity defined by sets of electrophysiological properties.

Certain intrinsic electrical properties and anatomical characteristics have been useful in defining cell types in other hypothalamic nuclei. For example, three categories of ventromedial neurons, each possibly subserving a separate biological function, were identified on the combined basis of their intracellular electrical properties and neuronal morphology (Minami et al. 1986a and b). Also, in the region of the paraventricular nucleus of the rat, magnocellular neurons, parvocellular neurons, and cells surrounding the nucleus were found to have distinct and identifying membrane properties. These included the capacity for low-threshold Ca^{2+} spikes (LTS), the linearity versus nonlinearity of current-voltage (I-V) relations, and membrane time-constant values (Hoffman et al. 1991; Tasker and Dudek 1991). Alternatively, despite anatomical heterogeneity, the MPOA could be comprised of neurons with mostly similar intrinsic membrane properties. In either situation, these electrophysiological properties would provide the substrate for integrating specific neuronal inputs or neurohumoral conditions that control reproduction and other biologically important processes associated with this region.

Synaptic transmission in the SDN-POA also has not been studied and has been little examined in the MPOA as a whole. Gamma-aminobutyric acid (GABA) is likely to be the

dominant inhibitory neurotransmitter in the hypothalamus (van den Pol et al. 1990). Spontaneous and evoked IPSPs that are mediated by GABA have been identified in other hypothalamic regions, including the paraventricular (Tasker and Dudek, in preparation), supraoptic (Randle et al. 1986), and suprachiasmatic (Kim and Dudek, 1990) nuclei. GABA may also be important for functions attributed to the MPOA and may mediate inhibitory synaptic transmission in this area. Regional GABA concentration is relatively high in the MPOA (Mansky et al. 1982), and many medial preoptic neurons stain for the GABA-synthesizing enzyme, glutamate decarboxylase (Flügge et al. 1986). GABA neurons in the MPOA may provide an important link in the feedback actions of gonadal steroids on the release of gonadotropic hormones and prolactin from the anterior pituitary (Jarry et al. 1991). Putative IPSPs have been identified in the MPOA of mice (Hodgkiss and Kelly, 1990) and rats (Curras et al., 1991), though neither study pharmacologically evaluated whether these events were due to GABA release. Collectively, these findings suggest that $GABA_A$-mediated inhibitory synaptic contacts are wide-spread throughout the MPOA; however, this remains to be shown with intracellular recordings from this region during bath application of GABA antagonists.

The present study compared the intrinsic and synaptic electrical properties of neurons in the SDN-POA with surrounding MPOA cells. Hodgkiss and Kelly (1990) obtained intracellular recordings from medial preoptic neurons in mice and identified LTS potentials in approximately half of these recorded cells. However, the focus of their study was to compare grafted preoptic cells with normal (control) neurons in tissue slices, and mice do not have an SDN-POA-like structure (Bleier et al., 1982). Curras et al. (1991) recorded

intracellularly from thermosensitive neurons in the MPOA and anterior hypothalamus of the rat, but they did not determine the precise cytoarchitectural location of their recordings, and they did not investigate the presence or absence of LTS potentials. Therefore, by combining intracellular recording with intracellular staining and histology, we tested three hypotheses: (1) Neurons in the SDN-POA are electrophysiologically homogeneous but differ from cells elsewhere in the MPOA; (2) Specific types of medial preoptic neurons generate LTS potentials; (3) GABA-mediated synaptic inhibition is wide-spread among these cells. Our results indicate that SDN-POA neurons do share common electrical properties, such as LTS potentials and $GABA_A$-mediated IPSPs, but they have these properties in common with other MPOA cells. Part of these data has been presented in abstract form (Hoffman et al. 1990).

METHODS

Slice Preparation

Hypothalamic slices containing the MPOA were obtained from adult Sprague-Dawley rats (150-300 g, Charles Rivers Breeding Laboratory) during the light phase of a 12-h light/dark cycle. Animals were anesthetized with nembutal (100 mg/kg intraperitoneal), decapitated, and their brains quickly removed and placed in chilled (1-4°C), oxygenated, artificial cerebrospinal fluid (ACSF). This consisted (in mM) of 124 NaCl, 26 $NaHCO_3$, 3 KCl, 1.3 $MgSO_4$, 1.4 NaH_2PO_4, 2.4 $CaCl_2$, and 11 glucose. A tissue block containing the hypothalamus was dissected and sectioned coronally at 400 μm on a vibroslice (Campden Instruments). The anterior commissure, optic chiasm, and third ventricle were landmarks used to identify the MPOA. Slices containing the MPOA (see Fig. 1) were placed in a ramp-type recording chamber, in which an interface between a humidified mixture of 95% O_2 and 5% CO_2 and the perfused ACSF (pH 7.4; 34 $\pm$ 1°C) was maintained. Slices were allowed to equilibrate in the recording chamber for 2-3 h before recording.

Electrophysiological Techniques

Micropipettes for intracellular recording were pulled from glass capillaries (1.0 mm OD, 0.5 mm ID, American Glass Co.), using a Flaming-Brown puller; they were filled with either 2 M K-acetate or 2 M K-acetate containing 2% biocytin (Sigma) and had tip resistances of 90-200 MΩ. Microelectrodes were advanced in 4-μm steps with a piezoelectric microdrive (Nanostepper), and cell impalements were achieved by oscillating the negative-

capacitance feedback. Electrical signals were recorded with an electrometer (Model IR183, Neurodata Instruments or Axoclamp-2A, Axon Instruments), which contained a bridge circuit. Signals were stored on video cassettes, using an analogue to digital converter (Neurocorder Model DR-484, Neurodata Instruments), and traces were generated (ISC67AVE system, RC Electronics) and printed on an X-Y plotter or a laser printer.

Stimulating electrodes were made from insulated platinum-iridium wire (diameter=75 μm). Constant-current stimulation was applied extracellularly to the dorsal preoptic region in a series of intensities (5-700 μA, 0.5 ms, 0.3 Hz) to evoke a complete range of synaptic responses. This stimulation site was chosen because it contains afferents to the medial preoptic nucleus (Simerly and Swanson 1986) and because stimulation applied to this site consistently elicited synaptic responses in recorded neurons.

Drug Application

In some experiments bicuculline methiodide (10 and 50 μM) was added to the ACSF perfusate to test whether GABA receptors mediated the IPSPs. Fast Na^+ spikes were blocked with bath application of tetrodotoxin (TTX, 50 μg/ml). To block Ca^{2+}-dependent potentials the ACSF was replaced with a solution containing (in mM) 125.5 NaCl, 3 KCl, 1.3 $MgCl_2$, 10 N-2-hydroxyethylpiperazine-N'-2-ethanesulphonic acid (HEPES), 11 glucose, 0.2 $CaCl_2$ and 0.5 $NiCl_2$.

Anatomy

Biocytin was iontophoresed intracellularly with negative current pulses (2 Hz, 100-300 ms, 200-500 pA), and injected cells were histologically processed as previously described (Horikawa and Armstrong 1988; Tasker et al. 1991). Briefly, slices were immersion-fixed for at least 12 h in 4% paraformaldehyde in 0.1 M Na-cacodylate buffer (pH 7.25; 5°C) and sectioned on a sliding microtome. An avidin-biotinylated horseradish peroxidase bridge was attached (Vectastain Elite kit, Vector Laboratories) and an opaque reaction product formed using a glucose-oxidase procedure and diaminobenzidine(-4HCl) (Sigma) as the chromogen (Smithson et al. 1984). Sections were mounted onto gelatin-coated slides and counterstained with cresyl violet or toluene blue.

RESULTS

General Electrophysiological Properties

Intracellular recordings were obtained from 46 medial preoptic neurons, all of which had overshooting action potentials $\geq$ 50 mV measured from threshold to peak (mean $\pm$ SEM = 61.2 $\pm$ 1.6 mV) and apparent resting potentials at or more negative than -50 mV (mean = -60.7 $\pm$ 2.2 mV, where each resting potential could be verified at the end of an experiment, n = 33). All recordings included in this study were stable for at least 10 min. Most of the recordings (94%) were made in slices from males; however, 3 medial preoptic neurons from ovariectomized females were included in analyses of LTS potentials, which were similar to those recorded in male tissue. In terms of intrinsic and synaptic electrophysiological properties examined in this study, neurons in the SDN-POA did not significantly differ from other medial preoptic neurons (Table 1).

Insert Table 1 about here

Low-Threshold Potentials

The most salient intrinsic property of medial preoptic neurons was their capacity to generate low-threshold potentials (mean amplitude $\pm$ SEM = 29.2 $\pm$ 1.8 mV), as observed in 98% of all recorded cells (n=46) and 100% of those neurons that were stained and histologically identified within the SDN-POA and elsewhere in the MPOA. When these cells were hyperpolarized, application of depolarizing current pulses could activate low-threshold

potentials that typically generated up to three Na^+ spikes (Fig. 1A and B). The low-threshold potentials persisted during TTX block of fast, voltage-dependent Na^+ channels (n=1), but these potentials were blocked by bath application of Ni^{2+} in low $[Ca^{2+}]_o$ HEPES medium (n=3) (data not shown). These potentials were also observed as anodal-break spikes following the offset of hyperpolarizing current pulses (Fig. 1C and D). Anodal-break spikes were also blocked by Ni^{2+} in the low-Ca^{2+} medium. Varying the duration of the hyperpolarizing current pulse revealed that voltage-dependent deinactivation of the low-threshold conductance was also time dependent (Fig. 1C). Therefore, these events appear to be low-threshold Ca^{2+} (LTS) potentials.

In some medial preoptic neurons, LTS potentials appeared to underly oscillating membrane potentials, which followed the offset of hyperpolarizing current pulses and resultant anodal-break spikes (Fig 1D). These oscillations were not observed in all cells.

Insert Fig. 1 about here.

Other Membrane Responses to Current Injection

Along with LTS potentials, medial preoptic neurons were similar in terms of other intrinsic properties, such as membrane time constant and input resistance (Table 1). Most cells (n=25) had I-V relations that were linear, with little or no evidence of anomolous and time-dependent inward rectification at hyperpolarizing potentials up to and greater than 40 mV below resting potential (mean Vm $\pm$ SEM = -61.1 $\pm$ 1.6 mV) (Figure 2A and 2B, left). The hyperpolarizing I-V relations of only two neurons suggested inward rectification, and the I-V plots from these cells were only weakly curvilinear (Figure 2B, right). One of these

neurons was otherwise electrophysiologically similar to other recorded cells in this study (e.g., capacity for LTS potentials); however, the other cell was the only recorded neuron that failed to generate an obvious LTS potential (data not shown). This neuron was not injected with biocytin, and so its position within the MPOA could not be verified.

Insert Fig. 2 about here.

Depolarizing current pulses of different intensity were applied to evaluate repetitive firing of medial preoptic cells (n=21). In most neurons (88%), spike frequency increased as a function of current intensity; spike amplitude and frequency declined as a function of time during the pulse (i.e., spike-frequency adaptation) (Fig. 3). The degree of adaptation was variable across neurons, and only one or two action potentials could be evoked in 2 cells. In most neurons (83% of 24 cells), relatively small afterhyperpolarizations followed spike trains (following 7-11 spikes, mean $\pm$ SEM amplitude = -4.7 $\pm$ 0.5 mV; duration = 64 $\pm$ 13 ms, measured at half maximum amplitude) (Fig. 3).

Insert Fig. 3 about here.

Synaptic Responses

Extracellular stimulation (50-700 μA) of the dorsal preoptic region reliably evoked synaptic potentials (n=34 neurons). In most cells (73%), this stimulation produced a fast EPSP that was attenuated by a single fast IPSP (Fig. 4A, 5A and B). Average latencies ($\pm$ SEM) for evoked EPSPs and IPSPs were 2.7 $\pm$ 0.2 ms and 4.8 $\pm$ 0.5 ms, respectively.

Although a single IPSP was most typically observed (Fig. 5A), stimulation evoked multiple IPSPs in a few neurons (Fig 4A, top trace, and B). In some instances spikes occurred at the termination of large IPSPs (Fig. 4B), suggesting that the IPSPs deinactivated the conductance underlying the LTS potentials. Spontaneous PSPs were frequently recorded, and among these events IPSPs were prominent (Fig. 4C). The reversal potential of evoked IPSPs was -71 $\pm$ 5 mV (mean $\pm$ SEM, n=7) (Fig. 5A), and bath application of bicuculline (10 and 50 μM) blocked the evoked IPSPs (n=3). In neurons in which stimulation usually evoked only IPSPs in normal medium, bicuculline blocked the IPSPs and revealed EPSPs (Fig. 5B).

Insert Figs. 4 and 5 about here.

Medial Preoptic Subdivisions and Neuronal Morphology

After impalement with biocytin-filled electrodes and subsequent histological procedures, 24 neurons were recovered and located in the SDN-POA, the medial preoptic nucleus medialis (MPNm), and elsewhere in the MPOA. Stable recordings were obtained in 18 of these cells (see Table 1). Neurons varied with respect to their dendritic arbor: one set of cells (46% of stained neurons) had 1 or 2 primary dendrites (Fig. 6), and another set (54%) had multipolar dendritic arrays (Fig. 7). These morphological characteristics were not uniquely associated with specific medial preoptic subdivisions examined in the present study (Fig. 8). Soma sizes were similar in both sets of neurons: longest-axis soma diameters of neurons with 1 or 2 primary dendrites ranged from 11 to 34 μm and shortest-axis diameters from 10 to 22 μm. Soma diameters of multipolar cells ranged from 16 to 34 μm (longest axis) and from 10 to 16 μm (shortest axis). Dendritic arbors in both sets of neurons were

sparsely spiny or aspiny; only primary dendrites were observed on 38% of stained cells and both primary and secondary dendrites on 62% of the cells. Axons typically originated from primary dendrites and most often coursed in a medial to ventromedial direction (7 of 10 observations), in some cases giving off local collaterals (Fig. 9). Both primary axons and local collaterals contained varicosities (Figs. 6, 7 and 9). Regardless of cytoarchitectonic location or morphological appearance, stained neurons had similar electrical properties that did not differ from those recorded in most unstained (or non-anatomically recovered) neurons (see Table 1 and below).

Insert Figs. 6-9 about here

DISCUSSION

SDN-POA vs. Other MPOA Neurons

In the present study intrinsic membrane properties were studied in neurons that were histologically verified to reside in the SDN-POA, as well as in surrounding medial preoptic neurons. The hypothesis that sets of these properties were similar among SDN-POA neurons was confirmed, but the hypothesis that these properties differed between neurons in this nucleus with cells situated elsewhere in the MPOA was not. Instead, neurons with a common set of intrinsic properties appear to constitute the predominant electrophysiological cell type across medial preoptic subdivisions. Unstained neurons, whose precise cytoarchitectonic locations could not be determined, also had properties similar to those of stained cells with verified locations within the MPOA. It is unlikely that the homogeneity reflects selection of cells residing in a single location or having a common morphology, because the intracellular staining confirmed that the data were obtained from a variety of locations and cells with differing morphology. Among medial preoptic cells, the lack of covariations among sets of examined intrinsic properties indicates relative homogeneity at this level of analysis. Thus neurochemical and anatomical heterogeneity within this region (Simerly et al., 1986; Simerly and Swanson, 1986) may not be associated with a similar heterogeneity in neuronal membrane properties recorded under constant-temperature conditions.

This study does not rule out the possibility that a small subset of neurons with distinct electrophysiological properties also resides in the MPOA. In studies conducted in the corpus

striatum and zona compacta of the substantia nigra, principle neurons comprised 95% of recorded neurons, whereas 5% of cells at each site had different electrophysiological properties (Jiang and North, 1991; Lacey et al., 1989). If an analogous situation exists in the MPOA, approximately 2 cells would have shown different properties from the rest of the cells recorded in the present study. One neuron did fail to generate an obvious LTS potential, and, unlike all but one other medial preoptic neuron, it had inward rectifying I-V relations in the hyperpolarizing direction. Although the position of this atypical cell within the MPOA was not histologically verifiable, this recording is consistent with the possibility of a *small subset* of medial preoptic neurons with distinctly different properties from the majority of cells in this region.

It is also possible that the actual percentage of medial preoptic neurons constituting such a subset(s) would be underestimated in data from intracellular recordings, since a recording bias would be expected for larger neurons (e.g., Jiang and North, 1991). However, present data do suggest that, similar to the hypothalamic supraoptic nucleus (Andrew and Dudek, 1983; Andrew and Dudek, 1984 a and b; Bourque and Renaud, 1985), the medial preoptic area is *relatively* homogeneous in comparison with other hypothalamic nuclei, such as the paraventricular nucleus (Hoffman et al., 1991; Tasker and Dudek, 1991).

LTS

As hypothesized, medial preoptic neurons could generate LTS potentials, but these potentials did not differentiate cell types in this region. Unlike the paraventricular, ventromedial, and arcuate nuclei (Hoffman et al. 1991; Loose et al. 1990; Minami et al. 1986

a and b; Tasker and Dudek 1991), where only subsets of neurons display LTS potentials, all anatomically identified medial preoptic neurons recorded in the present investigation had the capacity for these potentials. This was also true for all but the one unstained neuron discussed above. This finding appears to contrast with previous recordings from grafted and non-grafted medial preoptic neurons in mice, in which a large proportion of cells were not identified as having LTS potentials (Hodgkiss and Kelly 1990). This apparent discrepancy could reflect a species difference or instead the different focus of the previous study (Hodgkiss and Kelly 1990). The LTS potentials recorded in the present investigation generally were not as large as those described in the inferior olivary nucleus (Llinás and Yarom 1981) and thalamus (Jahnsen and Llinás 1984). Nonetheless, they had similar voltage dependence, and they were likewise Ca^{2+} dependent in that bath application of Ni^{2+} in a low Ca^{2+}-containing medium blocked them. These data, plus the voltage dependence of these potentials, suggest mediation by channel openings responsible for transient (T) Ca^{2+} currents, which are particularly sensitive to Ni^{2+} (Fox et al. 1987). In medial preoptic neurons, LTS potentials generated only one or a few Na^{+} spikes and thus resembled hypothalamic parvocellular (type II) neurons in the paraventricular nucleus (Hoffman et al. 1991; Tasker and Dudek 1991). As recorded in paraventricular parvocellular neurons, LTS-mediated anodal-break spikes in medial preoptic neurons could trigger membrane oscillations. These oscillations, however, were not as robust as those reported for cells situated near but outside the paraventricular nucleus (type III neurons) (Hoffman et al. 1991; Tasker and Dudek 1991). Other membrane properties described below also indicate similarities between medial preoptic and paraventricular parvocellular

neurons.

Other Intrinsic Properties

Values for input resistance, membrane time constant, Na^+-spike amplitude and duration, and resting potential were similar among medial preoptic neurons. Most medial preoptic cells had linear I-V relations in the hyperpolarizing direction, with the I-V plots from two cells deviating slightly from linearity. Similar values and I-V relations were reported for paraventricular parvocellular neurons (Hoffman et al. 1991; Tasker and Dudek 1991). This suggests two main points: (1) a broad category of hypothalamic parvocellular neurons with a common set of intrinsic electrophysiological properties extends across certain hypothalamic regions, and (2) these properties are important for integrating responses to the several homeostatic stimuli known to affect the activity of cells in this region (Boulant and Silva 1989).

Fast Synaptic Events and GABA

Findings from this study support the hypothesis that medial preoptic neurons receive GABA receptor-mediated synaptic inhibition. Spontaneous EPSPs and IPSPs were consistently recorded in these cells, and an EPSP-IPSP sequence could often be evoked by applying electrical stimuli to the dorsal preoptic region. The evoked IPSPs were usually superimposed on the EPSPs, thus reducing the amplitude and duration of the evoked EPSPs. In some experiments, evoked EPSPs could be observed only when the IPSPs were blocked with bicuculline. This effect of bicuculline on IPSPs, coupled with an IPSP reversal near the

Cl^- equilibrium potential (Randle et al. 1986), indicates that ligand-binding at $GABA_A$ receptors mediates these events. Previous findings suggest that medial preoptic cells synthesize GABA (Mansky et al. 1982; Flügge et al. 1986) and that GABA-releasing neurons participate in synchronizing phasic gonadotropic activity (Jarry et al. 1991). Our findings relate to this latter possibility in two ways: (1) GABA appears to be the primary, if not the only, neurotransmitter mediating fast IPSPs in medial preoptic neurons; and (2) the axons of stained cells often ramified into an apparent network of local collaterals, possibly forming local circuits in this region.

Future Direction

Properties frequently encountered in medial preoptic recordings (e.g., LTS potentials and $GABA_A$-receptor-mediated synaptic inhibition) probably play a significant role in interneuronal communication in this region of the hypothalamus. Conceivably, these electrophysiological properties could be regulated by testicular hormones that also regulate the development of anatomical characteristics of the MPOA (Gorski et al. 1980; Jacobson et al. 1981; Raisman and Field 1973). Developmental studies and comparisons between males and females are required to assess possible electrophysiological "sexual dimorphism" and its regulation by gonadal steroids.

We thank Dr. P. Micevych for his advice and for the use of his histological specimens, both of which facilitated cytoarchitectural identifications. We also thank Dr. D. Birt for computer programming. The assistance of S. Sampogna and G. Allen in histologically processing tissue samples is gratefully acknowledged, as is the help provided by S. Belkin and C. Gray in preparing figures. This research was supported by a grant from the Air Force Office of Scientific Research (F. E. D.) and a National Institutes of Health postdoctoral fellowship (N.W. H.).

REFERENCES

Andrew, R.D., and Dudek, F.E. Burst discharge in mammalian neuroendocrine cells involves an intrinsic regenerative mechanism. *Science* 221: 1050-1052, 1983.

Andrew, R.D., and Dudek, F.E. Analysis of intracellularly recorded phasic bursting by mammalian neuroendocrine cells. *J. Neurophysiol.* 51: 552-566, 1984a.

Andrew, R.D., and Dudek, F.E. Intrinsic inhibition in magnocellular neuroendocrine cells of rat hypothalamus. *J. Physiol. (Lond.)* 353: 171-185, 1984b.

Bleier, R., Byne, W., and Siggelkow, I. Cytoarchitectonic sexual dimorphisms of the medial preoptic and anterior hypothalamic areas in guinea pig, rat, hamster, and mouse. *J. Comp. Neurol.* 212: 118-130, 1982.

Bloch, G.J., and Gorski, R.A. Cytoarchitectonic analysis of the SDN-POA of the intact and gonadectomized rat. *J. Comp. Neurol.* 275: 604-612, 1988.

Boulant, J.A. Hypothalamic control of thermoregulation: neurophysiological basis. In: *Handbook of the Hypothalamus* 3 (part A), edited by P.J. Morgane and J. Panksepp. New York: Dekker, 1980, p. 1-82.

Boulant, J.A., and Silva, N.L. Multisensory hypothalamic neurons may explain interactions among regulatory systems. *News in Physiological Sciences* 4: 245-248, 1989.

Bourque, C.W., and Renaud, L.P. Calcium-dependent action potentials in rat supraoptic neurosecretory neurons recorded in vitro. *J. Physiol. (Lond.)* 363: 419-428, 1985.

Cohn, J., and Gerall, A.A. Pre- and postpuberal medial preoptic area lesions and maternal behavior in the rat. *Physiol. Behav.* 46: 333-336, 1989.

Curras, M.C., Kelso, S.R., and Boulant, J.A. Intracellular analysis of inherent and synaptic activity in hypothalamic thermosensitive neurons in the rat. *J. Physiol. (Lond.)* 440: 257-271, 1991.

Flügge, G., Oertel, W.H., and Wuttke, W. Evidence for estrogen-receptive GABAergic neurons in the preoptic/anterior hypothalamic area of the rat brain. *Neuroendocrinology* 53: 261-267, 1986.

Fox, A.P., Nowycky, M C., Tsien, R.W. Kinetic and pharmacological properties distinguishing three types of calcium currents in chick sensory neurons. *J. Physiol. (Lond.)* 394: 149-172, 1987.

Giantonio, G.W., Lund, N.L., and Gerall, A.A. Effect of diencephalic and rhinencephalic lesions on the male rat's sexual behavior. *J. Comp. Physiol. Psychol.* 73: 38-46, 1970.

Gorski, R.A. Sexual dimorphisms of the brain. *J. Animal Sci.* 61: 38-61, 1985.

Gorski, R.A., Harlan, R.E., Jacobson, C.D., Shryne, J.E., and Southam, A.M. Evidence for the existence of a sexually dimorphic nucleus of the preoptic area. *J. Comp. Neurol.* 193: 529-539, 1980.

Hodgkiss, J.P., and Kelly, J.S. An intracellular study of grafted and *in situ* preoptic area neurones in brain slices from normal and hypogonadal mice. *J. Physiol. (Lond.)* 423: 111-135, 1990.

Hoffman, N.W., Kim, Y.I., Gorski, R.A., and Dudek, F.E. Electrical and morphological characteristics of neurons in the male sexually dimorphic nucleus (SDN) of the rat medial preoptic area (MPOA). *Soc. Neurosci. Abstr.* 16: 574, 1990.

Hoffman, N.W., Tasker, J.G., and Dudek, F.E. Immunohistochemical differentiation of

electrophysiologically defined neuronal populations in the region of the rat hypothalamic paraventricular nucleus. *J. Comp. Neurol.* 307: 405-416, 1991.

Horikawa, K., and Armstrong, W.E. A versatile means of intracellular labeling: Injection of biocytin and its detection with avidin conjugates. *J. Neurosci. Methods* 25: 1-11, 1988.

Jacobson, C.D., Csernus, V.J., Shryne, J.E., and Gorski, R.D. The influence of gonadectomy, androgen exposure, or gonadal graft in the neonatal rat on the volume of the sexually dimorphic nucleus of the preoptic area. *J. Neurosci.* 1: 1142-1142, 1981.

Jacobson, C.D., Terkel, J., Gorski, R.A., and Sawyer, C.H. Effects of small medial preoptic area lesions on maternal behavior: retrieval and nest building in the rat. *Brain Res.* 194: 471-478, 1980.

Jahnsen, H., and Llinás, R. Electrophysiological properties of guinea-pig thalamic neurons: An *in vitro* study. *J. Physiol. (Lond.)* 349: 205-226, 1984.

Jarry, H., Leonhardt, S., Wuttke, W. Gamma-aminobutyric acid neurons in the preoptic/ anterior hypothalamic area synchronize the phasic activity of the gonadotropin-releasing hormone pulse generator in ovariectomized rats. *Neuroendocrinology* 53: 261-267, 1991.

Jiang, J.-G., and North, R.A. Membrane properties and synaptic responses of rat striatal neurones *in vitro*. *J. Physiol. (Lond.)* 443: 533-553, 1991.

Kim, Y.I., and Dudek, F.E. Suprachiasmatic nucleus (SCN) neurons receiving retinal inputs are under the control of gamma-amino butyric acid (GABA). *Soc. Neurosci. Abstr.* 16: 574, 1990.

Lacey, M.G., Mercuri, N.B., and North, R.A. Two cell types in rat substantia nigra zona compacta distinguished by membrane properties and the actions of dopamine and opioids.

J. Neurosci. 9: 1233-1241, 1989.

Llinás, R., and Yarom, Y. Electrophysiology of mammalian inferior olivary neurons *in vitro*. Different types of voltage-dependent conductances. *J. Physiol. (Lond.)* 315: 549-567, 1981.

Loose, M.D., Ronnekleiv, O.K., and Kelly, M.J. Membrane properties and response to opioids of identified dopamine neurons in the guinea pig hypothalamus. *J. Neurosci.* 10: 3627-3634, 1990.

Mansky, T., Mestres-Ventura, P. and Wuttke, W. Involvement of GABA in the feedback action of estradiol on gonadotropin and prolactin release: hypothalamic GABA and catecholamine turnover rates. *Brain Res.* 231:353-364, 1982.

Minami, T., Oomura, Y., and Sugimori, M. Electrophysiological properties and glucose responsiveness of guinea-pig ventromedial hypothalamic neurones *in vitro*. *J. Physiol. (Lond.)* 380: 127-143: 1986a.

Minami, T., Oomura, Y., and Sugimori, M. Ionic basis for the electroresponsiveness of guinea-pig hypothalamic neurones *in vitro*. *J. Physiol. (Lond.)* 380: 145-156, 1986b.

Raisman, G. and Field, P.M. Sexual dimorphism in the neuropil of the preoptic area of the rat and its dependence on neonatal androgen. *Brain Res.* 54: 1-29, 1973.

Randle, J.C., Bourque, C.W., and Renaud, L.P. Characterization of spontaneous and evoked inhibitory postsynaptic potentials in rat supraoptic neurosecretory neurons in vitro. *J. Neurophysiol.* 56: 1703-1717, 1986.

Simerly, R.B., Gorski, R.A., and Swanson, L.W. Neurotransmitter specificity of cells and fibers in the medial preoptic nucleus: an immunohistochemical study in the rat. *J. Comp. Neurol.* 246: 343-363, 1986.

Simerly, R.B., and Swanson, L.W. The organization of neural inputs to the medial preoptic nucleus of the rat. *J. Comp. Neurol.* 246: 312-342, 1986.

Smithson, K.G., Cobbett, P., MacVicar, B.A., and Hatton, G.I. A reliable method for immunohistochemical identification of Lucifer Yellow injected peptide-containing mammalian central neurons. *J. Neurosci. Methods* 10: 59-69, 1984.

Swanson, L.W and Mogenson, G.J. Neural mechanism for the functional coupling of autonomic, endocrine and somatomotor responses in adaptive behaviors. *Brain Res. Rev.* 3: 1-34, 1981.

Tasker, J.G., and Dudek, F.E. Electrophysiological properties of neurons in the region of the paraventricular nucleus in slices of the rat. *J. Physiol. (Lond.)* 434, 271-293, 1991.

Tasker, J.G., Hoffman, N.W., and Dudek, F.E. Comparison of three intracellular markers for combined electrophysiological, morphological and immunohistochemical analyses. *J. Neurosci. Methods* 38: 129-143, 1991.

van den Pol, A. N., Wuarin, J.-P., and Dudek, F.E. Glutamate, the dominant excitatory transmitter in neuroendocrine regulation. *Science* 250: 1276-1278, 1990.

van Gemert, M., Miller, M., Carey, R.J., and Moses, A.M. Polyuria and impaired ADH release following medial preoptic lesioning in the rat. *Am. J. Physiol.* 228:1293-1297, 1975.

FIGURE LEGENDS

Figure 1. LTS potentials recorded in medial preoptic neurons. A: At rest a neuron fired a single action potential in response to the injection of a depolarizing current pulse (left). As a neuron was hyperpolarized with steady (DC) current, the same current pulse intensity triggered a regenerative depolarization to Na^+-spike threshold, resulting in a short burst of action potentials (middle). The size of this depolarization grew with increasing DC hyperpolarization, shown here during bath application of tetrodotoxin (TTX: 0.5 μg/ml) to a different neuron (right). B: Progressively increasing the intensity of a depolarizing current pulse from a hyperpolarized condition also progressively increased the size of the LTS potential (calibration bars in B also apply to A). C: Time dependence of LTS potentials. Hyperpolarizing current pulses had to be sufficiently long for an LTS potential to occur with the offset of the pulse, whether the Na^+ spikes were unblocked (left) or blocked (right) with TTX. D: An anodal-break spike could generate a burst of Na^+ spikes, and a post-burst afterhyperpolarization could then trigger a membrane oscillation (or series of oscillations) (voltage trace in D is the average of 4 traces). In this and in subsequent figures, top traces are current, the bottom traces are voltage, and dotted lines indicate resting potential. Traces in A (right) and C (right) are from a female rat.

Figure 2. I-V relations of medial preoptic neurons. Rectangular current pulses of 100-300 ms duration of increasing intensity were injected and the voltage responses recorded. Current pulses were typically injected from rest (mean $\pm$ SEM = 61.1 $\pm$ 1.6 mV) or

occasionally from a slightly hyperpolarized (DC) condition to reduce spontaneous firing (64.7 $\pm$ 0.33 mV). Membrane time constant and input resistance values were calculated from averaged voltage deflections (n=5-30) in response to weak current pulses (-50 pA or -100 pA) (see Table 1). A: Voltage deflections of a medial preoptic cell in response to current injections. B (left): I-V plots of several representative medial preoptic neurons. Both A and B (left) show linear I-V relations in the hyperpolarizing direction. B (right): I-V plots from the only 2 neurons with non-linear I-V relations suggesting inward rectification in the hyperpolarizing direction. Traces in A are the average of 4-7 traces except that indicated by the arrowhead, which was averaged across 22 traces for membrane time constant measurement.

Figure 3. Spike trains in response to different intensities of depolarizing current pulses. With greater current-pulse intensity, spike frequency increased but also typically showed moderate adaptation across the duration of the pulse. Afterhyperpolarizations usually followed spike trains of sufficient frequency (dotted line indicates resting potential).

Figure 4. Evoked and spontaneous postsynaptic potentials recorded in medial preoptic neurons. A: In most medial preoptic cells, an EPSP-IPSP sequence could be evoked by extracellular stimulation of the dorsal preoptic region but only at certain stimulus intensities. In this neuron, increasing stimulus intensity only slightly increased IPSP amplitude until an intensity was reached that evoked an EPSP-IPSP sequence (voltage traces are averaged across 4 traces). B: In a few medial preoptic cells, extracellular stimulation of the dorsal

preoptic region evoked one or more IPSPs. The four traces are from the same neuron, where multiple IPSPs were evoked by a 30 μA stimulus. Note that depolarizations generating action potentials (clipped in this figure) occasionally followed the large IPSPs. C: Spontaneous PSPs, including IPSPs, were frequently recorded in medial preoptic neurons, shown here by four separate traces from the same cell recorded at rest. Arrowhead in A and B indicates stimulus artifact.

Figure 5. Properties of evoked IPSPs. A: In this medial preoptic neuron, a 300-μA extracellular stimulus to the dorsal preoptic region evoked an EPSP-IPSP complex. The IPSP reversed near -72 mV. B: In another medial preoptic cell, a 200-300 μA stimulus to the dorsal preoptic region evoked only an IPSP (top) in normal medium. Bath application of the $GABA_A$ antagonist, bicuculline (BIC, 10 μM), blocked the evoked IPSP and revealed an evoked EPSP (middle). The effect of bicuculline was reversible (bottom) and was not accompanied by appreciable changes in input resistance (right traces). During this experiment, the cell was hyperpolarized with 11 pA of steady current to prevent spontaneous firing. Voltage traces in B are averaged across 21-30 individual traces. Arrowheads indicate stimulus artifacts.

Figure 6. Morphology of a bipolar medial preoptic neuron. Camera lucida drawing (top) and photomicrographs (bottom) showing a biocytin-injected neuron with 2 primary dendrites. As shown at lower power (left), this cell was situated in the sexually dimorphic nucleus of the preoptic area. Calibration bars = 50 μm; iii = third ventricle.

Figure 7. Morphology of a multipolar medial preoptic neuron. Camera lucida drawing (right) and photomicrographs (center and left) showing a biocytin-injected neuron with a multipolar array of primary dendrites. This neuron was located in the medial preoptic nucleus medialis (lower power photomicrograph). Calibration bars = 50 μm; iii = third ventricle.

Figure 8. Schematic diagram of the approximate location of recorded and stained neurons with respect to medial preoptic subdivisions. A-D represents a rostral-caudal progression through the medial preoptic area (MPOA). Stained neurons are schematicized in terms of their numbers of primary dendrites. Other abbreviations: ac = anterior commissure; ADP = anterodorsal preoptic nucleus; AVP = anteroventral periventricular nucleus, BST = bed nucleus of the stria terminalis; BSTenc = BST encapsulated portion; DBB = diagonal band of Broca; LPOA = lateral preoptic nucleus; MPNm = medial preoptic nucleus medialis; MePO = median preoptic nucleus; ox = optic chiasm; PVN = paraventricular nucleus; PSCN = preoptic suprachiasmatic nucleus; SDN = sexually dimorphic nucleus of the preoptic area; SCN = suprachiasmatic nucleus; SO = supraoptic nucleus; iii = third ventricle. Schematics were adapted with permission from Simerly and Swanson (1986).

Figure 9. Axon collaterals from a medial preoptic neuron. Camera lucida drawing and photomicrograph of a bipolar neuron located in the sexually dimorphic nucleus of the preoptic area. Note that its axon (a) arose from a primary dendrite (d) and ramified locally. Axon collaterals were covered with varicosities (arrowheads). Calibration bars = 50 μm; iii

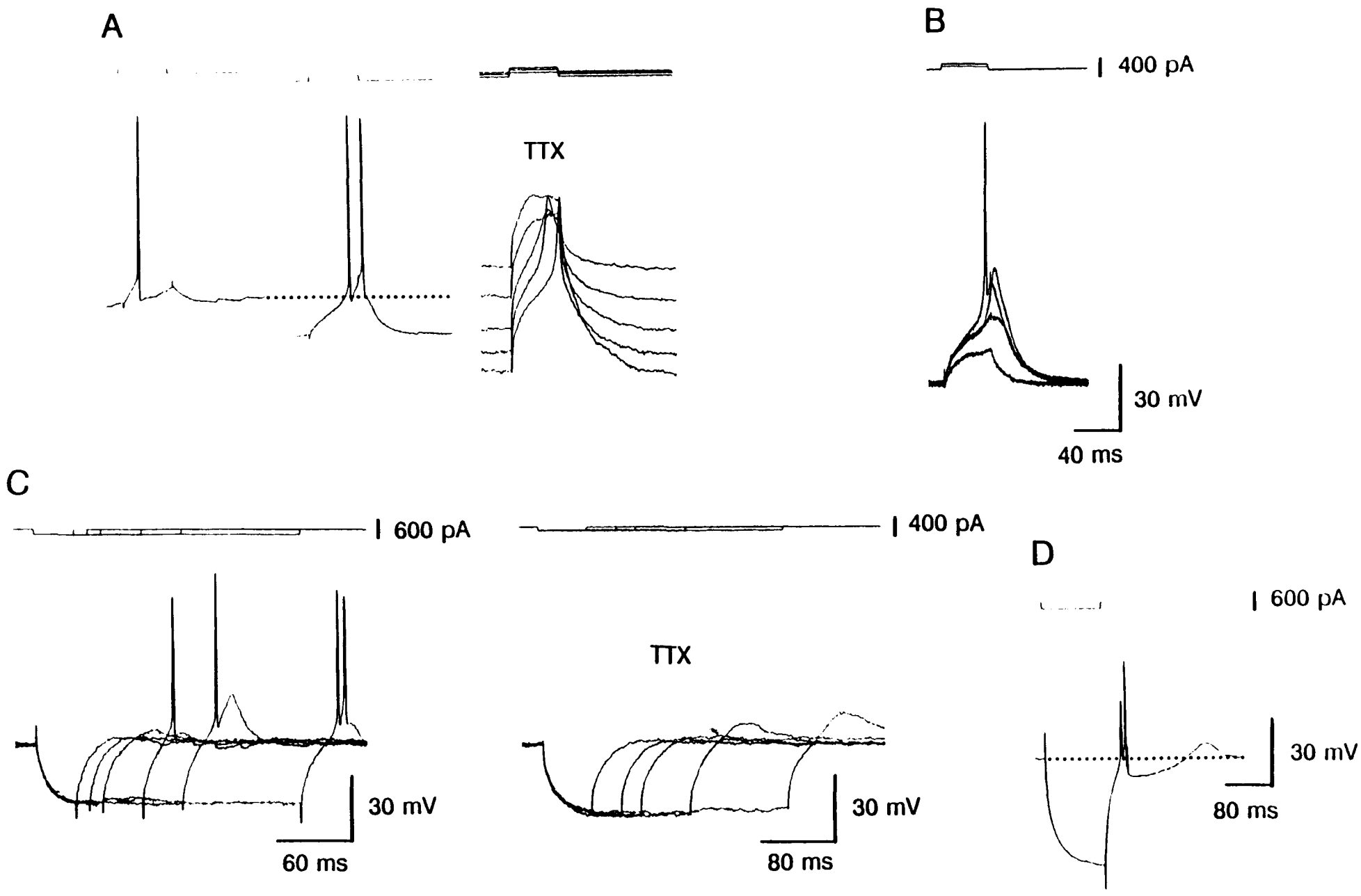
A
TTX
B
400 pA
30 mV
40 ms
C
600 pA
400 pA
30 mV
60 ms
TTX
30 mV
80 ms
D
600 pA
30 mV
80 ms

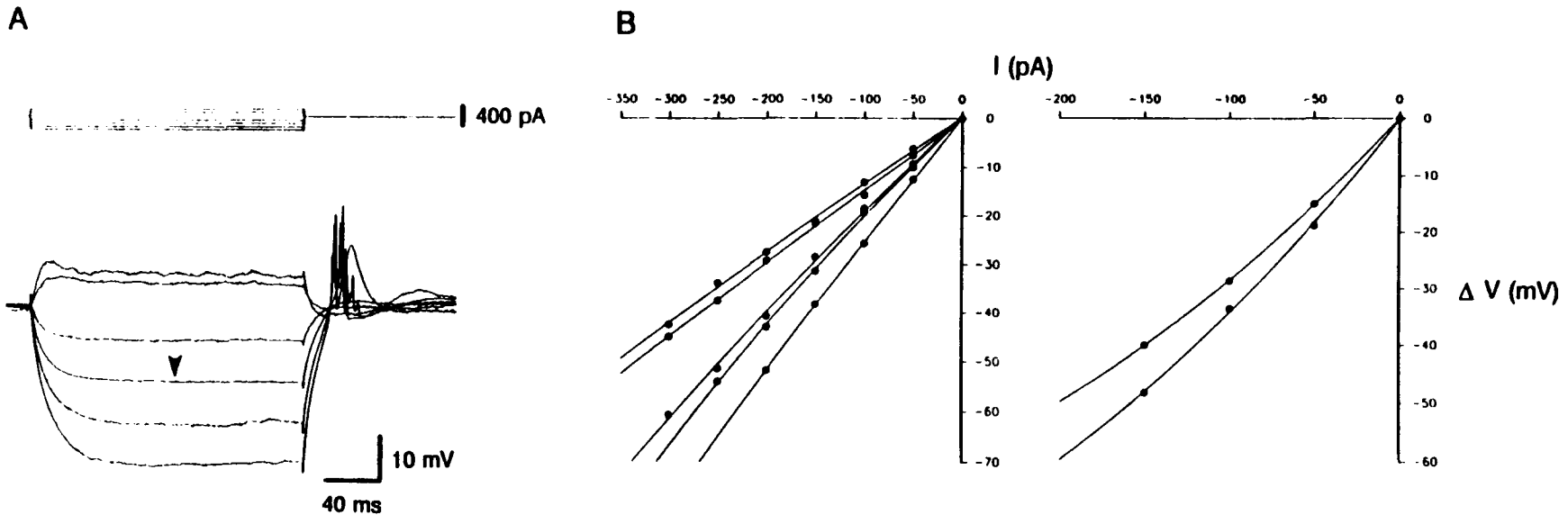
A
400 pA
10 mV
40 ms
B
I (pA)
-350 -300 -250 -200 -150 -100 -50 0
0 -10 -20 -30 -40 -50 -60 -70
-200 -150 -100 -50 0
0 -10 -20 -30 -40 -50 -60
Δ V (mV)

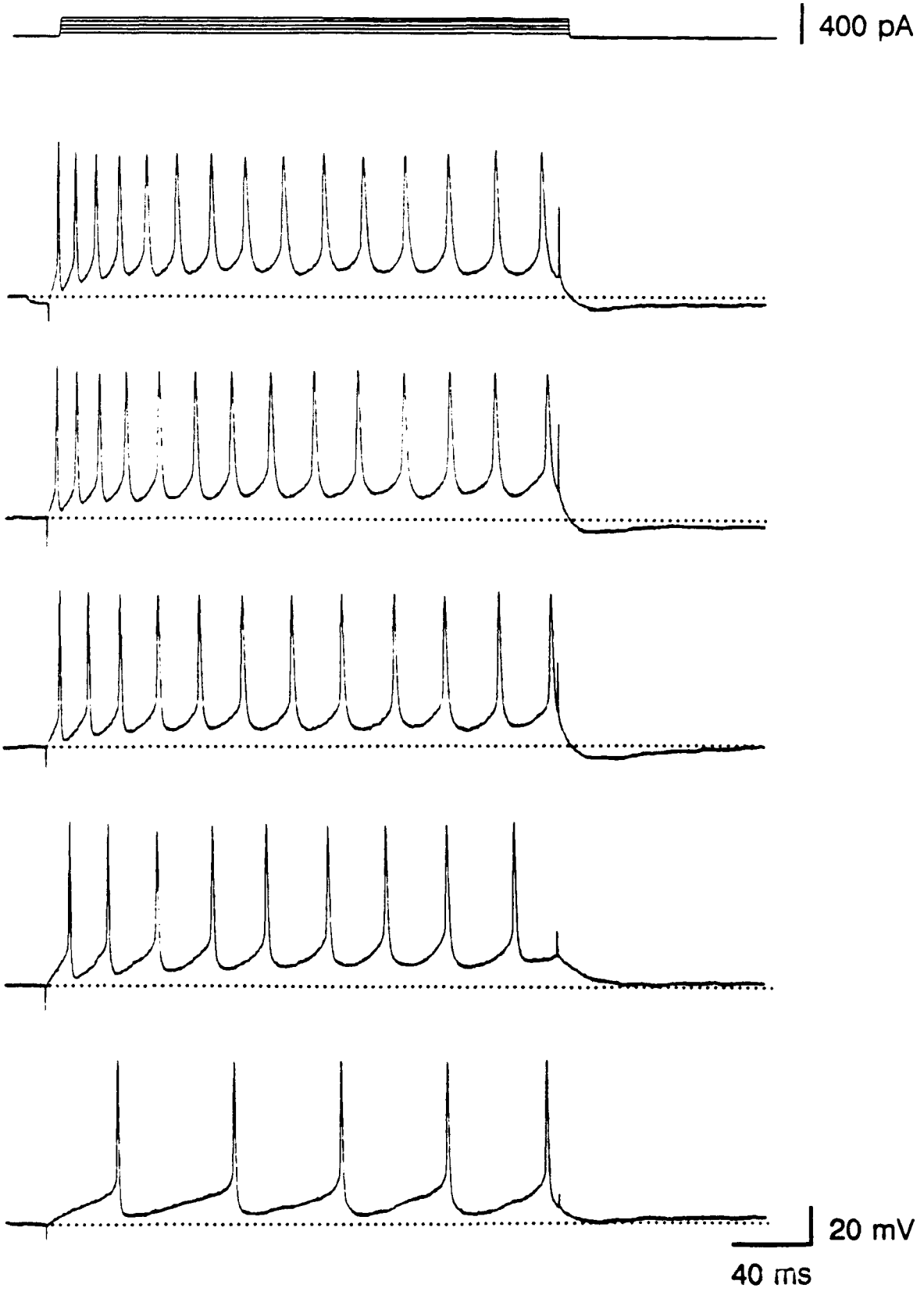

Fig. 3

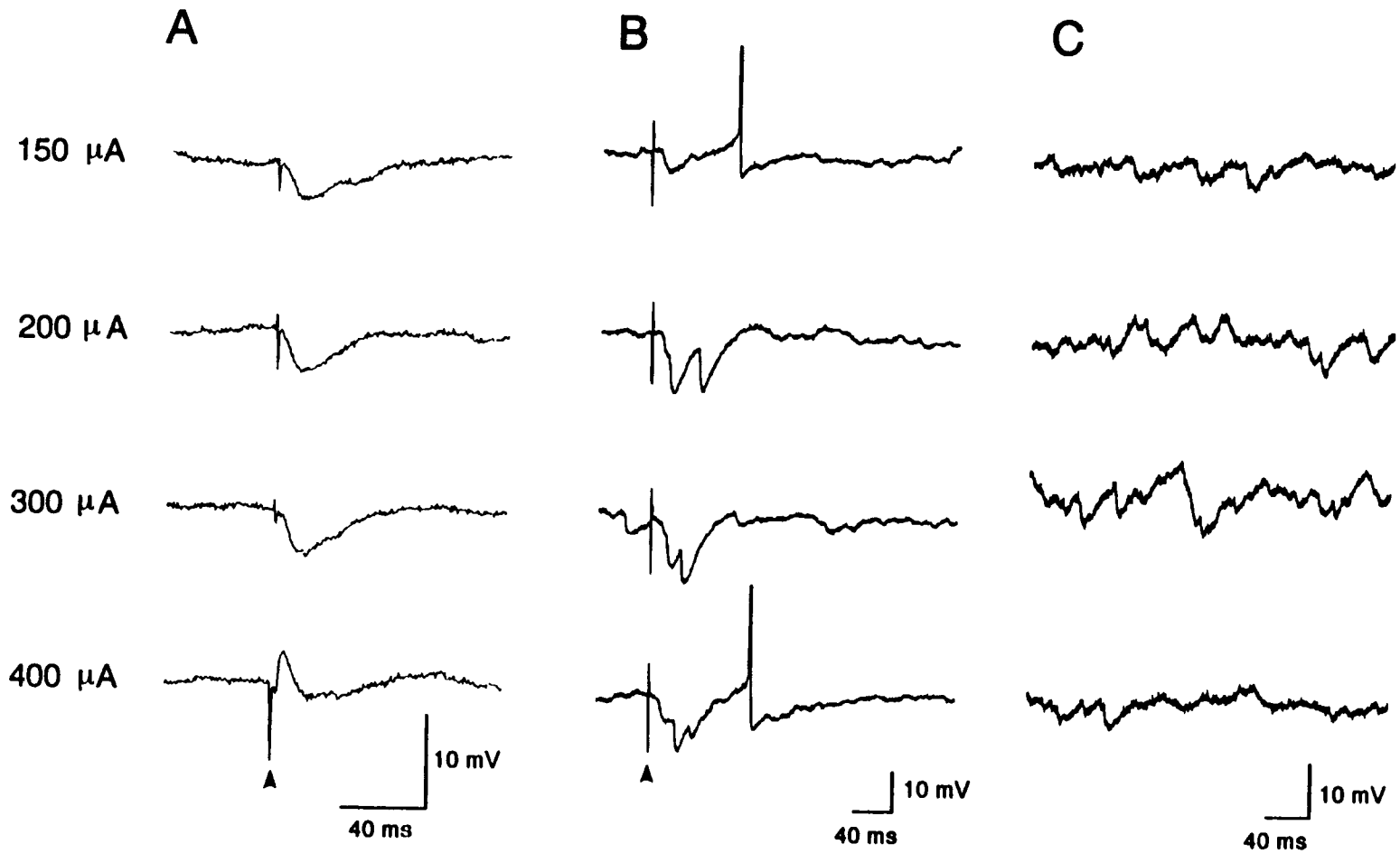
A
B
C
150 µA
200 µA
300 µA
400 µA
A
10 mV
40 ms
A
10 mV
40 ms
10 mV
40 ms

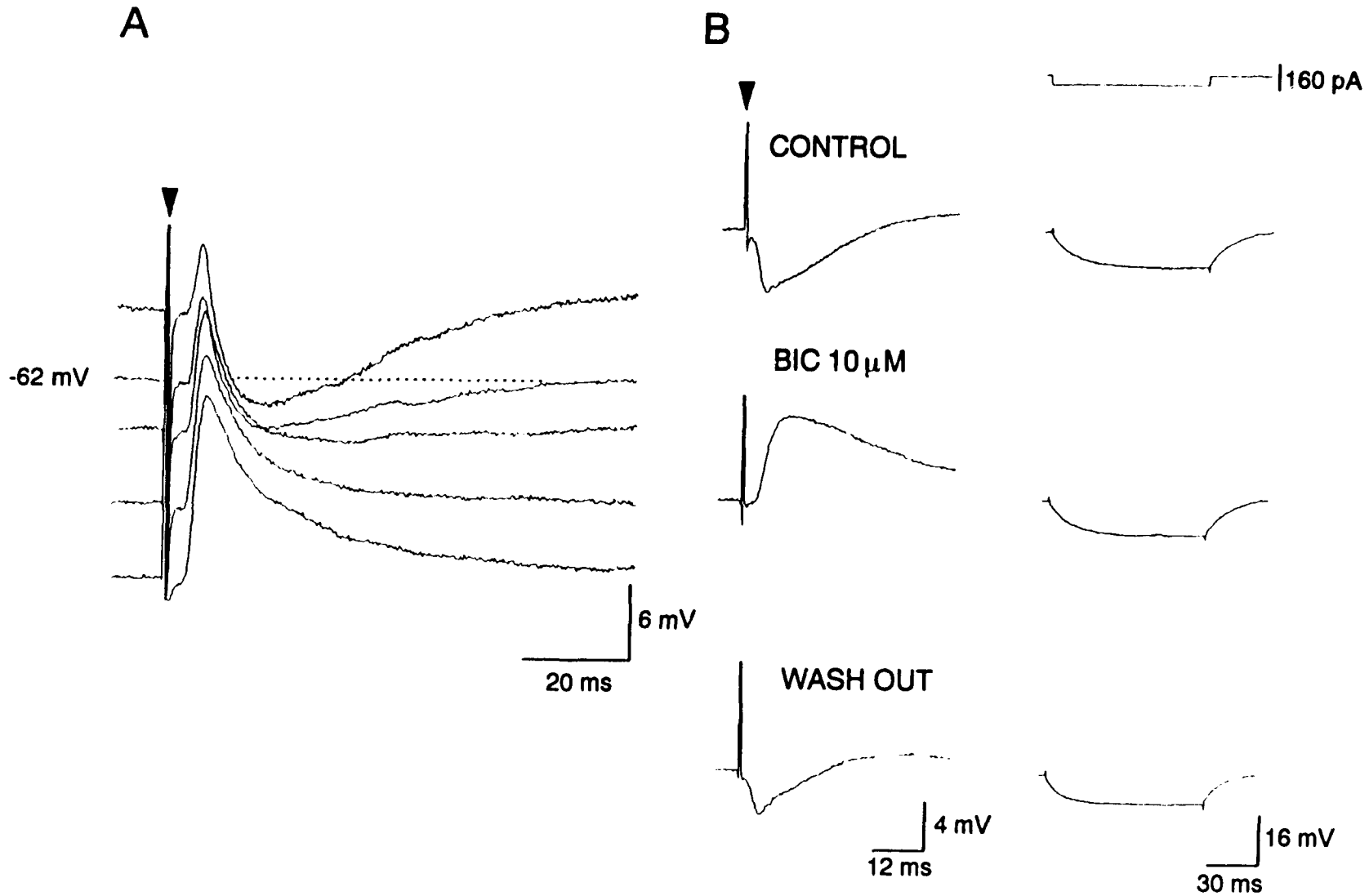
A
-62 mV
6 mV
20 ms
B
160 pA
CONTROL
BIC 10 μM
WASH OUT
4 mV
12 ms
16 mV
30 ms

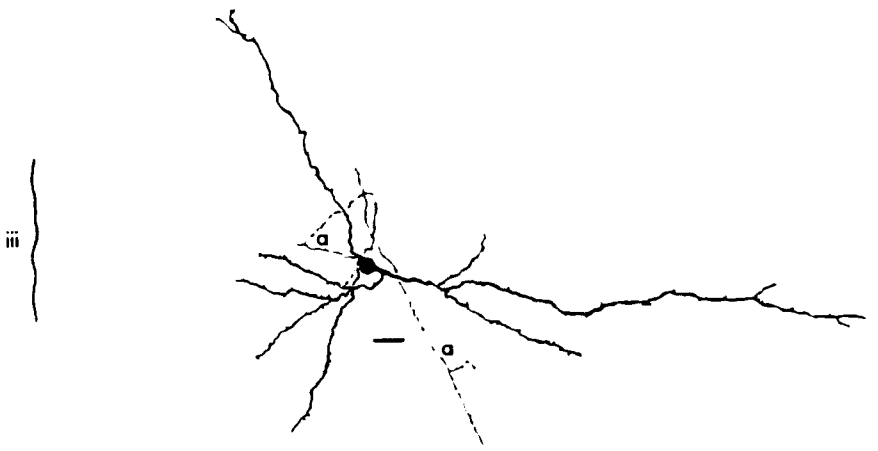

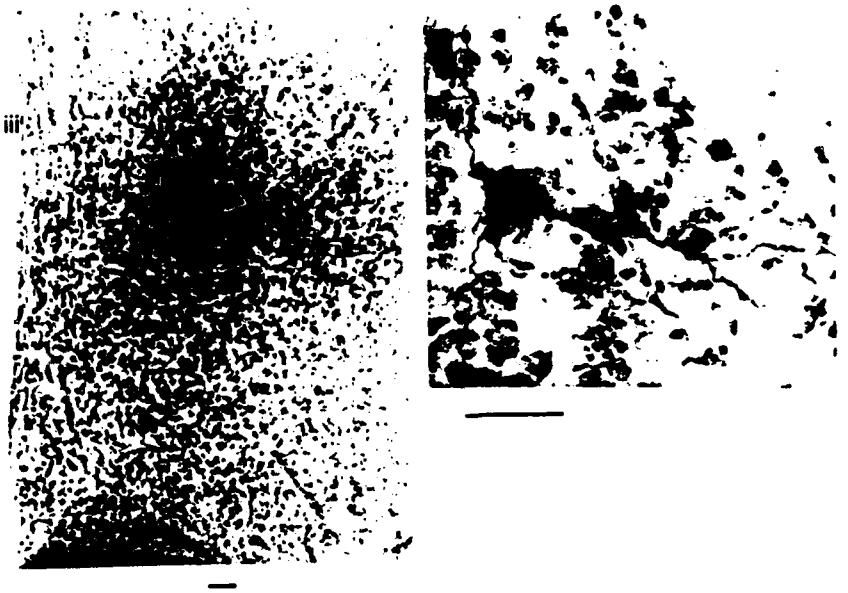

Fig 6

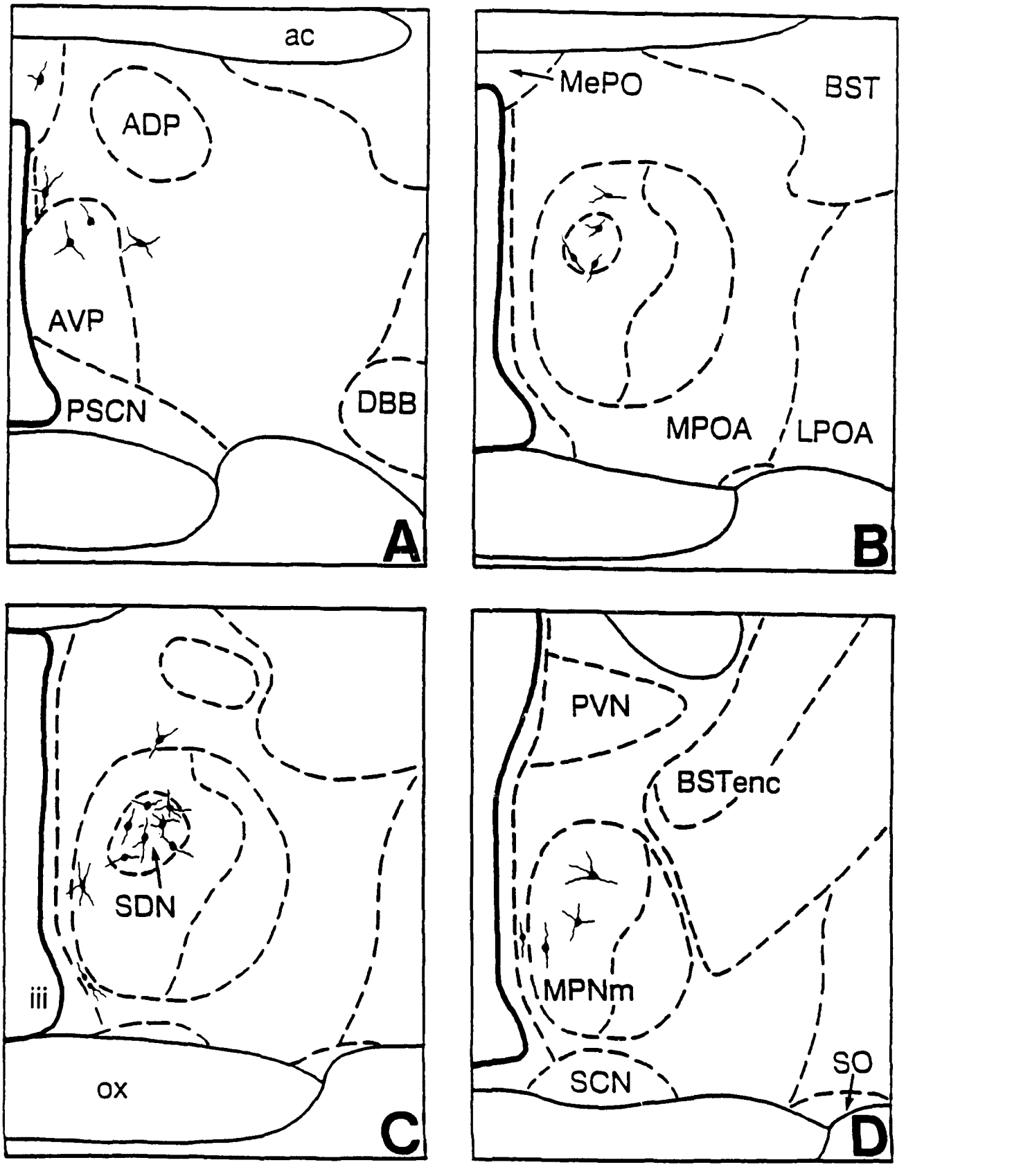
ac
ADP
AVP
PSCN
DBB
A
MePO
BST
MPOA
LPOA
B
SDN
iii
ox
C
PVN
BSTenc
MPNm
SCN
SO
D

Fig 8

Table 1. Basic electrophysiological properties of medial preoptic neurons.

	SDN-POA	MPOA	Undetermined Location
Resting Potential (mV):	-57.8 ± 1.7 (6)	-61.9 ± 2.8 (10)	-61.2 ± 2.1 (17)
Input Resistance (MΩ):	164 ± 15 (5)	191 ± 24 (9)	209 ± 19 (16)
Membrane Time Constant (ms):	16.8 ± 4.5 (5)	13.8 ± 2.1 (8)	15.6 ± 1.7 (10)
Spike Amplitude from Threshold (mV):	61.1 ± 2.6 (7)	62.3 ± 1.7 (11)	60.7 ± 1.3 (27)
Spike Duration at Half Amplitude (ms):	0.71 ± 0.09 (7)	0.83 ± 0.08 (10)	0.80 ± 0.05 (21)

Properties are expressed as mean ± SEM (n). No statistically significant differences were observed (student's t-test, $p < 0.05$) between neurons in the sexually dimorphic nucleus of the preoptic area (SDN-POA) and those situated in other parts of the medial preoptic area (MPOA). Recorded neurons in the Undetermined Location category were either not injected with biocytin or were not histologically recovered after injection. The MPOA was also targeted for these recordings (note the similarity between obtained values and those of stained neurons in the SDN-POA and elsewhere in the MPOA).

Running title page

PATCH CLAMP ANALYSIS OF SPONTANEOUS SYNAPTIC CURRENTS IN SUPRAOPTIC NEUROENDOCRINE CELLS OF THE RAT HYPOTHALAMUS

Abbreviated title:

Spontaneous synaptic currents
in supraoptic neurons

Number of text pages: 16

Number of figures: 8

Number of table: 0

Correspondence:

F. Edward Dudek, Ph.D.
Department of Anatomy and Neurobiology
Colorado State University
Fort Collins, CO 80523
Tel: (303) 491-5847
FAX: (303) 491-7907

Key words:

hypothalamus, supraoptic nucleus, neurosecretion,
magnocellular neuroendocrine cells, amino acids,
synaptic currents, patch clamp

Title page

Dr. Charles F. Stevens

PATCH CLAMP ANALYSIS OF SPONTANEOUS SYNAPTIC CURRENTS IN SUPRAOPTIC NEUROENDOCRINE CELLS OF THE RAT HYPOTHALAMUS

Jean-Pierre Wuarin
F. Edward Dudek

Mental Retardation Research Center
and the Laboratory of Neuroendocrinology
of the Brain Research Institute
UCLA School of Medicine
Los Angeles, California 90024

Present address:

F. Edward Dudek
Jean-Pierre Wuarin
Department of Anatomy and Neurobiology
Colorado State University
Fort Collins, CO 80523

Acknowledgments:

This research was supported by a grant from the US Air Force Office of Scientific Research to F.E. Dudek and by a fellowship from the Swiss National Science Foundation to J.-P. Wuarin.
We thank A. Bienvenu for secretarial assistance.

Abstract

Spontaneous synaptic currents were recorded in supraoptic magnocellular neurosecretory cells using whole-cell patch-clamp techniques in the rat hypothalamic slice preparation. Numerous spontaneous excitatory and inhibitory postsynaptic currents (EPSCs and IPSCs) were observed in the 27 cells recorded. The rate of occurrence of the spontaneous currents and the relative proportion of EPSCs versus IPSCs varied significantly from cell to cell. Miniature EPSCs and IPSCs were clearly distinguished from background noise in tetrodotoxin (n=3 cells at 0.5 μg/ml). The frequency of EPSCs and IPSCs decreased by approximately 70% and the largest events were blocked in tetrodotoxin, but the peaks of the amplitude histograms were shifted by only a few millivolts. Bicuculline (n=10 cells at 10 μM and 2 cells at 20 μM) blocked completely all the IPSCs without any detectable effect on the frequency or amplitude of the EPSCs. No slow spontaneous outward currents, indicative of a K^+ current from activation of $GABA_B$ receptors, were observed. The α-amino-3-hydroxy-5-methyl-4-isoxazole propionic acid (AMPA)/kainate type glutamate receptor antagonist 6-cyano-2,3-dihydroxy-7-nitroquinoxaline (CNQX; n=7 cells at 10 μM) consistently blocked all EPSCs without any apparent effect on the frequency or amplitude of the IPSCs. No synaptic events could be detected when CNQX was applied in combination with bicuculline (n = 4). The decay phase of averaged spontaneous IPSCs and EPSCs recorded at resting membrane potential could be well fitted by single exponential functions in most cells. The time constants ranged from 1.3 to 3.0 ms for EPSCs (4 cells) and 5.5 to 6.6 ms for IPSCs (3 cells). A second, slower time constant of 4 to 15 ms was found in the largest averaged EPSCs (≥ 40 pA). The amplitude of this slow component was -2 to -4 pA. These results suggest that in magnocellular neurosecretory cells, glutamate mediates all the spontaneous EPSCs by acting primarily on AMPA/kainate type receptors at resting membrane potential and that activation of $GABA_A$ receptors mediates most if not all IPSCs.

Magnocellular neuroendocrine cells of the supraoptic nucleus have long been considered as a model system for a wide range of studies on neurosecretion. These neuroendocrine cells synthesize the neuropeptide hormones oxytocin and vasopressin and transport them, from their cell bodies in the supraoptic and paraventricular nuclei, along their axons to the neurohypophysis where they are secreted directly in the general circulation. The supraoptic nucleus has particular advantages for electrophysiological studies on neuroendocrine cells because, unlike other hypothalamic nuclei, virtually all of these cells project to the neurohyphophysis and are therefore neuroendocrine. Numerous substances (e.g., acetylcholine, norepinephrine, opioid peptides, dopamine, histamine, serotonin, substance P, vasopressin, oxytocin, cholecystokinin, somatostatin) have been proposed to regulate or modulate hypothalamic neurosecretion (for review of the neuropharmacology of this system, see Renaud and Bourque, 1991). A wide range of studies on conventional neurons, as opposed to hypothalamic neuroendocrine cells, suggest that these substances primarily serve as neuromodulators rather than neurotransmitters responsible of traditional synaptic potentials. Until recently, however, relatively few studies have directly tested the hypothesis that excitatory and inhibitory amino acids (i.e., glutamate and γ-aminobutyric acid (GABA)) mediate all fast synaptic transmission in the magnocellular neuroendocrine system (Gribkoff and Dudek, 1988; Gribkoff and Dudek, 1990; Wuarin and Dudek, 1991). Recent evidence suggests that most of the excitatory and inhibitory synapses, not only in the magnocellular system, but throughout the neuroendocrine hypothalamus may be glutamatergic and GABAergic respectively (van den Pol et al., 1990).

Studies using intracellular recordings showed that two broad-spectrum antagonists for excitatory amino acids, kynurenic acid and γ-d-glutamylglycine, inhibit electrically evoked and spontaneous excitatory postsynaptic potentials in the rat supraoptic nucleus (Gribkoff and Dudek, 1988, 1990). Most of the electrically induced excitatory synaptic input to magnocellular and

parvocellular neurons in the paraventricular nucleus and to neurons in the arcuate nucleus has been shown to be inhibited or blocked by 6-cyano-2,3-dihydroxy-7-nitroquinoxaline (CNQX), suggesting that glutamate mediates excitatory synaptic events mainly by activating AMPA/kainate type receptors (Wuarin and Dudek, 1991; Van den Pol et al. 1990). Immunohistochemical studies have shown glutamate-reactive presynaptic boutons in contact with dendrites and cells bodies in the supraoptic nucleus (Meeker et al., 1989; van den Pol et al., 1990). Therefore, recent electrophysiological and immunohistochemical observations have provided evidence that glutamate is a neurotransmitter at many excitatory synapses in the supraoptic nucleus and elsewhere in the hypothalamus.

A recent anatomical study using post-embedding surface staining with immunogold showed that GABA immunoreactive terminals compose approximately 50% of the synaptic input, non only to the supraoptic nucleus, but also to paraventricular, arcuate and suprachiasmatic nuclei. This observation strongly suggests that GABA is the most important inhibitory neurotransmitter in the magnocellular system and in the hypothalamus (Decavel and van den Pol, 1990). Intracellular recordings from supraoptic neurons obtained in the explant preparation showed an abundance of spontaneous IPSPs that were chloride-dependent and mediated by $GABA_A$-receptor activation (Randle et al., 1986). Extracellular stimulation in the diagonal band of Broca evoked IPSPs that closely resembled the spontaneous events. These results suggest that supraoptic magnocellular neurons receive an extensive and powerful inhibitory GABAergic input, originating at least in part in structures located rostral to the supraoptic nucleus.

The electrophysiological studies mentioned above used sharp microelectrodes for intracellular recording. This technique allows detection of spontaneous EPSPs but has limitations regarding the resolution of small events. Synaptic potentials mediated by substances other than glutamate or GABA may be relatively small and may not have been detected. Another potential problem of these previous studies is the use of extracellular electrical stimulation to evoke synaptic responses. The

stimuli were delivered through electrodes positioned near the supraoptic or paraventricular nucleus, a location that gave large and consistent synaptic responses. With this method, however, it is likely that only a fraction of the entire input to a nucleus is activated, and that afferent fibers releasing neurotransmitters other than amino acids were not stimulated. In the present study, we used whole cell patch-clamp recordings in conventional hypothalamic slices (Blanton et al., 1989) to address the two problems mentioned above. This technique provides a signal-to-noise ratio far superior than intracellular recording with sharp electrodes and allows detection of miniature synaptic events (Edwards et al., 1990; Otis et al., 1991). Testing the effects of amino acid receptors antagonists on spontaneous EPSCs and IPSCs would be expected to provide a more rigorous assessment of the importance of the excitatory and inhibitory amino acids (i.e., glutamate and GABA) as transmitters for the neuroendocrine cells in the supraoptic nucleus.

The aims of this study were 1) to establish the properties of spontaneous postsynaptic currents in supraoptic magnocellular neuroendocrine cells, 2) to determine if glutamate, acting on AMPA/kainate type receptors, mediates all detectable excitatory synaptic currents, 3) to test if $GABA_A$ receptors mediate all detectable IPSCs, and 4) to determine if activation of NMDA receptors contributes to the decay of EPSCs. The properties and components of the EPSCs and IPSCs were examined through analyses of the time course of the events, and the role of AMPA/kainate and $GABA_A$ receptors was evaluated with bath application of CNQX and bicuculline.

Materials and Methods

Slice preparation. Young male rats (50-80 g) were decapitated, their brain rapidly dissected and placed in ice-cold perfusion solution (see below) for 1 min. During the dissection, particular care was taken to cut the optic nerves without applying any tension on them. A block of tissue containing the hypothalamus was then trimmed and glued on the stage of a vibrating microtome. Usually two slices of 400-600 μm containing the supraoptic nucleus were cut in a frontal plan and immediately transferred in a ramp chamber (Haas et al., 1979) oxygenated with 95% O_2-5% CO_2 and thermoregulated at 34 °C. The perfusion solution contained (in mM) 124 NaCl, 26 $NaHCO_3$, 3 KCl, 1.3 $MgSO_4$, 1.4 NaH_2PO_4, 2.4 $CaCl_2$, and 10 glucose; pH 7.4. The following drugs were applied in the perfusion solution: bicuculline methiodide (10 and 20 μM), tetrodotoxin (0.5 μg/ml) (both from Sigma, St. Louis, MO) and CNQX (3 and 10 μM, from Tocris Neuramin, Buckhurst Hill, England)

Recording methods. Whole-cell current recordings (Hamill et al., 1981) were obtained using patch pipettes with open resistances of 2-5 MΩ. Seal resistances were 1 to 10 GΩ, series resistances were 5-25 MΩ compensated at >80%. Patch pipettes were filled with (in mM) 140 K-gluconate, 10 HEPES, 1 NaCl, 1 $CaCl_2$, 1 $MgCl_2$, 5 BAPTA, 4 ATP (pH 7.2). ATP was used to decrease the run down of IPSCs. Without 4 mM ATP, IPSCs gradually disappeared within the first 20 min (Stelzer et al., 1988). The pipettes were pulled from borosilicate glass of 1.7 mm diameter and 0.5 mm wall thickness. Currents were recorded using an Axopatch-1D amplifier, low-pass filtered at 2 kHz, digitized at 44 kHz (Neuro-Corder, Neurodata Inc.) and stored on video tapes. The amplitude and decay phases of spontaneous synaptic currents were measured on a personnal computer using pClamp programs (Axon Instruments).

Cell labeling. Six cells were recorded with pipettes containing biocytin (0.2% n=2 and 0.4% n=4). At the end of the experiment, the slice containing the marked cell was immersed in 4% paraformaldehyde in 0.1 M sodium cacodylate buffer overnight. The tissue was then cut at 50 µm and rehydrated. The sections were labeled with an avidin-biotinylated horseradish peroxydase reaction (Horikawa and Armstrong, 1988). To ascertain that the labeled cells were within the boundaries of the supraoptic nucleus, the slices were counter-stained with cresyl violet.

Results

Recordings were obtained from 27 cells in 23 slices. Once the whole-cell configuration was established, stable recordings were achieved for several hours without noticeable change in resting membrane potential or input resistance. Mean resting membrane potential was -63 ± 2.5 mV (mean ± SE, n = 21), and input resistances ranged from 400 to 1100 MΩ with a mean of 726 ± 50 MΩ (mean ± SE, n = 25). All recordings were made with the holding potential set to the same value as the resting membrane potential for the recorded cell.

Although it was relatively easy to position recording electrodes within the supraoptic nucleus under visual control using slices cut in the frontal plan, we also recorded from 6 cells with pipettes containing biocytin in order to label them and verify that we were indeed recording from magnocellular neurons. This confirmed that we were not recording from cells at the periphery of the nucleus which have been hypothetised to be GABAergic neurons (Theodosis et al., 1986). We recovered 4 cells, and they were located well within the boundaries of the supraoptic nucleus (2 cells could not be found in the stained sections).

Numerous spontaneous synaptic events were observed in all cells. Inward currents were defined as EPSCs and outward currents as IPSCs (Fig. 1). The IPSC amplitudes ranged from 10 to 80 pA, and the average amplitude for each cell was between 15 and 30 pA. The EPSC amplitudes ranged from -10 to more than -150 pA, and the average amplitude was from -10 to -50 pA. The rate of occurence of spontaneous EPSCs and IPSCs varied from < 1 Hz to > 10 Hz (Fig. 2). Three cells showed bursts of spontaneous IPSCs, and the maximum frequency of IPSCs during a burst was > 20 Hz (Fig. 3). The proportion of EPSCs versus IPSCs also varied from cell to cell; 4 cells showed mostly IPSCs and 2 cells showed only EPSCs.

Fig. 1 about here

Fig. 2 about here

Fig. 3 about here

Effects of tetrodotoxin on synaptic currents

We applied TTX in the perfusion solution at 0.5 μg/ml to test if synaptic activity could be detected after action potentials had been blocked (Fig. 4). In the 3 cells tested, miniature EPSCs and IPSCs could be clearly distinguished from baseline noise. Figure 5 shows an example of amplitude distributions of spontaneous EPSCs and IPSCs before and during the application of TTX.

Fig. 4+5 about here

Effect of bicuculline and CNQX on spontaneous synaptic currents

To determine if all the IPSCs were due to the activation of $GABA_A$ receptors, we tested bicuculline on 10 cells at 10 μM and on 2 cells at 20 μM. Bicuculline, at both concentrations, blocked completely all the IPSCs in all the cells tested. This block was reversible (Fig. 6). Bicuculline had no effect on the frequency and amplitude of EPSCs and it did not modify input resistance or resting membrane potential.

Fig. 6 about here

In order to test the hypothesis that all spontaneous EPSCs in magnocellular neuroendocrine cells are mediated by glutamate, we applied the non-NMDA receptor-selective antagonist, CNQX, in the perfusion solution. The antagonist was tested on 6 cells at 10 μM and on 1 cell at 3 μM. In the 7 cells tested, CNQX reversibly blocked all the EPSCs. In 3 cells, bicuculline (20 μM) was applied before CNQX to block IPSCs and isolate the EPSCs. When CNQX was then added to bicuculline in the perfusion solution, no synaptic activity could be detected (Fig. 7).

Fig. 7 about here

Time course of decay phase of spontaneous currents

Decays of spontaneous currents were measured from averaged EPSCs and IPSCs recorded

at resting membrane potential. The synaptic currents were averaged by using the first half of the rising phase to align them. Both EPSCs and IPSCs could be fitted by a single exponential function (Fig. 8). The fit was quite good for all the averaged IPSCs. Decays of the smaller averaged EPSCs (i.e. ≤30 -pA) could be well fitted by a single exponential (τ = 2.4 ± 0.38 ms; n = 4; e.g., Fig. 8, cells 1,3 and 4). However, in 4 of the larger averaged EPSCs (≥40 pA, e.g. Fig. 8, cells 2 and 5), the decay was better fitted by the sum of two exponentials. The second time constant second was 4 to 15 ms, and its amplitude was -2 to -4 pA.

Fig. 8 about here

Discussion

Patch-clamp and spontaneous currents versus previous studies

The present study is the first using the whole-cell patch-clamp technique in the "thick slice" (Blanton et al., 1989) to investigate the electrophysiology of the magnocellular system. All the previous studies of neurotransmission in the magnocellular system used sharp microelectrodes, which provide relatively low signal-to-noise ratio. The necessity of using particularly high-resistance electrodes to obtain stable recordings in magnocellular neuroendocrine cells compounded the problem of the low resolution of this type of electrode and made it difficult to record spontaneous events routinely. Only high-quality recordings allowed clear detection of spontaneous synaptic activity (Randle et al., 1986; Gribkoff and Dudek, 1990). The previous work was also based mostly on the study of electrically evoked synaptic responses. The rationale for this approach was to obtain responses that were large enough to allow accurate measurement of the effects of selective antagonists. After averaging, this allowed analysis of dose-response relations (Wuarin and Dudek, 1991). One of the weaknesses of the electrical stimulation technique is that one can only activate particular pathway(s), and therefore, evoked synaptic responses may not reveal all of the afferent inputs to a cell. Considering these limitations and the amount of evidence accumulated over the years in favor of other neurotransmitters in the magnocellular system, we reexamined the importance of glutamatergic and GABAergic neurotransmission in the magnocellular system by studying spontaneous synaptic events with a technique that allows greatly superior resolution over sharp microelectrodes.

The improved signal-to-noise ratio provided by patch pipettes allowed us to detect spontaneous miniature synaptic currents in all the cells tested with TTX. The amplitude of the

miniature EPSCs and IPSCs was well above noise level in each cell tested. It is therefore reasonable to assume that we would have been able to detect any spontanous EPSCs and IPSCS not mediated by glutamate or the activation of $GABA_A$ receptors when the non-NMDA receptor antagonist CNQX and bicuculline were present in the perfusion solution.

It has been shown that spontaneous GABA- and glutamate-mediated synaptic currents can be observed in an isolated mammalian central neuron (Drewe et al., 1988). These currents were Ca^{2+} dependent and blocked by γ-d-glutamylglycine and bicuculline. These results suggest that the presence of functional synaptic boutons attached to the postsynaptic cell is a sufficient condition for miniature spontaneous activity to occur, and that the cell bodies and the axons of the projecting cells are not necessary. Therefore, spontaneous activity in the slice may provide a qualitative means to study all of the inputs to a given cell.

One of the major limitations of the patch-clamp technique is the dialysis of the cell cytoplasm. The consequence is "rundown", which affects mainly currents dependent on the activation of G-protein coupled receptors. Ligand-gated channels generating fast events, such as the nicotinic acetylcholine receptor, seem to be less susceptible to washout. We did not detect any obvious decrease in the spontaneous activity within the first 3 min of recording, which suggests that rapid washout of synaptic currents after establisment of the whole-cell configuration did not occur. However, we found that Mg^{2+} in the intracellular solution was necessary to avoid washout of all IPSCs within 30 min. When Mg^{2+} was present in the pipette, we did not notice any obvious decrease in the frequency of spontaneous events, even over a period of several hours of recording. The fact that EPSCs and IPSCs recovered from the effect of CNQX and bicuculline, respectively, argues against the possibility that washout occured during application of the antagonists.

EPSCs and excitatory amino acids

The results obtained in the present study support and extend the earlier work showing that kynurenic acid, γ-d-glutamylglycine and CNQX inhibit evoked excitatory postsynaptic potentials in supraoptic and paraventricular magnocellular neuroendocrine cells (Gribkoff and Dudek, 1988; Gribkoff and Dudek, 1990; Wuarin and Dudek, 1991). As mentioned above, these studies used extracellular electrical stimulation to evoke synaptic responses and high-resistance sharp microelectrodes with re' ively low resolution. Although these results showed that excitatory amino acids are a major excitatory neurotransmitter in the magnocellular neuroendocrine system, the methods used did not allow one to exclude an important role of other neurotransmitters. There is an abundance of data showing that other neuroactive substances influence vasopressin and oxytocin secretion as well as increase the firing activity of magnocellular neurons. Among the most studied potential neurotransmitters with excitatory actions in the magnocellular system are acetylcholine, norepinephrine, dopamine, histamine, cholecystokinin and angiotensin (Renaud and Bourque, 1991). In other systems in the brain, these substances have been shown to have slow effects. In the magnocellular system, evidence has been presented suggesting the existence of a monosynaptic cholinergic input onto supraoptic neurons (Hatton et al., 1983). As described above, the signal-to-noise ratio obtained with patch pipettes would have allowed us to detect any small events mediated by neurotransmitters such as acetycholine or histamine (Yang and Hatton, 1989). We did not detect any inward current in the 7 cells tested with CNQX. The present results support the hypothesis that glutamate probably mediates all the fast EPSCs in magnocellular neuroendocrine cells.

NMDA receptors and EPSCs

Several recent studies have demonstrated that NMDA receptors are present in supraoptic cells. A dl-2-amino-5-phosphonopentanoic acid (AP-5) sensitive component to electrically evoked postsynaptic potentials could be revealed in the slice preparation when Mg^{2+} was deleted from the perfusion solution (Gribkoff 1991). The amplitude of excitatory synaptic potentials evoked by electrical stimulation of the organum vasculosum lamina terminalis was increased in Mg^{2+}-free medium and inhibited by AP-5 (Yang and Renaud, 1991). Depolarization (Hu and Bourque, 1991a) and rythmic bursting activity (Bourque and Hu, 1991; Hu and Bourque, 1991b) could be induced in magnocellular neurons by application of NMDA. These results suggest that NMDA receptors are present on these cells, that they influence their firing properties and that they play a role in synaptic transmission.

In hippocampal granule cells (Keller et al., 1991), NMDA-dependent evoked EPSCs recorded in cells voltage-clamped near resting membrane potential had a decay that could be fitted by a double exponential whose time constants were approximately 1 and 2 orders of magnitude larger than that of the non-NMDA component. These time constants were increased in nominally 0 Mg^{2+}. In the thin cerebellar slice, evoked EPSCs in granule neurons had a slow component that could be blocked by AP-5. Miniature EPSCs were composed of an initial fast non-NMDA component followed by clearly discernable NMDA channels (Silver et al., 1992). Averaging of these miniature currents revealed that the channel openings formed a second slower synaptic component. The amplitude of the slow NMDA component, in both spontaneous and induced EPSCs was approximately 10% of the fast component amplitude. To detect a potential NMDA component in the spontaneous EPSCs at resting membrane potential, we measured the time course of the decay phase using exponential functions. We found that the decay phase of averaged spontaneous EPSCs in magnocellular

neuroendocrine cells could be well fitted with one exponential in most cells. In a few cells, however, we found a second component characterized by a small amplitude (approximately 10% that of the fast component) and a time constant 5 to 10 times slower than the fast time constant. This slow phase of the decay of spontaneous EPSCs is reminiscent of an NMDA component, such as described in the studies mentioned above. Since most of the channels linked to the NMDA receptors are blocked at resting membrane potential by the Mg^{2+} present in the extracellular medium (Jahr and Stevens, 1990; Mayer et al., 1984; Nowak et al., 1984), NMDA currents are expected to be relatively small at that potential. Potential space clamp problems might have allowed the largest EPSCs to depolarize the membrane potential sufficiently to allow NMDA receptors to be activated. Taken together with results obtained using extracellular electrical stimulation in the paraventricular nucleus (Wuarin and Dudek, 1991), our results do not support the notion of an significant activation of NMDA receptors in spontaneous EPSCs of supraoptic magnocellular neurons at resting membrane potential. This contrasts with results obtained in cerebellar granule cells (Silver et al., 1992), hippocampal granule cells (Keller et al., 1991) and neocortical pyramidal cells (Wuarin et al., 1992) where a more consistent NMDA component to the excitatory synaptic responses was found. Future experiments designed to evaluate the voltage dependence of spontaneous EPSCs are needed for a more complete evaluation of the role played by the NMDA receptors in synaptic transmission in the magnocelluar neuroendocrine system.

GABA and IPSCs

GABA is considered to be the dominant inhibitory neurotransmitter in the magnocellular system (van den Pol, 1985; Jhamandas and Renaud, 1986; Randle et al., 1986; Renaud and Bourque, 1991) and throughout the hypothalamus (Decavel and van den Pol, 1990). However, other

neuroactive substances have been shown to inhibit vasopressin and oxytocin secretion and to decrease the firing rate of magnocellular neuroendocrine cells. Examples are norepinephrine (Armstrong et al., 1982; Arnaud et al., 1983) and opioid peptides (Wuarin and Dudek, 1990). Using the same strategy that we used for the EPSCs, we searched for small or relatively slow events, once all the fast $GABA_A$-receptors-mediated currents were blocked by bicuculline. We did not detect any outward currents in the 12 cells tested with the $GABA_A$ receptor antagonist bicuculline. To our knowledge, there is no report of spontaneous $GABA_B$-receptor-mediated synaptic currents. Although it is possible that these currents could have been washed out immediately after obtaining the whole cell recording configuration, no studies using sharp electrodes have presented evidence for spontaneous inhibitory synaptic events mediated by $GABA_B$ receptors. These results support the hypothesis that all IPSCs are mediated by activation of $GABA_A$ receptors.

Source of spontaneous currents

Studying spontaneous synaptic currents has advantages over electrically evoked responses for assessing the overall synaptic input to a cell. In the in vitro slice preparation, however, several factors are likely to influence spontaneous synaptic activity. Many afferent axons are cut during the preparation of the slice; all the afferents fibers from other parts of the brain and brain stem and from hypothalamic regions (Swanson and Sawchenko, 1983) not contained in the slice are obviously cut. Axons from some local cells that project to the supraoptic nucleus through a trajectory outside the plane of the slice are also cut. Part of the strong GABAergic input (van den Pol, 1985) to the supraoptic nucleus has been proposed to originate from GABA neurons located around the nucleus itself (Theodosis et al., 1986), therefore, GABAergic neurons projecting to supraoptic cells may still be present in the slice.

The striking differences that we observed between cells in terms of the frequency of events and the proportion of EPSCs versus IPSCs may be the result of different cells having different local input. The largest PSCs were most likely due to action potentials originating from cut axons or from local circuits containing the soma of the projecting cell and its axon. The bursts of IPSCs that we observed in some cells are likely to be caused by bursts of action potentials in a GABAergic cell projecting to the recorded cell. Therefore, GABAergic inhibitory and glutamatergic excitatory local circuits probably exist and are functional in the slice.

Conclusions

The concept of neurosecretion was established four decades ago (Sharrer and Sharrer, 1954), and the supraoptic magnocellular neuroendocrine cells are the classic model of neurosecretory cells (Hatton, 1990). Possible difference between conventional neurons and neuroendocrine cells in terms of passive membrane properties and synaptic transmission has been a long-standing question (Finlayson and Osborne, 1975; Mason and Bern, 1977; Yagi and Iwasaki, 1977). In the present study, the identification of neuroendocrine cells was unequivocal because we used direct visual identification of the supraoptic nucleus, and staining of cells showed that we were recording from cells in the nucleus. As reviewed by Renaud (1987, 1991), the intrinsic and synaptic properties that have been described in neuroendocrine cells are similar or identical to what is known to occur in neurons. Our observations on spontaneous EPSCs and IPSCs also support the hypothesis that neuroendocrine cells integrate electrical and chemical signals similarly to regular neurons. In particular, the present results support the hypothesis that 1) glutamate or related excitatory amino acids mediate all the fast excitatory synaptic input to magnocellular neuroendocrine cells, and 2) GABA acting on $GABA_A$ receptors mediates all the fast inhibitory input. The other neuroactive amines and peptides proposed

as neurotransmitter candidates in the magnocellular neuroendocrine system are perhaps not neurotransmitters such as defined in the neuromuscular junction (Katz, 1969), but rather neuromodulators. By changing cell membrane potential and input resistance over long periods of time, they influence directly the amplitude and duration of the fast synaptic currents and therefore indirectly modulate the secretion of oxytocin and vasopressin.

References

Armstrong WE, Sladek CD, Sladek JR (1982) Characterization of noradrenergic control of vasopressin release by organ-cultured rat hypothalamo-neurohypophysial system. Endocrinology 111:273-279.

Arnaud E, Cirino M, Layton BS, Renaud LP (1983) Contrasting actions of amino acids, acetylcholine, noradrenaline and leucine enkephalin on the excitability of supraoptic vasopressin-secreting neurons. Neuroendocrinology 36:187-196.

Blanton MG, Lo Turco JL, Kriegstein AR (1989) Whole cell recording from neurons in slices of reptilian and mammalian cerebral cortex. J Neurosci Methods 30:203-210.

Bourque CW, Hu B (1991) NMDA induces rhythmic bursting activity in rat magnocellular neurosecretory cells (MNCs) in vitro. Soc Neurosci Abstr 17:256.

Decavel C, van den Pol AN (1990) GABA: a dominant neurotransmitter in the hypothalamus. J Comp Neurol 302:1019-1037.

Drewe JA, Childs GV, Kunze DL (1988) Synaptic transmission between dissociated adult mammalian neurons and attached synaptic boutons. Science 241:1810-1813.

Edwards FA, Konnerth A, Sakmann B (1990) Quantal analysis of inhibitory synaptic transmission in the dentate gyrus of rat hippocampal slices: a patch-clamp study. J Physiol (Lond) 430:213-249.

Finlayson LH, Osborne MP (1975) Secretory activity of neurons and related electrical activity. Adv comp Physiol Biochem 6:165-258.

Gribkoff VK (1991) Electrophysiological evidence for N-methyl-D-aspartate excitatory amino acid receptors in the rat supraoptic nucleus in vitro. Neurosci Lett 131:260-262.

Gribkoff VK, Dudek FE (1988) The effects of the excitatory amino acid antagonist kynurenic acid on synaptic transmission to supraoptic neuroendocrine cells. Brain Res 442:152-156.

Gribkoff VK, Dudek FE (1990) Effects of excitatory amino acid antagonists on synaptic responses of supraoptic neurons in slices of rat hypothalamus. J Neurophysiol 63:60-71.

Haas HL, Schaerer B, Vosmansky MA (1979) A simple perfusion chamber for the study of nervous tissue slice in vitro. J Neurosci Methods 1:323-325.

Hamill OP, Marty A, Neher E, Sakmann B, Sigworth FJ (1981) Improved patch techniques for high-resolution current recordings from cells and cell-free patches. Pflügers Archiv 391:85-100.

Hatton GI, Ho YW, Mason WT (1983) Synaptic activation of phasic bursting in rat supraoptic nucleus neurones recorded in hypothalamic slices. J Physiol (Lond) 345:297-317.

Hatton GI (1990) Emerging concepts of structure-function dynamics in adult brain: the hypothalamo-neurohypophysial system. Prog Neurobiol 34:437-504.

Horikawa K, Armstrong WE (1988) A versatile means of intracellular labeling: injection of biocytin and its detection with avidin conjugates. J Neurosci Methods 25:1-11.

Hu B, Bourque CW (1991a) Functional N-methyl-D-aspartate and non-N-methyl-D-aspartate receptors are expressed by rat neurosecretory cells in vitro. J Neuroendocrinol 3:509-514.

Hu B, Bourque CW (1991b) Ionic basis of NMDA-induced rhytmic bursting activity in rat magnocellular neurosecretory cells (MNCs) in vitro. Soc Neurosci Abstr 17:256.

Jahr CE, Stevens CF (1990) A quantitative description of NMDA receptors-channel kinetic behavior. J Neurosci 10:1830-1837.

Jhamandas JH, Renaud LP (1986) A γ-aminobutyric-acid-mediated baroreceptor input to supraoptic vasopressin neurones in the rat. J Physiol (Lond) 381:595-606.

Katz B (1969) The release of neural transmitter substances. UK: Liverpool University Press.

Keller BU, Konnerth A, Yaari Y (1991) Patch clamp analysis of excitatory synaptic currents in granule cells of rat hippocampus. J Physiol (Lond) 435:275-293.

Mason CA, Bern HA (1977) Cellular biology of the neurosecretoy neuron. In: Handbook of Physiology, vol.1, pt. 2 (Kandel ER ed), pp. 651-689. Baltimore: Waverly Press.

Mayer ML, Westbrook GL, Guthrie PB (1984) Voltage-dependent block by Mg^{2+} of NMDA

responses in spinal cord neurones. Nature 309:261-263.

Meeker RB, Swanson DJ, Hayward JN (1989) Light and electron microscopic localization of glutamate immunoreactivity in the supraoptic nucleus of the rat hypothalamus. Neuroscience 33:157-167.

Nowak L, Bregestovski P, Ascher P, Herbet A, Prochiantz A (1984) Magnesium gates glutamate-activated channels in mouse central neurones. Nature 307:462-465.

Otis TS, Staley KJ, Mody I (1991) Perpetual inhibitory activity in mammalian brain slices generated by spontaneous GABA release. Brain Res 545:142-150.

Randle JCR, Bourque CW, Renaud LP (1986) Characterization of spontaneous and evoked postsynaptic potentials in rat supraoptic neurosecretory neurons in vitro. J Neurophysiol 56:1703-1717.

Renaud LP (1987) Magnocellular neuroendocrine neurons: update on intrinsic properties, synaptic inputs and neuropharmacology. Trends Neurosci 10:498-502.

Renaud LP, Bourque CW (1991) Neurophysiology and neuropharmacology of hypothalamic magnocellular neurons secreting vasopressin and oxytocin. Prog Neurobiol 36:131-169.

Scharrer E, Scharrer B (1954) Hormones produced by neurosecretory cells. Recent Prog Horm Res 10:183-232.

Silver RA, Traynelis SF, Cull-Candy SG (1992) Rapid-time-course miniature and evoked excitatory currents at cerebellar synapses *in situ*. Nature 355:163-166.

Stelzer A, Kay AR, Wong RKS (1988) $GABA_A$-receptor function in hippocampal cells is maintained by phosphorylation factors. Science 241:339-341.

Swanson LW, Sawchenko PE (1983) Hypothalamic integration: organization of the paraventricular and supraoptic nuclei. Annu Rev Neurosci 6:269-234.

Theodosis DT, Paut L, Tappaz ML (1986) Immunocytochemical analysis of the GABAergic innervation of oxytocin- and vasopressin-secreting neurons in the rat supraoptic nucleus. Neuroscience 19:207-222.

van den Pol AN (1985) Dual ultrastructural localization of two neurotransmitter-related antigens: colloidal gold-labeled neurophysin-immunoreactive supraoptic neurons receive peroxidase-labeled glutamate decarboxylase- or gold-labeled GABA-immunoreactive synapses. J Neurosci 5:2940-2954.

van den Pol AN, Wuarin J-P, Dudek FE (1990) Glutamate, the dominant excitatory transmitter in neuroendocrine regulation. Science 250:1276-1278.

Wuarin J-P, Dudek FE (1990) Direct effects of an opioid peptide selective for μ-receptors: intracellular recordings in the paraventricular and supraoptic nuclei of the guinea-pig. Neuroscience 36:291-298.

Wuarin J-P, Dudek FE (1991) Excitatory amino acid antagonists inhibit synaptic responses in the guinea pig hypothalamic paraventricular nucleus. J Neurophysiol 65:946-951.

Wuarin J-P, Peacock WJ, Dudek FE (1992) Single-electrode voltage-clamp analysis of the N-Methyl-D-aspartate component of synaptic responses in neocortical slices from children with intractable epilepsy. J Neurophysiol 67:84-93.

Yagi K, Iwasaki S (1977) Electrophysiology of the neurosecretory cell. Int Rev Cytol 48:141-186.

Yang CR, Renaud LP (1991) GABAergic- and glutamatergic-mediated synaptic inhibition and excitation in rat supraoptic neurons from activation of organum vasculosum. Soc Neurosci Abstr 17:257.

Yang QZ, Hatton GI (1989) Histamine and histaminergic inputs: responses of rat supraoptic nucleus neurons recorded intracellularly in hypothalamic slices. Biomed Res 10:135-144.

FIGURE LEGENDS

Figure 1. Whole-cell patch clamp recording of a supraoptic magnocellular neuroendocrine cell with both excitatory and inhibitory inputs. A-C are data from the same cell. A, spontaneous currents recorded at resting membrane potential (-66 mV), R_{in} was 700 MΩ. Traces are continuous. B and C, histograms showing distribution of the EPSC and IPSC amplitudes respectively. Current amplitudes were measured during 6-min epochs from data such as shown in A. Note that in this cell there were approximately 4 times more EPSCs than IPSCs.

Figure 2. Comparison of the rate of spontaneously occurring synaptic events in two different cells. Traces in panel A and B show two samples (5 s) of spontaneous synaptic activity at a relatively slow time scale. Upward deflections were IPSCs and downward defections were EPSCs. Frequency histograms of IPSCs and EPSCs (during 115 s) are shown for each cell. The average rate for IPSCs and EPSCs was 4.2 s^{-1} and 13 s^{-1} for cell A and 0.7 s^{-1} and 1.1 s^{-1} for cell B, respectively.

Figure 3. Whole-cell recording of a magnocellular neuron showing predominantly IPSCs. This cell showed bursts of IPSCs separated by periods of relative inactivity. A, example of a burst of IPSCs. Between bursts, the presynaptic cell was presumably silent (see top and bottom two traces). Traces are continuous. B, amplitude histogram of IPSCs from cell shown in A measured during a period of approximately 8 min. C, frequency of spontaneous IPSCs during a period of 2 min 20 s, including two bursts of IPSCs. The second peak corresponds to the burst shown in A. Recording was at resting membrane potential (-60 mV), R_{in} was 900 MΩ.

Figure 4. Comparison of spontaneous synaptic activity in normal perfusion solution (top panel)

and 20 min after addition of 0.5 μg/ml TTX (bottom panel). The cell R_{in} was 500 MΩ. Traces are continuous, and holding potential was the same as resting membrane potential (-55 mV).

Figure 5. Histograms of the amplitudes of EPSCs (left panel) and IPSCs (right panel) recorded from the cell shown in Fig. 4 in normal solution and in TTX-containing solution. In each condition, EPSCs and IPSCs were measured during a 1-min period. The filled columns represent the amplitudes of EPSCs and IPSCs recorded in the presence of 0.5 μg/ml TTX. Note that the peak of the EPSC amplitude histogram was decreased only from -9 to -8 pA by TTX. The peak of the IPSC amplitude distribution was decreased from -13 to -10 pA.

Figure 6. In bicuculline, no IPSCs were detected. Upper panel shows recording under control conditions. Middle panel shows the effect of bath-applied bicuculline (15 min at 10 μM). The IPSCs recovered from the block, but only after more than 90 min of washout (bottom panel). All traces are continuous, holding potential was -70 mV throughout the experiment, and cell R_{in} was 1 GΩ.

Figure 7. No spontaneous EPSCs or IPSCs were detected in the presence of bicuculline and CNQX. As shown in Fig. 6, no IPSCs were observed in bicuculline (20 μM, upper panel). When CNQX (10 μM) was added to the perfusion solution in addition to bicuculline (20 μM), all spontaneous synaptic currents were blocked (middle panel). The effect of CNQX could be reversed after approximately 120 min (bottom panel). Cell R_{in} was 600 MΩ, holding potential was resting membrane potential (-65 mV). Traces are continuous.

Figure 8. Decay phase of IPSCs and of most EPSCs was well fitted by single exponential functions. Traces are averaged spontaneous EPSCs and IPSCs from five different cells (1-5) obtained

at resting membrane potential in normal solution. Cell 4 did not show any IPSCs. The time constant of the fit (dotted line) is indicated for each averaged current. The number of averaged events is shown by n. Cell 5 is the same cell as shown in Fig 2A, however only EPSCs were averaged. Traces in 5a and 5b are identical (note different calibration bars for cells 1-4 and cell 5). The decay phase of cell 5 was poorly fitted with a single exponential function (5a). The sum of two exponential functions (5b) shows a small component (-4 pA) with a relatively slow time constant (τs) and a larger component (-34 pA) with a fast time constant (τf).

Fig. 1

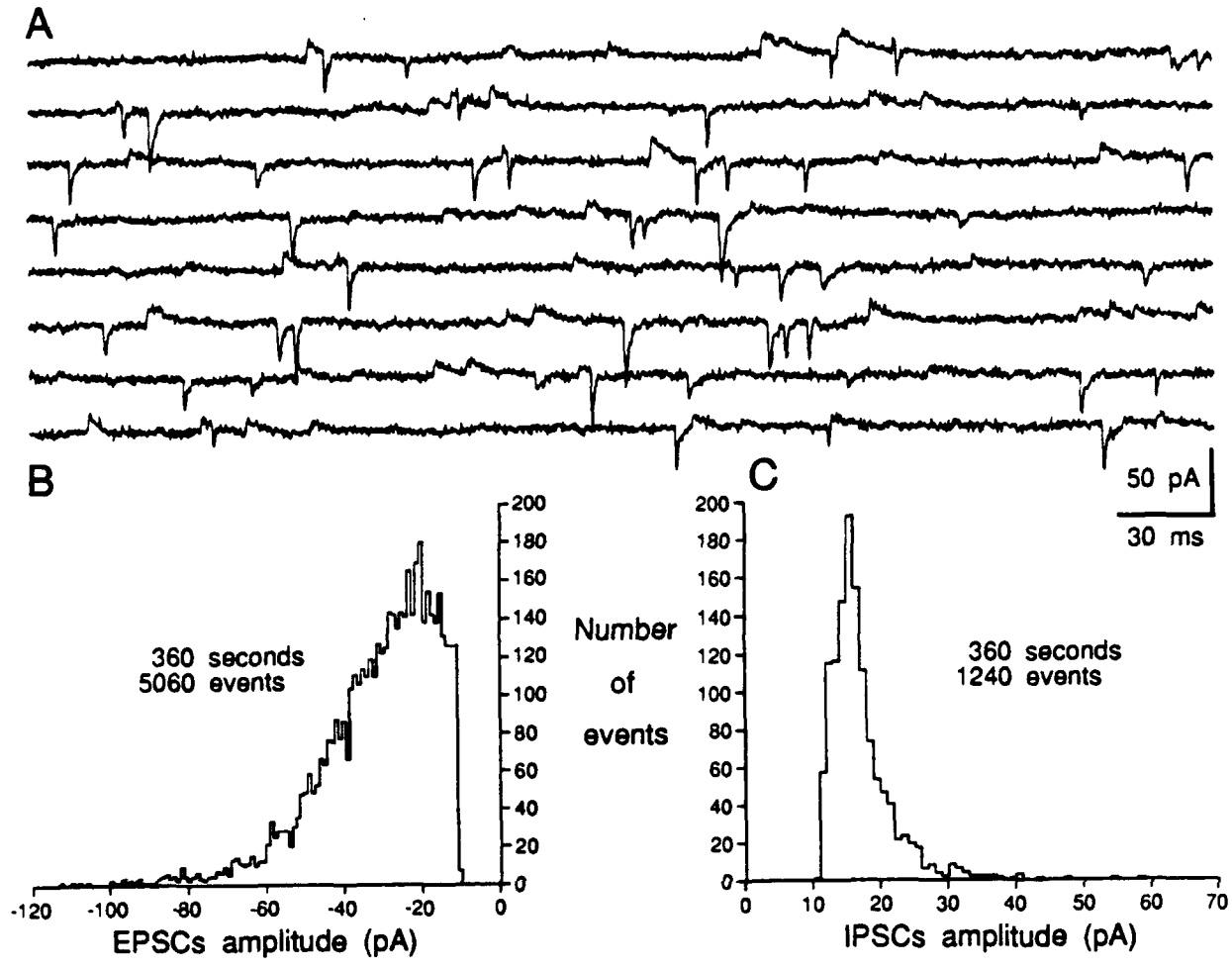
A
B
C
50 pA
30 ms
360 seconds
5060 events
360 seconds
1240 events
Number
of
events
EPSCs amplitude (pA)
IPSCs amplitude (pA)
-120
-100
-80
-60
-40
-20
0
10
20
30
40
50
60
70
0
20
40
60
80
100
120
140
160
180
200

Fig. 2

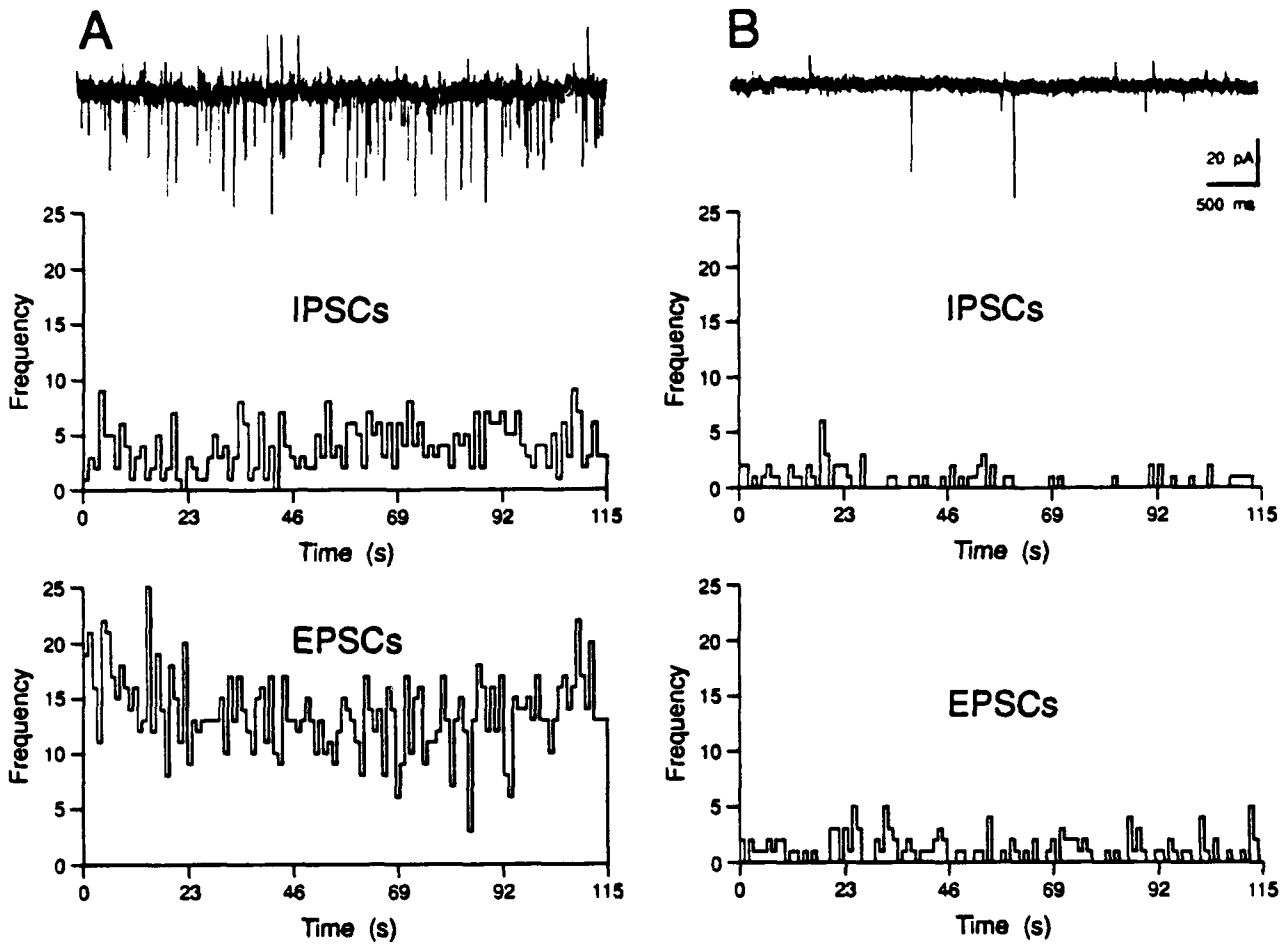
A
B
20 pA
500 ms
IPSCs
EPSCs
Frequency
Time (s)
0
23
46
69
92
115
5
10
15
20
25

Fig. 3

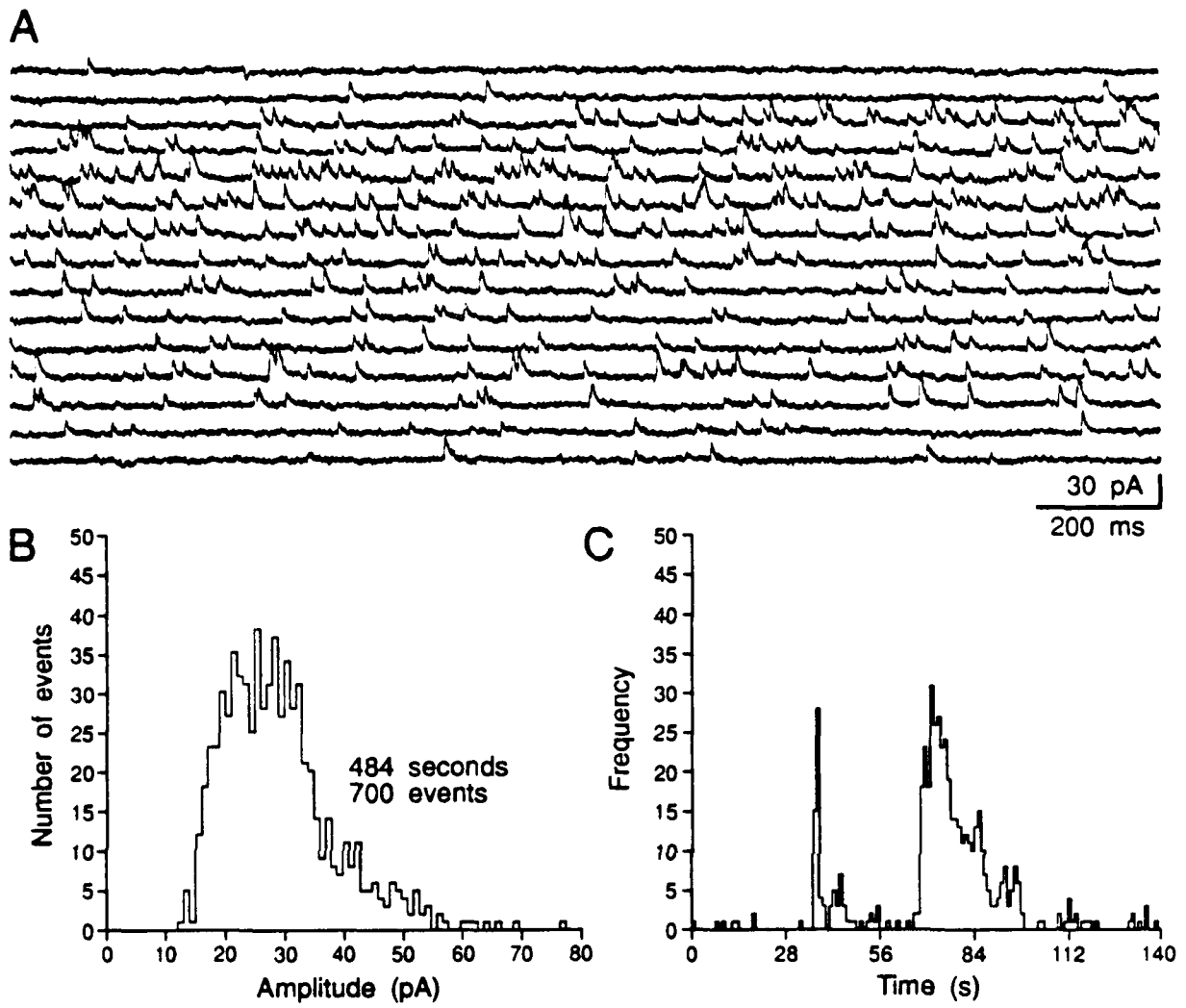
A
30 pA
200 ms
B
Number of events
484 seconds
700 events
Amplitude (pA)
C
Frequency
Time (s)

Fig. 4

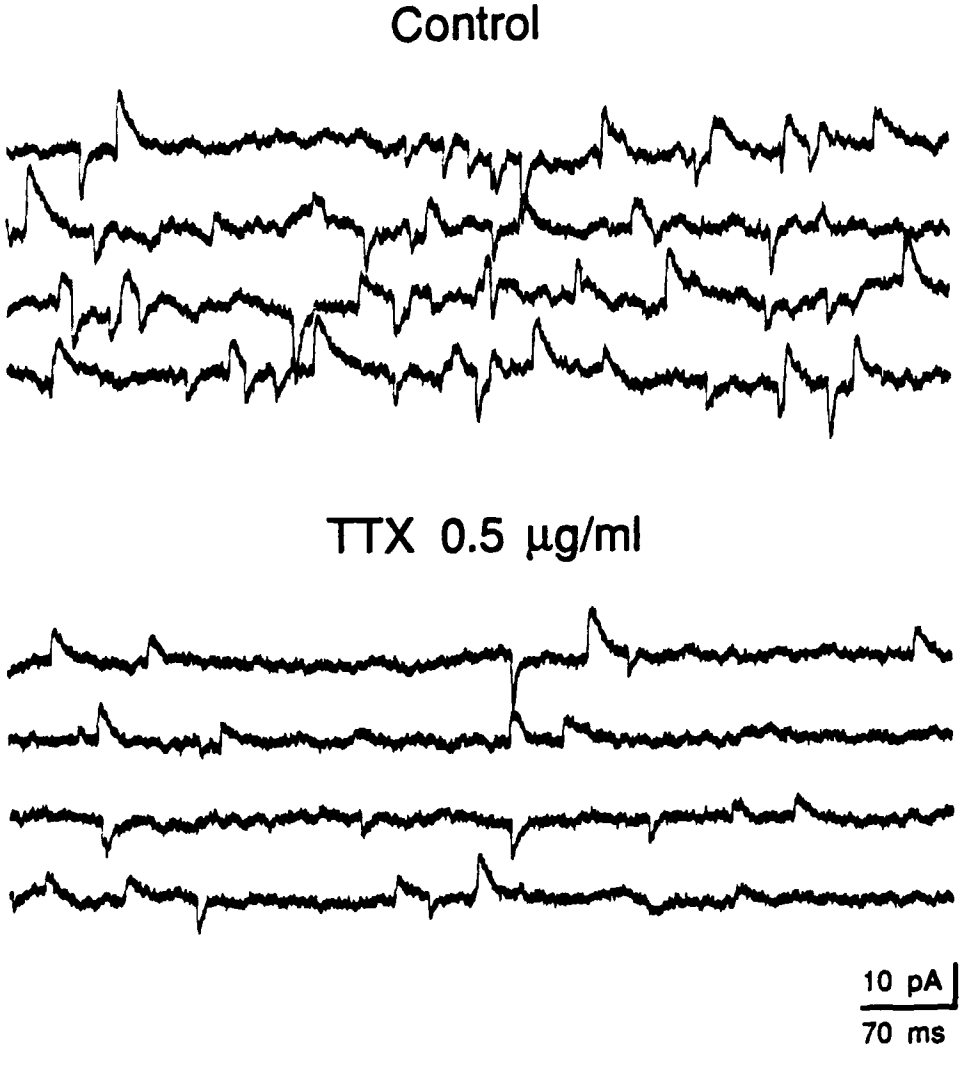

Fig. 5

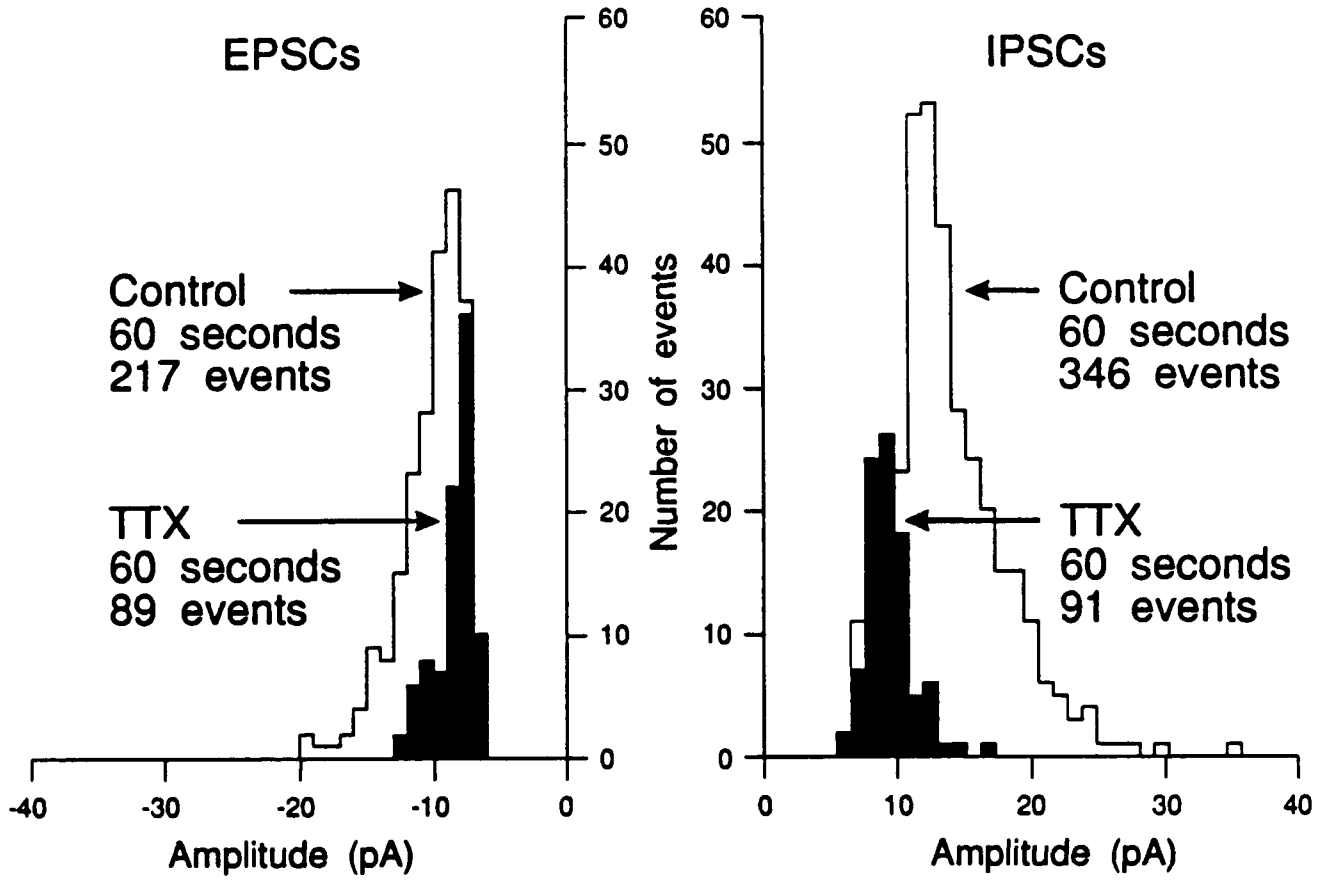
EPSCs
IPSCs
Control
60 seconds
217 events
TTX
60 seconds
89 events
Control
60 seconds
346 events
TTX
60 seconds
91 events
Number of events
Amplitude (pA)
Amplitude (pA)
60
50
40
30
20
10
0
-40
-30
-20
-10
0
10
20
30
40

Fig. 6

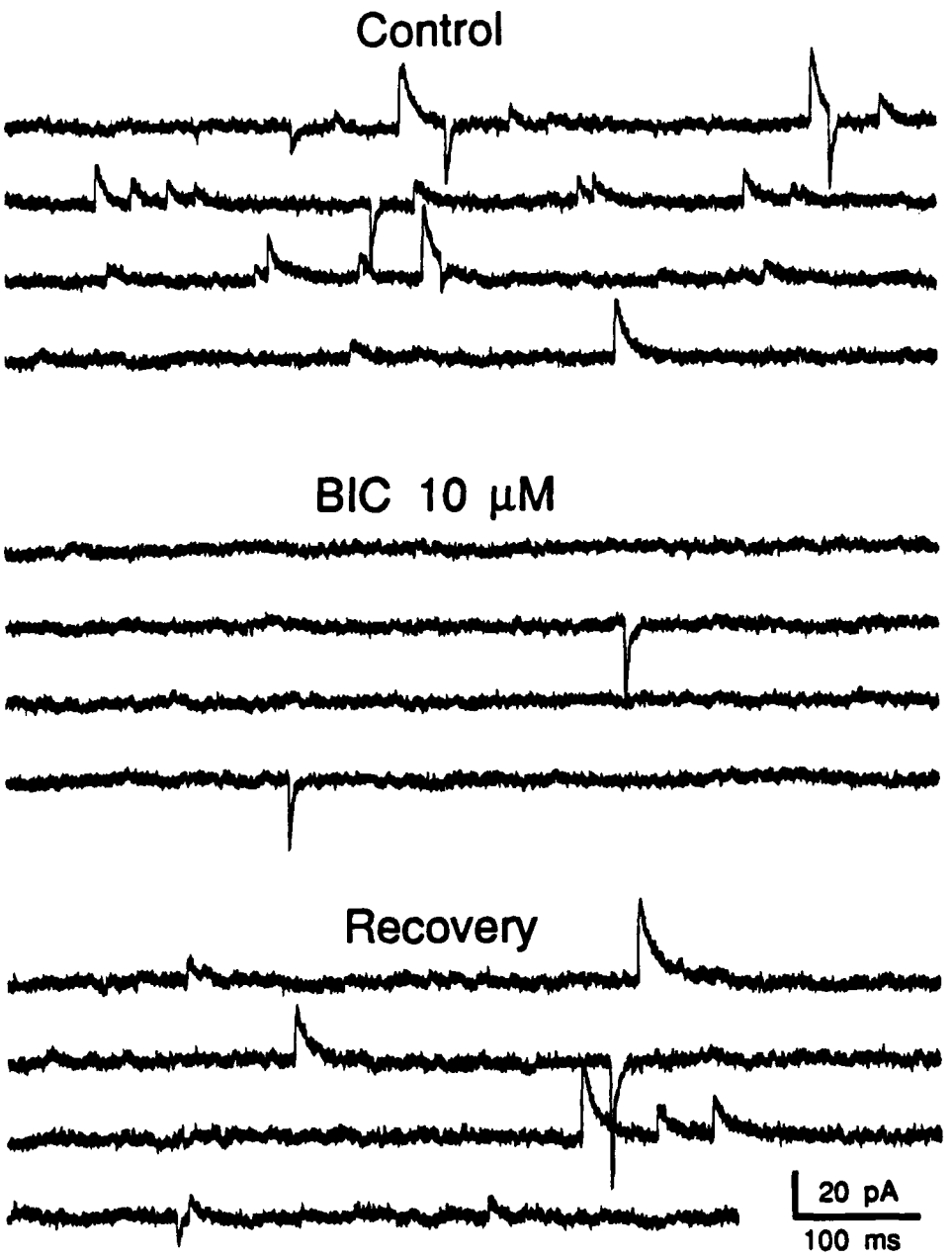

Fig. 7

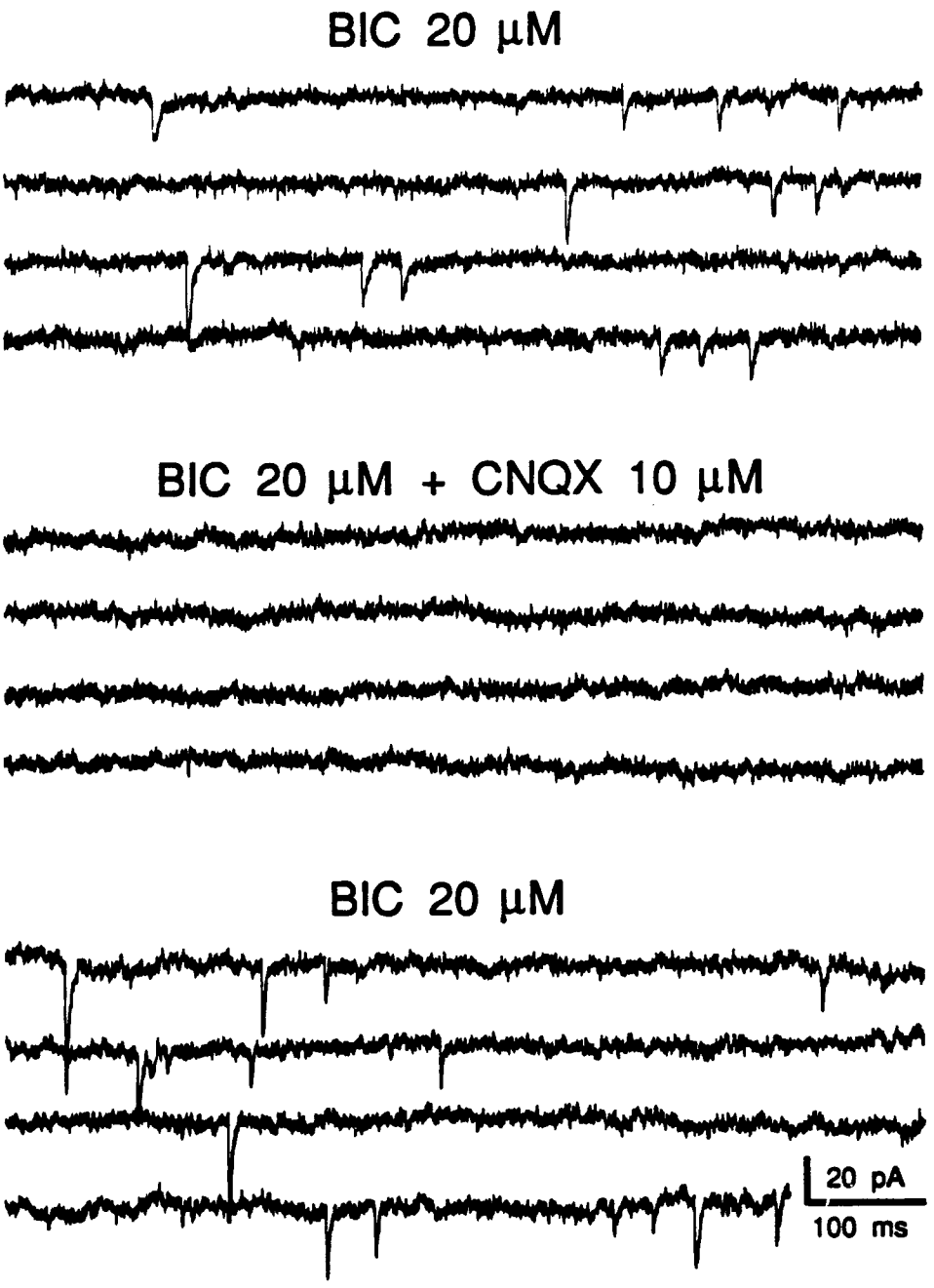

Fig. 3

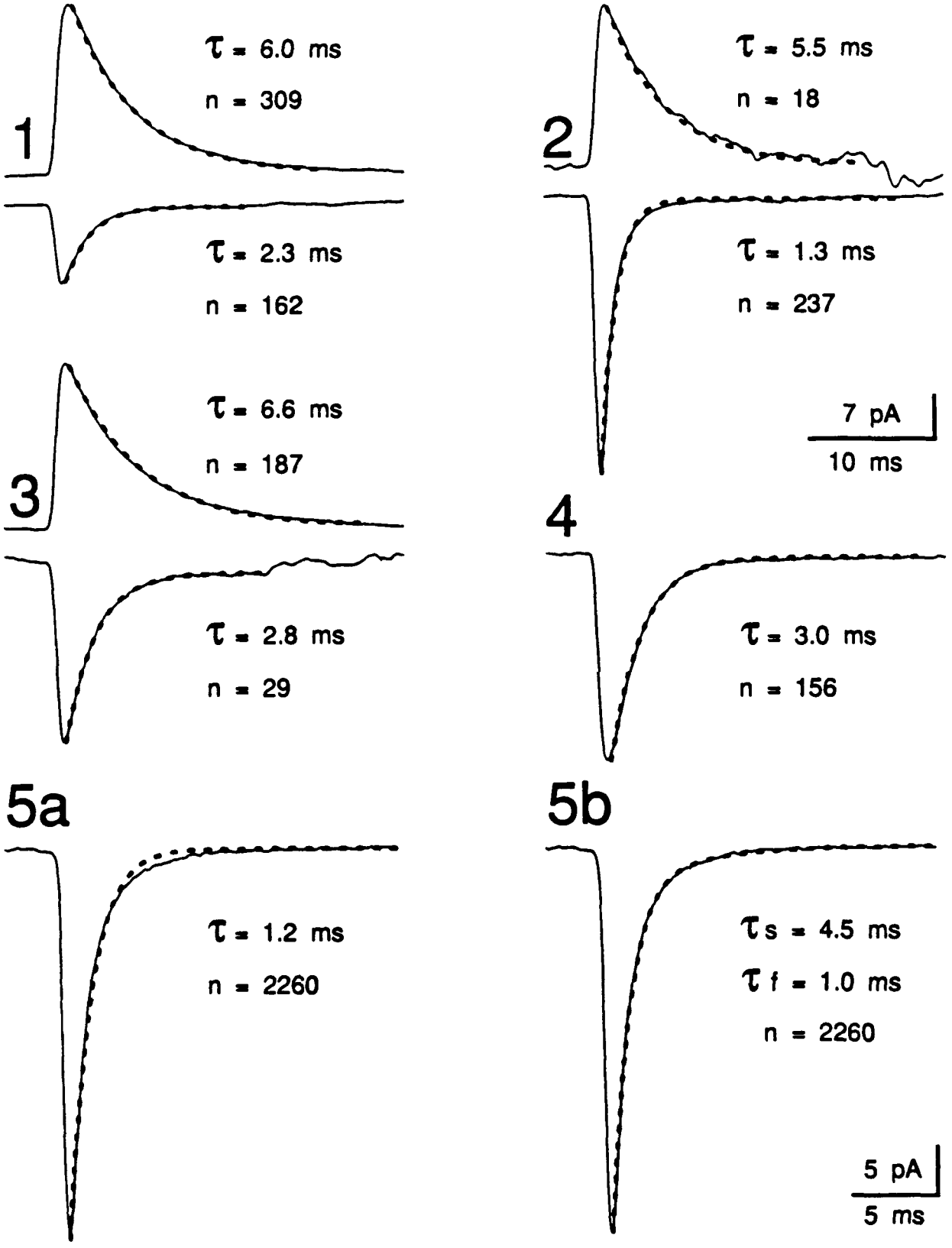
1
τ = 6.0 ms
n = 309
τ = 2.3 ms
n = 162
2
τ = 5.5 ms
n = 18
τ = 1.3 ms
n = 237
7 pA
10 ms
3
τ = 6.6 ms
n = 187
τ = 2.8 ms
n = 29
4
τ = 3.0 ms
n = 156
5a
τ = 1.2 ms
n = 2260
5b
τs = 4.5 ms
τf = 1.0 ms
n = 2260
5 pA
5 ms

Journal of Physiology (1991), **444**, pp. 269–287
With 10 figures
Printed in Great Britain

INTRACELLULAR ELECTROPHYSIOLOGICAL STUDY OF SUPRACHIASMATIC NUCLEUS NEURONS IN RODENTS: EXCITATORY SYNAPTIC MECHANISMS

BY YANG IN KIM* AND F. EDWARD DUDEK*†

*From the *Mental Retardation Research Center and †Brain Research Institute, UCLA School of Medicine, Los Angeles, CA 90024, USA*

(*Received 31 January 1991*)

SUMMARY

1. To study the synaptic mechanisms of excitatory transmission in the suprachiasmatic nucleus (SCN), we assessed the effects of excitatory amino acid receptor antagonists on excitatory postsynaptic potentials (EPSPs) recorded from SCN neurons in horizontal and parasagittal hypothalamic slice preparations from rats and guinea-pigs. The EPSPs were evoked by electrical stimulation of either optic nerve or a site near the SCN.

2. When evoked at membrane potentials between −60 and −100 mV, the EPSPs from optic nerve stimulation were conventional in shape; they rose to the peak quickly (6·2 ± 0·5 ms, mean ± S.E.M.; $n = 45$) and decayed gradually over 50–250 ms. When evoked at membrane potentials between −20 and −55 mV after blockade of outward K^+ currents and fast Na^+ spikes by intracellular injection of Cs^+ and QX-314 ($n = 5$ neurons), a slow depolarizing potential emerged near the fast peak of the EPSP. This slow potential, unlike the fast peak, was not linearly related to membrane potential.

3. An antagonist for kainate- and quisqualate-type excitatory amino acid receptors, 6,7-dinitroquinoxaline-2,3-dione (DNQX 1–10 μM), depressed in a concentration-dependent and reversible manner the EPSPs evoked by optic nerve stimulation at membrane potentials between −60 and −100 mV ($n = 9$). The effects of DNQX were not associated with any significant changes in the baseline input resistance or membrane potential of the postsynaptic neurons. The selective *N*-methyl-D-aspartate (NMDA) receptor antagonist, DL-2-amino-5-phosphonopentanoic acid (AP5, 50–100 μM), did not affect significantly and consistently the EPSPs evoked at these membrane potentials ($n = 7$). On the other hand, AP5 (50 μM) blocked or depressed the slow depolarizing component of the EPSPs evoked at membrane potentials between −20 and −55 mV ($n = 4$). No significant changes in baseline input resistance or membrane potential accompanied the effects of AP5.

4. Stimulation of a site lateral or dorsocaudal to the SCN evoked EPSPs distinct from those evoked by optic nerve stimulation. Again, DNQX (0·3–10 μM) depressed the EPSPs evoked at membrane potentials between −60 and −100 mV ($n = 4$) whereas AP5 (50 μM) had no effect ($n = 5$). When evoked at less negative membrane potentials (i.e. −20 to −55 mV) after intracellular injection of Cs^+ and QX-314, the

EPSPs had a slow depolarizing potential, similar to the EPSPs from optic nerve stimulation. The slow potential, which often triggered a presumed high-threshold Ca^{2+} spike, was blocked or depressed significantly by AP5 (50 μM, $n = 3$).

5. The present results suggest that, at resting or more negative membrane potentials, non-NMDA receptors mediate excitatory synaptic transmission for both retinal and non-retinal inputs to SCN neurons; at less negative potentials, however, NMDA receptors may also play a role in excitatory synaptic transmission.

INTRODUCTION

Increasing evidence suggests that the suprachiasmatic nucleus (SCN) of the hypothalamus is the major pacemaker for circadian rhythms in mammals (Rusak & Zucker, 1979; Takahashi & Zatz, 1982; Turek, 1985; Meijer & Rietveld, 1989). Bilateral lesion of the SCN eliminates endogenous behavioural and hormonal rhythms (Moore & Eichler, 1972; Stephan & Zucker, 1972; Reppert, Perlow, Ungerleider, Mishkin, Tamarkin, Orloff, Hoffman & Klein, 1981), whereas transplantation of neural tissue containing SCN neurons to the third ventricle of the SCN-lesioned arrhythmic host restores disrupted circadian rhythms (Ralph, Foster, Davis & Menaker, 1990).

Most of the circadian rhythms in mammals are entrained to the environmental light–dark cycle via the retina. Two well-defined pathways delivering photic information from the retina to the SCN are the retinohypothalamic tract (Hendrickson, Wagoner & Cowan, 1972; Moore & Lenn, 1972), a direct projection from the retinal ganglion cells to SCN neurons, and the geniculohypothalamic tract, an indirect photic afferent arising from the intergeniculate leaflet of the thalamus (Swanson, Cowan & Jones, 1974; Ribak & Peters, 1975). While the geniculohypothalamic tract does not appear essential for photic entrainment (Albers, Liou, Ferris, Stopa & Zoeller, 1991), the retinohypothalamic tract seems to be critical. This direct projection by itself is sufficient for photic entrainment (Moore, 1983).

The neurotransmitter(s) in the retinohypothalamic tract is unknown. A key experimental approach for identifying the neurotransmitter(s) is to determine which specific antagonists block the postsynaptic potentials (PSPs) of SCN neurons following activation of retinal afferents. Due to the difficulty of obtaining intracellular recordings from small SCN neurons (mean diameter: about 8–10 μm; van den Pol, 1980), only three intracellular electrophysiological studies have been published. Although they describe some electrical properties of SCN neurons (Wheal & Thomson, 1984; Sugimori, Shibata & Oomura, 1986; Thomson & West, 1990), only one of these reports mentioned briefly the excitatory postsynaptic potentials (EPSPs) following optic nerve stimulation, and the synaptic mechanism(s) responsible for the EPSPs was not investigated.

Recently, from the results obtained with extracellular recording and brain slice techniques, Shibata, Liou & Ueka (1986) suggested that excitatory amino acid (EAA) receptors of the *N*-methyl-D-aspartate (NMDA) subtype mediate retinohypothalamic transmission, whereas Cahill & Menaker (1989*b*) argued that non-NMDA receptors are responsible. The potential problems associated with these extracellular electrophysiological studies are that (1) it is not clear whether the evoked field potentials were actually a *direct* reflection of the synaptic events, and

(2) possible non-specific effects of the employed EAA receptor antagonists (e.g. effects on the baseline membrane potential or input resistance of postsynaptic neurons) were not tested.

In the present study, by using intracellular recording techniques, we could avoid these problems. In addition, we could assess the effects of employed antagonists on evoked EPSPs at various membrane potentials. Although the main focus of this study was on the EPSPs from optic nerve stimulation (i.e. retinal input), we also studied the EPSPs from the stimulation of non-retinal afferents, to test the hypothesis that all the fast EPSPs in the SCN are mediated by EAA receptors. These data support the hypothesis that, at resting or more negative membrane potentials, non-NMDA receptors mediate excitatory synaptic transmission for both the retinal and non-retinal inputs to SCN; at less negative membrane potentials, NMDA receptors also play a role. Preliminary accounts of these results have been published (Kim & Dudek, 1989).

METHODS

Animals

Male Sprague–Dawley rats (120–350 g) and guinea-pigs (150–450 g) were kept under a 12 h light–12 h dark cycle (light on at 07.00 h) for at least 1 week (mostly more than 2 weeks).

Preparation and maintenance of hypothalamic slices

In the morning (after 07.00 h) of the day of the experiment, the animals were injected with sodium pentobarbitone (I.P., 100 mg/kg wt) or were left untreated before being decapitated with a guillotine. After decapitation, the skull was opened and the cranial nerves were carefully cut. The brain was removed from the skull, put in ice-cold artificial cerebrospinal fluid (ACSF) (composition in mM: 124 NaCl, 1·4 NaH_2PO_4, 3 KCl, 2·4 $CaCl_2$, 26 $NaHCO_3$, 1·3 $MgSO_4$, 11 glucose) for about 1 min, and then blocked to contain the hypothalamus. Using a vibroslicer (Campden Instruments, USA), a horizontal or parasagittal slice(s) (450–750 μm) containing the SCN and the optic nerve(s) (rat, 2–5 mm; guinea-pig: 1–3 mm) was cut from the block. In one case, a sagittal slice was cut obliquely to contain the contralateral optic nerve. The slice was transferred to an interface-type recording chamber, which was constantly perfused with warmed ACSF (32–35 °C) at 0·7–1·0 ml/min. A humidified atmosphere of 95% O_2 and 5% CO_2 was maintained above the slice, which was equilibrated to the experimental conditions for at least 2 h before the commencement of experiments.

Intracellular recording

Intracellular micropipettes were pulled with a Flaming–Brown puller (Sutter Instruments, USA) and filled with 2–4 M-potassium acetate (pH = 7·4) or 5 mM-HEPES buffer containing 2 M-CsCl and 150 mM-QX-314, a quaternary lidocaine derivative (pH = 7·4). SCN neurons were impaled by advancing the micropipette recording electrode (90–360 MΩ) through the slice in 3 μm steps with a piezoelectric microdrive (Nano-stepper, List Medical) and oscillating the negative capacitance feedback. The signal from the recording electrode was passed through a high-impedance amplifier with a bridge circuit (Axoclamp-2A, Axon Instruments, USA). Voltage and current traces were displayed on an oscilloscope and a chart recorder. In addition, the traces were digitized (Neurocorder, Neurodata Instruments, USA) and stored on videotape for off-line data analysis with the IS'67AVE system (RC electronics, USA). Each of the voltage traces presented in this paper is an average of ten to thirty, unless stated otherwise.

Electrical stimulation

For electrical stimulation of the optic nerve (ipsi- or contralateral), a bipolar electrode made with Teflon-coated, 90% platinum–10% iridium wires (76 μm in diameter) was placed on the cut end of the nerve. The stimulation was with single monophasic pulses (0·5 ms) of intensities $\leq$ 70 V or $\leq$ 0·8 mA. To ensure the specificity of the stimulation, the regular bipolar electrode was

occasionally replaced by a suction electrode, which normally required much lower intensity stimulation (as low as 3–5 V), but tended to cause some physical damage to the nerve in long-term experiments. Despite the difference in the stimulus intensity, the onset latency and general shape of the PSPs evoked were similar, suggesting that the stimulation was specific in both cases.

In some experiments a second, bipolar electrode was placed in a site lateral or dorsocaudal to the SCN. By stimulating the site ($\leqslant$ 1·0 mA) simultaneously with the optic nerve, the specificity of the optic nerve stimulation was further assessed. This test was based on the assumption that if a postsynaptic response evoked by optic nerve stimulation is due to current spread to the site near the SCN, the postsynaptic response evoked by stimulation of this nearby site should block the response to optic nerve stimulation. In no case (none of eight neurons from seven slice preparations) was such a blockade observed, further suggesting the specificity of optic nerve stimulation. Finally, any uncertain response, such as immediate depolarization without reasonable onset latency, was excluded from the data analysis.

Pharmacological agents

The antagonists employed in the present study were applied to the brain slices by bath perfusion (> 15 min). Bicuculline methiodide (BIC, γ-aminobutyric acid$_A$ ($GABA_A$) receptor antagonist) and DL-2-amino-5-phosphonopentanoic acid (AP5, NMDA receptor antagonist) were dissolved in the ACSF to the final concentrations, while 6,7-dinitroquinoxaline-2,3-dione (DNQX, non-NMDA receptor antagonist) was pre-dissolved in dimethyl sulphoxide (DMSO) before the final dilution with the ACSF. The final concentration of DMSO was 0·01–0·1 %, which had no apparent effect on the passive membrane properties and synaptic transmission. BIC and AP5 were obtained from Sigma (USA) and DNQX was from Tocris Neuramin (UK).

RESULTS

The data presented in this paper were based on intracellular recordings (10 min to 6 h) from over 100 SCN neurons. Approximately three-quarters of the neurons were from rat slices and the remaining from guinea-pig slices. Since there was no obvious difference between rat and guinea-pig neurons in terms of the postsynaptic response to optic nerve stimulation (except the difference in the onset latency, which was presumably due to the difference in the length of the attached optic nerve; see Methods), the data from the two species were combined. Most of the SCN neurons were spontaneously active (up to 34 Hz). Therefore, isolation of synaptic potentials normally required removal of action potentials either by hyperpolarizing current injection or by direct blockade of the channels responsible for fast Na^+ currents (see below). For the neurons that were recorded with potassium acetate-filled electrodes and which exhibited a postsynaptic response to optic nerve stimulation, the input resistance and the action potential amplitude were 263 ± 21 MΩ (mean ± S.E.M., $n = 43$) and 58 ± 1 mV ($n = 45$), respectively. The input resistance was calculated from the slope of the linear portion of the current–voltage plot, and the action potential amplitude was measured from spike threshold.

Postsynaptic response of SCN neurons to optic nerve stimulation

Optic nerve stimulation evoked fast EPSPs (Fig. 1*A*) in thirty-one neurons impaled in BIC-free medium. The stimulation never evoked a pure, fast or slow inhibitory postsynaptic potential (IPSP) in these neurons or other neurons recorded in the absence of BIC. A fast IPSP followed an EPSP in only one neuron (Fig. 1*B*). BIC (50 μM) completely blocked this IPSP, whereas it had no significant effect on the EPSP (Fig. 1*B*). The EPSPs evoked in other neurons were also not affected by BIC

($n = 9$, Fig. 1*A*). In the presence of BIC and at membrane potentials more negative than -75 mV (i.e. below the reversal potential for $GABA_A$-receptor-mediated IPSPs), the amplitude and duration (at half-amplitude) of the EPSP were $98 \pm 5\%$ and $103 \pm 10\%$ of the values obtained in the BIC-free condition, respectively ($n = 4$).

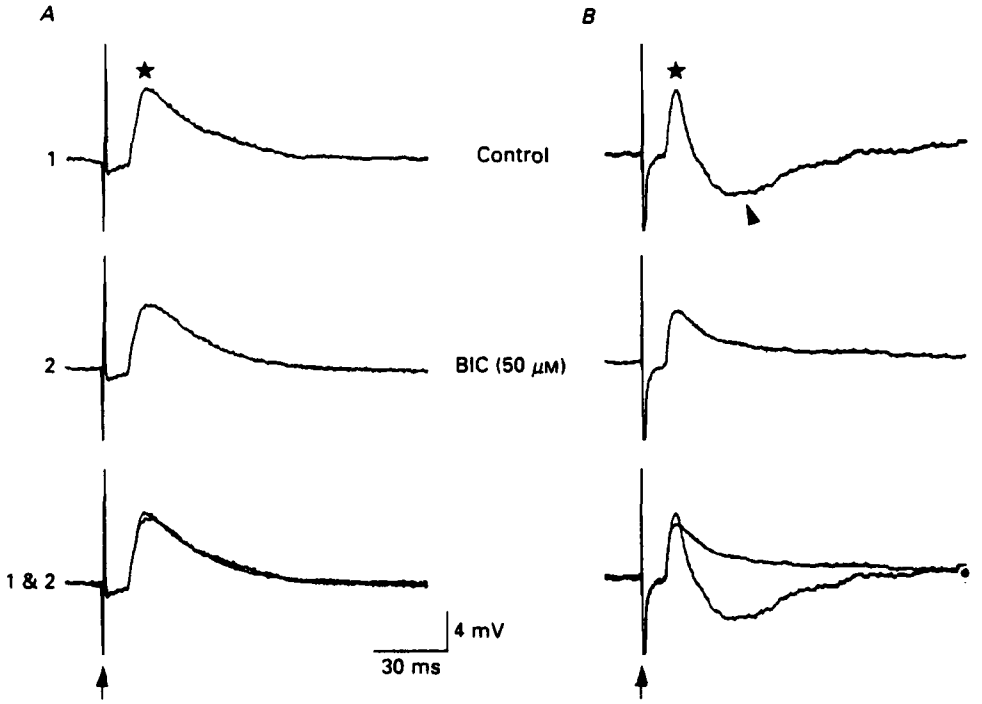

Fig. 1. PSPs from optic nerve stimulation (arrow), and the effects of BIC. Traces in *A* and *B* are from two different neurons recorded with potassium acetate-filled electrodes. Unless stated otherwise, the traces presented in all of the following figures were obtained with potassium acetate-filled electrodes. In *A* the evoked EPSP (★) was not associated with an IPSP, but the EPSP (★) in *B* was followed by an (IPSP) (arrow-head). In *A* and *B*, the PSPs before (1) and during (2) application of BIC are shown in the top and middle panels. Superimposed traces (1 & 2) are also provided in the bottom panel for direct comparison. In *B*, the IPSP following the EPSP was selectively blocked by BIC; the slight decrease in EPSP amplitude during BIC application was associated with and presumably due to a slight decrease in baseline input resistance (data not shown). Cells were current clamped to -60 mV (*A*) and -55 mV (*B*).

At membrane potentials less negative than -75 mV, the amplitude and duration were 94 ± 3 and $108 \pm 9\%$ of the values obtained in BIC-free medium, respectively ($n = 5$). Therefore, these EPSPs were not associated with a BIC-sensitive IPSP.

To insure that the EPSPs under study were not contaminated by a $GABA_A$-receptor-mediated synaptic component, we included BIC (50 μM) in the perfusing medium. Once a slice was bathed in BIC, no attempt was made to wash the BIC out of the bath, because a complete wash-out normally took > 1 h. As a result, several neurons were impaled in the continued presence of BIC. The PSP evoked in these neurons was always a pure EPSP ($n = 20$).

When evoked at membrane potentials between −60 and −100 mV, the EPSPs from optic nerve stimulation were of a conventional shape. In general, the EPSPs rose to their peaks quickly (6·2±0·5 ms, $n = 45$) (Fig. 2A), and decayed gradually over 50–250 ms. In many cases, the decay could be fitted reasonably well with a

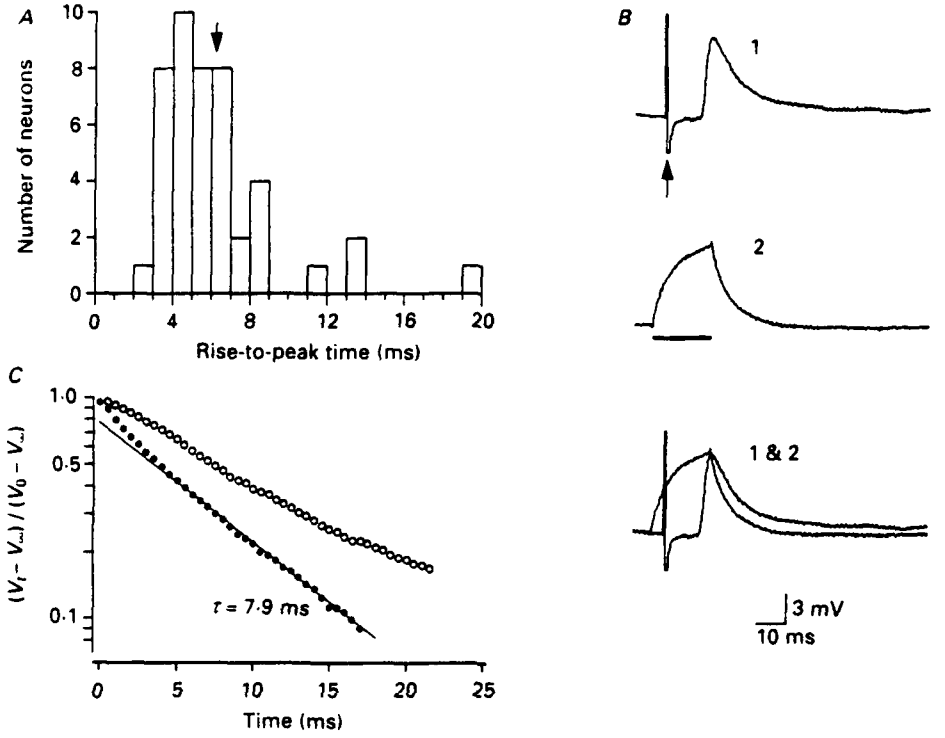

Fig. 2. Time course of the EPSPs evoked by optic nerve stimulation. *A*, frequency histogram for the rise-to-peak time of the EPSPs from forty-five neurons. Arrow indicates the mean. *B*, top and middle panels: EPSP evoked by optic nerve stimulation (arrow) and electrotonic potential evoked by a weak depolarizing current pulse (horizontal line), respectively. These potentials were evoked at the same baseline membrane potential (−72 mV). Bottom panel: superimposition of the top (1) and middle (2) traces for direct comparison. *C*, for the decay of the EPSP and electrotonic potential in *B*, the values of $(V_t - V_\infty)/(V_0 - V_\infty)$, taken at 0·5 ms intervals and integrated over ±0·1 ms, were plotted against time, where V_t is the voltage at time t, V_0 is the voltage at the beginning of the decay and V_∞ is the voltage at the baseline. A straight line was fitted by eye to the latter, linear portion of the plot for the electrotonic potential decay (●), and the apparent membrane time constant (τ) was calculated with the equation $\tau = -0{\cdot}4343/\text{slope of the line}$ (Rall, 1969). The plot for the decay of the EPSP (○) illustrates that the decay had a time constant greater than the apparent membrane time constant.

single exponential. The estimated time constant for the decay of the EPSPs was 20·2±1·8 ms ($n = 14$), and was always larger than the membrane time constant (12·0±1·2 ms), which was estimated from the latter portion of the charging phase of the averaged electrotonic potential elicited by a hyperpolarizing current pulse (delivered in the linear range of the current–voltage plot). Figure 2*B* and *C* shows that the decay of an evoked EPSP was slower than that of a depolarizing electrotonic

potential. Since these potentials were evoked at the same baseline membrane potential and were similar in amplitude, it is likely that the slower decay of the EPSP is due primarily to a mechanism other than a pure voltage-dependent conductance.

When evoked at membrane potentials between −20 and −55 mV after blockade of outward K^+ currents and fast Na^+ spikes by intracellular injection of Cs^+ and

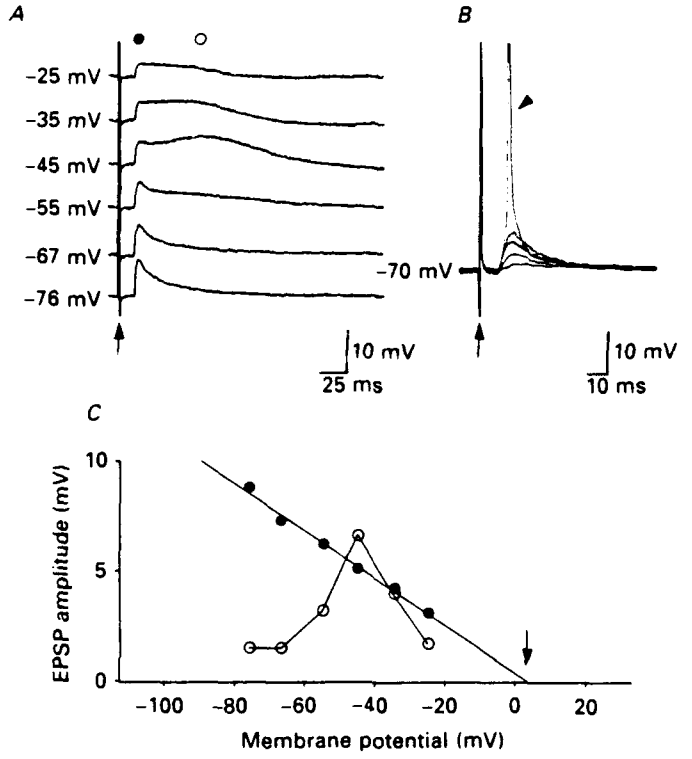

Fig. 3. Amplitude of the EPSPs from optic nerve stimulation (arrows in *A* and *B*) as a function of membrane potential and stimulus intensity. *A*. EPSPs evoked at different membrane potentials. Cs^+ and QX-314 were injected intracellularly to block outward K^+ currents and fast Na^+ spikes. Note the slow depolarizing potentials on the falling phase of the EPSPs evoked at membrane potentials between −25 and −55 mV. *B*. EPSPs evoked at a fixed baseline membrane potential (−70 mV) with different stimulus intensities (0·35–0·5 mA). At the highest intensity, the stimulus evoked an action potential (arrow-head; truncated). Note the same onset latency of the EPSPs. Each superimposed trace is an average of two to eight. Recorded with a pipette filled with potassium acetate (Cs^+ and QX-314 were absent). *C*, plot of the amplitude of the EPSPs in *A* against membrane potential. The amplitude was measured at 18·5 ms (●) and 76·5 ms (○) from the time of stimulation. These time points corresponded to the fast peak of the EPSP and the peak of the slow depolarizing potential, respectively. A linear regression line was fitted through the data points for the fast peaks to estimate the reversal potential (+3 mV; arrow).

QX-314, the EPSPs from optic nerve stimulation ($n = 5$) were quite different in shape from those evoked at more negative membrane potentials (Fig. 3*A*). Near the fast peak of the EPSP, a slow depolarizing potential was present; this component

was apparently absent in the responses evoked at membrane potentials more negative than −60 mV. The amplitude of the slow potential was non-linearly related to membrane potential, and was maximum at membrane potentials of around −45 mV (Fig. 3*A* and *C*).

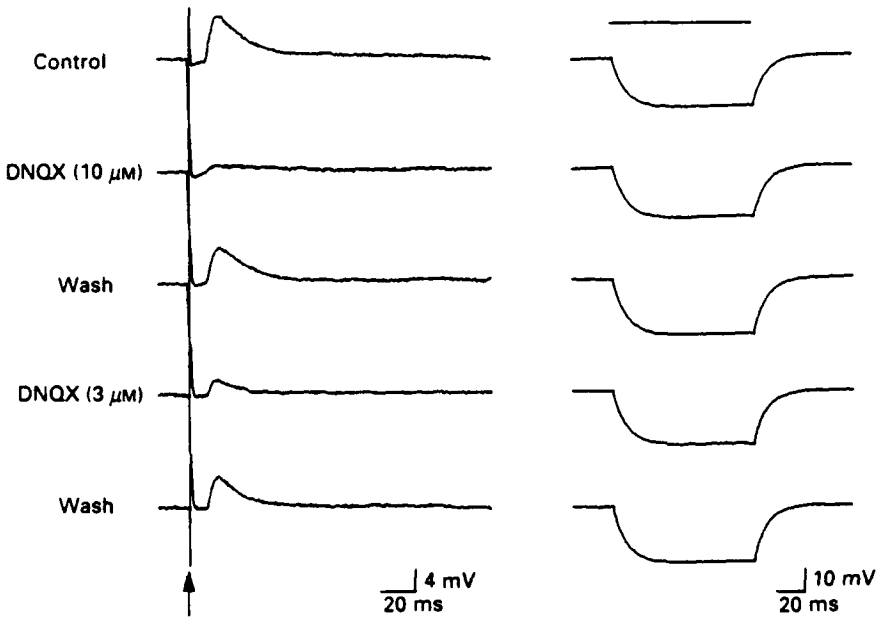

Fig. 4. Depression by DNQX of the EPSPs from optic nerve stimulation. Left panel. EPSPs from optic nerve stimulation (arrow) under each experimental condition. Note the concentration-dependent and reversible depression of EPSPs by DNQX. Also, note that DNQX, even at 10 μM concentration, did not completely block the early part of the EPSP. This residual response could be due to the competition between DNQX and endogenous ligand(s) for non-NMDA receptors. Right panel, electrotonic potentials induced by a hyperpolarizing current pulse (−50 pA, 100 ms; horizontal line) under each experimental condition. Note the lack of DNQX effect on the baseline input resistance. Current clamped to −65 mV.

The EPSP amplitude was a function of stimulus intensity (Fig. 3*B*). In addition, the amplitude of the fast peak of the EPSP was linearly related to membrane potential (Fig. 3*A* and *C*). The reversal potential of the fast peak was -1 ± 6 mV ($n = 7$ neurons) (Fig. 3*C*).

The EPSPs of SCN neurons did not follow high-frequency optic nerve stimuli. In about 20–30% of the cases, they failed to follow stimuli presented even at < 1 Hz. The mean onset latency of evoked EPSPs was variable across neurons (range: 6·5–12·1 ms, $n = 14$ neurons from three guinea-pig and eight rat preparations). Nevertheless, the onset latency of evoked EPSPs in a given neuron was virtually constant: the standard deviation of the onset latency of the EPSPs ($n = 10$–16) was 0·25 ms on average (range of the standard deviation: 0·14–0·53 ms). Across different neurons in a given slice preparation, the EPSPs were similar in onset latency; the difference in the mean onset latency between neurons was < 1 ms. Based on length

of the stimulated optic nerve and the mean onset latency of the evoked EPSPs, the conduction velocity of the optic nerve fibres innervating the SCN was estimated to be $0{\cdot}39 \pm 0{\cdot}02$ m/s (range: 0·31–0·56 m/s, $n = 12$ neurons from ten rat preparations).

Effects of DNQX and AP5 on the EPSPs from optic nerve stimulation

The effects of DNQX, a non-NMDA receptor antagonist, on the EPSPs evoked at membrane potentials between -60 and -100 mV were examined in nine neurons. In

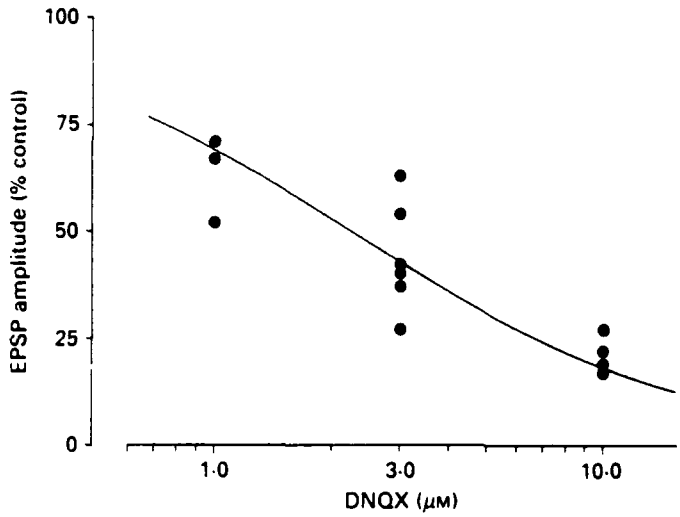

Fig. 5. Concentration–response curve for the DNQX effects on the EPSPs from optic nerve stimulation. This semilogarithmic plot is based on thirteen tests in nine neurons. Four of the nine neurons were tested with two different concentrations, while the remaining were with one. The concentration at which DNQX would produce half-maximal inhibition (IC_{50}) of the EPSP was calculated from the non-linear regression line fitted to the data points, assuming the following relationship: % EPSP = $100\ IC_{50}/(IC_{50} + [DNQX])$. In this figure the IC_{50} is 2·2 μM.

all of the nine neurons, application of DNQX (1–10 μM) resulted in a significant depression of the evoked EPSPs (Fig. 4). The maximum effect of DNQX was observed 15–60 min after the onset of application. The effects of DNQX were not associated with any significant changes in the baseline input resistance (105 ± 4% of the control, $n = 11$ tests in eight neurons) or membrane potential ($-3{\cdot}6 \pm 1{\cdot}7$ mV change from the control level, $n = 12$ tests in eight neurons) of the postsynaptic neurons, and were partially or almost completely reversible following 30–120 min wash ($n = 8$ tests in six neurons) (Fig. 4). The effects of DNQX were concentration dependent, as illustrated in Figs 4 and 5. The concentration at which DNQX would depress the EPSPs by 50% (IC_{50}) was estimated to be about 2 μM (Fig. 5).

In contrast to the strong effects of DNQX, AP5 had no consistent effects on the EPSPs evoked at membrane potentials between -60 and -100 mV (Fig. 6). The EPSP amplitude in 50–100 μM-AP5 was 89 ± 9% ($n = 7$) of control. On the other

hand. AP5 clearly affected the EPSPs that were evoked at membrane potentials between −20 and −55 mV. In each of the four neurons tested, AP5 (50 μM) blocked or depressed significantly the slow depolarizing potential that emerged at the falling phase of the EPSP, with little or no effect on the fast peak (Fig. 7). The AP5 effects

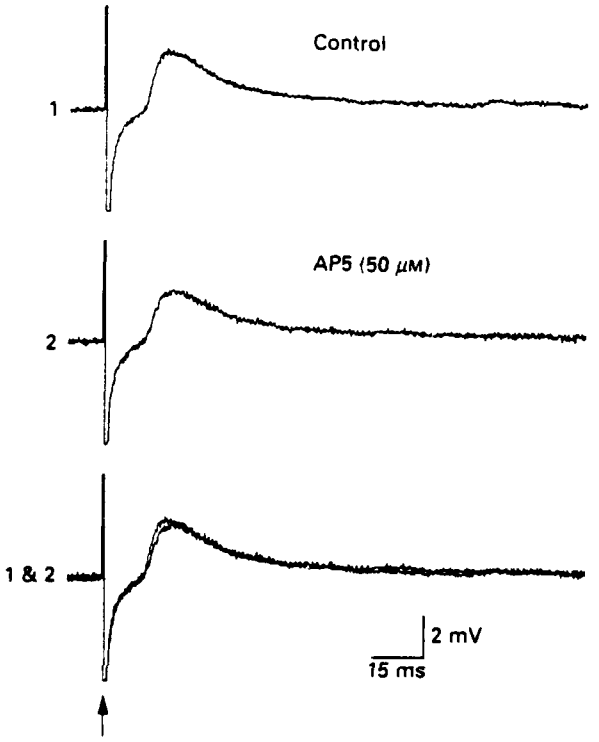

Fig. 6. Lack of effect of AP5 on the EPSPs from optic nerve stimulation (arrow). Top and middle panels, EPSPs before and during application of AP5. Bottom panel, superimposition of the traces in the top and middle panels. Current clamped to −78 mV.

were close to maximum at 10–15 min after the onset of application, and partially reversible after about 30 min wash ($n = 1$). The rapid effects of AP5 (as compared to the DNQX effects) might be due to the hydrophilic property of AP5. The effects of AP5 were not associated with any significant changes in the baseline input resistance (101 ± 13% of the control, $n = 3$) or membrane potential (−1·8 ± 2·3 mV change from the control level, $n = 4$) of the postsynaptic neurons.

Effects of DNQX and AP5 on the EPSPs from stimulation of a neighbouring site of the SCN

Stimulation of a site lateral or dorsocaudal to the SCN in BIC-treated slices often evoked fast EPSPs distinct from those from optic nerve stimulation. Here again, DNQX (0·3–10 μM) depressed by 15–90% the EPSPs evoked at membrane potentials between −60 and −100 mV ($n = 4$; Fig. 8). The concentration-dependent DNQX

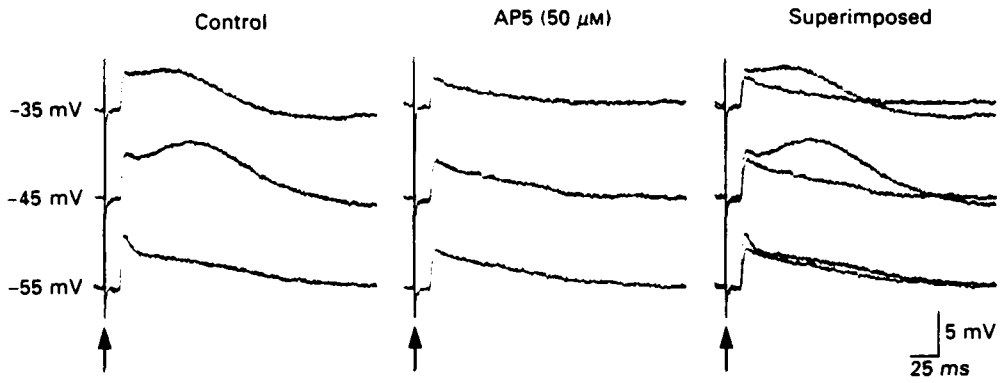

Fig. 7. Blockade by AP5 of the slow depolarizing potentials as a component of the EPSPs evoked by optic nerve stimulation (arrow). Left and middle panels. EPSPs evoked at −35, −45 and −55 mV membrane potentials before and during application of AP5. Right panel. the traces in the left and middle panels are superimposed. Recorded with CsCl- and QX-314-filled electrode.

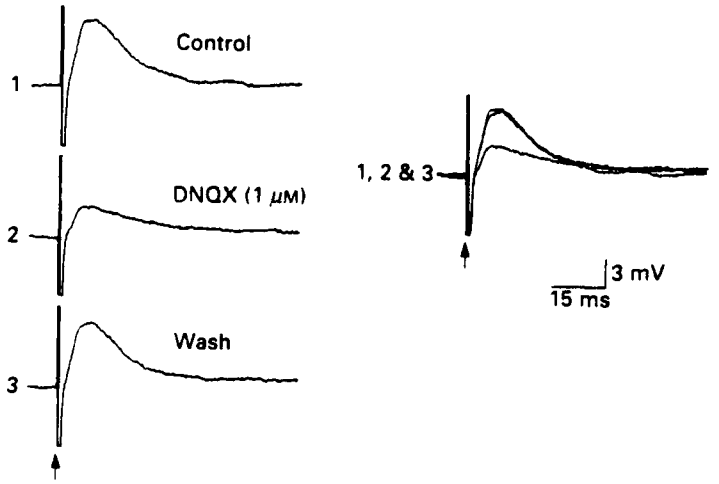

Fig. 8. Depression by DNQX of the EPSP from stimulation of a site lateral to the SCN. Left panel. EPSPs following stimulation (arrow) of the neighbouring site under each experimental condition. Right panel. the traces in the left panel are superimposed. Current clamped to −82 mV.

effect was reversible ($n = 2$), and was not associated with any significant changes in the baseline input resistance (99 ± 1 % of the control, $n = 3$) or membrane potential ($-2{\cdot}0 \pm 1{\cdot}2$ mV change from the control level, $n = 3$) of the postsynaptic neurons. In contrast to the consistent DNQX effects, AP5 had no significant effect on the EPSPs evoked at these membrane potentials (Fig. 9): in 50–100 μM-AP5 the EPSP amplitude was 103 ± 10 % ($n = 5$) of the control.

The EPSPs evoked at membrane potentials between −20 and −55 mV after

blockade of outward K^+ currents and fast Na^+ spikes with Cs^+ and QX-314 contained a slow depolarizing potential, similar to the EPSPs from optic nerve stimulation. A presumed high-threshold Ca^{2+} spike (Llinás & Yarom, 1981; Connors & Prince, 1982) often arose from the slow potential (Fig. 9). As expected, AP5 (50 μM) blocked

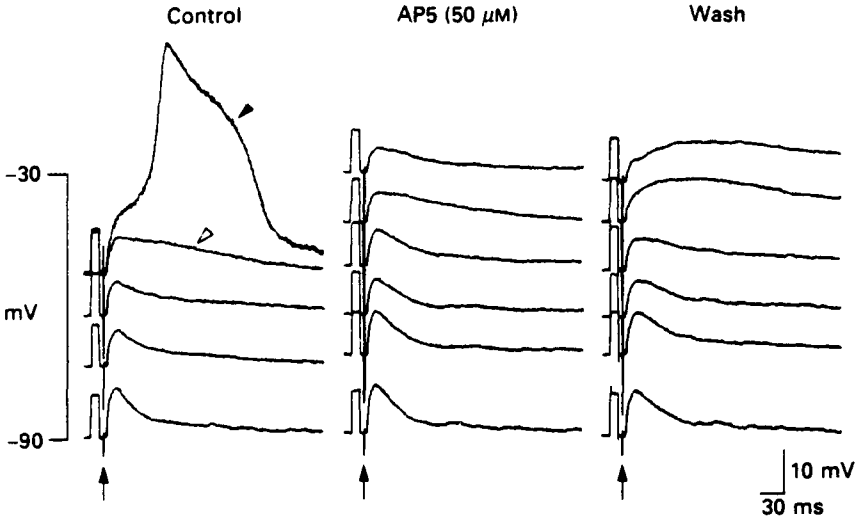

Fig. 9. Effects of AP5 on the EPSPs evoked by stimulation (arrow) of a site dorsocaudal to the SCN. For each experimental condition, several EPSPs were evoked at membrane potentials between -30 and -90 mV. A calibration pulse (10 mV, 10 ms) preceded the dorsocaudal stimulation by 5 ms. The top trace in the left panel exhibiting a presumed high-threshold Ca^{2+} spike (arrow-head) is an individual trace (i.e. not averaged), and each of the remaining traces is an average of six to ten. *During the control period (left panel)*, the EPSPs evoked at a membrane potential of about -50 mV contained a slow depolarizing potential (open arrow-head) at the falling phase. This slow potential often triggered a presumed high-threshold Ca^{2+} spike. During application of AP5 (middle panel), the slow potential was almost completely blocked. After wash-out AP5 (right panel), the slow potential reappeared without triggering the presumed Ca^{2+} spikes. Recovery from the AP5 blockade was more apparent for the EPSPs evoked at less negative membrane potentials. Recorded with CsCl- and QX-314-filled electrode.

or attenuated the slow potential ($n = 3$; Fig. 9). Again, the effect was partially reversible ($n = 2$), and was not associated with any significant changes in baseline input resistance ($103 \pm 13\%$ of the control, $n = 3$) or baseline membrane potential ($-1{\cdot}0 \pm 2{\cdot}1$ mV change from the control level, $n = 3$).

Depression of spontaneously occurring EPSPs by DNQX

Because SCN neurons in these slice preparations rarely exhibited spontaneous EPSPs of an amplitude and frequency adequate for testing of the antagonist, the effects of DNQX on spontaneous EPSPs were examined in only two neurons, recorded with potassium acetate-filled electrodes. At concentrations of 1–10 μM, DNQX depressed the amplitude of the spontaneous EPSPs by over 50% with no significant effect on the passive membrane properties (Fig. 10). In one neuron, a

concentration dependence of the DNQX effect was observed (data not shown). We did not attempt to assess the possible effects of DNQX on the frequency of the EPSPs.

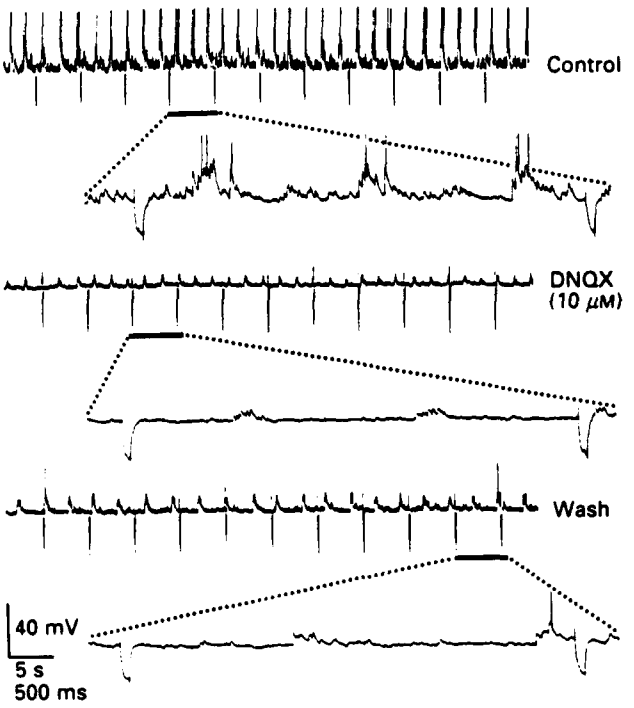

Fig. 10. Depression by DNQX of spontaneously occurring EPSPs. In each panel the underlined portion of the upper trace is shown at a 10 times faster speed (the lower trace). The downward deflections of the traces are electrotonic potentials induced by hyperpolarizing current pulses (−100 pA, 100 ms). During control period large compound EPSPs gave rise to action potentials (truncated). Between the large compound EPSPs were interposed smaller EPSPs. DNQX greatly depressed the EPSPs. The effect of DNQX was only partially reversible after 2 h wash. DNQX did not affect the baseline input resistance. Over the course of the experiment the interval of the large compound EPSPs increased gradually. All of the traces in this figure are individual (not averaged). Current clamped to a membrane potential of about 25 mV below threshold (accurate membrane potential not available).

DISCUSSION

Postsynaptic response of SCN neurons to optic nerve stimulation

Whether inputs from retinal ganglion cells to SCN neurons are excitatory or inhibitory has been an unsettled issue. In anaesthetized rats and hamsters the firing rate of a subpopulation of SCN neurons was shown either to increase or to decrease in response to either retinal illumination or direct electrical stimulation of optic nerve (Nishino, Koizumi & Brooks, 1976; Groos & Mason, 1978; Sawaki, 1979; Groos, Mason & Meijer, 1983; Groos & Meijer, 1985; Meijer, Groos & Rusak, 1986).

Although the prevalent type of response was excitation (i.e. an increase in firing rate in about 75%), inhibition was also present in some units, even after bilateral lesion of the lateral geniculate nucleus (Groos & Mason, 1978). On the other hand, *in vitro* studies with rat and mouse brain slice preparations (Shibata, Oomura, Hattori & Kita, 1984; Cahill & Menaker, 1989*a*) have suggested that an initial increase in firing rate is the predominant type of response immediately after optic nerve stimulation. In these *in vitro* studies a pure decrease in firing rate after optic nerve stimulation was rarely observed, although some neurons following the initial excitation showed an inhibitory or oscillatory firing pattern. Our results agree relatively well with those from other *in vitro* studies, because all the PSPs of SCN neurons to optic nerve stimulation were EPSPs, as indicated by the following: (1) The estimated reversal potential of the PSPs was near 0 mV, similar to the reported values for EPSPs of other central nervous system neurons (Brown & Johnston, 1983; Crunelli, Kelly, Leresche & Pirchio, 1987; Gallagher & Hasuo, 1989) and (2) EAA receptor antagonists blocked the PSPs in a concentration-dependent and reversible manner (see below). The discrepancy between the present results and those from the previous *in vivo* studies may be due to the difference in the type of stimulation (i.e. retinal illumination *vs.* optic nerve stimulation), stimulation parameters (e.g. repetitive *vs.* discrete single shocks to the optic nerve) and/or anaesthesia. Alternatively, it may be due to the fact that in the present study many of the non-retinal afferents to the SCN were severed in the course of hypothalamic slice preparation and, as a result, complications associated with indirect inputs were reduced or eliminated.

The results that optic nerve stimulation never evoked pure IPSPs in any of the neurons recorded in BIC-free medium, and that BIC had no effect on the EPSPs from optic nerve stimulation, strongly suggest GABA is not a neurotransmitter directly responsible for retinohypothalamic transmission. In addition, the absence of pure evoked IPSPs also suggests that the local GABAergic neurons in SCN are not relay neurons between retinal ganglion cells and other SCN neurons. Nevertheless, our data do not exclude the possibility that GABAergic neurons participate in photic information processing. The observation that one of the thirty-one neurons showing an EPSP to optic nerve stimulation also showed a subsequent BIC-sensitive IPSP rather argues for such a possibility.

The EPSPs evoked by optic nerve stimulation appeared to be monosynaptic, because the evoked EPSPs in a given neuron and also across different neurons in a given slice preparation were virtually constant in onset latency; in a given neuron the standard deviation of the EPSP onset latency was only 0·25 ms on average, and across different neurons in a given slice preparation the difference in the mean onset latency was < 1 ms. On the other hand, the failure of SCN neurons to follow high-frequency optic nerve stimuli with EPSPs is consistent with polysynaptic connections, and could imply that some EPSPs are mediated through local interneurons. However, the fragility of the EPSPs could simply be due to axonal conduction block in presynaptic terminals and may be a characteristic specific for the retinal input to SCN neurons (i.e. a consistent following with EPSPs may not be as critical for photic information processing in SCN as in thalamus and cortex).

The estimated conduction velocity of the retinohypothalamic tract in the present study roughly matches that from the previous extracellular electrophysiological

studies conducted with rat and mouse slice preparations (Shibata *et al.* 1984; Cahill & Menaker, 1989*a*), and suggests that the optic nerve fibres innervating SCN neurons are unmyelinated. This conclusion is consistent with the anatomical evidence that optic nerve fibres within rat SCN are unmyelinated (Güldner, 1978).

Mediation by non-NMDA receptors of retinohypothalamic transmission at resting or more negative membrane potentials

The present results demonstrate that DNQX, a non-NMDA receptor antagonist, reversibly depressed the EPSPs, evoked by optic nerve stimulation at membrane potentials between −60 and −100 mV. Also, the data illustrate that the effects of DNQX were not associated with any significant changes in the baseline input resistance or membrane potential of the postsynaptic neurons, suggesting a specific action of DNQX. The estimated concentration at which DNQX depressed the EPSPs by 50% roughly matches the concentrations that were reported to inhibit by 50% the binding of [^{3}H]kainate and [^{3}H]AMPA (α-amino-3-hydroxy-5-methyl-4-isoxazole propionic acid), a quisqualate agonist, to a rat cortical membrane preparation (Honoré, Davies, Drejer, Fletcher, Jacobsen, Lodge & Nielsen, 1988). The match in the DNQX concentrations again suggests that the DNQX effects in the present study were via action at the specific binding sites. In addition, the effects of DNQX were not likely due to its interaction with the strychnine-insensitive, glycine binding site on the NMDA receptor complex (Birch, Grossman & Hayes, 1988; Lester, Quarum, Parker, Weber & Jahr, 1989), because AP5 had no significant and consistent effects on the EPSPs even at high concentrations.

Our results confirm the general conclusion of the previous extracellular electrophysiological studies that EAA receptors mediate retinohypothalamic transmission (Shibata *et al.* 1986; Cahill & Menaker, 1987, 1989*b*), and further provide *direct* intracellular electrophysiological evidence that at resting or more negative membrane potentials retinohypothalamic transmission is mediated by non-NMDA receptors.

Involvement of NMDA receptors in retinohypothalamic transmission at less negative membrane potentials

The role of NMDA receptors in retinohypothalamic transmission is controversial. In support of a role, Shibata *et al.* (1986) showed that the field potentials recorded in the SCN of rat hypothalamic slice preparations following optic nerve stimulation were depressed by a moderately selective NMDA receptor antagonist, DL-2-amino-adipic acid (Watkins & Evans, 1981). However, the antagonist concentration that resulted in approximately 50% depression of the field responses was 1 mM. At this concentration the antagonist may not be selective for NMDA receptors, as pointed out by Cahill & Menaker (1989*b*). Recently, Rusak & Robertson (1989) reported that pre-treatment with MK-801, a non-competitive NMDA receptor antagonist, blocked the light-induced increase in the immunoreactivity of *fos*, the product of the *c-fos* proto-oncogene, in the SCN of hamsters. Also, Colwell, Ralph & Menaker (1990) demonstrated that intraperitoneal injection of MK-801 blocked in a dose-dependent manner the phase-shifting effects of light on the circadian rhythm of wheel-running

activity in hamsters. Although the results from these studies suggest a possible role for NMDA receptors in photic information processing, they do not provide information on the exact location of the NMDA receptors.

A recent *in vitro* extracellular electrophysiological study by Cahill & Menaker (1989*b*) does not support the hypothesis that NMDA receptors participate in retinohypothalamic transmission. According to these investigators, omission of Mg^{2+} from the superfusate did not reveal any AP5-sensitive component (i.e. NMDA component) in the postsynaptic field potentials recorded in the SCN following optic nerve stimulation. Since the absence of an NMDA component could be due to the residual Mg^{2+} in the tissue, which could have been enough to maintain the voltage-dependent block of the NMDA receptor-linked channels (Mayer, Westbrook & Guthrie, 1984; Nowak, Bregestovski, Ascher, Herbet & Prochiantz, 1984), we took the strategy of altering baseline membrane potential, instead of using Mg^{2+}-free medium, in testing for the presence of an NMDA component. In our experiments, at membrane potentials between −20 and −55 mV, optic nerve stimulation evoked slow, as well as fast, depolarizing potentials, whose relationship to membrane potential was non-linear, as expected for NMDA receptor-mediated events. Since these experiments were conducted under a condition where Ca^{2+} channels were not blocked, pure voltage-dependent Ca^{2+} conductances activated by the fast depolarizing potentials might have initiated the slow depolarizing potentials. The selective blockade of the slow potentials by AP5, however, suggests that this is not the case. When coupled with the observation that AP5 had little or no effect on the EPSPs evoked at membrane potentials between −60 and −100 mV, these results suggest that at resting or more negative membrane potentials, NMDA receptors do not contribute or contribute only minimally to retinohypothalamic transmission, whereas at less negative membrane potentials NMDA receptors play a role.

Despite the evidence in the present study for involvement of NMDA receptors in retinohypothalamic transmission at less negative membrane potentials, the extent to which NMDA receptors contribute to excitatory synaptic transmission is unclear. In the current experiments we did not add to the perfusing medium glycine, which is known to allosterically modulate the NMDA receptors (Johnson & Ascher, 1987). We assumed that the sub-synaptic concentration of glycine was high enough for the modulation (Thomson, 1989). If this assumption was incorrect, we might have underestimated the contribution of the NMDA component. In the future, whole-cell voltage-clamp experiments with patch pipettes (Blanton, Lo Turco & Kriegstein 1989) in medium with different concentrations of glycine and Mg^{2+} are expected to allow a more rigorous and quantitative analysis of the NMDA component.

Contribution of both NMDA and non-NMDA receptors to non-retinal synaptic transmission to SCN

The EPSPs evoked by stimulation of a site near to the SCN at membrane potentials between −60 and −100 mV were sensitive to DNQX, but not to AP5. On the other hand, those evoked at less negative membrane potentials contained an AP5-sensitive component. These results, coupled with the fact that the spontaneous EPSPs in hyperpolarized cells were also sensitive to DNQX, support the hypothesis that the synaptic mechanisms underlying other excitatory inputs to SCN are basically the same as those of the retinohypothalamic tract (i.e. at resting or more

negative membrane potentials, mainly non-NMDA receptors mediate excitatory synaptic transmission, while at less negative membrane potentials NMDA receptors also play a role).

Up to now, no serious attention has been paid to the potential role of the EAAs in non-retinal neurotransmission in the SCN, probably because more emphasis has been put on other putative neurotransmitters (e.g. neuropeptide Y). Many of the non-retinal afferents containing other putative neurotransmitters may also utilize glutamate or similarly related EAAs for fast excitatory neurotransmission. In this case, the other putative transmitters may have modulatory roles.

In conclusion, the data obtained from these experiments suggest that: (1) the direct retinal input to SCN is excitatory, and GABA is not the neurotransmitter, and (2) at resting or more negative membrane potentials, non-NMDA receptors mediate excitatory synaptic transmission for both retinal and non-retinal inputs to SCN neurons. At less negative membrane potentials, however, NMDA receptors may also play a role.

We are grateful to Dr D. Birt for developing neurophysiological data analysis routines, to T. Valdes and D. Weber for technical assistance, and to S. Morris for secretarial help. This research was supported by grants from the United States Air Force Office of Scientific Research (87-0361 and 90-0056) to F. E. D.

REFERENCES

ALBERS, H. E., LIOU, S-Y., FERRIS, C. F., STOPA, E. G. & ZOELLER, R. T. (1991). Neurochemistry of circadian timing. In *The Suprachiasmatic Nucleus: The Mind's Clock*, ed. KLEIN, D. C., MOORE, R. Y. & REPPERT, S. M., pp. 263–288. Oxford University Press, Oxford.

BIRCH, P. J., GROSSMAN, C. J. & HAYES, A. G. (1988). 6,7-Dinitro-quinoxaline-2,3-dion and 6-nitro,7-cyano-quinoxaline-2,3-dion antagonise responses to NMDA in the rat spinal cord via an action at the strychnine-insensitive glycine receptor. *European Journal of Pharmacology* **156**, 177–180.

BLANTON, M. G., LO TURCO, J. J. & KRIEGSTEIN, A. R. (1989). Whole cell recording from neurons in slices of reptilian and mammalian cerebral cortex. *Journal of Neuroscience Methods* **30**, 203–210.

BROWN, T. H. & JOHNSTON, D. (1983). Voltage-clamp analysis of mossy fiber synaptic input to hippocampal neurons. *Journal of Neurophysiology* **50**, 487–507.

CAHILL, G. M. & MENAKER, M. (1987). Kynurenic acid blocks suprachiasmatic nucleus responses to optic nerve stimulation. *Brain Research* **410**, 125–129.

CAHILL, G. M. & MENAKER, M. (1989*a*). Responses of the suprachiasmatic nucleus to retinohypothalamic tract volleys in a slice preparation of the mouse hypothalamus. *Brain Research* **479**, 65–75.

CAHILL, G. M. & MENAKER, M. (1989*b*). Effects of excitatory amino acid receptor antagonists and agonists on suprachiasmatic nucleus responses to retinohypothalamic tract volleys. *Brain Research* **479**, 76–82.

COLWELL, C. S., RALPH, M. R. & MENAKER, M. (1990). Do NMDA receptors mediate the effects of light on circadian behavior? *Brain Research* **523**, 117–120.

CONNORS, B. W. & PRINCE, D. A. (1982). Effects of local anesthetic QX-314 on the membrane properties of hippocampal pyramidal neurons. *Journal of Pharmacology and Experimental Therapeutics* **220**, 476–481.

CRUNELLI, V., KELLY, J. S., LERESCHE, N. & PIRCHIO, M. (1987). On the excitatory post-synaptic potential evoked by stimulation of the optic tract in the rat lateral geniculate nucleus. *Journal of Physiology* **384**, 603–618.

GALLAGHER, J. P. & HASUO, H. (1989). Excitatory amino acid-receptor-mediated EPSPs in rat dorsolateral septal nucleus neurones *in vitro*. *Journal of Physiology* **418**, 353–365.

GROOS, G. & MASON, R. (1978). Maintained discharge of rat suprachiasmatic neurons at different adaptation levels. *Neuroscience Letters* **8**, 59–64.

GROOS, G., MASON, R. & MEIJER, J. (1983). Electrical and pharmacological properties of the suprachiasmatic nuclei. *Federation Proceedings* **42**, 2790–2795.

GROOS, G. A. & MEIJER, J. H. (1985). Effects of illumination on suprachiasmatic nucleus electrical discharge. *Annals of the New York Academy of Sciences* **453**, 134–146.

GÜLDNER, F. H. (1978). Synapses of optic nerve afferents in the rat suprachiasmatic nucleus. *Cell and Tissue Research* **194**, 17–35.

HENDRICKSON, A. E., WAGONER, N. & COWAN, W. M. (1972). An autoradiographic and electron microscopic study of retino-hypothalamic connections. *Zeitschrift für Zellforschung und Mikroskopische Anatomie*. **135**, 1–26.

HONORÉ, T., DAVIES, S. N., DREJER, J., FLETCHER, E., JACOBSEN, P., LODGE, D. & NIELSEN, F. E. (1988). Quinoxalinediones: Potent competitive non-NMDA glutamate receptor antagonists. *Science* **241**, 701–703.

JOHNSON, J. W. & ASCHER, P. (1987). Glycine potentiates the NMDA response in cultured mouse brain neurons. *Nature* **325**, 529–531.

KIM, Y. I. & DUDEK, F. E. (1989). Antagonism of fast excitatory postsynaptic potentials in suprachiasmatic nucleus neurons by excitatory amino acid antagonists. *Society for Neuroscience Abstracts* **15**, 1088.

LESTER, R. A. J., QUARUM, M. L., PARKER, J. D., WEBER, E & JAHR, C. E. (1989). Interaction of 6-cyano-7-nitroquinoxaline-2.3-dione with the *N*-methyl-*D*-aspartate receptor-associated glycine binding site. *Molecular Pharmacology* **35**, 565–570.

LLINÁS, R. & YAROM, Y. (1981). Electrophysiology of mammalian inferior olivary neurones in vitro. Different types of voltage-dependent ionic conductances. *Journal of Physiology* **315**, 549–567.

MAYER, M. L., WESTBROOK, G. L. & GUTHRIE, P. B. (1984). Voltage-dependent block by Mg^{2+} of NMDA response in spinal cord neurones. *Nature* **309**, 261–263.

MEIJER, J. H., GROOS, G. A. & RUSAK, B. (1986). Luminance coding in a circadian pacemaker: the suprachiasmatic nucleus of the rat and the hamster. *Brain Research* **382**, 109–118.

MEIJER, J. H. & RIETVELD, W. J. (1989). Neurophysiology of the suprachiasmatic circadian pacemaker in rodents. *Physiological Reviews* **69**, 671–707.

MOORE, R. Y. (1983). Organization and function of a central nervous system circadian oscillator: the suprachiasmatic hypothalamic nucleus. *Federation Proceedings* **42**, 2783–2789.

MOORE, R. Y. & EICHER, V. B. (1972). Loss of a circadian adrenal corticosterone rhythm following suprachiasmatic lesions in the rat. *Brain Research* **42**, 201–206.

MOORE, R. Y. & LENN, N. J. (1972). A retinohypothalamic projection in the rat. *Journal of Comparative Neurology* **146**, 1–14.

NISHINO, H., KOIZUMI, K. & BROOKS, C. McC. (1976). The role of the suprachiasmatic nuclei of the hypothalamus in the production of circadian rhythm. *Brain Research* **112**, 45–59.

NOWAK, L., BREGESTOVSKI, P., ASCHER, P., HERBET, A. & PROCHIANTZ, A. (1984). Magnesium gates glutamate-activated channels in mouse central neurones. *Nature* **307**, 462–465.

RALL, W. (1969). Time constants and electrotonic length of membrane cylinders and neurons. *Biophysical Journal* **9**, 1483–1508.

RALPH, M. R., FOSTER, R. G., DAVIS, F. C. & MENAKER, M. (1990). Transplanted suprachiasmatic nucleus determines circadian period. *Science* **247**, 975–978.

REPPERT, S. M., PERLOW, M. J., UNGERLEIDER, L. G., MISHKIN, M., TAMARKIN, L., ORLOFF, D. G., HOFFMAN, H. J. & KLEIN, D. C. (1981). Effects of damage to the suprachiasmatic area of the anterior hypothalamus on the daily melatonin and cortisol rhythms in the rhesus monkey. *Journal of Neuroscience* **12**, 1414–1425.

RIBAK, C. E. & PETERS, A. (1975). An autoradiographic study of the projections from the lateral geniculate body of the rat. *Brain Research* **92**, 261–294.

RUSAK, B. & ROBERTSON, H. A. (1989). Induction of c-fos expression in the suprachiasmatic nucleus (SCN) of hamsters by light exposure. *Society for Neuroscience Abstracts* **15**, 493.

RUSAK, B. & ZUCKER, I. (1979). Neural regulation of circadian rhythms. *Physiological Reviews* **59**, 449–526.

SAWAKI, Y. (1979). Suprachiasmatic nucleus neurons: excitation and inhibition mediated by the direct retino-hypothalamic projection in female rats. *Experimental Brain Research* **37**, 127–138.

SHIBATA, S., LIOU, S. Y. & UEKI, S. (1986). Influence of excitatory amino acid receptor antagonists and of baclofen on synaptic transmission in the optic nerve to the suprachiasmatic nucleus in slices of rat hypothalamus. *Neuropharmacology* **25**, 403–409.

SHIBATA, S., OOMURA, Y., HATTORI, K. & KITA, H. (1984). Responses of suprachiasmatic nucleus neurons to optic nerve stimulation in rat hypothalamic slice preparation. *Brain Research* **302**, 83–89.

STEPHAN, F. K. & ZUCKER, I. (1972). Circadian rhythms in drinking behavior and locomotor activity of rats are eliminated by hypothalamic lesions. *Proceedings of the National Academy of Sciences of the USA* **69**, 1583–1586.

SUGIMORI, M., SHIBATA, S. & OOMURA, Y. (1986). Electrophysiological bases for rhythmic activity in the suprachiasmatic nucleus of the rat: an in vitro study. In *Emotions: Neuronal and Chemical Control*, ed. OOMURA, U., pp. 199–206. S. Karger, Basel, Switzerland.

SWANSON, L. W., COWAN, W. M. & JONES, E. G. (1974). An autoradiographic study of the efferent connections of the ventral lateral geniculate nucleus in the albino rat and cat. *Journal of Comparative Neurology* **156**, 143–163.

TAKAHASHI, J. S. & ZATZ, M. (1982). Regulation of circadian rhythmicity. *Science* **217**, 1104–1111.

THOMSON, A. M. (1989). Glycine modulation of the NMDA receptor/channel complex. *Trends in Neurosciences* **12**, 349–353.

THOMSON, A. M. & WEST, D. C. (1990). Factors affecting slow regular firing in the suprachiasmatic nucleus in vitro. *Journal of Biological Rhythms* **5**, 59–75.

TUREK, F. W. (1985). Circadian neural rhythms in mammals. *Annual Review of Physiology* **47**, 49–64.

VAN DEN POL, A. N. (1980). The hypothalamic suprachiasmatic nucleus of rat: Intrinsic anatomy. *Journal of Comparative Neurology* **191**, 661–702.

WATKINS, J. C. & EVANS, R. H. (1981). Excitatory amino acid transmitters. *Annual Review of Pharmacology and Toxicology* **21**, 165–204.

WHEAL, H. V. & THOMSON, A. M. (1984). The electrical properties of neurones of the rat suprachiasmatic nucleus recorded intracellularly in vitro. *Neuroscience* **13**, 97–104.

Journal of Physiology (1992), 000. *pp.* 000–000
With 7 figures
Printed in Great Britain

'Press'

INTRACELLULAR ELECTROPHYSIOLOGICAL STUDY OF SUPRACHIASMATIC NUCLEUS NEURONS IN RODENTS: INHIBITORY SYNAPTIC MECHANISMS

BY YANG IN KIM* AND F. EDWARD DUDEK*†

*From the *Mental Retardation Research Center and †Brain Research Institute, UCLA School of Medicine, Los Angeles, CA 90024, USA*

(*Received 31 October 1991*)

SUMMARY

1. The mechanisms responsible for evoked and spontaneous fast inhibitory postsynaptic potentials (IPSPs) in the hypothalamic suprachiasmatic nucleus (SCN) were studied with intracellular recording. SCN neurons, primarily ones identified as receiving excitatory optic nerve input, were recorded in rat and guinea-pig brain slice preparations maintained *in vitro*.

2. In normal medium, electrical stimulation of a site dorsocaudal to the SCN evoked IPSPs from thirty-three of thirty-six neurons. The evoked IPSPs rose to the peak quickly ($8{\cdot}7 \pm 0{\cdot}9$ ms, mean ± S.E.M.; $n = 15$ neurons) and decayed gradually with a time constant of 25 ± 3 ms. Spontaneous IPSPs were present in each of the thirty-six neurons. These IPSPs had a rise-to-peak time of $7{\cdot}2 \pm 1{\cdot}0$ ms ($n = 6$ neurons) and a decay time constant of 14 ± 5 ms.

3. When recorded with potassium acetate-filled electrodes, the evoked and spontaneous IPSPs were hyperpolarizing at resting membrane potential (less negative than −70 mV) and had a reversal potential of around −75 mV. On the other hand, when recorded with potassium chloride-filled electrodes, the IPSPs were depolarizing at membrane potentials more negative than −50 mV and had an estimated reversal potential less negative than spike threshold.

4. Bath application of bicuculline (10–50 μM), a γ-aminobutyric acid$_A$ ($GABA_A$) receptor antagonist, resulted in a complete blockade of both the ~~evoked~~ ($n = 16$) and spontaneous ($n = 13$) IPSPs. The bicuculline effects were reversible, and were not associated with any significant and consistent change in baseline membrane potential or input resistance. The neurons impaled in bicuculline-containing medium ($n = 11$) exhibited neither spontaneous IPSPs nor evoked IPSPs.

5. In some neurons bicuculline-resistant hyperpolarizing potentials, which were similar to the fast IPSPs in time course, occurred spontaneously or were evoked by electrical stimulation of the optic nerve or the dorsocaudal site. A fast prepotential always preceded the hyperpolarizing potential, and hyperpolarizing currents blocked these events, indicating that they were not synaptic in origin. No slow IPSPs were detected.

6. The results suggest that fast IPSPs from non-retinal afferents exist in virtually

SCN neurons receiving excitatory retinal input, and that $GABA_A$ receptors associated with Cl^- channels mediate the fast IPSPs.

INTRODUCTION

In mammals the major pacemaker for circadian rhythms appears to be located in the hypothalamic suprachiasmatic nuclei (SCN) (for reviews, see Takahashi & Zatz, 1982; Moore, 1983; Turek, 1985; Meijer & Rietveld, 1989). Several studies have pointed to the possibility that γ-aminobutyric acid (GABA), via its action at the level of the SCN, may participate in mammalian circadian time keeping. The SCN contains GABAergic neurons (Tappaz, Brownstein & Kopin, 1977; Card & Moore, 1984; van den Pol & Tsujimoto, 1985; van den Pol, 1986; Okamura, Bérod, Julien, Geffard, Kitahama, Mallet & Bobillier, 1989), and nearly 50% of synaptic boutons in the SCN are immunoreactive for GABA (Decavel & van den Pol, 1990). Furthermore, exogenously applied GABA and its related agents alter the single-unit activity of a significant proportion of SCN neurons (Shibata, Liou & Ueki, 1983; Liou & Albers, 1990; Liou, Shibata, Albers & Ueki, 1990; Mason, Biello & Harrington, 1991).

Agents that alter GABAergic neurotransmission have been reported to affect the circadian rhythms of rodents. Single intraperitoneal injections of triazolam, a short-acting benzodiazepine, induce a permanent phase shift in free-running behavioural and endocrine rhythms (for review, see Turek & Van Reeth, 1988), while bicuculline, a $GABA_A$ receptor antagonist, blocks the light-induced phase delays of free-running locomotor rhythm (Ralph & Menaker, 1985). It is not clear where and how these GABAergic drugs act to influence the circadian time-keeping system. A recent study by Johnson, Smale, Moore & Morin (1988) suggests that the lateral geniculate nucleus of the thalamus might be the critical site for the triazolam-induced phase shifts. On the other hand, more recent studies by Smith, Inouye & Turek (1989) and by Smith, Turek & Slater (1990) suggest that the SCN might be an important site for GABAergic drug action. According to their reports, microinjection of muscimol, a selective $GABA_A$ receptor agonist, into the SCN led to a permanent phase advance or delay of free-running locomotor rhythms of hamster; the phase advance was selectively blocked by the $GABA_A$ receptor antagonists, bicuculline and picrotoxin, but not by the $GABA_B$ receptor antagonist, phaclofen.

Several studies have suggested a neurotransmitter role for GABA in the hypothalamus. The evidence includes the presence of numerous GABAergic boutons and axons in various hypothalamic nuclei (Tappaz *et al.* 1977; Decavel & van den Pol, 1990), and the sensitivity to $GABA_A$ receptor antagonist of inhibitory postsynaptic potentials (IPSPs) recorded in some hypothalamic nuclei (Randle, Bourque & Renaud, 1986; Tasker & Dudek, 1988; Hoffman, Kim, Gorski & Dudek, 1990). With regard to the SCN, strong morphological evidence exists for a neurotransmitter role for GABA, but solid physiological evidence is lacking.

The present study was designed to provide physiological evidence that GABA, acting on $GABA_A$ receptors to increase chloride conductance, is the dominant fast inhibitory transmitter in the SCN. In this study, we tested whether bicuculline, a $GABA_A$ receptor antagonist, blocked the spontaneous and evoked IPSPs recorded in the SCN. Since the results of our previous study indicated that optic nerve input to

SCN neurons is excitatory (Kim & Dudek, 1991), we attempted to evoke IPSPs by stimulating other, non-retinal afferents. Here we present intracellular electrophysiological evidence that $GABA_A$ receptors mediate fast IPSPs in the SCN and that fast IPSPs are present in the vast majority of, if not all, SCN neurons. A preliminary account of these results has been published (Kim & Dudek, 1990).

METHODS

Animals

Male Sprague–Dawley rats ($n = 26$, 120–350 g) and guinea-pigs ($n = 5$, 150–450 g) purchased from Charles River Company (USA) were housed in a temperature controlled vivarium (22–23 °C) under a 12 h light/12 h dark cycle (light on at 07·00 h, pacific time) for at least 1 week (mostly more than 2 weeks) prior to use.

Preparation and maintenance of hypothalamic slices

In the morning (after 07.00 h) of the day of the experiment each animal was decapitated with a guillotine under sodium pentobarbitone (I.P., 100 mg/kg wt) anaesthesia. Immediately after decapitation, the brain was removed from the skull and placed in ice-cold physiological saline (composition in mM: 124 NaCl, 1·4 NaH_2PO_4, 3 KCl, 2·4 $CaCl_2$, 26 $NaHCO_3$, 1·3 $MgSO_4$, 11 glucose). After approximately 1 min, the brain was trimmed to a small block to contain the hypothalamus and optic nerves. Then, using a vibroslicer (Campden Instruments, UK), two 500 μm thick parasagittal slices containing the SCN and optic nerve were cut from the block. In one case (rat), a coronal slice was cut from the block. The slices were immediately transferred to and maintained in an interface-type recording chamber which was constantly perfused with warmed (32–35 °C) physiological saline at 0·7–1·0 ml/min. In some experiments, bicuculline methiodide (Sigma, USA) was added to the perfusing medium. A humidified atmosphere of 95% O_2 and 5% CO_2 was maintained above the slice throughout the experiments. Electrophysiological experiments were begun at least 2 h after the slice preparation.

Intracellular recordings and electrical stimulation

Intracellular micropipettes were filled with either 2 M potassium acetate or 2–3 M potassium chloride (90–360 MΩ). Current-clamp recordings were obtained using a high-impedance amplifier with a bridge circuit (Axoclamp-2A, Axon Instruments, USA). Bipolar electrodes were used to stimulate the optic nerve ($\leqslant$ 0·8 mA, 0·5 ms) and a site dorsocaudal to the SCN ($\leqslant$ 1·0 mA, 0·5 ms). The electrode placement in the dorsocaudal aspect varied among different experiments (i.e. more dorsal in some, more caudal in others). The distance of the electrode from the SCN was also variable among experiments (range, 0·5–3 mm).

RESULTS

The data presented in this paper were from forty-eight SCN neurons (thirty-six rat and twelve guinea-pig neurons), which were recorded between 10·00 h and 21·00 h and whose mean ($\pm$S.E.M.) action potential amplitude (measured from spike threshold) and input resistance (estimated from the slope of the linear portion of current–voltage plot) were 60 ± 1 mV ($n = 28$) and 255 ± 27 MΩ ($n = 28$), respectively. The spontaneous firing rate (0–19 Hz) did not appear to correlate with the time of recording. In terms of the properties of postsynaptic potentials, rat and guinea-pig neurons were not obviously different; therefore, the data from the two species were combined.

Characteristics of evoked and spontaneous IPSPs

In bicuculline-free medium electrical stimulation of optic nerve evoked an excitatory postsynaptic potential (EPSP) in a subpopulation of SCN neurons (~~about~~ ~30–40%). However, stimulation of a site dorsocaudal to the SCN evoked an IPSP in

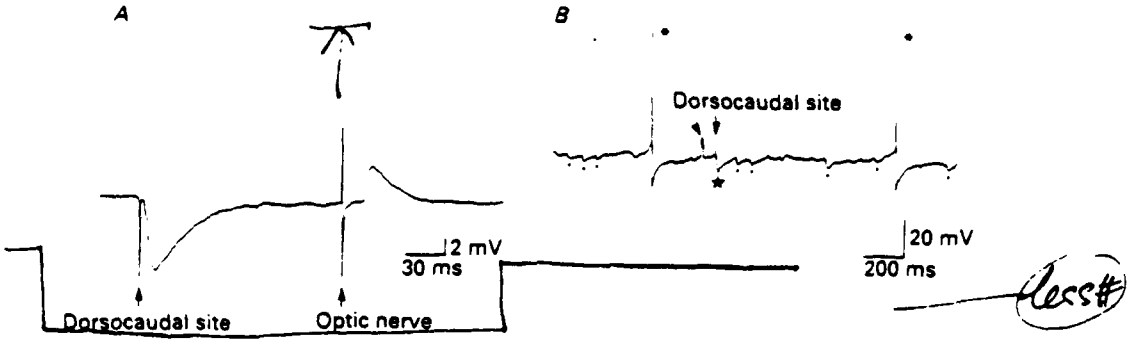

Fig. 1. Convergence of the excitatory optic nerve and inhibitory non-optic nerve inputs to SCN neurons. *A*, an IPSP and an EPSP evoked by stimulation (arrow) of a site dorsocaudal to the SCN and optic nerve, respectively. The trace is an average of twenty response. *B*, individual trace showing spontaneous (●) and evoked (★) IPSPs recorded from another neuron that responded to optic nerve stimulation with an EPSP (not shown). A 10 mV, 10 ms calibration pulse (arrow-head) preceded dorsocaudal stimulation (arrow). Action potentials are labelled with asterisks. Cells were recorded with potassium acetate-filled electrodes and current-clamped to −61 mV (*A*) and −52 mV (*B*). Unless stated otherwise, all the records presented in the following figures were obtained with potassium acetate-filled electrodes.

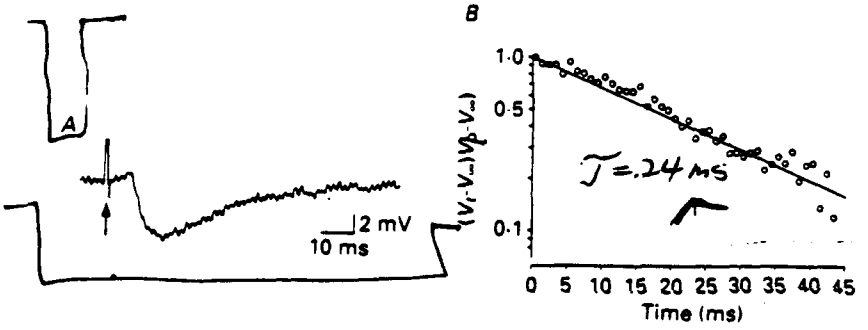

Fig. 2. The IPSPs decayed exponentially. *A*, an IPSP evoked by dorsocaudal stimulation (arrow). *B*, for the decay of the evoked IPSP in *A*, the values of $(V_t-V_\infty)/(V_0-V_\infty)$, taken at 1 ms intervals and integrated over ±0·2 ms, were plotted against time, where V_t is the voltage at time t, V_0 is the voltage at the beginning of the decay and V_∞ is the voltage at the baseline. A linear regression line was fitted to the plot to calculate the time constant ($\tau = -0{\cdot}4343$/slope of the line; Rall, 1969). The cell was at resting membrane potential (−58 mV).

most of the neurons examined (thirty-three of thirty-six neurons). Figure 1*A* illustrates that neurons that responded to optic nerve stimulation with an EPSP ($n = 26$) also responded to dorsocaudal site stimulation with an IPSP ($n = 23$).

Across different neurons the latency of the evoked IPSPs (measured at 50 % of the IPSP peak) varied significantly (range, 5·5–13·5 ms), presumably due to differences in the distance between the recording and stimulation sites. Within a given neuron, however, the latency was virtually constant; the mean latency had a standard deviation of 0·47 ms on average (range of standard deviation across seven neurons, 0·17–0·69 ms; 7–16 IPSPs per neuron). In every neuron tested ($n = 5$), the IPSPs could follow 10 or 20 Hz stimulation.

The evoked IPSPs rose to the peak in 3·9–18·6 ms (8·7 ± 0·9 ms, $n = 15$ neurons), and decayed gradually over 50–150 ms (Fig. 2*A*). In most cases, the decay could be fitted reasonably well with a single time constant (25 ± 3 ms; range 12–52 ms, $n = 15$ neurons, Fig. 2*B*). Neither the rise-to-peak time nor the decay time constant of

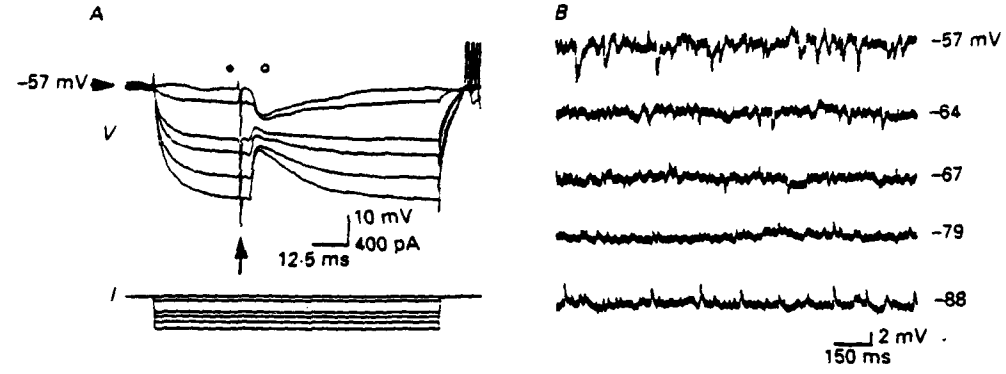

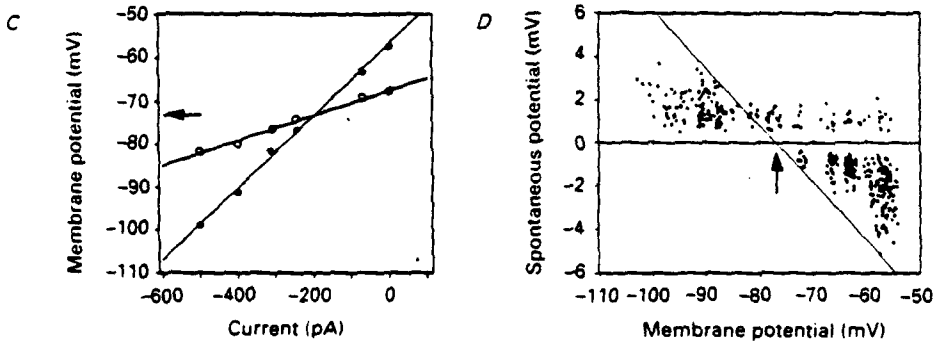

Fig. 3. IPSP reversal potential. *A*, IPSPs evoked by dorsocaudal stimulation (arrow) at the peak of the electrotonic potentials (*V*) elicited by injecting hyperpolarizing current pulses of various amplitudes (*I*). Each voltage trace is an average of three to six responses. *B*, spontaneous IPSPs recorded at the membrane potentials indicated to the right of each trace. These IPSPs were from the same neuron as *A*. Both the evoked and spontaneous IPSPs were hyperpolarizing at membrane potentials less negative than −70 mV, and depolarizing at membrane potentials more negative than −80 mV. *C*, current–voltage plots constructed from the data in *A*. Voltage measurements were obtained immediately before the stimulation (●) and at the peak of the IPSP (○). The slopes of the linear regression lines fitted to the plots were compared to estimate the change in input resistance during the IPSP; input resistance decreased by about 67 % at the peak of the IPSP. The membrane potential where the regression lines cross (arrow, −73 mV) was taken as the reversal potential for the IPSP. *D*, the amplitude of spontaneous IPSPs in *B* was plotted against membrane potential. Other spontaneous IPSPs not shown in *B* were also included in the plot. The points in the upper right quadrant of this plot correspond presumably to spontaneous EPSPs. The continuous line shows the upper limit of the variation in the IPSP amplitude. The intercept of this line with the abscissa (arrow, −77 mV) was taken as the reversal potential for the spontaneous IPSPs.

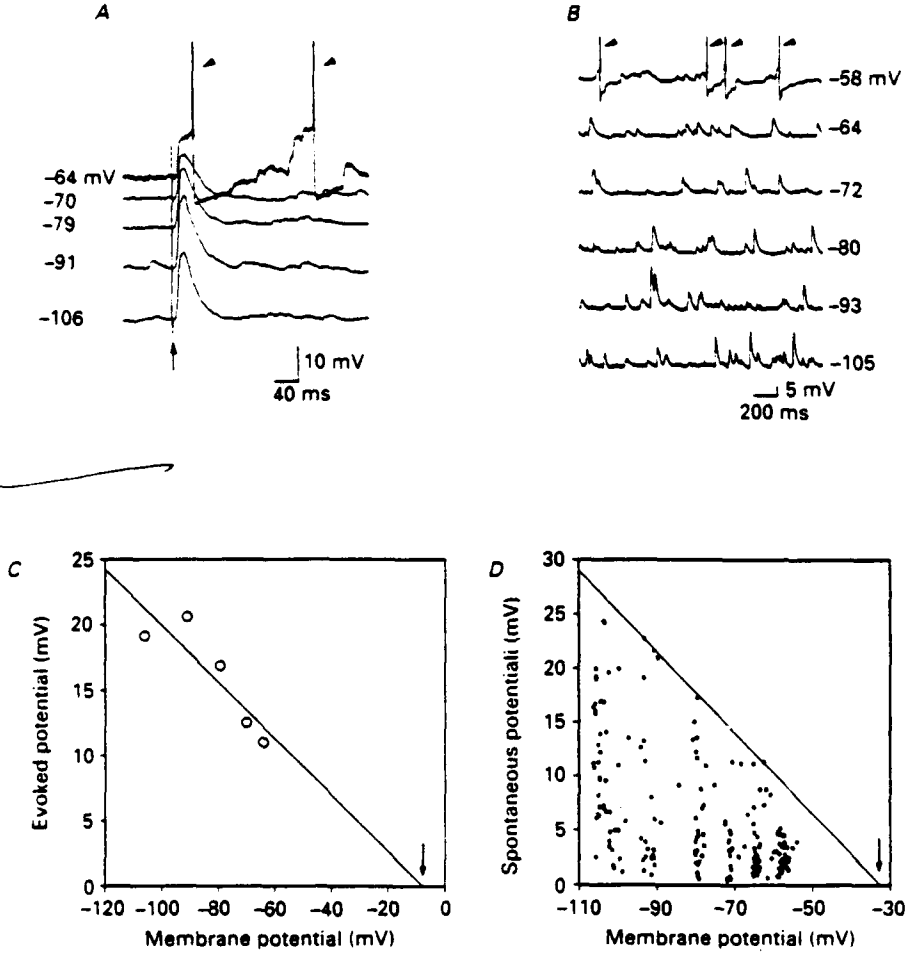

Fig. 4. Reversal of the polarity of IPSP by intracellular Cl^- loading. *A*, depolarizing postsynaptic potentials evoked by stimulation of the dorsocaudal site (arrow) at the membrane potentials indicated to the left of each trace. This cell was recorded with potassium chloride-filled electrode. All of the traces except the top one are an average of eight to fifteen responses. The action potentials (arrow-heads) in the top trace are truncated. *B*, spontaneous depolarizing postsynaptic potentials recorded at the membrane potentials indicated to the right of each trace. Thee potentials were from the same neuron as in *A*. The postsynaptic potentials recorded in this neuron were always depolarizing at membrane potentials more negative than −50 mV, and could support action potentials (arrow-heads; truncated). *C* and *D*, the amplitude of the postsynaptic potentials in *A* and *B* was plotted against membrane potential in *C* and *D*, respectively. For the plot in *D*, extra data points other than those shown in *B* were also included. A linear regression line was fitted to the plot in *C* to estimate the reversal potential (arrow, −7 mV) of the evoked postsynaptic potential. The continuous line in *D* shows the upper limit of the variation in the spontaneous postsynaptic potential amplitude. The intercept of this line with abscissa (arrow, −32 mV) was taken as the reversal potential.

the IPSPs appeared to vary with the time of day or season. At the peak of the IPSP, input resistance decreased by 48±6% (range 31–67%; $n = 6$, Fig. 3*C*).

Spontaneous IPSPs occurred in all thirty-seven neurons recorded in bicuculline-

free medium (Fig. 1*B*), and their frequency of occurrence was normally high (> 10 IPSPs/s in eighteen out of twenty-five neurons). Similar to the evoked IPSPs, the spontaneous IPSPs rose to their peaks quickly and decayed gradually. For six neurons where 10–30 spontaneous IPSPs (≥ 2 mV) were analysed, the rise-to-peak

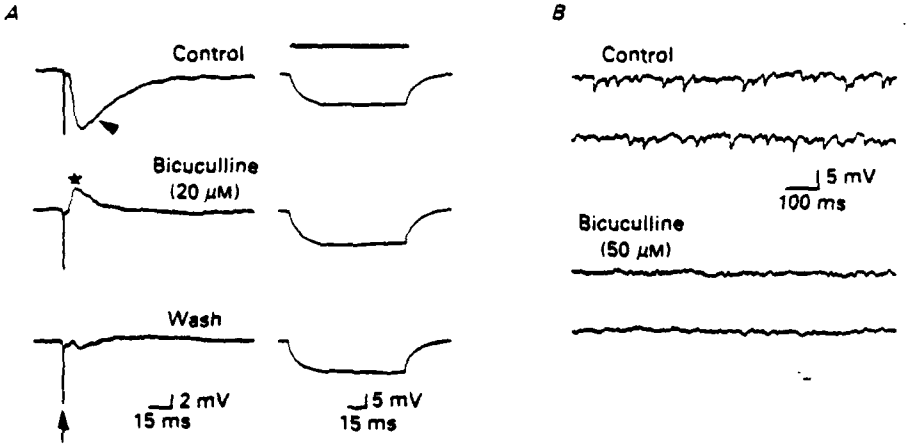

Fig. 5. Blockade of IPSPs by bicuculline. *A*, synaptic responses (left panel) evoked by stimulation (arrow) of the dorsocaudal site and electrotonic potentials (right panel) elicited by injecting a hyperpolarizing current pulse (−50 pA, 100 ms; continuous line) under each experimental condition. Each trace is an average of ten to twenty responses. The blockade by bicuculline (20 μM) of the evoked IPSP (arrow-head) revealed an EPSP (★), which was shunted by the IPSP during control condition. Wash-out of bicuculline resulted in disappearance of the EPSP and reappearance of the IPSP of a smaller magnitude. Note the lack of a slow hyperpolarizing component (i.e. slow IPSP) in any of the experimental conditions. Also, note that bicuculline had no significant effect on the baseline input resistance. *B*, individual traces showing spontaneous IPSPs (upper panel) and the effects of bicuculline (50 μM) on these IPSPs (lower panel). The data in *A* and *B* were obtained from two different neurons, current-clamped to −61 (*A*) and −57 mV (*B*).

time was 7·2 ± 1·0 ms (range 3·9–11·2 ms) and the decay time constant was 14 ± 5 ms (range 8–20 ms).

Dependence of the IPSP reversal potential on Cl^- concentration gradient

When recorded with potassium acetate-filled electrodes, the evoked and spontaneous IPSPs were hyperpolarizing at resting membrane potential (less negative than −70 mV) and depolarizing at membrane potentials more negative than −80 mV (Fig. 3*A* and *B*). The estimated reversal potentials for the evoked and spontaneous IPSPs (Fig. 3*C* and *D*) were −75 ± 2 mV (range −70– −83 mV, $n = 6$) and −74 ± 1 mV (range −70– −77 mV, $n = 4$), respectively. These values are close to the Cl^- equilibrium potential (−75 mV) calculated with the assumption that intracellular Cl^- concentration is 8 mM (McCormick, 1990), suggesting that Cl^- may be the current carrier for the IPSPs.

If the IPSPs are due to an increase in Cl^- conductance, then changes in the Cl^- concentration gradient across the cell membrane should be accompanied by changes in the IPSP reversal potential. By recording with potassium chloride-filled electrodes ($n = 7$), cells were loaded with Cl^-, which altered the Cl^- concentration gradient.

Immediately after impalement of the cells with these electrodes, hyperpolarizing postsynaptic potentials similar to the IPSPs recorded with potassium acetate-filled electrodes were present (data not shown). Over 1–2 min, however, depolarizing postsynaptic potentials (Fig. 4*A* and *B*) gradually replaced the hyperpolarizing

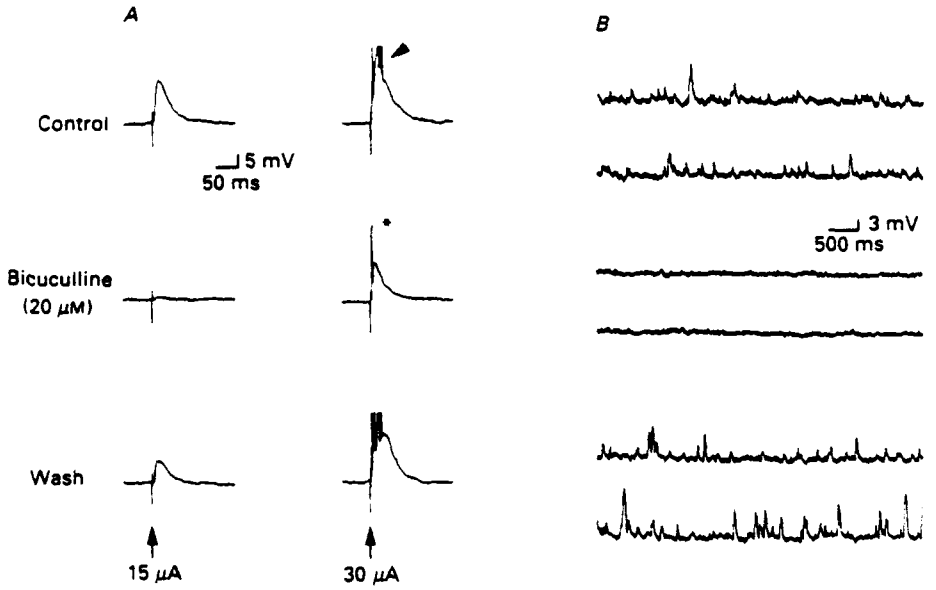

Fig. 6. Blockade of the depolarizing IPSPs (potassium chloride-filled electrode) by bicuculline. *A*, synaptic responses evoked under each experimental condition by stimulation (arrow) of the dorsocaudal site at 15 (left panel) and 30 μA (right panel). Each trace is an average of six responses. Note that, under the control condition, the 30 μA stimulation triggered a burst of action potentials (arrow-head; truncated). Also, note that the response from 15 μA stimulation had very little bicuculline-resistant component while the one from 30 μA stimulation had a significant bicuculline-resistant component, which generated an action potential (asterisk; truncated). *B*, individual traces obtained under each experimental condition from the same neuron in *A*, showing the effects of bicuculline on spontaneous depolarizing postsynaptic potentials. The bicuculline effects both in *A* and *B* were not associated with any significant changes in the baseline input resistance (data not shown). The cell was current-clamped to −77 mV.

postsynaptic potentials, presumably due to gradual increase in the intracellular Cl^- concentration. The estimated reversal potential for the depolarizing postsynaptic potentials was always less negative than spike threshold ($n = 4$ neurons, Fig. 4*C* and *D*). These results further support the hypothesis that Cl^- is the current carrier for the IPSPs in the SCN.

Blockade of IPSPs by bicuculline

Bath-applied bicuculline (10–50 μM) blocked both the evoked ($n = 13$) and spontaneous ($n = 10$) IPSPs recorded with potassium acetate-filled electrodes (Fig. 5). The blockade of the evoked IPSP was accompanied by either an emergence of an EPSP (Fig. 5*A*) or a significant increase in the amplitude of the EPSP that

sometimes preceded the IPSP. The blockade of IPSPs was complete within 10–15 min after the onset of bicuculline application, and was reversed by wash of bicuculline; in neurons where a 15–90 min wash was possible without losing the impalement, a partial to full recovery from the bicuculline effects was clearly

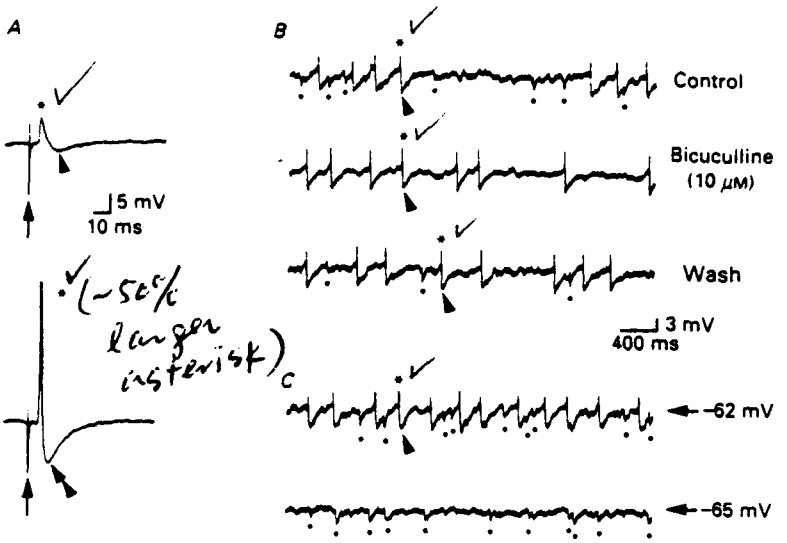

Please replace the asterisk in Fig 7A (top panel), 7B & 7C with ★ (star). Please also replace the asterisk in Fig 7A (bottom panel) with a slightly larger asterisk (~50%)

(~50% larger asterisk)

Fig. 7. Fast prepotential and its associated hyperpolarizing after-potential resembling fast IPSP. *A*, fast prepotential (~~point~~) and hyperpolarizing after-potential (arrow-head) evoked by dorsocaudal stimulation (arrow) in 50 μM bicuculline (upper panel). Occasionally, the fast prepotential could trigger an action potential (asterisk; truncated) (lower panel). The hyperpolarizing after-potential associated with the action potential (double arrow-heads) was of a greater magnitude. The cell was current-clamped to −74 mV. *B*, effect of bicuculline on spontaneous fast prepotentials and their associated *hyperpolarizing after-potentials*. Unlike spontaneously occurring fast IPSPs (●), ~~and~~ fast prepotentials (★) and the hyperpolarizing after-potentials (arrow-head) were not blocked by bicuculline. The cell was current-clamped to −63 mV. *C*, effect of membrane potential change on the fast prepotentials and the hyperpolarizing after-potentials. In bicuculline-free condition, the cell was current-clamped to the membrane potentials indicated to the right of each trace. Unlike fast IPSPs, fast prepotentials and the hyperpolarizing after-potentials were absent at membrane potentials more negative than −65 mV. The traces in *B* and *C* were from the same neuron.

★/

the/

achieved for both evoked (6 out of 6 neurons) and spontaneous (4 out of 6 neurons) IPSPs. The bicuculline effects were not associated with any significant changes in the baseline input resistance of postsynaptic neurons (105 ± 10% of the control, $n = 6$, Fig. 5*A*) and, in most cases, the baseline membrane potential was steady during bicuculline application; in a few cases, however, a depolarization of 5–10 mV followed bicuculline application. The depolarizing postsynaptic potentials recorded with potassium chloride-filled electrodes were also sensitive to bicuculline (20–50 μM). The evoked depolarizing postsynaptic potentials were partially blocked by bicuculline and had a bicuculline-resistant component, which was presumably an EPSP (Fig. 6*A*, $n = 3$). The spontaneous depolarizing postsynaptic potentials were

completely blocked by bicuculline (Fig. 6*B*, $n = 3$). Again, the effects of bicuculline were reversible and not associated with any significant change in baseline membrane potential or input resistance.

The neurons impaled with potassium acetate-filled electrodes in the continued presence of bicuculline (50 μM) in the perfusing medium never exhibited either evoked or spontaneous IPSPs ($n = 11$). In bicuculline, stimulation of the dorsocaudal site (as well as optic nerve) evoked only an EPSP, an action potential and/or a fast prepotential. The evoked fast prepotentials were occasionally followed by hyperpolarizing after-potentials with a time course that resembled the fast IPSPs (Fig. 7*A*). Hyperpolarizing after-potentials also followed the spontaneously occurring fast prepotentials observed in three neurons (Fig. 7*B* and *C*). Although bicuculline did not affect these potentials (Fig. 7*B*), hyperpolarization of the neuron beyond a certain point completely arrested the fast prepotentials and the associated hyperpolarizing after-potentials (Fig. 7*C*), indicating a non-synaptic nature of their origin. In the present study, we did not detect any slow IPSPs.

DISCUSSION

$GABA_A$ receptors mediate the IPSPs in the SCN

Numerous anatomical studies have suggested a neurotransmitter role for GABA in the SCN. The results of the present study provide physiological evidence for such a role. In addition, our data suggest that $GABA_A$ receptors mediate inhibitory transmission in the SCN. This conclusion is consistent with the one drawn by Thomson & West (1990) from their preliminary results that ionophoretically applied bicuculline blocked spontaneous IPSPs in the SCN. Also, the conclusion is supported by recent reports by Liou *et al.* (1990) and Mason *et al.* (1991) that bicuculline antagonized the depression of neuronal firing in the SCN caused by exogenously applied GABA, $GABA_A$ receptor agonist muscimol and/or benzodiazepines. The current findings that bicuculline-sensitive spontaneous IPSPs were present in all the neurons recorded in normal medium and that stimulation of a site dorsocaudal to the SCN also evoked bicuculline-sensitive IPSPs from most of these neurons are in line with the observation made by Decavel & van den Pol (1990) in their immunocytochemical study that all the SCN neurons examined were innervated by GABA-positive axons. Taken together, these results strongly support the hypothesis that GABA, acting on $GABA_A$ receptors, is the dominant inhibitory neurotransmitter in the SCN.

Type of IPSPs in the SCN

Both evoked and spontaneous IPSPs had a fast rising phase, and their decay could be fitted with a single time constant in most cases. This observation, coupled with the findings that the IPSPs were associated with a postsynaptic increase in Cl^- conductance and completely blocked by the $GABA_A$ receptor antagonist bicuculline, strongly suggests that the IPSPs were of the fast type, and not mixed with slow IPSPs (see below). The IPSPs observed in our study were similar to those recorded from supraoptic nucleus neurons in hypothalamic explants (Randle *et al.* 1986), in terms of the time course, dependence on Cl^- conductance and sensitivity to

bicuculline. $GABA_A$ receptors may thus mediate fast inhibitory synaptic transmission throughout the hypothalamus.

Lack of slow IPSPs in the SCN

$GABA_B$ receptor-mediated, slow IPSPs have been documented in many brain regions (Dutar & Nicoll, 1988; Hasuo & Gallagher, 1988; Soltesz, Haby, Leresche & Crunelli, 1988; Karlsson & Olpe, 1989; McCormick, 1989). However, the results of our study do not provide support for the presence of slow IPSPs in the SCN, because, as mentioned above, the blockade of IPSPs by bicuculline was complete without leaving any obvious bicuculline-resistant, slow hyperpolarizing component. The bicuculline-resistant hyperpolarizing after-potentials that followed fast prepotentials were fast in time course, and appeared to be non-synaptic events (i.e. not slow IPSPs). The lack of any significant and consistent effects of bicuculline at the concentrations used here (10–50 μM) on the passive membrane properties of postsynaptic neurons suggests that the blockade of IPSPs by bicuculline was specific. Comparable concentrations of bicuculline were reported to block the fast IPSPs recorded from the supraoptic (Randle *et al.* 1986) and paraventricular (Tasker & Dudek, 1988) nuclei in the hypothalamus. In the dorsal lateral geniculate nucleus of the thalamus, 50 μM bicuculline was shown to block fast, but not slow, IPSPs (Soltesz, Lightowler, Leresche & Crunelli, 1989). This suggests that bicuculline at concentrations $\leqslant 50\ \mu$M is selective for $GABA_A$ receptors.

Several explanations need to be considered for the lack of slow IPSPs in these recordings. The inability to detect slow IPSPs might have been due to the low signal-to-noise ratio associated with the high resistance sharp electrodes used. However, when slow IPSPs were present in other neurons, they could be recorded with similar high resistance electrodes. The employed stimulus intensity (up to 1 mA) may not have been sufficient to evoke slow IPSPs (Dutar & Nicoll, 1988). It is also possible that the perfusion rate was so high that effective concentrations of GABA for $GABA_B$ receptor activation (i.e. for slow IPSP) could not be achieved with the electrical stimulation. These explanations seem unlikely, because lower intensity stimulation ($< 0{\cdot}1$ mA) at a similar perfusion rate could evoke slow IPSPs in slices from other parts of the brain (Y. I. Kim & F. E. Dudek, unpublished observation). The lack of slow IPSPs might be due to the particular site of electrical stimulation (i.e. due to limited stimulation of the afferents that would evoke only fast IPSPs) or to the fact that the electrical stimulation of the presynaptic sites was not equivalent to physiological synaptic activation.

The absence of slow IPSPs in the SCN could be viewed as evidence against the existence of postsynaptic $GABA_B$ receptors. However, it would not exclude the possibility that functional $GABA_B$ receptors exist at other locations, such as extrasynaptic sites or serotonergic axonal elements (François-Bellan, Héry, Faudon & Héry, 1988; Bosler, 1989). It might be through these receptors that the $GABA_B$ receptor agonist, baclofen, depressed the neuronal discharge in the rat SCN (Liou *et al.* 1990) and phase-advanced the hamster circadian rhythm of locomotor activity (Smith *et al.* 1990).

Does GABAergic input arise locally?

The present data indicate that afferents other than the optic nerve are the source of inhibitory GABAergic input to SCN neurons. The techniques employed in this study, however, do not allow determination of whether the input arises locally from GABAergic cells in the SCN (Tappaz *et al.* 1977; Card & Moore, 1984; van den Pol & Tsujimoto, 1985; van den Pol, 1986; Okamura *et al.* 1989) or from cells outside the SCN. That the evoked IPSPs had a virtually constant onset latency and followed stimuli presented at 10 or 20 Hz only suggests that the GABAergic input is monosynaptic. Further studies with other techniques, such as glutamate microdrop application (Christian & Dudek, 1988), may provide more direct answers to these questions.

Role of GABAergic input to SCN neurons

Several lines of research have suggested that GABA is an important neurotransmitter in circadian time keeping. A series of studies by Ralph & Menaker (1985, 1986 & 1980) has provided evidence that light-induced phase shifts of the circadian locomotor rhythm of hamsters involve GABAergic regulation. Conceivably, the SCN neurons receiving optic nerve input (i.e. light) might be an important site for the GABAergic regulation. The direct GABAergic innervation of the retinorecipient neurons demonstrated in the present study supports this idea. Nevertheless, the exact functional significance of the GABAergic transmission in SCN neurons remains to be determined. As argued by Smith *et al.* (1990), the GABAergic transmission in the SCN may not be normally involved in circadian timing system.

The finding that spontaneous IPSPs occurred frequently in most of the neurons studied differs from the data of Wheal & Thomson (1984) that spontaneous synaptic activity was absent in SCN neurons, but agrees with the more recent report by Thomson & West (1990) that spontaneous IPSPs occurred frequently. The spontaneous IPSPs occurring at high rates suggest that significant ongoing synaptic inhibition is present in the SCN maintained *in vitro*. This pronounced synaptic inhibition may also exist in *in vivo* conditions and contribute significantly in controlling the baseline membrane potential of postsynaptic neurons. The depolarization (5–10 mV) that followed the bicuculline blockade of spontaneous IPSPs in some neurons supports this hypothesis.

In summary, fast IPSPs in SCN neurons are associated with a postsynaptic increase in Cl^- conductance, and are blocked by bicuculline. All the SCN neurons examined, including those identified as receiving excitatory optic nerve input, had fast IPSPs; this suggests that $GABA_A$ receptor-mediated, fast inhibitory synaptic input is present in most, if not all, SCN neurons.

We are grateful to Dr D. Birt for developing neurophysiological data analysis routines, to T. Valdes and D. Weber or technical assistance, and to J. Wang for secretarial help. This research was supported by grants from the United States Air Force Office of Scientific Research (87-0361 and 90-0056) to F.E.D.

REFERENCES

BOSLER, O. (1989). Ultrastructural relationships of serotonin and GABA terminals in the rat suprachiasmatic nucleus. Evidence for a close interconnection between the two afferent systems. *Journal of Neurocytology* **18**, 105–113.

CARD, J. P. & MOORE, R. Y. (1984). The suprachiasmatic nucleus of the golden hamster: Immunohistochemical analysis of cell and fiber distribution. *Neuroscience* **13**, 415–431.

CHRISTIAN, E. P. & DUDEK, F. E. (1988). Electrophysiological evidence from glutamate microapplications of local excitatory circuits in the CA1 area of rat hippocampal slices. *Journal of Neurophysiology* **59**, 110–123.

DECAVEL, C. & VAN DEN POL, A. N. (1990). GABA: A dominant neurotransmitter in the hypothalamus. *Journal of Comparative Neurology* **302**, 1019–1037.

DUTAR, P. & NICOLL, R. A. (1988). A physiological role for $GABA_B$ receptors in the central nervous system. *Nature* **332**, 156–158.

~~FRANÇOIS-BELLAN~~, A. M., HÉRY, M., FAUDON, M. & HÉRY, F. (1988). Evidence for GABA control of serotonin metabolism in the rat suprachiasmatic area. *Neurochemistry International* **13**, 455–462.

HASUO, H. & GALLAGHER, J. P. (1988). Comparison of antagonism by phaclofen of baclofen induced hyperpolarizations and synaptically mediated late hyperpolarizing potentials recorded from rat dorsolateral septal neurons. *Neuroscience Letters* **86**, 77–81.

HOFFMAN, N. W., KIM, Y. I., GORSKI, R. A. & DUDEK, F. E. (1990). Electrical and morphological characteristics of neurons in the region of the male sexually dimorphic nucleus (SDN) of the rat medial preoptic area (MPOA). *Society for Neuroscience Abstracts* **16**, 574.

JOHNSON, R. F., SMALE, L., MOORE, R. Y. & MORIN, L. P. (1988). Lateral geniculate lesions block circadian phase-shift responses to a benzodiazepine. *Proceedings of the National Academy of Sciences of the USA* **85**, 5301–5304.

KARLSSON, G. & OLPE, H.-R. (1989). Late inhibitory postsynaptic potentials in rat prefrontal cortex may be mediated by $GABA_B$ receptors. *Experientia* **45**, 157–158.

KIM, Y. I. & DUDEK, F. E. (1990). Suprachiasmatic nucleus (SCN) neurons receiving retinal inputs are under the control of gamma-aminobutyric acid (GABA). *Society for Neuroscience Abstracts* **16**, 574.

KIM, Y. I. & DUDEK, F. E. (1991). Intracellular electrophysiological study of suprachiasmatic nucleus neurons in rodents: Excitatory synaptic mechanisms. *Journal of Physiology* **444**, 269–287.

LIOU, S. Y. & ALBERS, H. E. (1990). Single unit response of neurons within the hamster suprachiasmatic nucleus to GABA and low chloride perfusate during day and night. *Brain Research Bulletin* **25**, 93–98.

LIOU, S. Y., SHIBATA, S., ALBERS, H. E. & UEKI, S. (1990). Effects of GABA and anxiolytics on the single unit discharge of suprachiasmatic neurons in rat hypothalamic slices. *Brain Research Bulletin* **25**, 103–107.

MCCORMICK, D. A. (1989). GABA as an inhibitory neurotransmitter in human cerebral cortex. *Journal of Neurophysiology* **62**, 1018–1027.

MCCORMICK, D. A. (1990). Membrane properties and neurotransmitter actions. In *The Synaptic Organization of the Brain*, ed. SHEPHERD, G. M., pp. 32–66. University Press, Oxford.

MASON, R., BIELLO, S. M. & HARRINGTON, M. E. (1991). The effects of GABA and benzodiazepines on neurones in the suprachiasmatic nucleus (SCN) of Syrian hamsters. *Brain Research* **552**, 53–57.

MEIJER, J. H. & RIETVELD, W. J. (1989). Neurophysiology of the suprachiasmatic circadian pacemaker in rodents. *Physiological Reviews* **69**, 671–707.

MOORE, R. Y. (1983). Organization and function of a central nervous system circadian oscillator: the suprachiasmatic hypothalamic nucleus. *FASEB Journal* **42**, 2783–2789.

OKAMURA, H., BÉROD, A., JULIEN, J.-F., GEFFARD, M., KITAHAMA, K., MALLET, J. & BOBILLIER, P. (1989). Demonstration of GABAergic cell bodies in the suprachiasmatic nucleus: in situ hybridization of glutamic acid decarboxylase (GAD) mRNA and immunocytochemistry of GAD and GABA. *Neuroscience Letters* **102**, 131–136.

RALL, W. (1969). Time constants and electrotonic length of membrane cylinders and neurons. *Biophysical Journal* **9**, 1483–1508.

FRANÇOIS-BELLAN

Please move the reference before McCormick (1989).

RALPH, M. R. & MENAKER, M. (1985). Bicuculline blocks circadian phase delays but not advances. *Brain Research* **325**, 362–365.

RALPH, M. R. & MENAKER, M. (1986). Effects of diazepam on circadian phase advances and delays. *Brain Research* **372**, 405–408.

RALPH, M. R. & MENAKER, M. (1989). GABA regulation of circadian responses to light. I. Involvement of $GABA_A$-benzodiazepine and $GABA_B$ receptors. *Journal of Neuroscience* **9**, 2858–2865.

RANDLE, J. C. R., BOCRQUE, C. W. & RENAUD, L. P. (1986). Characterization of spontaneous and evoked inhibitory postsynaptic potentials in rat supraoptic neurosecretory neurons in vitro. *Journal of Neurophysiology* **56**, 1703–1717.

SHIBATA, S., LIOU, S. Y. & UEKI, S. (1983). Different effects of amino acids, acetylcholine and monoamines on neuronal activity of suprachiasmatic nucleus in rat pups and adults. *Neuroscience Letters* **39**, 187–192.

SMITH, R. D., INOUYE, S. T. & TUREK, F. W. (1989). Central administration of muscimol phase-shifts the mammalian circadian clock. *Journal of Comparative Physiology A* **164**, 805–814.

SMITH, R. D., TUREK, F. W. & SLATER, N. T. (1990). Bicuculline and picrotoxin block phase advances induced by GABA agonists in the circadian rhythm of locomotor activity in the golden hamster by phaclofen-insensitive mechanism. *Brain Research* **530**, 275–282.

SOLTESZ, I., HABY, M., LERESCHE, N. & CRUNELLI, V. (1988). The $GABA_B$ antagonist phaclofen inhibits the late K^+-dependent IPSP in cat and rat thalamic and hippocampal neurones. *Brain Research* **448**, 351–354.

SOLTESZ, I., LIGHTOWLER, S., LERESCHE, N. & CRUNELLI, V. (1989). Optic tract stimulation evokes $GABA_A$ but not $GABA_B$ IPSPs in the rat ventral lateral geniculate nucleus. *Brain Research* **479**, 49–55.

TAKAHASHI, J. S. & ZATZ, M. (1982). Regulation of circadian rhythmicity. *Science* **217**, 1104–1111.

TAPPAZ, M. L., BROWNSTEIN, M. J. & KOPIN, I. J. (1977). Glutamate decarboxylase (GAD) and gamma-aminobutyric acid (GABA) in discrete nuclei of hypothalamus and substantia nigra. *Brain Research* **125**, 109–121.

TASKER, J. G. & DUDEK, F. E. (1988). Local circuit interactions between neurons in the region of the rat paraventricular nucleus. *Society for Neuroscience Abstracts* **14**, 1178.

THOMSON, A. M. & WEST, D. C. (1990). Factors affecting slow regular firing in the suprachiasmatic nucleus in vitro. *Journal of Biological Rhythms* **5**, 59–75.

TUREK, F. W (1985). Circadian rhythms in mammals. *Annual Review of Physiology* **47**, 49–64.

TUREK, F. W. & VAN REETH, O. (1988). Altering the mammalian circadian clock with the short-acting benzodiazepine, triazolam. *Trends in Neurosciences* **11**, 535–541.

VAN DEL POL, A. N. (1986). Gamma-aminobutyrate, gastrin releasing peptide, serotonin, somatostatin, and vasopressin: Ultrastructural immunocytochemical localization in presynaptic axons in the suprachiasmatic nucleus. *Neuroscience* **17**, 643–659.

VAN DEN POL, A. N. & TSUJIMOTO, K. L. (1985). Neurotransmitters of the hypothalamic suprachiasmatic nucleus: Immunocytochemical analysis of 25 neuronal antigens. *Neuroscience* **15**, 1049–1086.

WHEAL, H. V. & THOMSON, A. M. (1984). The electrical properties of neurones of the rat suprachiasmatic nucleus recorded intracellularly in vitro. *Neuroscience* **13**, 97–104.

(final copy)

MEMBRANE PROPERTIES OF RAT SUPRACHIASMATIC NUCLEUS NEURONS RECEIVING OPTIC NERVE INPUT

Yang In Kim

and

F. Edward Dudek

Mental Retardation Research Center and
Brain Research Institute,
UCLA School of Medicine
760 Westwood Plaza, NPI 58-258
Los Angeles, CA 90024
U.S.A.

in press
J. Physiol., London

Running title: Membrane properties of SCN neurons

Address for correspondence:

F. Edward Dudek, Ph.D.
Department of Anatomy & Neurobiology,
Colorado State University
Fort Collins, CO 80523
U.S.A.

SUMMARY

1. The electrophysiological properties of suprachiasmatic nucleus (SCN) neurons (n=33) receiving optic nerve input were studied with intracellular recordings in rat hypothalamic slices maintained *in vitro*. Our major goal was to provide baseline data concerning the intrinsic membrane properties of these neurons and to test the hypothesis that the neurons are homogeneous electrophysiologically.

2. Action potentials were short in duration and followed by a pronounced hyperpolarizing afterpotential. Spike amplitude (58.2 ± 1.1 mV, mean ± S.E.M.; measured from threshold), spike duration (0.83 ± 0.03 ms; measured at half amplitude) and hyperpolarizing afterpotential amplitude (23.9 ± 1.0 mV; measured from threshold) appeared unimodally distributed and did not co-vary.

3. Intracellular injection of depolarizing current pulses evoked spike trains, and spike inactivation, spike broadening and frequency accommodation were always present. An afterhyperpolarization followed the spike train in all but one neuron.

4. Membrane time constant ranged from 7.5 to 21.1 ms (11.4 ± 0.7 ms, n=27), and its distribution appeared to be unimodal with the peak at ~10 ms. Input resistance ranged from 105 to 626 MΩ (301 ± 23 MΩ, n=33); the distribution also appeared unimodal with its peak at ~250 MΩ.

5. A subpopulation (16 of 33, 48%) of the neurons exhibited slight (6-29%) time-dependent inward rectification in their voltage responses to hyperpolarizing current injection. Of the neurons lacking the time-dependent rectification, some (n=5) exhibited time-independent inward rectification of 6-20% and others showed no (or <3%) such rectification. The degree of inward rectification was

correlated with neuronal excitability ($r=0.60$, $p<0.002$; assessed by measuring the steepness of the primary slope of the frequency-current plot) and with the spontaneous firing rate ($r=0.49$, $p<0.007$). Furthermore, the neurons with >6% inward rectification (neurons with time-dependent and -independent rectification were combined) were more excitable [362 ± 43 Hz/nA (n=15) vs. 221 ± 37 Hz/nA (n=9), $p<0.05$] and had a higher spontaneous firing rate [11.1 ± 1.9 Hz (n=19) vs. 3.9 ± 1.5 Hz (n=11), $p<0.02$] than the neurons with no or negligible (i.e., <3%) inward rectification. The two groups, however, were not significantly different in membrane time constant and input resistance.

6. When adequately hyperpolarized, 12 of 17 (71%) neurons generated small low-threshold spike (LTS) potentials in response to depolarizing current pulses. The neurons with LTS potentials were not significantly different from other neurons (n=5, 29%) in spontaneous firing rate, excitability, membrane time constant and input resistance. The capacity to generate LTS potentials was not related to the presence of inward rectification.

7. Spontaneous firing (up to 34 Hz) was present in all but 6 neurons. In general, neurons with a firing rate >6 Hz (71%) had a regular firing pattern, whereas neurons that fired at <4 Hz (25%) had an irregular firing pattern. Altering the firing rate with intracellular current injection changed the firing pattern. Therefore, depending on the firing rate, a given neuron could show either a regular or an irregular firing pattern.

8. These results suggest that the retinorecipient neurons in the SCN do not form a completely homogeneous group nor clearly distinct classes in terms of intrinsic membrane properties. Furthermore, the data suggest inward rectification may be related to enhanced excitability and firing rate.

INTRODUCTION

Several lines of evidence suggest that, in mammals, the suprachiasmatic nucleus (SCN) of the hypothalamus contains the biological clock responsible for circadian rhythms (for review, see Takahashi & Zatz, 1982; Moore, 1983; Turek, 1985; Meijer & Rietveld, 1989). Entrainment of these rhythms to the daily light-dark cycle is an important process that allows maximal adaptation of an organism to its external environment. In mammals, the photic entrainment is mediated exclusively through the photoreceptors in the retina (Richter, 1965; Nelson & Zucker, 1981). The photic information delivered to the SCN via the retinohypothalamic tract, a direct projection from the retina to the SCN (Hendrickson, Wagoner & Cowan, 1972; Moore & Lenn, 1972), is apparently sufficient, if not essential, to maintain entrainment of circadian rhythms (Rusak & Boulos, 1981; Moore, 1983; Albers, Liou, Ferris, Stopa & Zoeller, 1991).

Realization of the potentially critical role of the retinohypothalamic pathway in photic entrainment has stimulated research concerning the SCN neurons that receive direct retinal input. Immunohistochemical evidence indicates that a subpopulation of these neurons contain vasoactive intestinal polypeptide (Ibata, Takahashi, Okamura, Kawakami, Terubayashi, Kubo & Yanaihara, 1989), and electrophysiological results strongly suggest that excitatory amino acid receptors mediate the fast retinal input to these neurons (Shibata, Liou & Ueki, 1986; Cahill & Menaker, 1987, 1989b; Kim & Dudek, 1991a). Limited information is available concerning intrinsic membrane properties of retinorecipient SCN neurons. Although Wheal & Thomson (1984) described several intrinsic membrane properties of SCN neurons, including the current-voltage relation, they did not determine whether the neurons received synaptic input from the optic nerve. They also did not evaluate quantitatively whether the neurons were homogeneous electrophysiologically. More recently, Sugimori, Shibata & Oomura (1986) reported that SCN neurons receiving synaptic input from the

optic nerve expressed low-threshold Ca^{2+} spike potentials and time-dependent inward rectification. However, they did not report how many cells were recorded for their study and what proportion of the cells had these intrinsic properties. Other studies with extracellular recordings from single SCN neurons have reported differences in firing pattern across the retinorecipient cells (Shibata, Oomura, Hattori & Kita, 1984; Cahill & Menaker, 1989a), which suggests that these neurons have heterogeneous intrinsic membrane properties.

In the present study, we aimed to provide baseline data concerning the intrinsic membrane properties of retinorecipient cells in rat SCN and to test the hypothesis that the neurons form an electrophysiologically homogeneous population. We also sought to determine if any intrinsic membrane properties were related to neuronal excitability or spontaneous firing rate. The data from these intracellular electrophysiological experiments suggest that the neurons are relatively homogeneous in many intrinsic membrane properties; however, they are also heterogeneous in some properties, such as inward rectification, which might be related to neuronal firing. A preliminary account of these results has been published (Kim & Dudek, 1991b).

METHODS

Animals

Male Sprague-Dawley rats (n=23, 120-350 g) purchased from Charles River company (USA) were used for this study. Prior to electrophysiological experiments, the rats were housed in a temperature-controlled room (22-23 ^{o}C) under a 12-h light/ 12-h dark cycle (light on at 0700 h; pacific standard time) for at least 1 wk (mostly >2 wk).

Hypothalamic slices

The methods employed for the preparation and maintenance of the slices were the same as those described earlier (Kim & Dudek, 1991a). In brief, a rat was decapitated with a guillotine under sodium-pentobarbitone (I.P., 100 mg/kg) anesthesia induced after 0700 h (i.e., after light on), and the brain was removed and submerged in ice-cold physiological saline (composition in mM: 124 NaCl, 1.4 NaH_2PO_4, 3 KCl, 2.4 $CaCl_2$, 26 $NaHCO_3$, 1.3 $MgSO_4$, 11 glucose). After about 1-min chilling, the brain was trimmed to a block containing the entire hypothalamus and optic nerves. Two 500-μm thick parasagittal slices containing the optic nerve and SCN were cut from the block with a vibrating microtome (Campden Instruments, UK). The slices were quickly transferred to an interface-type recording chamber and perfused with physiological saline (32-35 ^{o}C) at 0.7-1.0 ml/min. A humidified mixture of 95% O_2 and 5% CO_2 was blown over the slice for the entire experimental period. Electrophysiological recordings started 2 h after the slice preparation.

Intracellular recordings and electrical stimulation

Intracellular recordings were obtained with micropipettes filled with 2-4 M potassium acetate (90-360 MΩ). Voltage recordings in current-clamp mode were performed with a high-impedance amplifier having a bridge circuit (Axoclamp-2A, Axon Instruments, USA). A bipolar metal electrode (90% platinum-10% iridium) was placed in the cut end of the optic nerve for stimulation (≤0.8 mA, 0.5-ms monophasic pulse).

RESULTS

The results presented in this paper were from 33 SCN neurons that responded to optic nerve stimulation with an excitatory postsynaptic potential (Kim & Dudek, 1991a). Stable recordings for >10 min (up to 6 h) were obtained between 1100 h and 2100 h. None of the intrinsic membrane properties examined in this study appeared to be a function of the time of recording.

Action potentials

The shape and characteristics of action potentials were similar across neurons. Figure 1A illustrates a typical action potential. The spike amplitude (measured from threshold) was in the range of 50-65 mV (58.2 ± 1.1 mV, mean ± S.E.M.), and the spike duration (measured at half amplitude) was relatively short (0.83 ± 0.03 ms). A pronounced (normally >20 mV) hyperpolarizing afterpotential (23.9 ± 1.0 mV; measured from threshold) usually followed each spike. Spike amplitude, spike duration and hyperpolarizing afterpotential amplitude appeared unimodally distributed (Fig. 1B, C & D) and did not co-vary (data not shown).

Figure 1 around here

Spike train and afterhyperpolarization

In every neuron examined, intracellular injection of depolarizing current pulses of sufficient intensity elicited spike trains. Spike inactivation, spike broadening and frequency accommodation

(Fig. 2) were always present, although there was some variability across the neurons. In all but one

---

Figure 2 around here

---

neuron, an afterhyperpolarization followed each of the evoked spike trains. The amplitude of the afterhyperpolarization was a function of current intensity (Fig. 3A), and its polarity reversed at around -85 to -90 mV (i.e., near the K^+ equilibrium potential) (Fig. 3B). The decay of the afterhyperpolarization lasted up to 1 s, and usually could be fitted well with a single exponential.

Figure 3 around here

Membrane time constant and input resistance

The membrane time constant, which was estimated from the averaged electrotonic potential elicited by a small hyperpolarizing current pulse delivered in the linear portion of the current-voltage (I-V) plot, ranged from 7.5 to 21.1 ms (11.4 ± 0.7 ms, n=27). The distribution of the membrane time constant appeared to be unimodal with the peak at ~10 ms (Fig. 4A).

The input resistance, which was calculated from the slope of the linear portion of the I-V plot, was in the range of 105-626 MΩ (301 ± 23 MΩ, n=33). Its distribution (Fig. 4B) appeared to be unimodal with the peak at ~250 MΩ.

Figure 4 around here

Inward rectification

In 16 of the 33 neurons (48%), time-dependent inward rectification was observed in their voltage responses to hyperpolarizing current injection (Fig. 5). The degree of the time-dependent rectification across the neurons ranged from 6 to 29% (mostly 12-29%). The I-V plots for the neurons lacking the time-dependent rectification revealed that five of these neurons had time-independent inward rectification of 6-20%; for other neurons this rectification was <3% or absent. The degree of rectification was calculated by comparing the maximum and minimum apparent input resistances; the maximum was estimated from a -9 to -22 mV electrotonic potential in the linear portion of the I-V plot, while the minimum was from a potential of -36 to -63 mV falling in the most non-linear portion of the I-V plot. The electrotonic potentials were evoked from a baseline membrane potential of -56 to -77 mV. The baseline potential was often adjusted with continuous hyperpolarizing current to prevent spontaneous spiking. In silent cells (n=6), the potential was equal to the resting potential.

Figure 5 around here

The degree of inward rectification was correlated with the neuronal excitability [r=0.60, p<0.002; quantified by measuring the steepness of the primary slope of the frequency-current plot (Fig. 6A)] and with the spontaneous firing rate (r=0.49, p<0.007). Furthermore, the neurons with >6% inward rectification (neurons with time-dependent and -independent rectification were combined), compared to those with no or negligible (i.e., <3%) inward rectification, were more excitable [362 ± 43 Hz/nA (n=15) vs. 221 ± 37 Hz/nA (n=9), p<0.05, Fig. 6] and had a higher spontaneous firing rate [11.1 ± 1.9 Hz (n=19) vs. 3.9 ± 1.5 Hz (n=11), p<0.02, Fig. 7]. Between the

two groups, however, membrane time constant [11.8 ± 0.9 ms (n=15) vs. 10.9 ± 1.0 ms (n=12), p>0.5] and input resistance [331 ± 29 MΩ (n=21) vs. 248 ± 32 MΩ (n=12), p>0.05] were not significantly different.

Figure 6 & 7 around here

LTS potentials

Low-threshold spike (LTS) potentials were detected in 12 of 17 (71%) neurons. These potentials were evoked only when the cell was hyperpolarized adequately (Fig. 8A) and only by depolarizing potentials of sufficient amplitude (Fig. 8B). The LTS potentials were small; in general, they barely supported single action potentials (Fig. 8A), and only rarely 2-3 action potentials (Fig. 8B). Spontaneous firing rate [8.9 ± 2.8 Hz (n=12) vs. 9.3 ± 3.3 Hz (n=5), p>0.8], excitability [384 ± 71 Hz/nA (n=9) vs. 208 ± 44 Hz/nA (n=5), p>0.1], membrane time constant [12.8 ± 1.4 ms (n=11) vs. 9.4 ± 0.7 ms (n=5), p>0.1] and input resistance [327 ± 42 MΩ (n=12) vs. 240 ± 46 MΩ (n=5), p>0.2] were not significantly different between the groups of neurons that did and did not generate the LTS potentials. The capacity of a given neuron to generate an LTS potential was not related to the presence of inward rectification; 7 of 12 neurons that generated LTS potentials had inward rectification, and 2 of 5 that did not generate them had inward rectification (χ^2=0.48, p>0.25).

Figure 8 around here

Firing rate and pattern

All of the neurons except 6 were spontaneously active. In 71% of the cells, the spontaneous firing rate was >6 Hz (up to 34 Hz), and in 25% it was <4 Hz. In general, the pattern of >6-Hz firing was quite regular, whereas the pattern of <4-Hz firing was irregular (Fig. 9A). An oscillatory or bursting pattern of firing was never detected. Both the firing pattern (i.e., regular vs. irregular) and rate could be altered by intracellular current injection. Figure 9B illustrates that a given neuron could have both regular and irregular firing patterns, and the expression of these patterns depended on the firing rate.

Figure 9 around here

DISCUSSION

Homogeneity vs. heterogeneity of membrane properties

One of the major goals of the present study was to test the hypothesis that the SCN neurons receiving optic nerve input are electrophysiologically homogeneous. These neurons did appear relatively homogeneous in terms of action potential waveform, evoked spike train and its associated properties, membrane time constant and input resistance. With respect to some other intrinsic membrane properties (i.e., inward rectification and LTS potentials), however, the neurons appeared heterogeneous. The heterogeneity could reflect different physiological states manifested as a function of circadian time. This notion, however, is not consistent with the finding that different neurons recorded at the same time of day were heterogeneous, and no apparent relation was detected between a given membrane property and the time of recording. Taken together, our results do not support the hypothesis that the SCN neurons form a homogeneous group electrophysiologically. Neither do they support the idea that the neurons can be classified into a few distinct cell types, such as the cells in the paraventricular nucleus (Hoffman, Tasker & Dudek, 1991; Tasker & Dudek, 1991) or ventromedial hypothalamus (Minami, Oomura & Sugimori, 1986a & 1986b). Perhaps, the neuronal population consists of several subgroups, and the inherent variability in this type of recording obscured the differences.

Extracellular single-unit studies have reported that the retinorecipient (as well as other) cells in the SCN exhibit different firing patterns (Shibata et al., 1984; Cahill & Menaker, 1989a), which may be interpreted to mean that the cells have heterogeneous intrinsic membrane properties. The present results suggest that the firing pattern of a given retinorecipient neuron is not an absolute neuronal signature, but more or less a function of firing rate. The different firing patterns of

retinorecipient cells could be due to the membrane potential-dependent expression of different subsets of intrinsic membrane properties. More systematic studies considering firing rate might be needed to elucidate the potential link between firing patterns and particular intrinsic membrane properties.

Action potentials

The action potentials recorded in this study looked similar to those of SCN neurons recorded in coronal slices by Wheal & Thomson (1984), except that the action potentials of our neurons had significantly smaller amplitude than theirs (58.2 mV vs. 83.8 mV, $p<0.001$). This is not likely due to poorer impalements, since our neurons had significantly higher input resistance (301 MΩ vs. 147 MΩ, $p<0.001$) and longer membrane time constant (11.4 ms vs. 6.7 ms, $p<0.001$). The smaller spike amplitude could be related to the observation that our neurons were more depolarized; most of our neurons were spontaneously active and had an estimated resting membrane potential that was less negative than -50 mV, whereas their neurons were normally silent and had an average resting potential of -59 mV. Alternatively, it may be due to the difference in rat strain (Sprague-Dawley vs. Wistar) and/or experimental condition such as the time of recording. Lastly, the two studies may have dealt with different neuronal populations (cells with optic nerve input vs. cells without the input).

Spike train and post-train afterhyperpolarization

The SCN neurons receiving optic nerve input had similar spike train properties (i.e., spike inactivation, spike broadening & frequency accommodation) to those SCN neurons recorded in coronal slices (Wheal & Thomson, 1984; their synaptic connection with optic nerve was unknown).

In addition, almost all the neurons that did not respond to optic nerve stimulation had similar spike train properties (unpublished observation); however, the lack of response could be due to the possible destruction during slice preparation of the afferent from the optic nerve. These results suggest that the spike train properties are not limited only to the neurons that receive optic nerve input, instead, they may be common properties across all SCN neurons.

The post-train afterhyperpolarizations observed in this study were very similar to those described by Wheal & Thomson (1984) for the SCN neurons recorded in coronal slices. Also, they resembled the post-train afterhyperpolarizations observed in other hypothalamic regions. The afterhyperpolarizations in these sites appear to be caused by Ca^{2+}-dependent (Andrew & Dudek, 1984; Bourque, Randle & Renaud, 1985; Minami et al, 1986b; Bourque & Brown, 1987) and voltage-dependent K^+ conductances (Minami et al., 1986b). The Ca^{2+}-dependent K^+ conductance in magnocellular supraoptic neurons has been suggested to contribute to frequency adaptation (Andrew & Dudek, 1984; Bourque et al., 1985) and the long-term (seconds) spike inhibition following high-frequency firing that occurs in a variety of physiological contexts (Andrew & Dudek, 1984). The post-train afterhyperpolarizations in retinorecipient cells may have similar ionic mechanisms and functions. The estimated reversal potential of the post-train afterhyperpolarization in this study suggests that K^+ is the underlying current carrier.

Inward rectification

A significant proportion of the rat SCN neurons recorded in this study had time-dependent inward rectification, and some had time-independent rectification. Although not as strong as that seen in other central nervous system neurons, such as cerebellar Purkinje cells (Llinás & Sugimori, 1980a & 1980b), the inward rectification in SCN neurons was clearly detectable. Sugimori et al.

(1986) reported that guinea-pig SCN neurons had time-dependent inward rectification, and the degree of rectification was comparable to that in the present study. On the other hand, other investigators reported that rat SCN neurons recorded in coronal slices were usually linear in their I-V relations (Wheal & Thomson, 1984) and had little or no inward rectification in the hyperpolarizing direction (Thomson & West, 1990). The apparent inconsistency of these reports with our results may be explained by different methods of data analysis (e.g., degree of quantification of results). Alternatively, the discrepancy might be due to the difference in rat strain, experimental condition or neuronal population.

Inward rectification has been observed in a variety of cells, and different functions have been ascribed to it. In mouse dorsal root ganglion neurons, inward rectification can contribute to the anodal break excitation process (Mayer & Westbrook, 1983), while in sinoatrial node it is a part of the pace-making apparatus (Brown & DiFrancesco, 1980; Brown, 1982). The present results demonstrating the relationship of the degree of inward rectification with neuronal excitability and with spontaneous firing rate suggest that inward rectification might be somehow related to or involved in the control of neuronal firing.

LTS potentials

The LTS potentials recorded in SCN neurons did not appear as pronounced as the LTS potentials recorded in other central nervous system sites such as the thalamus (Jahnsen & Llinás, 1984), inferior olive (Llinás & Yarom, 1981) and areas near the paraventricular nucleus (Poulain & Carette, 1987; Hoffman et al, 1991; Tasker & Dudek, 1991). Nevertheless, the LTS potentials exhibited very similar voltage dependencies. In inferior olivary (Llinás & Yarom, 1981) and thalamic neurons (Jahnsen & Llinás, 1984), LTS potentials have been suggested to contribute to the

oscillation of the membrane potential (i.e., oscillatory firing behavior). However, a similar role for the LTS potentials appears less likely in retinorecipient cells, considering that we have not detected an oscillatory firing pattern in these neurons. The result that SCN neurons with and without the capacity to generate LTS potentials were not significantly different in spontaneous firing rate and excitability suggests that, at least in the present experimental condition, the capacity to generate LTS potentials does not significantly affect neuronal firing.

Concluding remarks

The results of the present study suggest that the SCN neurons receiving optic nerve input are relatively homogeneous in several intrinsic membrane properties. The study also provides evidence that these neurons are heterogeneous in some other properties, which may or may not be related to neuronal firing. Whether or not this electrophysiological heterogeneity is correlated with morphological and/or histochemical heterogeneity (van den Pol, 1980; Card & Moore, 1984; van den Pol & Tsujimoto, 1985) remains to be elucidated. Answers to these questions may provide an insight to whether or not individual neurons receiving retinal input have different roles in the photic entrainment of circadian rhythms.

ACKNOWLEDGEMENTS

We are grateful to Dr. D. Birt for developing neurophysiological data analysis routines, to T. Valdes and D. Weber for technical assistance, and to J. Wang for secretarial help. This research was supported by grants from the United States Air Force Office of Scientific Research (87-0361 and 90-0056) to F.E.D.

REFERENCES

ALBERS, H.E., LIOU, S.Y., FERRIS, C.F., STOPA, E.G. & ZOELLER, R.T. (1991). Neurochemistry of circadian timing. In *The Suprachiasmatic Nucleus: The mind's Clock.* eds. KLEIN, D.C., MOORE, R.Y. & REPPERT, S.M., pp. 263-288. Oxford University Press, Oxford.

ANDREW, R.D. & DUDEK, F.E. (1984). Intrinsic inhibition in magnocellular neuroendocrine cells of rat hypothalamus. *Journal of Physiology* **353**, 171-185.

BOURQUE, C.W. & BROWN, D.A. (1987). Apamin and d-tubocurarine block the afterhyperpolarization of rat supraoptic neurosecretory neurons. *Neuroscience Letters* **82**, 185-190.

BOURQUE, C.W., RANDLE, J.C.R. & RENAUD, L.P. (1985). A calcium-dependent potassium conductance in rat supraoptic nucleus neurosecretory neurons. *Journal of Neurophysiology* **54**, 1375-1382.

BROWN, H. (1982). Electrophysiology of the sinoatrial node. *Physiological Reviews* **62**, 505-530.

BROWN, H. & DIFRANCESCO, D. (1980). Voltage-clamp investigations of membrane currents underlying pace-maker activity in rabbit sino-atrial node. *Journal of Physiology* **308**, 331-351.

CAHILL, G.M. & MENAKER, M. (1987). Kynurenic acid blocks suprachiasmatic nucleus responses to optic nerve stimulation. *Brain Research* **410**, 125-129.

CAHILL, G.M. & MENAKER, M. (1989a). Responses of the suprachiasmatic nucleus to retinohypothalamic tract volleys in a slice preparation of the mouse hypothalamus. *Brain Research* **479**, 65-75.

CAHILL, G.M. & MENAKER, M. (1989b). Effects of excitatory amino acid receptors antagonists and agonists on suprachiasmatic nucleus responses to retinohypothalamic tract volleys. *Brain Research* **479**, 76-82.

CARD, J.P. & MOORE, R.Y. (1984). The suprachiasmatic nucleus of the golden hamster: immunohistochemical analysis of cell and fiber distribution. *Neuroscience* **13**, 415-431.

HENDRICKSON, A.E., WAGONER, N.A. & (1972). An autoradiographic and electron microscopic study of retino-hypothalamic connections. *Z.Zellforsch.* **135**, 1-26.

HOFFMAN, N.W., TASKER, J.G. & DUDEK, F.E. (1991). Immunohistochemical differentiation of electrophysiologically defined neuronal populations in the region of the rat hypothalamic paraventricular nucleus. *Journal of Comparative Neurology* **307**, 405-416.

IBATA, Y., TAKAHASHI, Y., OKAMURA, H., KAWAKAMI, F., TERUBAYASHI, H., KUBO, T. & YANAIHARA, N. (1989). Vasoactive intestinal peptide (VIP)-like immunoreactive neurons located in the rat suprachiasmatic nucleus receive a direct retinal projection. *Neuroscience Letters* **97**, 1-5.

JAHNSEN, H. & LLINAS, R. (1984). Electrophysiological properties of guinea-pig thalamic

neurones: an in vitro study. *Journal of Physiology* **349**, 205-226.

KIM, Y.I. & DUDEK, F.E. (1991a). Intracellular electrophysiological study of suprachiasmatic nucleus neurons in rodents: excitatory synaptic mechanisms. *Journal of Physiology* **444**, 269-287.

KIM, Y.I. & DUDEK, F.E. (1991b). Electrical heterogeneity of suprachiasmatic nucleus (SCN) neurons that receive optic nerve input. *Society for Neuroscience Abstracts* **17**, 669.(Abstract)

LLINAS, R. & SUGIMORI, M. (1980a). Electrophysiological properties of *in vitro* Purkinje cell somata in mammalian cerebellar slices. *Journal of Physiology* **305**, 171-195.

LLINAS, R. & SUGIMORI, M. (1980b). Electrophysiological properties of *in vitro* Purkinje cell dendrites in mammalian cerebellar slices. *Journal of Physiology* **305**, 197-213.

LLINAS, R. & YAROM, Y. (1981). Electrophysiology of mammalian inferior olivary neurones *in vitro*. Different types of voltage-dependent ionic conductances. *Journal of Physiology* **315**, 549-567.

MAYER, M.L. & WESTBROOK, G.L. (1983). A voltage-clamp analysis of inward (anomalous) rectification in mouse spinal sensory ganglion neurones. *Journal of Physiology* **340**, 19-45.

MEIJER, J.H. & RIETVELD, W.J. (1989). Neurophysiology of the suprachiasmatic circadian pacemaker in rodents. *Physiological Reviews* **69**, 671-707.

MINAMI, T., OOMURA, Y. & SUGIMORI, M. (1986a). Electrophysiological properties and glucose

responsiveness of guinea-pig ventromedial hypothalamic neurones in vitro. *Journal of Physiology* **380**, 127-143.

MINAMI, T., OOMURA, Y. & SUGIMORI, M. (1986b). Ionic basis for the electroresponsiveness of guinea-pig ventromedial hypothalamic neurones in vitro. *Journal of Physiology* **380**, 145-156.

MOORE, R.Y. (1983). Organization and function of a central nervous system circadian oscillator: the suprachiasmatic hypothalamic nucleus. *Federation Proceedings* **42**, 2783-2789.

MOORE, R.Y. & LENN, N.J. (1972). A retinohypothalamic projection in the rat. *Journal of Comparative Neurology* **146**, 1-14.

NELSON, R.J. & ZUCKER, I. (1981). Absence of extraocular photoreception in diurnal and nocturnal rodents exposed to direct sunlight. *Comparative Biochemical Physiology.* **69A**, 145-148.

POULAIN, P. & CARETTE, B. (1987). Low-threshold calcium spikes in hypothalamic neurons recorded near the paraventricular nucleus in vitro. *Brain Research Bulletin* **19**, 453-460.

RICHTER, C.P. (1965). *Biological Clocks in Medicine and Psychiatry.* Thomas, C., Springfield, Illinois.

RUSAK, B. & BOULOS, Z. (1981). Pathways for photic entrainment of mammalian circadian rhythms. *Photochemistry and Photobiology* **34**, 267-273.

SHIBATA, S., LIOU, S.Y. & UEKI, S. (1986). Influence of excitatory amino acid receptor

antagonists and of baclofen on synaptic transmission in the optic nerve to the suprachiasmatic nucleus in slices of rat hypothalamus. *Neuropharmacology* **25**, 403-409.

SHIBATA, S., OOMURA, Y., HATTORI, K. & KITA, H. (1984). Responses of suprachiasmatic nucleus neurons to optic nerve stimulation in rat hypothalamic slice preparation. *Brain Research* **302**, 83-89.

SUGIMORI, M., SHIBATA, S. & OOMURA, Y. (1986). Electrophysiological bases for rhythmic activity in the suprachiasmatic nucleus of the rat: an in vitro study. In *Emotions: Neuronal and Chemical Control*, ed. OOMURA, Y., pp. 199-206. S. Karger, Basel, Switzerland.

TAKAHASHI, J.S. & ZATZ, M. (1982). Regulation of circadian rhythmicity. *Science* **217**, 1104-1111.

TASKER, J.G. & DUDEK, F.E. (1991). Electrophysiological properties of neurones in the region of the paraventricular nucleus in slices of rat hypothalamus. *Journal of Physiology* **434**, 271-293.

THOMSON, A.M. & WEST, D.C. (1990). Factors affecting slow regular firing in the suprachiasmatic nucleus in vitro. *Journal of Biological Rhythms* **5**, 59-75.

TUREK, F.W. (1985). Circadian rhythms in mammals. *Annual Review of Physiology* **47**, 49-64.

VAN DEN POL, A.N. (1980). The hypothalamic suprachiasmatic nucleus of the rat: intrinsic anatomy. *Journal of Comparative Neurology* **191**, 661-702.

VAN DEN POL, A.N. & TSUJIMOTO, K.L. (1985). Neurotransmitters of the hypothalamic suprachiasmatic nucleus: immunocytochemical analysis of 25 neuronal antigens. *Neuroscience* **15**, 1049-1086.

WHEAL, H.V. & THOMSON, A.M. (1984). The electrical properties of neurones of the rat suprachiasmatic nucleus recorded intracellularly in vitro. *Neuroscience* **13**, 97-104.

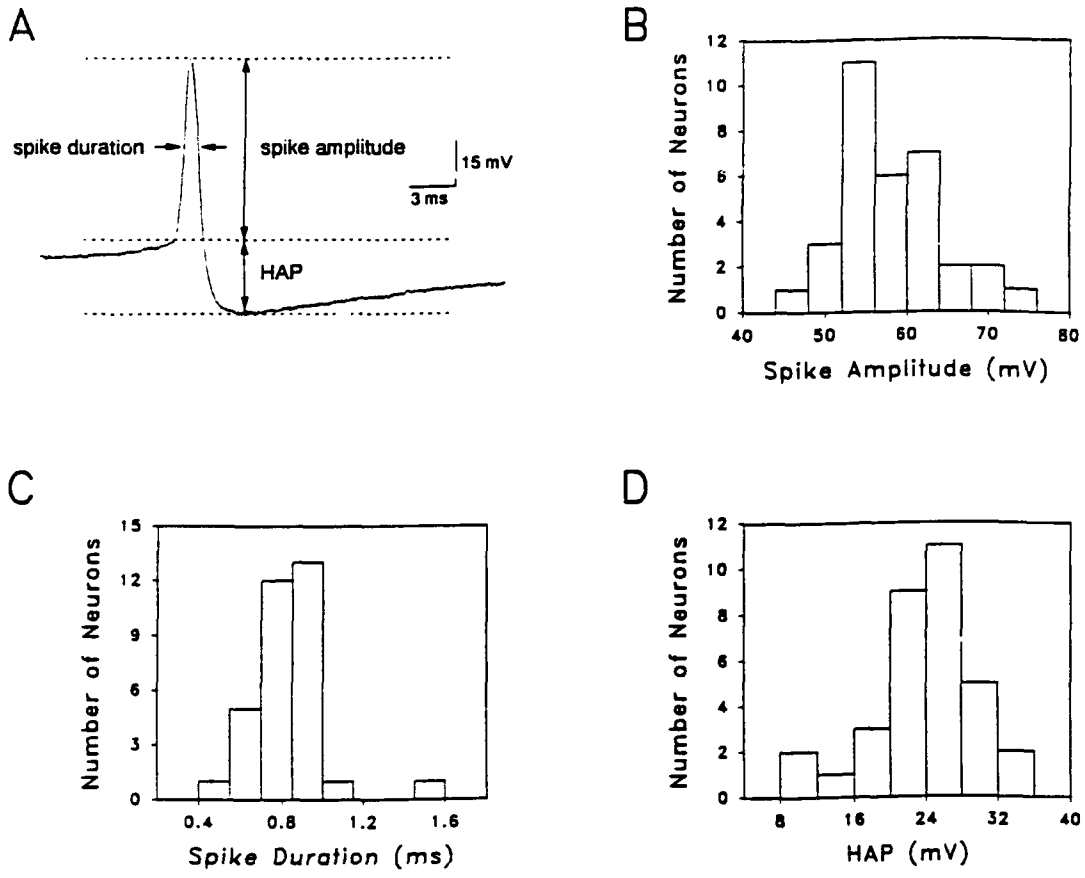

Figure 1 Characteristics of action potentials. *A*, A representative action potential recorded from an SCN neuron. *B, C & D,* Frequency histograms (33 neurons) for spike amplitude (*B*), spike duration (*C*) and hyperpolarizing afterpotential (*D*).

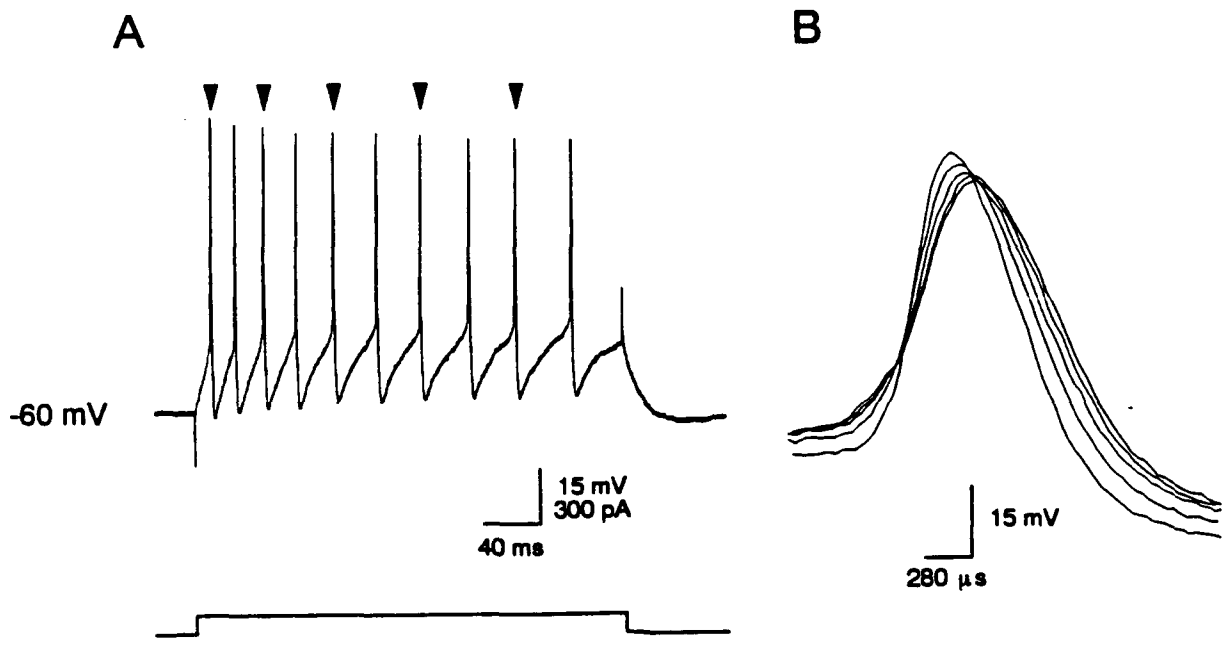

Figure 2 Properties of the spike train evoked by depolarizing current pulse. *A*, An evoked action potential train exhibiting spike inactivation and frequency accommodation. *B*, The spikes (arrowheads) in *A* are superimposed to illustrate progressive spike broadening and inactivation. Cell was current-clamped to -60 mV.

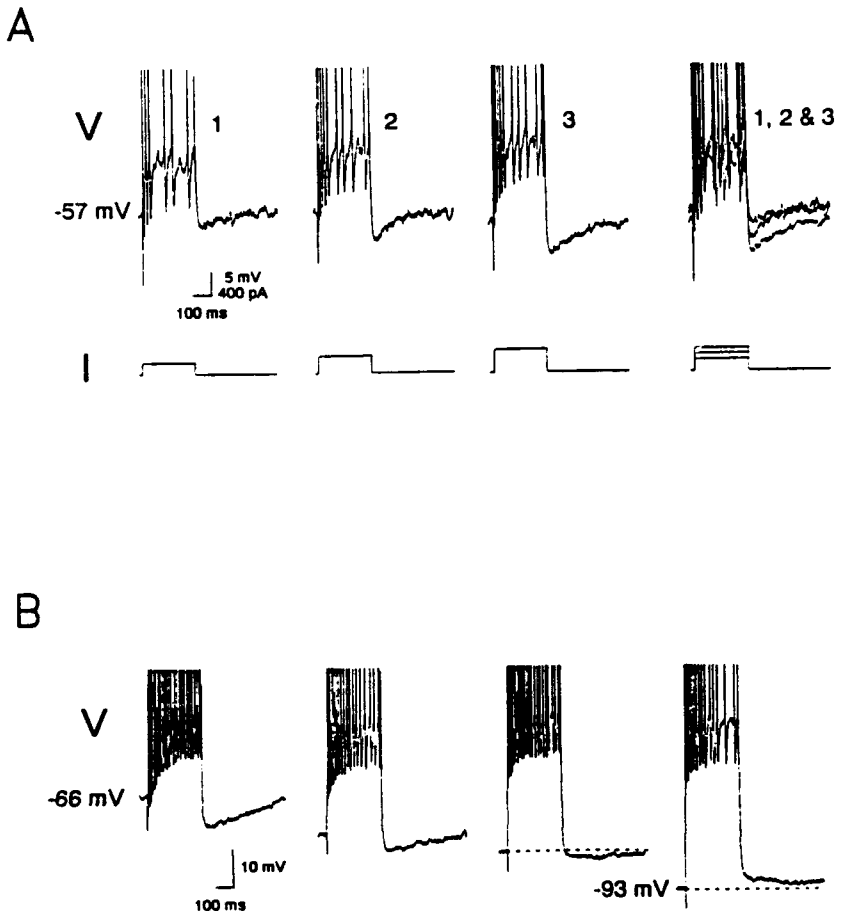

Figure 3 Properties of the post-train afterhyperpolarization. *A*, Spike trains evoked by three different intensities of current pulses. The amplitude of the post-train afterhyperpolarization was a function of current intensity. Cell was current-clamped to -57 mV. *B*, In another neuron, spike trains evoked at four different membrane potentials. The polarity of the post-train afterhyperpolarization reversed at around -90 mV.

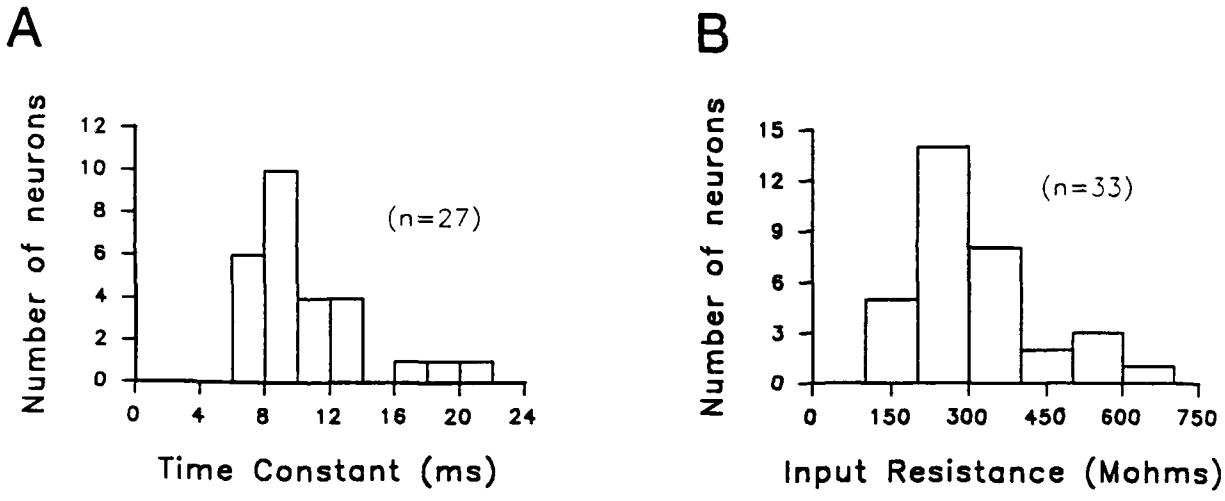

Figure 4 Frequency histograms for membrane time constant (*A*) and input resistance (*B*).

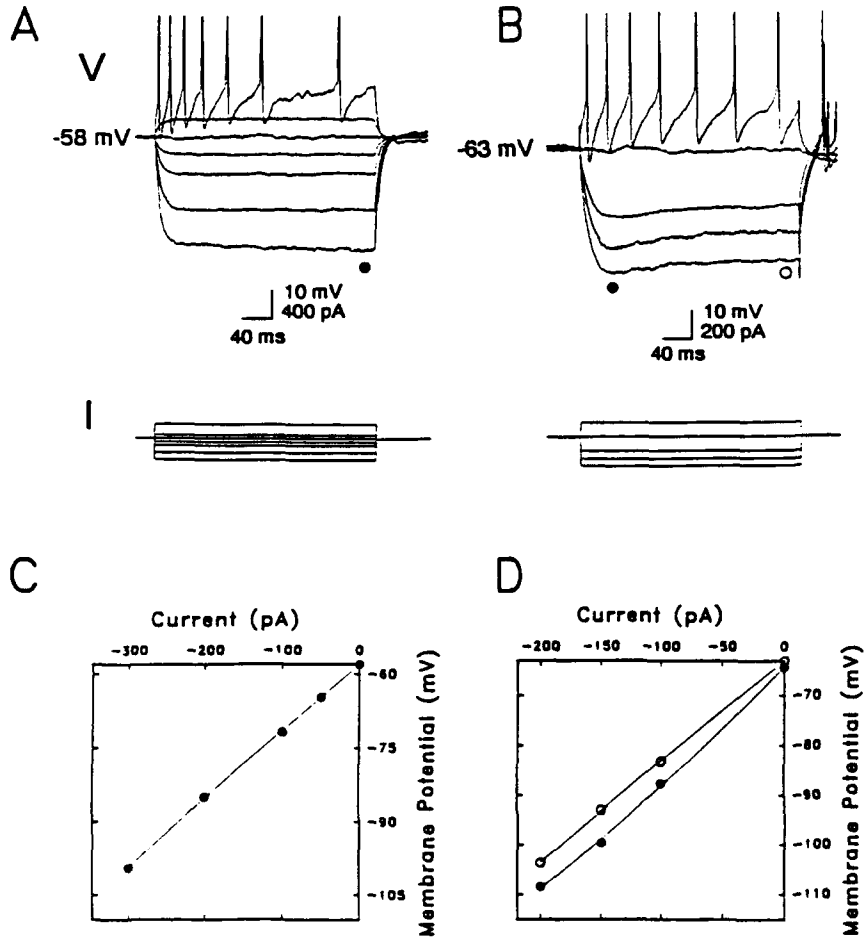

Figure 5 Time-dependent inward rectification. *A & B*, Voltage responses (upper panel) of two different neurons to intracellularly injected current pulses (lower panel). Action potentials are truncated. Cells were current-clamped to -58 mV (*A*) and -63 mV (*B*). *C & D*, I-V plots for the data in *A & B*, respectively. Voltage measurements were made at the time points indicated with closed and open circles. The data in *A & C* indicate the lack of inward rectification, whereas those in *B & D* illustrate the presence of time-dependent inward rectification.

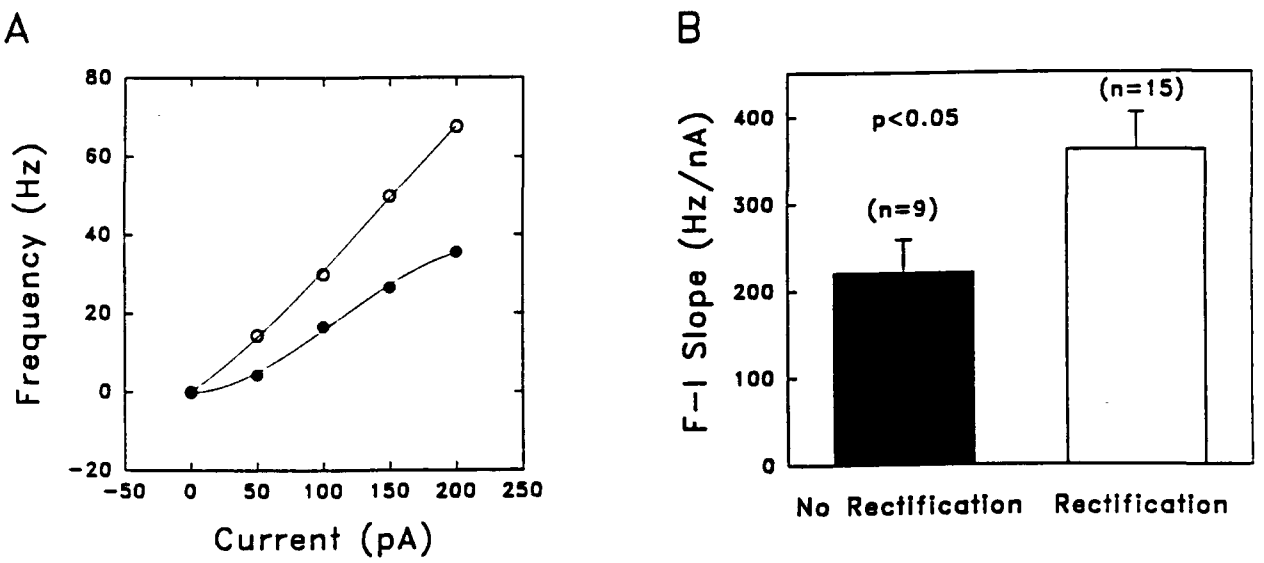

Figure 6 Neurons with inward rectification were more excitable. *A*, Frequency-current (F-I) plots for two neurons with (open circles) and without (filled circles) inward rectification. Cells were current-clamped to -69 and -70 mV, respectively. Spike frequency was calculated from the averaged number of spikes evoked by 300-ms current pulses of a given intensity (up to 500 pA). *B*, Comparison of the mean (±SEM) primary F-I slope (Hz/nA) between neurons with >6% inward rectification (open bar) and those with no or negligible (i.e., <3%) rectification (filled bar).

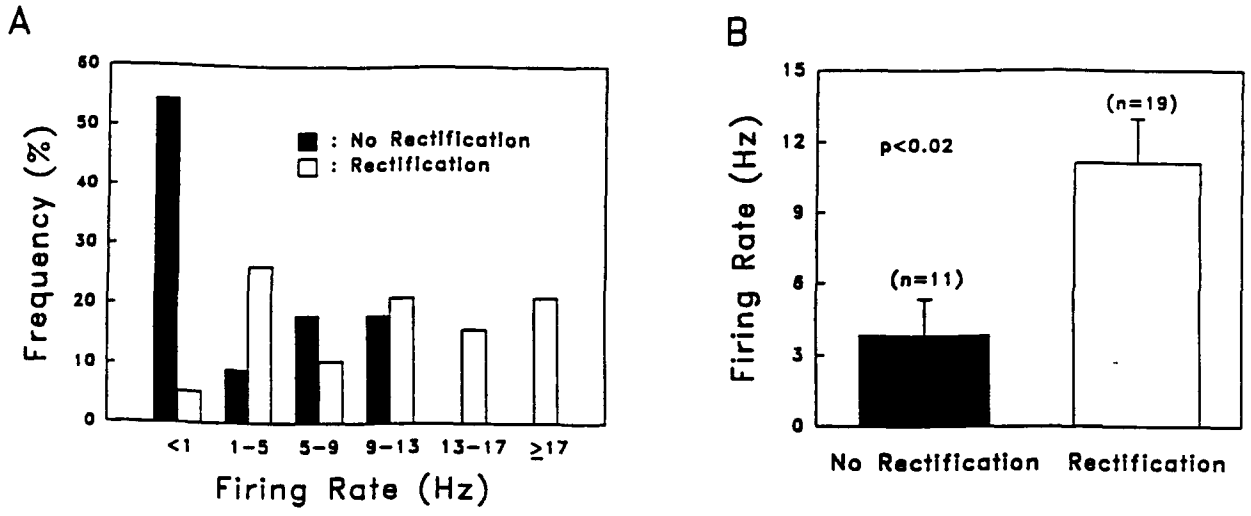

Figure 7 Neurons with inward rectification had higher spontaneous firing rate. *A*, Frequency histogram for firing rate. Note that over half of the cells with no or negligible (i.e., <3%) inward rectification (filled bars) had a firing rate of <1 Hz (most were silent) and over half of the cells with >6% rectification (open bars) had a firing rate of >9 Hz. *B*, Comparison of the mean (±SEM) firing rate between the two neuronal groups.

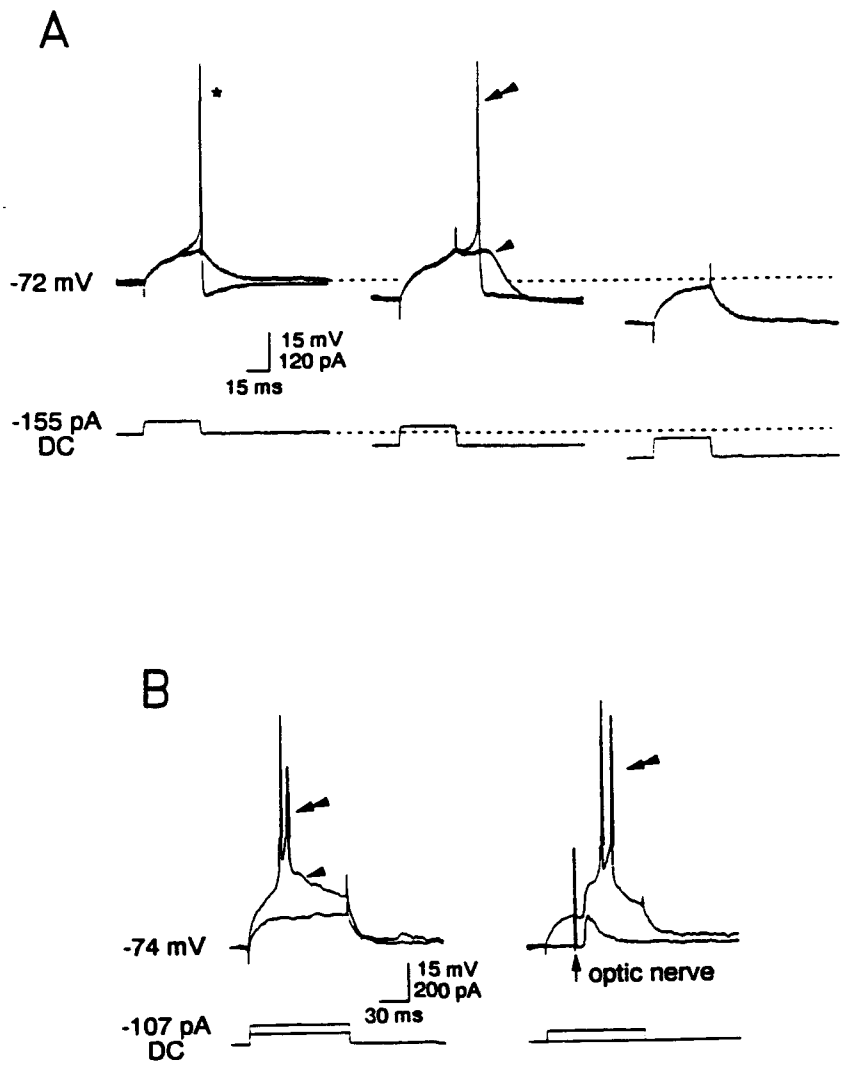

Figure 8 Characteristics of LTS potentials. *A*, Adequate hyperpolarization removed the inactivation of LTS conductance. Left: at a membrane potential of -72 mV, a depolarizing current pulse evoked an electrotonic potential or action potential (asterisk). Middle: when the cell was hyperpolarized to about -80 mV, a depolarizing current pulse could evoke a small LTS potential (arrowhead). Occasionally, an action potential (double arrowheads) arose from the LTS potential. Right: when

the cell was hyperpolarized to about -90 mV, a current pulse of the same intensity as the one in the middle panel did not evoke an LTS potential. *B*, Depolarizing potentials of only sufficient amplitude evoked LTS potentials. Data from another cell hyperpolarized to -74 mV. Left: of the two different intensities of current pulses injected, the higher one evoked an LTS potential (arrowhead) that supported two action potentials (double arrowheads). Right: when superimposed on a depolarizing electrotonic potential, the excitatory postsynaptic potential (EPSP) from optic nerve stimulation (arrow) evoked an LTS potential similar to the one in the left panel. Two action potentials (double arrowheads) arose from the LTS potential that emerged at the falling phase of the EPSP.

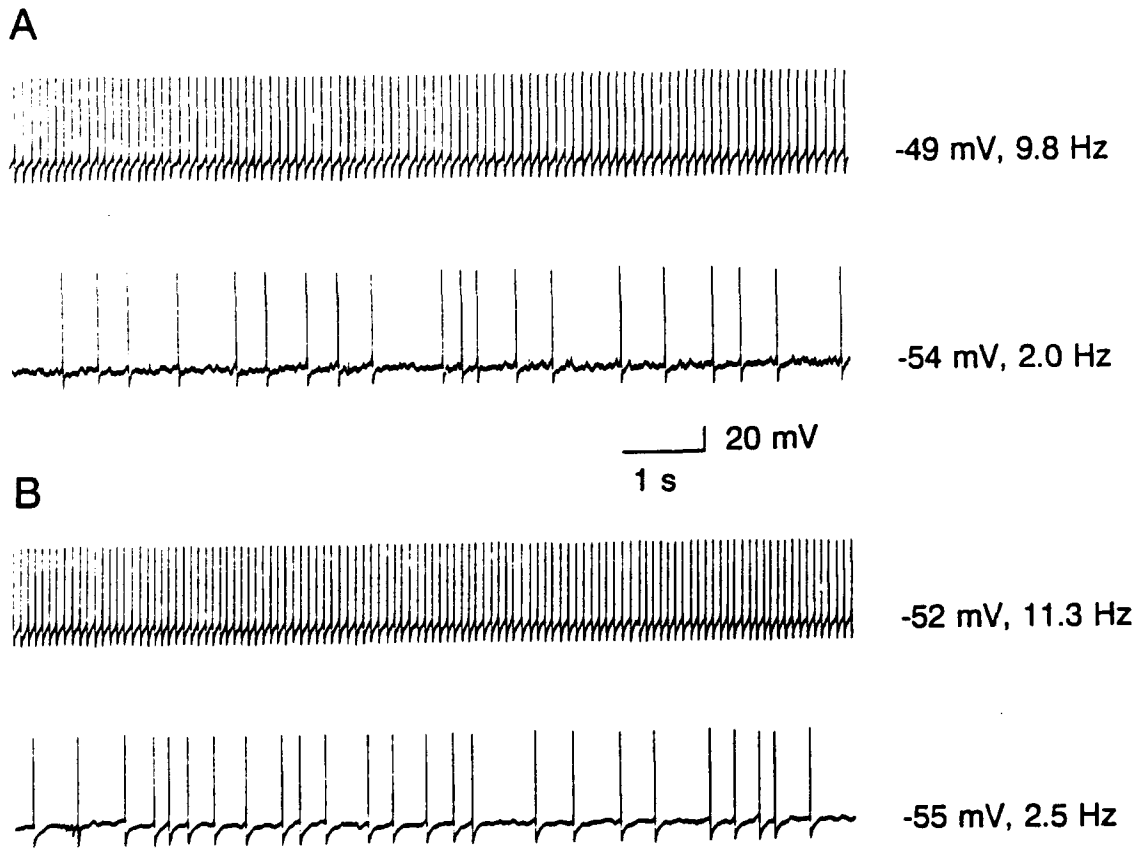

Figure 9 Firing patterns were related to firing rate. *A*, Regular *(upper panel)* and irregular (*lower panel*) spontaneous firing patterns observed in two different neurons at rest. *B*, A regular firing pattern observed in a neuron recorded at rest (*upper panel*), and an irregular pattern recorded from the same neuron at a more negative membrane potential (*lower panel*). The hyperpolarization was with intracellular injection of cathodal current. In *A* & *B*, the baseline membrane potential and firing rate are indicated to the right of each trace.

Classification: **Neurobiology**

Neuronal synchronization without calcium-dependent synaptic transmission in the hypothalamus

(suprachiasmatic nucleus/intercellular communication/patch-clamp)

Yona Bouskila[*] and F. Edward Dudek[*†]

Mental Retardation Research Center and Brain Research Institute, University of California, Los Angeles, School of Medicine, Los Angeles, CA 90024, U.S.A.

[*]Present address: Department of Anatomy and Neurobiology, Colorado State University, Fort Collins, CO 80523.

[†]To whom reprint requests should be addressed.

Abbreviations: SCN, suprachiasmatic nucleus; NMDA, N-methyl-D-aspartic acid; GABA, γ-aminobutyric acid; MUA, multiple-unit activity; PSP, postsynaptic potential; AP5, 2-amino-5-phosphonopentanoic acid; DNQX, 6,7-dinitroquinoxaline-2,3-dione.

ABSTRACT A critical question in understanding the mammalian brain is how populations of neurons become synchronized. This is particularly important for the neurons and neuroendocrine cells of the hypothalamus, which are activated synchronously to control endocrine glands and the autonomic nervous system. It is widely accepted that communication between neurons of the adult mammalian brain is mediated primarily by Ca^{2+}-dependent synaptic transmission. Here we report that synchronous neuronal activity can occur in the hypothalamic suprachiasmatic nucleus without active Ca^{2+}-dependent synaptic transmission. Simultaneous extracellular recordings of neuronal activity in the suprachiasmatic nucleus, which contains the mammalian biological clock (1, 2), confirmed a circadian rhythm of *synchronized* activity in hypothalamic slices. Ca^{2+}-free medium, which blocks chemical synaptic transmission (3-5) and increases membrane excitability (6), produced periodic and *synchronized* bursts of action potentials in a large population of SCN neurons with diverse firing patterns. N-methyl-D-aspartic acid, non-N-methyl-D-aspartic acid and γ-aminobutyric acid type A receptor antagonists had no effect on burst synchrony. Whole-cell patch-clamp recordings confirmed that the Ca^{2+}-free solution blocked evoked postsynaptic potentials and that the

mixture of antagonists blocked the remaining spontaneous postsynaptic potentials. Therefore, mechanisms other than Ca^{2+} dependent synaptic transmission can synchronize neurons in the mammalian hypothalamus, and may be important wherever neuronal networks are synchronized.

There is virtually no physiological information on local neuronal interactions in the hypothalamus, even though synchronization of the neuronal and neuroendocrine elements of the hypothalamus is a critical and fundamental process in the neurobiology of hormone secretion and homeostasis. In freely-moving animals the neuronal activity in the suprachiasmatic nucleus (SCN) of the hypothalamus exhibits a circadian rhythm where peak activity occurs at mid-light phase, even in a surgically isolated hypothalamus (7) or in vitro brain slice (8-11). Because these data are derived from neuronal populations, they also imply that the electrical activity generating the pacemaker is synchronized. Determining the mechanism(s) underlying this synchronization is critical to an understanding of circadian rhythm generation and neuronal interactions in the hypothalamus. The Ca^{2+}-independent non-synaptic mechanism(s) of synchronization we describe here in the SCN provides a crucial clue for understanding the cellular processes underlying circadian rhythm generation, since it is quite likely that the circadian rhythm incorporates the same mecnanism.

Most of the studies on neuronal networks in the mammalian brain have been directed toward chemical synaptic transmission, while other non-

conventional forms of communication between neurons have been relatively neglected and probably underestimated. Previous studies have suggested that certain areas of the brain (e.g., hippocampus, inferior olive and locus coeruleus) exhibit synchronization independent of chemical synaptic transmission, but the activity appears to be tightly synchronized (see **DISCUSSION**). Here we show that neuronal activity in the hypothalamus can be loosely synchronized after chemical synaptic transmission has been blocked. This significantly extends the brain areas in which a non-chemical synaptic mechanism has been shown to synchronize activity of large neuronal populations in the adult mammalian brain.

MATERIALS AND METHODS

Slice preparation. Coronal hypothalamic slices (350-500 μm) were prepared 2 h before the dark phase from Sprague-Dawley male rats (100-400 g, except 40-85 g for patch-clamp experiments). Rats were obtained from a single colony for circadian rhythm experiments and maintained on a 12:12 light:dark schedule for $\geq$14 days. The slices were studied in an interface chamber (33-35°C, in humidified 95% O_2 and 5% CO_2).

Solutions. For the circadian rhythm experiments (Fig. 1), slices were

bathed in a physiological solution containing (in mM): 124 NaCl, 3 KCl, 1.4 NaH_2PO_4, 2.4 $CaCl_2$, 1.3 $MgSO_4$, 11 glucose, 26 NaH_2CO_3. Control solutions in the other experiments (Figs. 2 and 3) were similar to those in Fig. 1 except for 134 mM NaCl, 10 mM HEPES as a buffer and 8 mM NaOH to adjust for pH 7.4. In the Ca^{2+}-free medium $MgCl_2$ was substituted for $CaCl_2$ and 0.1 mM 1,2-bis(2-aminophenoxy)ethane-,N,N,N',N'-tetraacetic acid (BAPTA), a specific Ca^{2+} chelator, was added. Blockade of N-methyl-D-aspartic acid (NMDA), non-NMDA and γ-aminobutyric acid type A ($GABA_A$) receptors was achieved by bath application of DL-2-amino-5-phosphonopentanoic acid (AP5), 6,7-dinitroquinoxaline-2,3-dione (DNQX) and bicuculline.

Extracellular recordings. Multiple-unit activity (MUA) was recorded simultaneously with two metal electrodes (90% platinum and 10% iridium wire coated with teflon, diameter = 76 μm). The signals were amplified with a differential amplifier (bandwidth filter = 0.3-3 KHz). Discharges above a threshold (signal to noise ratio ≥1.5-2.0:1) were counted in 5-min bins and then averaged in 1-h bins. Single-unit activity was recorded using glass micropipettes filled with 1 M NaCl (resistance = 30-40 MΩ).

Whole-cell patch-clamp recordings. Glass pipettes were filled with

solution containing (in mM): 120 K-gluconate, 1 NaCl, 1 $CaCl_2$, 1 $MgCl_2$, 10 HEPES, 4 Mg-ATP, 5 BAPTA and adjusted to pH 7.2 with KOH. Electrode resistance before seal formation was 4-7 MΩ. Extracellular stimulation applied through a platinum/iridium bipolar electrode to a site 2-3 mm dorsal to the SCN (0.2-1.6 mA and 0.5 ms) evoked an excitatory postsynaptic potential (PSP) starting after a 2-5 ms delay with 5-16 mV peak amplitude and duration of 60-120 ms. Input resistance was 657 ± 80 MΩ (mean ± SE, n=12, range of 350 to 1150 MΩ) at membrane potentials of -70 to -90 mV. During PSP blockade, no reduction was observed in input resistance (n=5), indicating that PSPs were not shunted by a leak in the membrane.

RESULTS

Simultaneous recordings of MUA with two electrodes positioned on the slice surface were made for 25 h. One electrode was located in the mid-ventral SCN and the other in the dorsal SCN (100-250 μm separation). These recordings confirmed that a circadian rhythm can be obtained in an isolated slice (Fig. 1A); peak activity occurred at 06:29 ± 0:26 h circadian time (mean ± SE, n=6; lights on from 00:00 to 12:00 h circadian time),

in agreement with other in vivo and in vitro studies (7-11). The correlation between the two hourly MUA counts across the circadian rhythm in the same SCN was high ($r=0.99$ Fig. 1B; 0.73, 0.61, 0.87 and 0.93 in other cases, d.f.=23, $p<0.0015$), thus confirming synchrony in circadian neuronal activity (Fig. 1B).

Fig. 1 here

To test whether chemical synaptic transmission is required for synchronization of SCN neurons, we bathed *hypothalamic slices in* Ca^{2+}-free solution to block evoked chemical PSPs. After 2.5-5.5 h, periodic bursts of neuronal activity appeared in the SCN. Simultaneous MUA recordings from two locations within one SCN revealed that the bursts always occurred simultaneously (n=11, Fig. 2A). Bursts were never synchronized in opposite SCNs (n=9, Fig. 2B) and differed in phase as well as in interval. Burst synchrony was maintained for 18.5 h (n=2) and normal activity could be restored within 12 min in normal-Ca^{2+} solution. Simultaneous single-unit and MUA recordings revealed that 61% of all neurons (n=23) generated bursts and that most neurons (79% of the

bursting neurons or 57% of all neurons) fired action potential(s) only during the MUA bursts. Intraburst interval and burst duration varied considerably between neurons and between consecutive bursts of the same neuron (Fig. 2C). That bursts of action potentials in individual cells occurred simultaneously with periodic increases of MUA amplitude, which demonstrates directly that MUA bursts represent action potentials from a population of bursting neurons.

Fig. 2 here

Excitatory amino acid receptor antagonists and bicuculline block all evoked and spontaneous postsynaptic events in SCN neurons (12-15). Although unlikely, spontaneous Ca^{2+}-independent release of neurotransmitters [*i.e.*, not mediated by action potentials] could conceivably contribute to burst synchronization. To test this hypothesis, we bath applied glutamate (NMDA and non-NMDA) and $GABA_A$ receptor antagonists (AP5 - 100 μM, DNQX - 50 μM and bicuculline - 50 μM) in the Ca^{2+}-free solution. These antagonists never altered MUA burst synchrony (n=6, tested 60-100 min), indicating that spontaneous release of

excitatory and inhibitory amino acids was not required for synchronization. Intracellular recordings have revealed only *fast* PSPs mediated by NMDA, non-NMDA and $GABA_A$ receptors in the nucleus (12-14, 16, 17) (also Fig. 3). Since all detectable PSPs were blocked, this result also rules out synchronization of SCN neurons through Ca^{2+}-independent transmitter release, which has previously been demonstrated in fish retinal neurons (18).

To assess directly the effect of the Ca^{2+}-free solution and the receptor antagonists on chemical synaptic transmission in SCN neurons, we recorded spontaneous and evoked PSPs using the whole-cell patch-clamp technique, which allows high resolution of synaptic events. Evoked excitatory PSPs were blocked in Ca^{2+}-free solution or during bath application of the amino acid antagonists (Fig. 3A and B). Spontaneous PSPs were not blocked in the Ca^{2+}-free solution (n=5, not shown), but were always abolished after application of the antagonists (Fig. 3C). Therefore, high-resolution whole-cell recordings directly demonstrated that all detectable chemical synaptic transmission was blocked in conditions that induced synchronized bursting when antagonists were present.

Fig. 3 here

DISCUSSION

The synchronized bursts in Ca^{2+}-free solution represent a loose type of neuronal synchronization (*i.e.,* many neurons firing within the same time window, but with variable discharge patterns and burst durations). This type of Ca^{2+}-independent synchronization has not been described previously in the mammalian brain. Normal synchronization of SCN activity during the circadian rhythm (see Fig. 1B) has similarities to that seen in Ca^{2+}-free conditions, since at any given time a sample of neurons show a wide range of firing frequencies (8-11) while still being loosely synchronized. The persistence of the synchronous bursts induced by Ca^{2+}-free solution, despite complete block of all detectable chemical synaptic transmission, demonstrates that a communication mechanism(s) other than Ca^{2+}-dependent synaptic transmission must operate in the SCN. This mechanism can synchronize neuronal activity within a nucleus but not between opposite nuclei (Fig. 2B). Communication between opposite nuclei is probably mediated by chemical synaptic transmission (16, 19) and therefore was blocked in the absence of Ca^{2+}.

Neurons in the inferior olive (20) and locus coeruleus (21) generate Ca^{2+}-dependent subthreshold oscillations that are rhythmic and synchronous. Although these oscillations are synchronized by gap junctions, and thus also seem to be independent of chemical synaptic mechanisms, they are Ca^{2+}-dependent and therefore different from the bursts described here. In hippocampal slices, low-Ca^{2+} solutions produce synchronized bursts in the absence of active chemical synapses (22-24), but the action potentials are tightly synchronized and generate population spikes during these bursts. The SCN bursts differ from the hippocampal activity (*i.e.*, weaker synchronization whereby action potentials do not occur one-for-one) and therefore represent a different type of synchronization of neuronal activity in the mammalian brain.

The neuronal synchronization in the hypothalamus that we are reporting here opens several new lines of investigation. This Ca^{2+}-independent mechanism(s) of synchronization in the SCN may depend on electrotonic coupling via gap junctions, electrical field effects (ephaptic interactions) and/or changes in the concentration of extracellular ions (25). Among these three possible mechanisms, electrical field effects seem the most unlikely to operate in the SCN due to the lack of parallel

arrangement of neuronal processes in .. nucleus. Electrotonic coupling and ionic interactions are more likely to facilitate synchronization in the nucleus, since many SCN cell bodies are tightly packed together with extensive regions of membrane apposition between them (19). Although there is evidence for electrotonic coupling in some areas of the hypothalamus (26), nearly all of the data are derived from anatomical rather than electrophysiological studies, and virtually no data are available for most hypothalamic areas including the SCN. It should now be possible to determine which hypothetical mechanisms of neuronal interaction are present in the SCN, and the role they play in synchronization.

Previous indirect evidence has suggested that neurons in the SCN can be synchronized via non-synaptic mechanisms. The circadian rhythm of glucose utilization that occurs across cells in the SCN is expressed before chemical synapses are functional (27). Tetrodotoxin application, which blocks synaptic transmission mediated by action potentials in axons, also blocks the circadian rhythm of motor activity while leaving the coordinated timing mechanism of the cellular clock in the SCN unimpaired (28). The non-synaptic mechanism(s) demonstrated here could explain both observations, since neuronal activity could be synchronized by electrical

and/or ionic interactions. A Ca^{2+}-independent mechanism(s) of neuronal synchronization may coordinate the cellular elements in the SCN responsible for circadian rhythms in mammals. Synchronization of neuronal activity in the SCN and other areas of the hypothalamus must be critical to execute the widespread behavioral, physiological and endocrine effects. Non-synaptic communication between mammalian neurons has largely been ignored, but recent studies - such as from intact animals (29) and the present in vitro data - suggest that non-synaptic mechanisms have a major role in many regions of the mammalian brain.

We thank D. Birt, Y.I. Kim, C. Meier, D. Weber and J.P. Wuarin for advice and assistance, and Y. I. Kim, C. Meier, J. Strecker and J. P. Wuarin for constructive comments on drafts of the manuscript. Supported by a grant from the United States Air Force Office of Scientific Research to F.E.D.

1. Meijer, J. H. & Rietveld, W. J. (1989) *Physiol. Rev.* **69**, 671-707.

2. Ralph, M. R., Foster, R. G., Davis, F. C. & Menaker, M. (1990) *Science* **247**, 975-978.

3. del Castillo, J. & Stark, L. (1952) *J. Physiol. (London)* **116**, 507-515.

4. Katz, B. & Miledi, R. (1967) *J. Physiol. (London)* **192**, 407-436.

5. Douglas, W. W. (1978) *Ciba Fnd. Symp.* **54**, 61-87.

6. Frankenhaeuser, B. & Hodgkin, A. L. (1957) *J. Physiol. (London)* **137**, 218-244.

7. Inouye, S. T. & Kawamura, H. (1979) *Proc. Natl. Acad. Sci. U.S.A.* **76**, 5962-5966.

8. Green, D. J. & Gillette, R. (1982) *Brain Res.* **245**, 198-200.

9. Groos, G. & Hendriks, J. (1982) *Neurosci. Lett.* **34**, 283-288.

10. Shibata, S., Oomura, Y., Kita, H. & Hattori, K. (1982) *Brain Res.* **247**, 154-158.

11. Prosser, R. A. & Gillette, M. U. (1989) *J. Neurosci.* **9**, 1073-1081.

12. Kim, Y. I. & Dudek, F. E. (1991) *J. Physiol. (London)* **444**, 269-287.

13. Thomson, A. M. & West, D. C. (1990) *J. Biol. Rhythms* **5**, 59-75.

14. Kim, Y. I. & Dudek, F. E. *J. Physiol. (London)* (in the press).

15. Cahill, G. M. & Menaker, M. (1989) *Brain Res.* **479**, 76-82.

16. Wheal, H. V. & Thomson, A. M. (1984) *Neuroscience* **13**, 97-104.

17. Sugimori, M., Shibata, S. & Oomura, Y. (1986) in *Emotions: Neuronal and Chemical Control*, ed. Oomura U. (Japan Scientific Societies, Japan), pp. 199-206.

18. Schwartz, E. A. (1987) *Science* **238**, 350-355.

19. van den Pol, T. N. (1980) *J. Comp. Neurol.* **191**, 661-702.

20. Llinàs, R. & Yarom, Y. (1986) *J. Physiol. (London)* **376**, 163-182.

21. Christie, M. J., Williams, J. T. & North, R. A. (1989) *J. Neurosci.* **9**, 3584-3589.

22. Jefferys, J. G. R. & Haas, H. L. (1982) *Nature* **300**, 448-450.

23. Konnerth, A., Heinemann, U. & Yaari, Y. (1983) *Nature* **307**, 69-71.

24. Taylor, C. P. & Dudek, F. E. (1982) *Science* **218**, 810-812.

25. Dudek, F. E., Snow, R. W. & Taylor, C. P. (1986) *Adv. Neurol.* **44**, 593-617 .

26. Hatton, G. I. (1990) *Prog. Neurobiol.* **34**, 437-504.

27. Moore, R. Y., Reppert, S. M. & Weaver, D. R. (1991) in *Suprachiasmatic Nucleus*, eds. Klein, D. C., Moore, R. Y. & Reppert, S. M. (Oxford University, New York), pp. 391-418.

28. Schwartz, W. J., Gross, R. A. & Morton, M. T. (1987) *Proc. Natl. Acad.*

Sci. USA **84**, 1694-1698.

29. Buzsàki, G., Horvàth, Z., Urioste, R., Hetke, J. & Wise, K. (1992) *Science* **256**, 1025-1027.

FIGURE LEGENDS

Fig. 1. Circadian rhythm of neuronal activity and comparison of activity recorded simultaneously from two locations in the SCN. (A) Average of normalized MUA (●) at each circadian hour from six rats. Normalized MUA was computed by dividing each hourly MUA count by the maximum hourly MUA count of each animal. (B) Averaged MUA count per 5-min at each circadian hour from one animal. MUA from the ventral SCN (●) and from 200 μm dorsal in the same SCN (▽) were counted simultaneously. Vertical lines are standard errors. Solid bars represent dark hours and open bars represent light hours.

Fig. 2. Simultaneous extracellular recordings during bursting activity in Ca^{2+}-free solution. (A) Simultaneous recordings of MUA from two locations in the same SCN (right side) indicate synchronous bursts. Interburst interval gradually increased from 1 s to a maximum of up to 10 s after several hours and the burst duration ranged from 0.5 to 2.0 s. (B) Simultaneous recordings of MUA from opposite SCNs (left and right) indicate that the bursts were not synchronous and had different interburst intervals (recorded in the same slice as A). (C) Single-unit activity (SUA) recording during a MUA burst in the same SCN; the SUA bursts coincided

with the MUA bursts.

Fig. 3. The effect of Ca^{2+}-free solution or glutamate and $GABA_A$ antagonists on PSPs recorded with the whole-cell patch-clamp technique. (A) Upper trace shows an excitatory PSP evoked by extracellular stimulation dorsal to the SCN. The excitatory PSP was completely blocked (lower trace) after 17 min (range of 9-26 min, n=4) in Ca^{2+}-free solution. Full recovery was obtained after 10 min in normal Ca^{2+} solution (not shown). The membrane potential in both traces was -66 mV. (B) Upper trace shows an evoked excitatory PSP from another neuron, which was blocked in 100 μM AP5, 50 μM DNQX and 50 μM bicuculline (BIC) mixture (lower trace) after 13 min (range of 9-13 min, n=3). The membrane potential in both traces was -78 mV. (C) The three upper left traces show continuous recordings of spontaneous PSPs in the same neuron as in (B). The lower left trace shows two spontaneous PSPs at faster sweep speed and higher gain. The three right traces show a continuous recording during complete blockade of spontaneous PSPs after 12 min (range of 9-14 min, n=6) in the antagonist mixture. All traces in (C) were recorded at membrane potential of -78 mV. Traces (A) and (B) contain a calibration pulse (10 mV, 10 ms) before the truncated stimulus artifact.

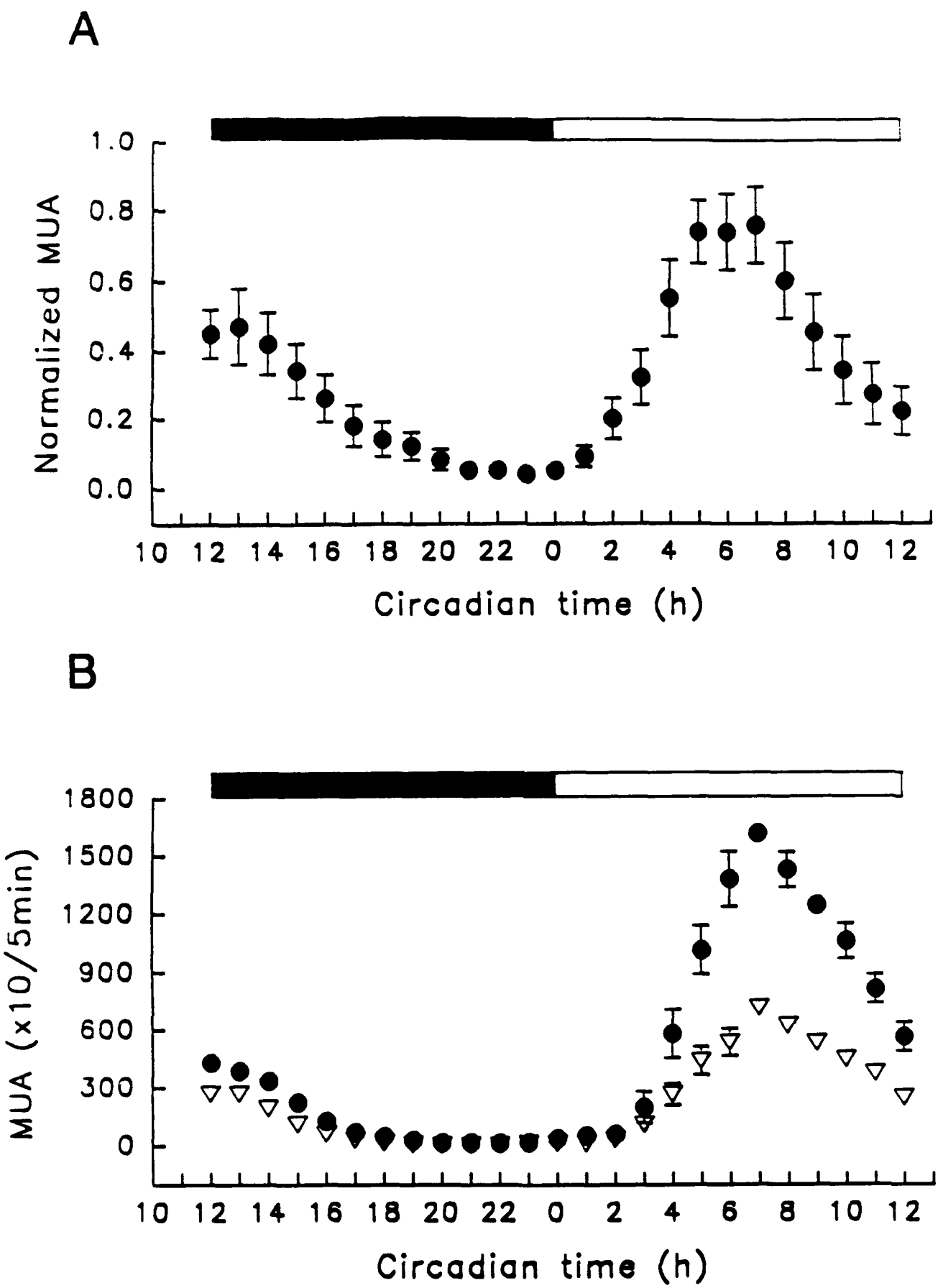
A
Normalized MUA
1.0
0.8
0.6
0.4
0.2
0.0
10 12 14 16 18 20 22 0 2 4 6 8 10 12
Circadian time (h)
B
MUA (x10/5min)
1800
1500
1200
900
600
300
0
10 12 14 16 18 20 22 0 2 4 6 8 10 12
Circadian time (h)

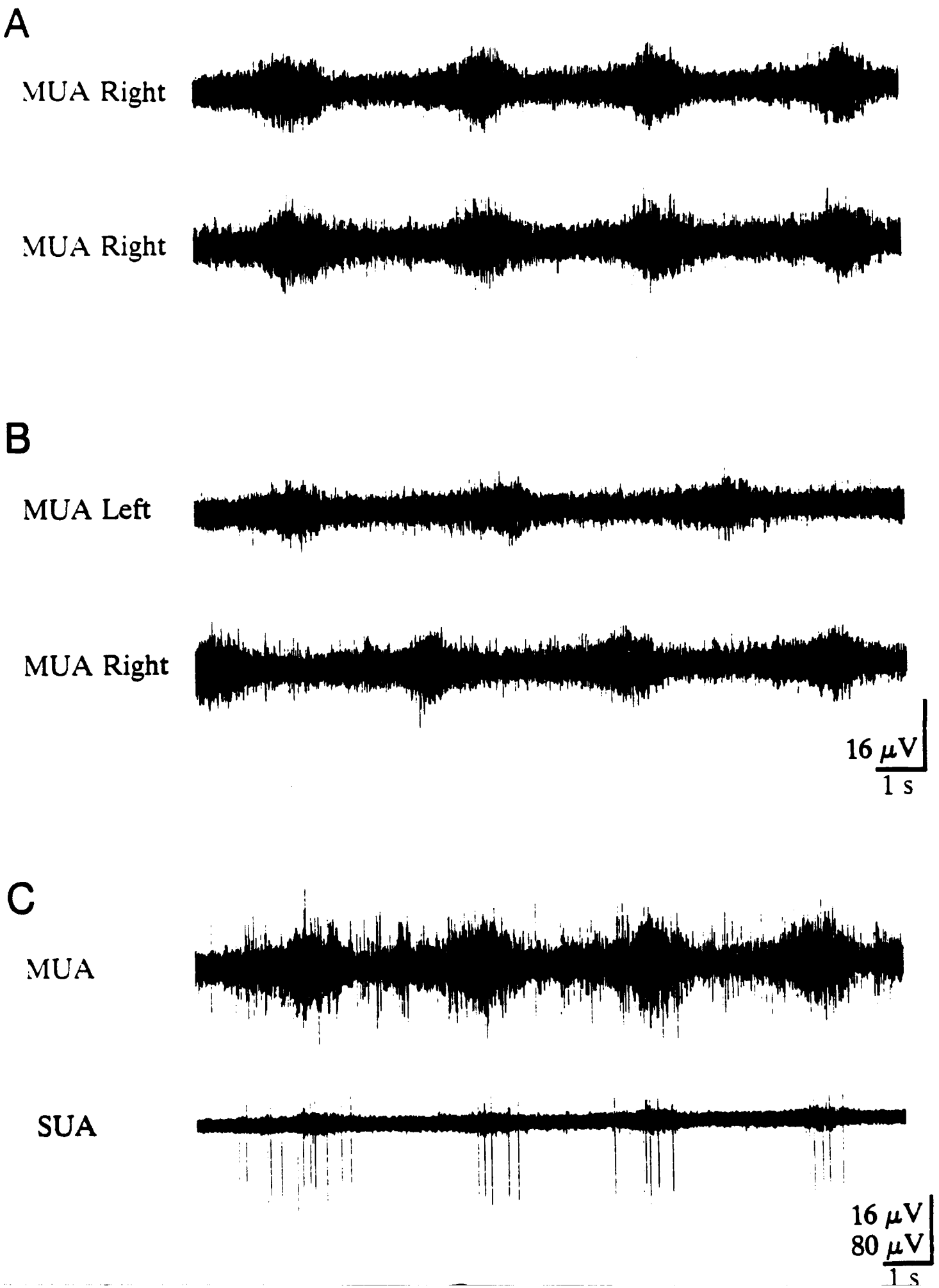
A
MUA Right
MUA Right
B
MUA Left
MUA Right
16 μV
1 s
C
MUA
SUA
16 μV
80 μV
1 s

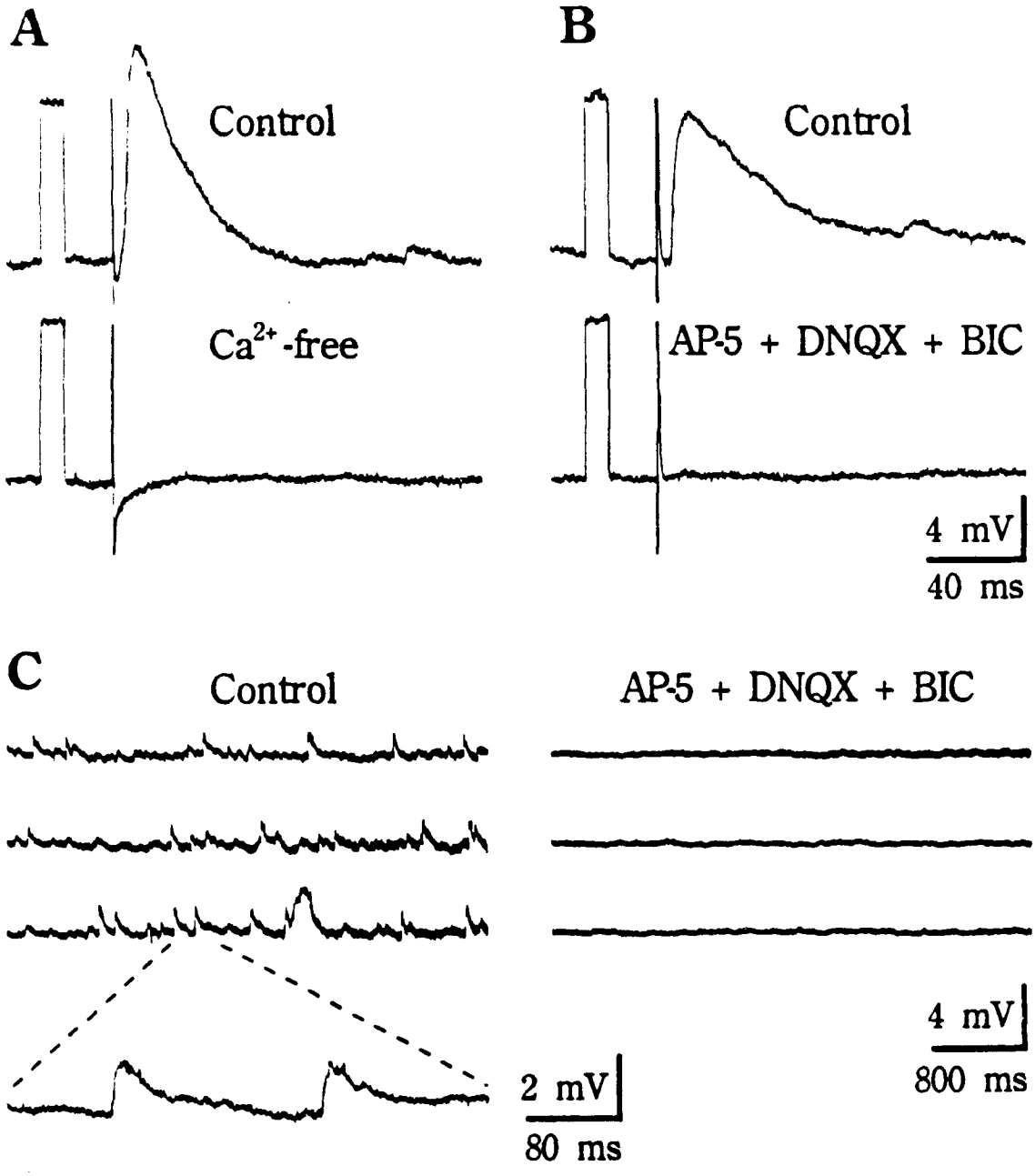
A
Control
Ca2+-free
B
Control
AP-5 + DNQX + BIC
4 mV
40 ms
C
Control
AP-5 + DNQX + BIC
4 mV
800 ms
2 mV
80 ms